Polypurine reverse Hoogsteen hairpins as a gene therapy tool: *in vitro* development and *in vivo* validation

Laura Rodríguez Gallego

UNIVERSITAT DE BARCELONA

FACULTAT DE FARMÀCIA

DEPARTAMENT DE BIOQUÍMICA I BIOLOGIA MOLECULAR

Programa de doctorat en Biotecnologia

Polypurine reverse Hoogsteen hairpins as a gene therapy tool: *in vitro* development and *in vivo* validation

LAURA RODRÍGUEZ GALLEGO

Barcelona, 2015

UNIVERSITAT DE BARCELONA

FACULTAT DE FARMÀCIA

DEPARTAMENT DE BIOQUÍMICA I BIOLOGIA MOLECULAR

Programa de doctorat en Biotecnologia

Polypurine reverse Hoogsteen hairpins as a gene therapy tool: *in vitro* development and *in vivo* validation

Memòria presentada per Laura Rodríguez Gallego per optar al títol de doctor per la Universitat de Barcelona

Dr. Carlos J. Ciudad Gómez
Director

Dra. Verónica Noé Mata
Directora

Laura Rodríguez Gallego

Barcelona, 2015

Learn from yesterday, live for today, hope for tomorrow
Albert Einstein

Durante esta etapa he conocido a mucha gente con la que he compartido momentos especiales y que me han aportado lecciones importantes. Me gustaría hacer especial mención a:

Carlos y Vero. Gracias a vosotros he aprendido cosas tanto a nivel profesional como personal. He aprendido muchas más cosas de las que inicialmente pensaba que aprendería y eso os lo tengo que agradecer especialmente. Gracias a vosotros me siento preparada para afrontar lo que venga. Porque lo duro no es empezar, sino perseverar.

A las que ya no están en el lab, pero que siempre estas presentes: al escuchar una canción, al consultar un protocolo, al hacer estadística etc.

Núria, la meva "mare" científica. Un terme una mica estrany però que té tot el sentit del món. Al cap i a la fi, no és cert que acabem sent una petita família? La Núria em va ensenyar tot a l'inici d'aquest camí i li agrairé sempre com em va transmetre la il·lusió per la ciència.

Carlota, si algo he aprendido de ti es a ser perseverante. Tienes un corazón enorme y fue un placer compartir lab contigo. Ojalá más adelante nos encontremos en este mundo que es la ciencia.

A las que siguen estando, ¿que hubiéramos hecho sin esas charlas post-lab? Porque la ciencia es poyata pero es también ser crítica y divagar.

Xenia, por esas conversaciones profundas de quién somos y a dónde vamos. Tal vez todavía no lo tengamos del todo claro, pero en ello estamos.

Anna, m'alegro molt d'haver-te conegut, ets una persona no només amb sentit de l'humor sinó amb una energia que ens has transmès cada dia. Tens una forma d'enfocar la vida molt sabia nena!

Claudia, crack! Si algún adjetivo te puede describir es proactiva, y tener alguien así al lado es una motivación continua. Estoy segura de que llegarás a donde te propongas! Por supuesto a Malu, por ser tan buena compi de lab.

Agradecer a todos esos estudiantes que han pasado por el lab, y que nos han enseñado también a nosotras: a cómo enseñar, a cómo tener paciencia, a cómo volver a tener ilusión. Mencionar especialmente a "mis" niñas: Iris, Alba, Carolina, y

Cristina Salado. También a los estudiantes de Erasmus: Sabine, Susana, Mila y Gizem.

A mi familia, por estar ahí durante estos años. Especialmente a mi hermana, Mariví, porque aunque esté lejos, siempre la siento muy cerca. Y a mi prima Ana, vivir esta etapa en paralelo nos ha unido aún más, gracias por todo! A mis amigos, por esas risas que te hacen desconectar de todo. Porque cada uno de ellos es especial.

A todos los doctorantes y estudiantes del Departamento. Por supuesto también a los profesores del Departamento y con especial mención a Laura Baldomà por la buena gestión del Departamento.

A José Luis, Sheila y Laura por su contribución en el primer artículo, gracias por haber estado al pie del cañón y darme la oportunidad de echar un ojo a lo que es una empresa biotec por dentro.

A Maria Tintoré y Sonia Pérez por ayudarme con los estudios de absorción UV. A Ramon Eritja por dedicarnos tiempo y explicaciones químicas.

A Gaël y Patricia por ayudarme con el estudio de líneas de linfoma, gracias a sus explicaciones y curiosidad científica.

Gracias a Jaume Coma y Chari, de los Servicios Científico-técnicos por ser de gran ayuda en los experimentos de Citometría de flujo.

Gracias a la Generalitat de la Catalunya por la beca FI que ha subvencionado estos estudios de doctorado y al Ministerio de Economía y competitividad por subvencionar los proyectos dentro de los cuáles he llevado a cabo la tesis.

"*Life isn't about finding yourself, it's about creating yourself*"

ABBREVIATIONS

A	Adenine
APRT	Adenine phosphoribosyltransferase
ASO	Antisense oligodeoxynucleotide
ATCC	American Type Culture Collection
Bak	BCL2-antagonist/killer
BAN	Biological Association Network
Bax	BCL2-associated X protein
Bcl	B-cell CLL/lymphoma
BH3	Bcl-2 Homology domain 3
bp	Base pair
C	Cytosine
cDNA	Complementary DNA
cpm	Counts per minute
CRPC	Castration-Resistant Prostatic Cancer
DHFR	Dihydrofolate Reductase
DNA	Desoxyribonucleic acid
dNTPs	Deoxynucleotide Triphosphate
DOTAP	N-[1-(2,3-Dioleoyloxy)propyl]-N,N,Ntrimethylammonium methylsulfate
dTMP	Thymidine monophosphate
dUMP	Uridine monophosphate
EDTA	Ethylene diamine tetraacetic acid
EMSA	Electrophoretic Mobility Shift Assay
FGF21	Fibroblast growth factor 21
FITC	Fluorescein isothiocyanate
FS	Forward scatter
G	Guanine
GHT-	F12 medium without glycine, hypoxanthine and thymidine
GnRH	Gonadotrophin-releasing hormone
GSH	Reduced glutathione
GST	Glutathione S-Transferases
h	hour
HpF	Fluorescently labeled hairpin
IAP	Inhibitor of Apoptosis
IHPK2	Inositol hexaphosphate kinase 2
IP	Propidium iodide
LNA	Locked nucleic acids
Luc	Luciferase
M, mM, µM, nM	Molar, miliMolar, mcroMolar, nanoMolar
MAPK	Mitogen-activated Protein Kinase
Mcl-1	Myeloid cell leukemia 1
MDR	Multidrug resistance
miRNA	microRNA

Mis	Mismatch
MOE	Methoxyethyl
mRNA	Messenger ribonucleic acid
MTX	Methotrexate
nt	Nucleotide
PBS	Phosphate-buffer saline
PCR	Polymerase chain reaction
PI3K	phosphoinositide 3-kinase
PPRHs, Hp	Polypurine reverse Hoogsteen hairpins
PS	Phosphorothioate
qRT-PCR	Quantitative real time polymerase chain reaction
r-H	Reverse-Hoogsteen bonds
RAB20	RAB20, member RAS oncogene family
Rho123	Rhodamine 123
RISC	RNA-induced silencing complex
RNA	Ribonucleic acid
RNAi	RNA interference
RNAse	Ribonuclease
rRNA	Ribosomal ribonucleic acid
RTK	Tyrosine kinase receptors
Sc	Scrambled
siRNA	Small interfering RNA
SMAC	Second mitochondria-derived activator of caspase
Sp	Specificity Protein
SS	Side scatter
T	Thymidine
TERT	Telomerase Reverse Transcriptase
TFO	Triplex Forming Oligonucleotide
TLR	Toll-like Receptor
T_m	Melting temperature
TMPD	Tetramethylphenylenediamine
TNF	Tumor necrosis factor
TP53	Tumor protein p53
TRAIL	TNF-related Apoptosis-inducing ligands
TTS	Triplex-forming oligonucleotide target sequences
U	Uracil
U2AF65	U2 small nuclear RNA auxiliary factor 2
UTR	Untranslated region
VEGF	Vascular Endothelial Growth Factor
WC	Watson-Crick
WHO	World Health Organization
WT	Wild-type

INDEX

PRESENTATION

The work presented is focused on the study of Polypurine Reverse Hoogsteen hairpins (PPRHs) as gene silencing tools. The main goals were to study the mechanism of action of these molecules, to establish their proof of principle for *in vivo* applications, and to improve their design in terms of specificity and efficacy.

The research in our group included the usage of gene silencing tools such as ASOs, TFOs or siRNAs. However, all these molecules present hurdles, such as their stability, effect or cost. With the aim to overcome those problems, PPRHs were developed using the properties of Hoogsteen bonds.

PPRHs are double-stranded DNA molecules formed by two antiparallel homopurine domains linked by a 5-thymidine loop, which form intramolecular reverse Hoogsteen bonds. The *in vitro* study of their binding led to the finding that PPRHs bind to their pyrimidine target sequence inducing the displacement of the polypurine strand, at physiological conditions. As it is difficult to find pure polypurine/polypyrimidine stretches within the genome, and interruptions may disrupt binding, it was proved that the best base to use in front of the interruptions was an adenine (Coma et al. 2005) . Once their binding was proved *in vitro*, there was the need to prove their effect in cells. As our group had expertise in *dhfr* gene regulation, PPRHs against either the template or the coding strand of intronic sequences of the *DHFR* gene were tested *in vitro* and their mechanisms of action were studied. PPRHs were able to decrease the mRNA levels of the targeted gene and to decrease the cell viability when designed against *DHFR*. This was also the case for other genes important for cell proliferation (de Almagro et al. 2009; de Almagro et al. 2011) .

The experiments in this work explore the effect of PPRHs against anti-apoptotic targets, specifically, *survivin* and *Bcl-2*. We performed a comparative study of the *in vitro* efficacy of different PPRHs in cancer cell lines. We investigated the mechanism of action of the most efficient PPRHs and administered the best candidate in a xenograft tumor model to test the feasibility of their therapeutic use.

To improve their design, we explored the effect of different variables, such as the length and the presence of pyrimidine interruptions in the PPRH sequence. We also compared PPRHs and TFOs and designed a new molecule based on PPRHs, the so-called Wedge-PPRH. Finally, we analyzed the uptake of PPRHs into different cell lines.

1. INTRODUCTION

1.1. PPRHs and other silencing technologies

1.1.1. Triplex Forming Oligonucleotides

One of the most important discoveries of the 20th century was the structure of the DNA in 1953. From this moment on, enormous possibilities arose. Ten years later, the discovery of Hoogsteen bonding explained the existence of triple-stranded nucleic acids, when a single stranded DNA was capable of binding to the major groove of the DNA structure (Felsenfeld & Rich 1957; Hoogsteen 1963). That opened the possibility to design molecules to specifically target sequences within the genome. However, it was not until the late 80s that these molecules were suggested to play a role in gene expression (Wells & Collier 1988).

Triplex Forming Oligonucleotides (TFOs) are molecules that bind to the purine strand of the double-stranded DNA by hydrogen bonds, specifically Hoogsteen or reverse Hoogsteen bonds. There are three types of TFOs that vary in the composition and orientation of the third strand relative to the purine strand of the duplex, and therefore, in the type of bonds formed with the DNA (Figure 1).

- Purine TFOs (G,A-TFOs) are anti-parallel relative to the purine strand and form reverse Hoogsteen bonds.
- Pyrimidine TFOs (T,C-TFOs) are parallel to the purine strand and form Hoogsteen bonds. Cytosines must be protonated for this kind of binding, which occurs at acidic pH.
- Mixt TFOs (G,T-TFO) might be either parallel, thus forming Hoogsteen bonds, or anti-parallel forming reverse Hoogsteen bonds.

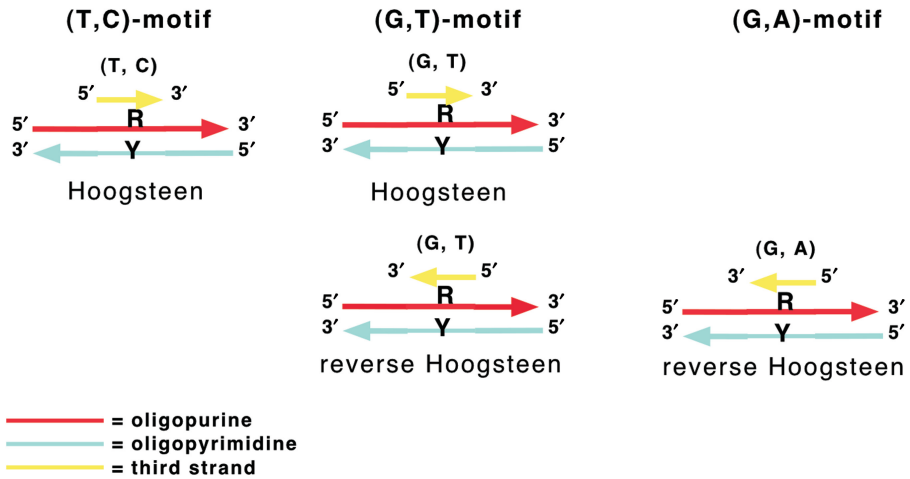

Figure 1. Types of TFOs depending on the composition and type of hydrogen bonds formed (Duca et al. 2008).

Purine TFOs have several advantages over pyrimidine TFOs because they bind to their target sequence in a pH-independent manner, with higher affinity and faster kinetics (Faucon et al. 1996). Design of TFOs is limited to location of stretches of polypurine/polypyrimidine sequences. Goñi et al. found that these sequences were overrepresented in the genome, mainly in regulatory regions, such as promoters and introns (Goñi et al. 2004). According to *in silico* analyses, genes presenting triplex-forming oligonucleotide target sequences (TTS) in their promoters were usually involved in physiological processes. Moreover, these regions tended to be conserved between species, implying a functional role of TTS. They also postulated that even when TTS were not directly targeted by transcription factors, they might be of importance for gene functionality by acting as spacing fragments to help the correct positioning of transcription factors(Goñi et al. 2006).

The study of the mechanism of action concluded that TFOs interfered with the transcription process (Praseuth et al. 1999). The first study of this inhibitory effect was conducted by Postel et al., that determined that a TFO against *c-myc* was capable of decreasing its mRNA levels in HeLa cells (Postel et al. 1991). Other TFOs have been suggested to interfere in the binding of transcription factors, such as those directed against the E-1 motif within the tie-1 promoter for the binding of Ets transcription factors, which are important for blood vessel formation (Hewett et al. 2006). Apart from binding to DNA, TFOs can bind to mRNA, thus blocking mRNA translation (François et al. 1999).

The *in vivo* application of TFOs displayed several problems, namely, stability, affinity and ability to form a triplex at physiological pH without forming secondary structures. To address stability, chemical modifications of the structure have been studied (Duca et al. 2008). In order to increase the affinity, Kool and co-workers found out that purine sequences in a hairpin or a circular structure could form triplexes with their single-stranded pyrimidine target sequence with a higher binding affinity in terms of melting temperature (T_m). With regard to their binding, it is worth mentioning that G-rich oligonucleotides can aggregate in the presence of potassium, hence competing for the binding with the target sequence. However, Kool also found that both hairpin and circular structures formed triplexes with their target sequence even in the presence of potassium (Vo et al. 1995).

1.1.2. Polypurine reverse Hoogsteen hairpins

1.1.2.1. Mechanism of action

Polypurine reverse Hoogsteen Hairpins (PPRHs) are non-modified DNA molecules, formed by two antiparallel purine domains linked by a 5-thymidine loop. These domains form intramolecular reverse Hoogsteen bonds, giving the molecule a hairpin structure. It was previously demonstrated in our group the ability of PPRHs to bind to their polypyrimidine target sequence of different lengths by Watson-Crick bonds. The PPRH was able to bind with high stability to its single-stranded target sequence. Moreover, the PPRH also bound to the double-stranded target sequence thus causing the displacement of the polypurine strand of the duplex (Coma et al. 2005). In Figure 2, bonds forming the triplex structure are shown.

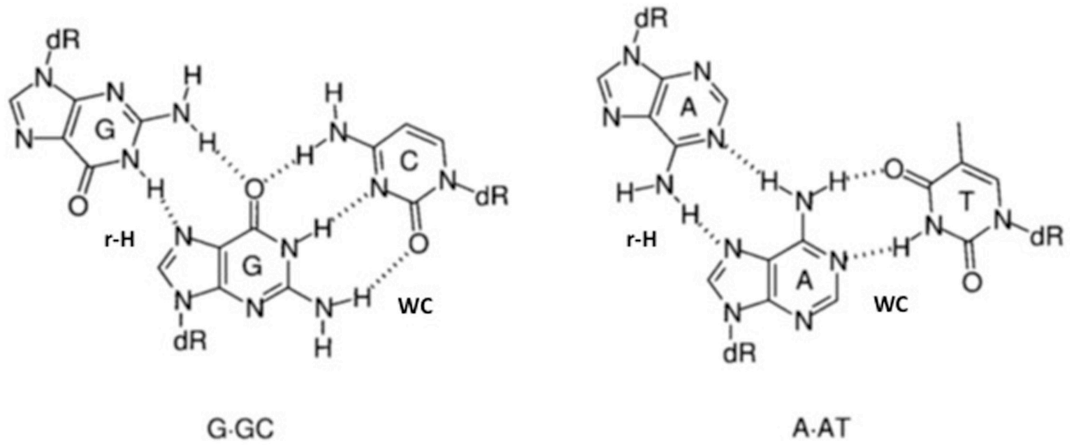

Figure 2. Reverse Hoogsteen bonds (r-H) and Watson-Crick bonds (WC) formed in the triplex structure. Modified from (Gowers & Fox 1999).

PPRHs can be designed against either of the strands of the DNA, depending on the location of the polypirimidine target sequence. Consequently, we could define two types of PPRHs: Template-PPRHs bind to the template strand of the DNA and Coding-PPRHs are directed against the coding strand, and can bind to DNA and mRNA because both strands have the same sequence and orientation. Both types of PPRHs against polypyrimidine target sequences in intronic sequences of the *DHFR* gene were designed and tested in terms of cell viability and gene expression. DHFR is an enzyme involved in the *de novo* synthesis of purine and thymidine monophosphate. It was found that a PPRH against a sequence in intron 3 in the template strand of the *DHFR* gene caused a decrease in *DHFR* mRNA, protein and

activity levels. Incubation of this PPRH in breast cancer cells using –GHT medium – a selective media not containing the final products of the enzyme-, decreased cell viability. Furthermore, it was demonstrated that this Template-PPRH displayed a higher effect when the two domains of the PPRH were bound by reverse Hoogsteen bonds (HpB) than when the sequence did not allow the formation of those bonds (Hp-NH) (de Almagro et al. 2009).

Subsequently, a Coding-PPRH directed against another intronic sequence of the *DHFR* gene, but in the coding strand, was tested. This study showed that binding of the Coding-PPRH to the pre-mRNA sequence within intron 3 of the *DHFR* gene prevented the binding of the splicing factor U2AF65, specific for that sequence. The lack of binding of that factor avoided correct splicing, leading to a decrease in DHFR protein levels (de Almagro et al. 2011). In Figure 3 the mechanisms of action of both PPRHs against the *DHFR* gene are shown.

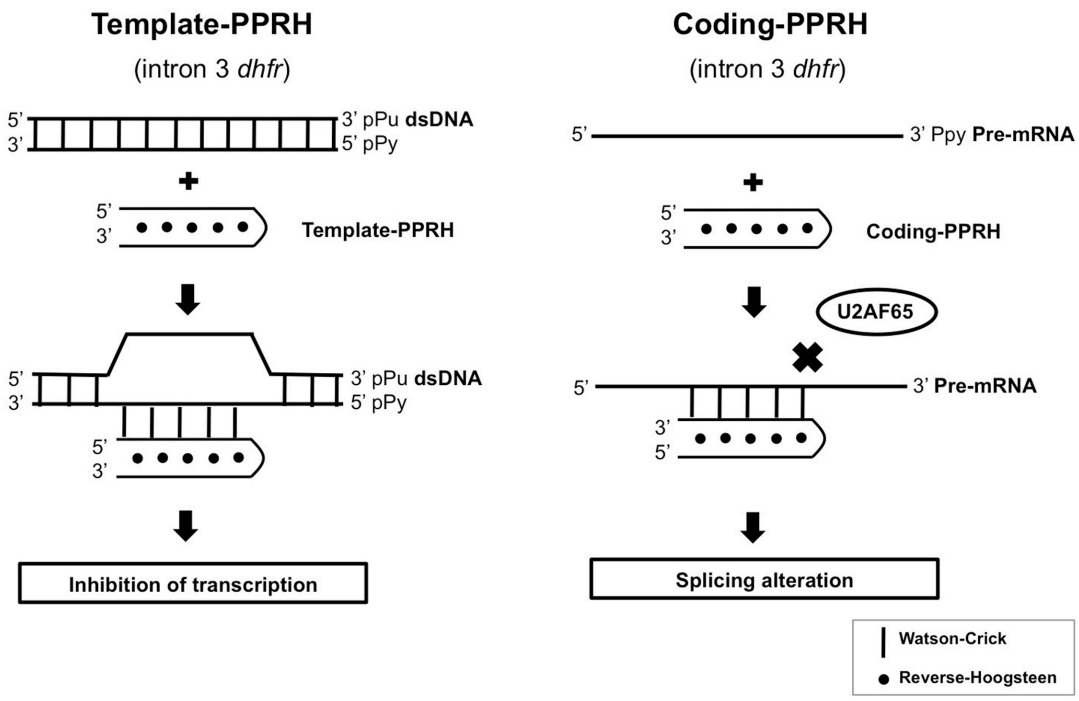

Figure 3. Mechanism of action of Template and Coding-PPRHs directed against two regions of intron 3 of the *DHFR* gene.

1.1.2.2 Properties of PPRHs

According to the previous description, Template-PPRHs act through an antigene strategy and Coding PPRHs may act through both antigene and antisense strategies.

The synthesis of PPRHs is inexpensive and straightforward due to the fact that they are non-modified DNA molecules. In addition, PPRHs are much more stable and resistant to nucleases than other gene silencing molecules (Coma et al. 2005; de Almagro et al. 2009).

For any silencing molecule, specificity is an important concern. Length and the presence of interruptions are the main points to address this issue. To properly design either ASOs or TFOs is essential to check for unintended targets, but it was stated that 17-nucleotide oligonucleotides should bind to a unique sequence in the genome (François et al. 1999). In our group, PPRHs of 20-nucleotides have been used successfully to target different genes. The polypurine/polypyrimidine sequences found in the genome are not always pure stretches and present interruptions. In the past, we tested different options to determine the best base to use in front of the interruptions and found that the use of adenines in both domains of the PPRH sequence maintained the binding to the target sequence while keeping a pure polypurine hairpin (Coma et al. 2005). This approach was then tested *in vitro* using PPRHs against the *DHFR* gene carrying several interruptions substituted by adenines. These PPRHs were useful to decrease survival in breast cancer cell lines through a decrease in *DHFR* mRNA levels, without inducing a decrease in various non-related genes (de Almagro et al. 2009).

1.1.3. Antisense Oligonucleotides and siRNAs

Apart from TFOs and PPRHs, other gene silencing technologies are worth mentioning, such as antisense oligonucleotides (ASOs) and small interfering RNAs (siRNA).

ASOs are single-stranded DNA molecules that bind to their complementary sequence in the mRNA. The consequent DNA-RNA hybrid is recognized and degraded by RNAse H1. ASOs can also act through blockade of translation or modulation of splicing when targeted against the pre-mRNA (Wu et al. 2004).

The discovery that introduction of double-stranded RNA in *C.elegans* decreased the levels of the targeted gene (Gall et al. 1998) and the following realization of this mechanism in other organisms, including mammalian cells (Elbashir et al. 2001) prompted the research in their mechanism and possible applications. siRNAs are dsRNA molecules of around 20 bp with a 2-nt 3' overhang, which are recognized by the RNA-induced silencing complex (RISC); this complex loads one of the strands (guide strand) and scans for complementary sequences, when the complementary mRNA sequence is found, the endonuclease Argonaute will degrade it (Siomi & Siomi 2009).

Both ASOs and siRNAs are used as common tools in laboratory research and are currently under development as target-directed therapeutic approaches. However, several obstacles have hampered their progress, such as stability, *in vivo* delivery and off-target effects. During the last years, much effort has been undertaken to overcome these problems.

Stability is a necessary property to ensure a longer half-life and a good biodistribution of the molecule. Stability limitations of gene silencing molecules have lead to the introduction of chemical modifications, such as phosphorothioate (PS) linkages to increase nuclease resistance (Watts & Corey 2012).

Another important problem when moving forward to the clinics is the delivery of such molecules to the specific cells. In *in vitro* approaches, this means using liposomal reagents or other vehicles for transfection. *In vivo* delivery is more challenging because to reach the appropriate cell, the molecule must pass through the blood vessel wall, the interstitial space and the extracellular matrix. Moreover, the nucleic acid based molecule needs to avoid the immune system and nuclease degradation, and when it is finally in the appropriate cell membrane, it needs to

enter the cell and escape from the endosome to exert its function. In this respect, the intrinsic stability of the molecule takes on importance. For both ASOs and siRNAs, chemical modifications are required to avoid nuclease degradation, to increase their stability and their potency. But besides these modifications, new vehicles to protect and specifically deliver the silencing molecule are necessary. For this reason, the choice of a vehicle has been a hot topic in the gene-therapy field in the last years. Researchers have been exploring new delivery methods such as lipids, cationic polymers, and lately, nanoparticles (Duca et al. 2008; Watts & Corey 2012; Burnett et al. 2012). Besides that, there is research about new strategies to direct targeting by using aptamers (Ferreira et al. 2008) or antibodies (Rodríguez et al. 2002), among others.

In terms of specificity, off-target effects are another important concern, mainly caused by the binding of the silencing molecule to unintended targets. One way to address them is by using modifications, such as LNA (locked nucleic acid), to increase affinity. In this aspect, siRNAs are especially problematic as they may exert off-target effects through two different routes. On the one hand, Jackson et al. reported several siRNAs reducing the levels of nonspecific genes that contained partial sequence identity with the siRNA and suggested they were playing a similar role to miRNAs (Jackson et al. 2003). On the other hand, there is an association between the use of siRNAs and activation of the innate immunity that might cause undesirable toxicities *in vivo* (Robbins et al. 2009). Recent reports have described effects of non-targeted siRNAs due to the activation of TLRs, causing anti-angiogenic and inflammation effects (Kleinman et al. 2008).

Despite all of these obstacles, gene silencing technologies are currently in the pipeline of pharmaceutical companies to treat a broad range of diseases. Two ASOs have been approved by the FDA: fomivirsen, for the treatment of citomegalovirus retinitis in 1998 (Grillone & Lanz 2001) and mipomersen, for Homozygous familial hypercholesterolemia in 2013 (Hair et al. 2013). Furthermore, a dozen ASOs are in Phase II and III against a variety of diseases, including cancer (Jiang 2013). Regarding siRNAs, even though more than 20 siRNAs are in phase II clinical trials, none has been approved yet by the FDA; in fact, two siRNAs against VEGF were withdrawn from clinical trials because of unspecific activation of the immune system via TLR3 (Kleinman et al. 2008).

Therefore, there is room for the development of other gene silencing technologies, such as PPRHs, with the aim to improve several properties that impair the development of the above-mentioned molecules.

1.2. Cancer:

In 2011, Hanahan and co-workers reassessed the main keys leading to tumorigenesis, or as they called them, the hallmarks of cancer. This review summarized the six previously described hallmarks (Hanahan & Weinberg 2000) and included four more taking into account the progress made in cancer research during the last years (Figure 4).

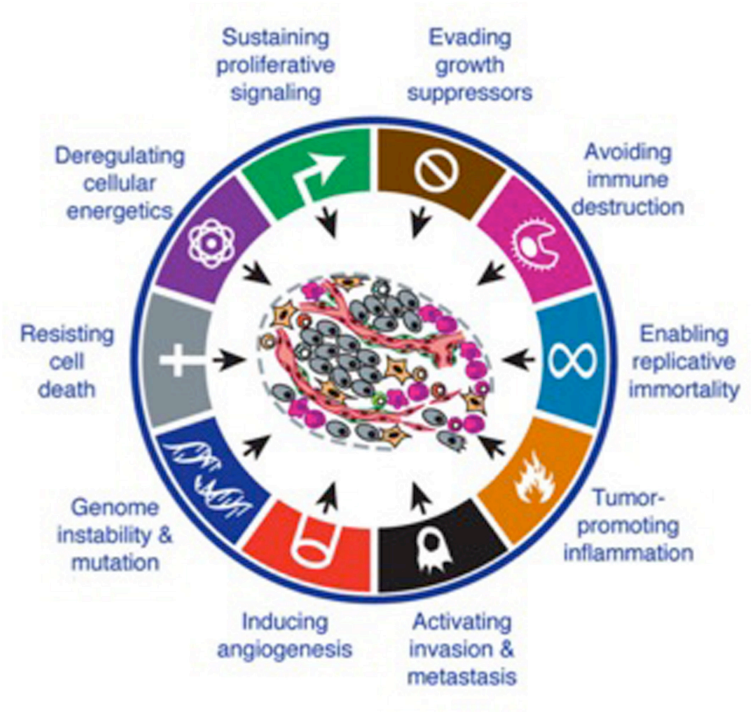

Figure 4. Hallmarks of cancer . From (Hanahan & Weinberg 2011)

Among these 10 hallmarks, one of the most studied has been the resistance to cell death. Apoptosis is triggered by stress signals, both from the extracellular and the intracellular environment, which converge in effector caspases that execute cell death. There are two apoptotic pathways: the extrinsic pathway and the intrinsic or mitochondrial pathway. Both pathways are constituted by upstream regulators: extracellular and intracellular proteins, and downstream effectors: caspases. Whereas the extrinsic pathway is activated by cell death receptors in the membrane, the intrinsic is triggered by different stresses, such as intracellular damage, and involves the mitochondria. Apoptosis activation depends upon the balance of pro and anti-apoptotic proteins and it is tightly regulated. It is

established that apoptosis, specifically the intrinsic pathway, is a programmed cell death that avoids cancer development (Hanahan & Weinberg 2011).

The extrinsic pathway consists in the activation of receptors of the tumor necrosis factor (TNF) family or TNF-related apoptosis-inducing ligands (TRAILs), that cause the recruitment and activation of caspase-8, which leads to proteolysis and activation of the effector caspase-3.

The intrinsic pathway causes the release of cytochrome *c* and second mitochondria-derived activator of caspase (SMAC) from the mitochondria, which will activate effector caspases that execute cellular degradation (Zielinski et al. 2013).

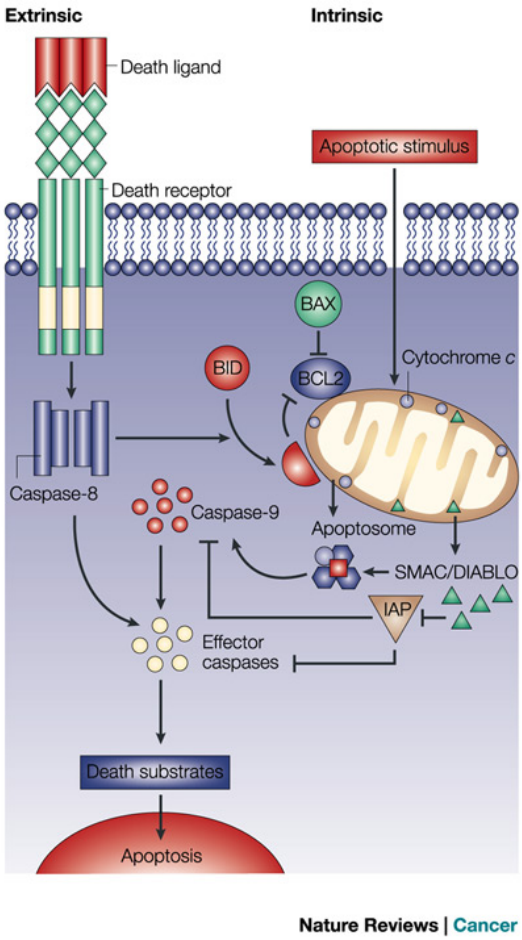

Figure 5. Apoptotic pathways. From (Altieri 2003b)

Impairment of apoptosis offers a clonal advantage for preneoplastic cells to survive even while bearing abnormalities (Adams & Cory 2007). Tumor cells have evolved several strategies to evade apoptosis, such as loss of TP53 or overexpression of anti-apoptotic regulators.

Another hallmark of cancer is the induction of angiogenesis. As tumors grow, they have a high requirement for nutrients and oxygen, and this need guides the formation of new vessels to sustain tumor growth. There are several angiogenic regulators involved in this process, such as *VEGF-A* and *survivin*.

Survivin and *Bcl-2* are anti-apoptotic proteins that stand out among other apoptosis regulators as good therapeutic targets. That is the reason why we chose them to develop our gene silencing strategy.

1.2.1. Prostate cancer

Prostate cancer is the second most common cancer and the fifth cause of death from cancer in men, as in 2012. Approximately 1.1 million men were diagnosed worldwide and 307,000 died from this cause in 2012, with a higher incidence in Western world and developed regions. Figure 6 shows incidence and mortality among regions (WHO 2012).

Prostate cancer is a heterogeneous disease where different genetic and epigenetic changes lead to its development, including loss of heterozygosity, activation of oncogenes and loss of tumor suppressor genes, among others. Other risk factors such as old age, black ethnicity and environmental risk factors, also play a role in prostate cancer (Felgueiras et al. 2014).

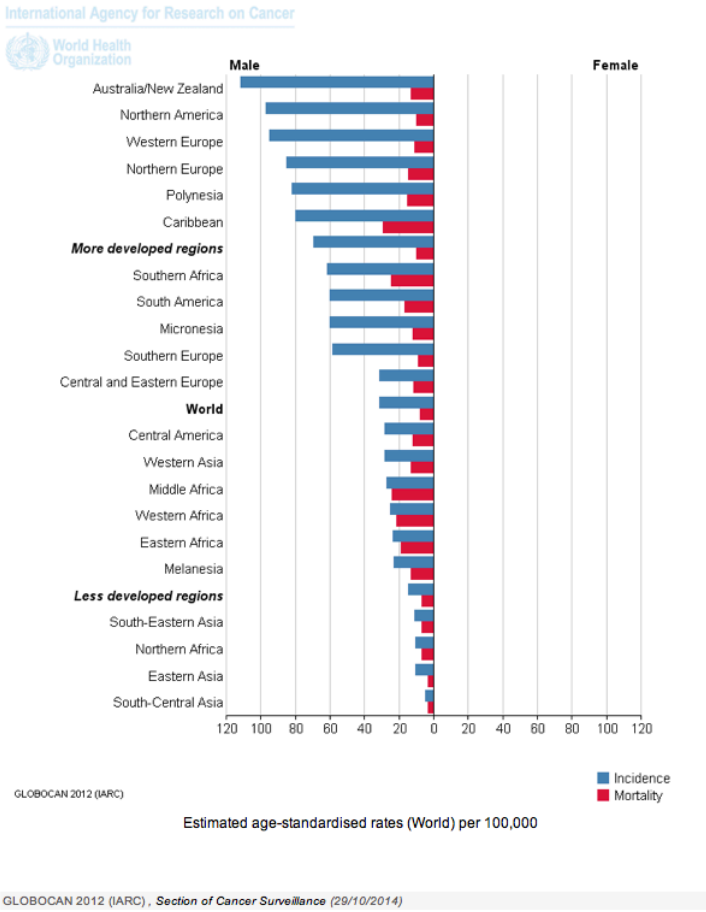

Figure 6. Incidence and Mortality rate in the world in 2012.

Treatment for prostate cancer depends on the stage of the disease, which is divided in: hormone-sensitive, androgen-independent, symptomatic metastatic, and advanced metastatic or anaplastic. Surgery and/or radiotherapy are the treatments of choice in early stages or when the cancer is localized. These procedures are usually combined with hormone ablation therapies - such as anti-androgens or GnRH analogues (gonadotrophin-releasing hormone)-, which is also the choice when metastatic disease appears. However, fewer effective treatments are available for hormone-resistant prostate cancer (the recommended term is CRPC). Currently, chemotherapy and combination treatments are under study for CRPC (Ramsay & Leung 2009; Felgueiras et al. 2014).

The study of the signaling pathways participating in the development of the disease has generated information about prospective new therapeutic targets. Of great importance is the androgen receptor pathway, which regulates development and progression of cancer. However, CRPC finds ways to overcome hormone dependency by altering the cascades of tyrosine kinase receptors (RTKs), thus activating pathways such as PI3K (phosphoinositide 3-kinase)/Akt and MAPK (mitogen-activated protein kinase). Another important hallmark of CRPC is its ability to overcome apoptosis, via overexpression of anti-apoptotic proteins like *survivin* and *Bcl-2* (Felgueiras et al. 2014).

Several target-directed strategies have been under development in the past years, using as targets the above mentioned genes. Both small molecules and antibodies are used to inhibit RTKs, with different mechanisms of action and efficacies. Whereas chemical inhibitors present higher efficacy, they often exert multi-target effects; on the other side, monoclonal antibodies are much more specific but display less effect. Combination therapies could be an option to increase the effect of the available therapies. Moreover, antisense oligonucleotides, such as oblimersen, have been under study without much success up until now (Ramsay & Leung 2009).

Even though the comprehension of the mechanism underneath the development of prostate cancer gave rise to a number of therapeutic targets, to date, none of these therapies is adequate for routine usage. Therefore, the development of new approaches to improve the current treatments is needed.

1.2.2. Targets

1.2.2.1 Survivin

The *survivin* gene is located at 17q25 in the human genome and encodes for the smallest member of the inhibitor of apoptosis (IAPs) family, with a molecular weight of 16.5 kDa. The involvement of *survivin* in apoptosis is broadly demonstrated either through its overexpression, which caused inhibition of cell death, or by decreasing its levels using different antagonists, which induced apoptosis. Even though its mechanism of action has been controversial, Dohi et al. proved that in response to stress, mitochondrial *survivin* protected the cell from apoptosis by preventing activation of initiator caspase-9 (Dohi et al. 2004).

Besides its role as an anti-apoptotic protein, *survivin* is also involved in mitosis and angiogenesis. *Survivin* expression depends on cell cycle and it is strictly regulated by its short half-life, being more abundant during mitosis, where it exerts a controlling function that is still under study (Altieri 2003a). It has been suggested that *survivin* may interact with caspase-9 at cell division to prevent apoptosis (O'Connor, et al. 2000). Regarding angiogenesis, *survivin* is known to be upregulated in endothelial cells during angiogenesis, which contributes to the inhibition of apoptosis via suppression of caspase-3 activity, and therefore, maintenance of viability (O'Connor et al. 2000). Previously in our group, the role of *survivin* in angiogenesis was investigated. Incubation of endothelial cells with either siRNAs or ASOs against *survivin* induced inhibition of migration and capillary formation, besides causing inhibition of growth, apoptosis and cell division defects (Coma et al. 2004).

Survivin is overexpressed in different tumors, including prostate (Ambrosini et al. 1997), colon (Kawasaki et al. 1998) and pancreas (Satoh et al. 2001). On the contrary, its levels are undetectable in most differentiated normal tissues, with the exception of thymus (Ambrosini et al. 1997), CD34+ bone-marrow-derived stem cells at low levels (Carter et al. 2001) and the basal colonic epithelium (Gianani et al. 2001). Thus, *survivin* is not only essential for cell survival, but its expression is very differentiated between normal and cancer cells, which makes *survivin* an ideal therapeutic target.

In particular, target-directed therapy to inhibit *survivin* is a good option in prostate cancer because it is associated with androgen resistance (Zhang et al.

2005) and with aggressive phenotypes (Shariat et al. 2004). In fact, several Phase-II clinical trials using either small-molecule inhibitors -YM155- or antisense therapy -LY2181308- have been conducted for castration-resistant prostatic cancer (CRPC), after showing apoptosis in prostate cancer cell lines and regression of tumor growth in xenografts (Nakahara et al. 2007).

YM155 is a small inhibitor of *survivin* that caused growth inhibition and an increase in apoptosis in different prostate cancer cell lines, as well as in subcutaneous and orthotopic xenografts models of prostate tumors (Nakahara et al. 2007). However, in phase II clinical trials, YM155 showed a rather modest activity (Tolcher et al. 2012). Further Phase II studies in combination with docetaxel are being conducted but no results have been posted so far (Astellas Pharma Inc 2007).

LY2181308 is a second-generation antisense oligonucleotide (ASO) that contains not only the phosphorothioate backbone but also the 2'-MOE modification of the ribose of the first 4 and last 4 nucleotides of the ASO, with the goal to increase potency, stability and decrease toxicity. This molecule, through the decrease in *survivin* levels, proved to induce apoptosis in a panel of different cancer cell lines, inhibited tumor growth in two xenograft models and sensitized the tumors to different chemotherapeutic agents in a synergistic fashion (Carrasco et al. 2011). However, a randomized phase-II trial with LY2181308 in combination with docetaxel showed no improvement in the efficacy of the treatment (Wiechno et al. 2014).

1.2.2.2 *Bcl-2*

Bcl-2 is a member of a family of proteins that control apoptosis through the intrinsic or mitochondrial apoptotic pathway. This control depends on the balance and interactions between the two opposite players of the family: the pro-apoptotic proteins that promote cell death -Bax, Bak and Bok- and the anti-apoptotic proteins that protect cells -Bcl-2, Bcl-X_L, Bcl_W and Mcl-1, among others-. There is another subfamily, the so-called BH3-only proteins, with the least homology -that include Bik, Bad, Bid, Bim, Bmf, Hrk, Noxa and Puma-, which have a monitoring and cytotoxic function (Willis & Adams 2005). Specifically, Bcl-2 and other proteins from its family (Bcl-x_L, Bcl-w, Mcl-1, A1) are inhibitors of apoptosis that exert their function by binding to the pro-apoptotic members of their family (Bax and Bak). In normal conditions, the anti-apoptotic proteins prevent the action of Bax or Bak. When apoptosis is triggered, Bax and Bak are released to disrupt the integrity of the outer membrane of the mitochondria, releasing other pro-apoptotic proteins such as cytochrome *c*, which activates a cascade of caspases that will ultimately cause apoptosis (Adams & Cory 2007; Azmi et al. 2011).

The first association between *Bcl-2* and cancer was established in follicular lymphomas bearing the translocation t(14;18) (McDonnell & Korsmeyer 1991). After that, Bcl-2 overexpression has been proved to correlate with cancer progression and resistance to chemotherapy in multiple cell lines (Azmi et al. 2011). In prostate cancer, *Bcl-2* expression increases along with the progression of the disease (Krajewska et al. 1996; Furuya et al. 1996). *Bcl-2* expression has also been related to recurrent prostate cancer after treatment with radiotherapy (Osser et al. 2003). Regarding other solid tumors, Bcl-2 content has been related to increased resistance to gemcitabine for the treatment of pancreatic cancer cell lines, proving that it is a good biomarker to predict response to therapy and to increase sensitivity to this drug (Bold et al. 1999). Relative to colon cancer, Pramanicim-A proved to cause apoptosis through an up and down-regulation of several members of the Bcl-2 family in HCT116 colon cancer cells (Bodur et al. 2013).

Nowadays, there are a wide variety of molecules against Bcl-2 under development and among the most important we found antisense oligonucleotides -oblimersen sodium- and small molecules - BH3 mimetics-.

Oblimersen is a phosphorothioate ASO directed against the first 6 codons of the open reading frame of human *Bcl-2* mRNA. This ASO was tested in several preclinical models and later in clinical trials in combination with chemotherapeutic agents for different types of cancer (Chi 2005). However, the first randomized phase II trial to evaluate the effect of this ASO previous to the administration of docetaxel in CRPC, found no benefit. The authors suggested that the determination of *Bcl-2* levels in CRPC patients to discriminate between populations might enhance the efficacy of this combination (Sternberg et al. 2009).

Regarding small molecules, both natural compounds -such as gossypol or its derivatives- and rationally designed ones - ABT derivatives- have been tested as *Bcl-2* inhibitors. Rational development has been necessary to improve specificity of compounds such as gossypol, a BH3-mimetic that inhibits not only Bcl-2 but also several members of its family. There has been a progress in more specific inhibitors, such as ABT-737 and ABT-263, but currently, they are still in preclinical development for tumors in the genitourinary tract (Hall et al. 2013).

Whereas small drugs have advantages as practical use and cost-efficiency *in vivo*, it is important to take into account drawbacks such as challenging pharmacokinetic profile and side effects due to unspecificity. On the other hand, ASOs are meant to be more specific, but their short half-life and DNAse-mediated degradation limits their action. Similar to antisense therapy, the *in vivo* use of antibodies and ribozymes, which are also under investigation, is limited by their lack of stability and effective delivery. Although much effort has been made to develop target-directed therapies against either *survivin* or *Bcl-2*, none of these approaches has been proven to be useful in the clinic (Scarfò & Ghia 2013).

2. GOALS

The major aim of this work was to study and develop PPRHs as a gene silencing tool. To do so, we established two main goals:

I. Validation of PPRHs both *in vitro* and *in vivo* to establish the proof of principle for their use as a therapeutic tool.
   - Comparison between Template- and Coding-PPRHs against *survivin* and *Bcl-2*.
   - Exploration of the mechanism of action of PPRHs.
   - *In vivo* administration of the best candidate in a xenograft tumor model.
   - Application of PPRHs to functionally validate targets in proliferation and in chemotherapeutic resistance.

II. Improvement of PPRHs properties to increase their efficacy and expand their applications:
   - Study of length importance for the design of PPRHs.
   - Comparison with TFOs against the same target, at the levels of binding and effect.
   - Study of interruptions to prevent off-target effects.
   - Development of new molecules based on PPRHs.
   - Study of the uptake of PPRHs in different cell lines.

3. MATERIALS AND METHODS

Most of the methodology used in this work is included in the Methods sections of the enclosed articles. Nevertheless, statement of the cell lines, media and oligonucleotides used in all the studies, and a more profound description of some of the methods, are detailed in this section.

3.1. Materials

3.1.1. Cell lines

All cell lines either from solid tumors or hematopoietic malignancies, used in the different studies, are specified in Table 1.

Table 1. Cell lines used in the experiments including information about cell type, organism and cell line repository.

Name	Cell type	Organism	Repository
Solid tumors			
PC3	Prostate adenocarcinoma	*Homo sapiens*	ECACC
SKBR3	Breast adenocarcinoma	*Homo sapiens*	ATCC
MiaPaCa2	Pancreas carcinoma	*Homo sapiens*	ATCC
HCT116	Colorectal carcinoma	*Homo sapiens*	ATCC
HeLa	Cervical adenocarcinoma	*Homo sapiens*	ATCC
MCF7	Breast adenocarcinoma	*Homo sapiens*	ATCC
SaOs 2	Bone osteosarcoma	*Homo sapiens*	ATCC
Hematopoietic malignancies cell lines			
Jurkat	Acute T cell leukemia	*Homo sapiens*	ATCC
K562	Chronic myelogenous leukemia	*Homo sapiens*	ATCC
EL4.BU	Lymphoma	*Mus musculus*	ATCC
THP-1	Acute monocytic leukemia	*Homo sapiens*	ATCC
Granta-519	B cell lymphoma	*Homo sapiens*	DSMZ
HBL-2	B cell lymphoma	*Homo sapiens*	(Peng et al. 1985)
WSU-FSCCL	Low-grade follicular small cleaved cell lymphoma	*Homo sapiens*	(Mohammad et al. 1993)
Negative Controls			
HUVEC	Human Umbilical Vein Endothelial Cells	*Homo sapiens*	Lonza
4T1	Breast carcinoma	*Mus musculus*	ATCC
CT26	Colon carcinoma	*Mus musculus*	ATCC

3.1.2. Media

Cell lines from solid tumors, including those from *Mus musculus*, were grown in Ham's F-12 medium supplemented with sodium bicarbonate (14mM, Applichem), Penicillin G sodium salt (100U/mL, Sigma-Aldrich), streptomycin (100mg/L, Sigma-Aldrich) and 7% fetal bovine serum (FBS, GIBCO, Invitrogen). Cells were incubated at 37º and 5% of CO_2. Trypsinization to expand cells was performed using 0,05% Trypsin with 0,02% EDTA (Sigma-Aldrich) in PBS 1X (154mM NaCl, 3,88mM H_2NaPO_4, 6,1mM $HNaPO_4$, pH 7,4).

Jurkat, K562, EL4.BU and THP-1 cells were grown in the above-mentioned conditions. Subculture did not need trypsin, but instead dilution into new medium depending on confluency was performed.

Granta-519 cells were grown in DMEM, containing sodium bicarbonate (44mM, Applichem), Penicillin G sodium salt (100U/mL, Sigma-Aldrich) and streptomycin (100mg/L, Sigma-Aldrich). HBL-2 and WSU-FSCCL cells were grown in RPMI-1640, containing sodium bicarbonate (23.8mM, Applichem), Penicillin G sodium salt (100U/mL, Sigma-Aldrich), streptomycin (100mg/L, Sigma-Aldrich), Sodium Pyruvate (1mM, Sigma-Aldrich) and HEPES (1mM, Sigma-Aldrich). Both media were supplemented with 10% FBS (GIBCO, Invitrogen). Granta-519 cells were diluted at a ratio 1/3 and HBL-2 and WSU-FSCCL cells at a ratio 1/4, every other day.

HUVEC cells were cultured in Endothelial cell Basal Medium EBM (Lonza), supplemented with hEGF, hydrocortisone, brain bovine extract, gentamicine (EGM, Lonza) and 10% FCS (Invitrogen).

3.1.3. PPRHs and other oligonucleotides

PPRHs and other molecules designed against every target tested in the experiments are detailed in the Tables below.

Nomenclature of the oligonucleotides used in the studies is described below:

- Hp: PPRH hairpin; TFO: Triplex Forming Oligonucleotide.
- Gene: s for *survivin*; t for *TERT;* bcl2 for *Bcl-2*; d for *DHFR*.
- Location within the gene sequence: Pr for promoter; I for intron; E for exon. Number indicates which intron or exon.
- Type of PPRH: -T for Template-PPRH; -C for Coding-PPRH; WT for Wild-type PPRH.
- Negative controls: WC for a hairpin with intramolecular Watson-Crick bonds; Sc for a molecule with a scrambled sequence and no target in the human genome.

Tables are divided by targets and/or applications.

Table 2. PPRHs, TFOs and Wedge-PPRHs directed against the *survivin* gene. Negative controls. DNA sequences used in the binding experiments.

Name	Sequence (5'-3')*	Location
PPRHs against *survivin*		
HpsPr-T	GGGGAGGG**A**GGGG**A**GGGGG**A**AAGAAATTTTTAAAGAA**A**GGGGG**A**GG GG**A**GGGAGGGG	Promoter -1009
HpsPr-C	AGGGGAGGGA**A**GGAG**A**G**A**AGTTTTTGA**A**G**A**GAGG**A**AGGGAGGGGA	Promoter -525
HpsI1-C	GGGGA**A**AAAG**A**AGGGAGGGGAGGTTTTTGGAGGGGAGGGA**A**GAAA**A** AGGGG	Intron 1 +413
HpsE4-C	A**A**GA**A**AGGGAGGAGGG**A**GAATTTTTAAG**A**GGGAGGAGGGA**A**AG**A**A	3'UTR +10413
Wild-type PPRHs against *survivin*		
HpsPr-T WT	GGGGAGGG**T**GGGG**C**GGGGG**T**AAGAAATTTTTAAAGAA**T**GGGGG**C**GGG G**T**GGGAGGGG	Promoter -1009
HpsPr-T WT 2	GGGGAGGG**A**GGGG**A**GGGGG**A**AAGAAATTTTTAAAGAA**T**GGGGG**C**GGG G**T**GGGAGGGG	Promoter -1009
HpsPr-C WT	AGGGGAGGGA**T**GGAG**T**G**C**AGTTTTTGA**C**G**T**GAGG**T**AGGGAGGGGA	Promoter -525

TFOs against *survivin*		
TFO-sPr-T	GA**A**G**A**GAGG**A**AGGGAGGGGA	Promoter -525
TFO-sPr-C	GGGGAGGG**A**GGGG**A**GGGGG**A**AAGAAA	Promoter -1009
Wedge-PPRHs against *survivin*		
Wedge-PPRH (23)	CTCCCACCCCGCCCCCATTCTTTTTTTTAAAGAA**T**GGGGG**C**GGGG**T**GG GAGGGGTTTTTGGGGAGGG**T**GGGG**C**GGGGG**T**AAGAAA	Promoter -1009
Wedge-PPRH (17)	CCCCGCCCCCATTCTTTTTTTTAAAGAA**T**GGGGG**C**GGGG**T**GGGAGGGG TTTTTGGGGAGGG**T**GGGG**C**GGGGG**T**AAGAAA	Promoter -1009
Negative controls		
Hps-WC	CCCCTCCCTCCCCTCCCCCTTTCTTTTTTTTAAAGAAAGGGGGAGGGGAGGGAGGGG	
Hps-Sc	AAGAGAAAAAGAGAAAGAAGAGAGGGTTTTTGGGAGAGAAGAAAGAGAAAAAGAGA A	
TFO-Sc	GGAAAAAGGAGGA	
Wedge-PPRH WC	CCCCGCCCCCATTCTTTTTTTTAAAGAA**T**GGGGG**C**GGGG**T**GGGAGGGGTTTTTCCCCT CCCACCCCGCCCCCATTCTTT	
Binding experiments		
Forward target sequence for HpsPr-T	ATTAAAGAATGGGGGCGGGGTGGGAGGGGTGG	
Reverse target sequence for HpsPr-T	CCACCCCTCCCACCCCGCCCCCATTCTTTAAT	
Forward target sequence for HpsPr-C	CTGCTGCACTCCATCCCTCCCCTGTT	
Reverse target sequence for HpsPr-C	AACAGGGGAGGGATGGAGTGCAGCAG	
Sp1 consensus sequence	ATTCGATCGGGGCGGGGCGAGC	
GATA consensus sequence	CACTTGATAACAGAAAGTGATAACTCT	
non-related sequence	AGGAACTCGCGTCCCAGCCA	

*Mismatches and its wild-type base are in bold. Polypyrimidine target sequences for PPRHs are underlined.

Table 3. DNA oligonucleotides sequences and PPRHs of different lengths against the telomerase (*TERT*) gene.

Name	Sequence (5'-3')*	Length (nt) #
PPRHs against *TERT*		
HptI10-T	AGGA**A**AAGGAAG**A**GGGAGGAAGG**A**AGGAGGTTTTTGGAGG**A**AGGAA GGAGGG**A**GAAGGAA**A**AGGA	30

HptI10-T2	AAGGAAG**A**GGGAGGAAGG**A**AGGAGGTTTTTGGAGGA**A**GGAAGGAGG G**A**GAAGGAA	25
HptI10-T3	GAAG**A**GGGAGGAAGG**A**AGGATTTTTAGGA**A**GGAAGGAGGG**A**GAAG	20

Binding experiments	
Forward target sequence	CAGGCAGGACAAGGAAGCGGGAGGAAGGCAGGAGGCTCTT
Reverse target sequence	AAGAGCCTCCTGCCTTCCTCCCGCTTCCTTGTCCTGCCTG

*Mismatches are in bold. Polypyrimidine target sequence for PPRHs is underlined.
#Length of the sequence of the PPRH that binds to the polypirimidine target sequence. Total length of the PPRH will be the specified length multiplied by two plus 5 thymidines.

Table 4. PPRHs directed against the *Bcl-2* gene.

Name	Sequence (5'-3')*	Location
PPRHs against *Bcl-2*		
HpBcl2Pr-C	GG**A**GAGGGG**A**GGGGAGAAGGAGGTTTTTGGAGGAAGAGGGG**A**GGG GAG**A**GG	Promoter -378
HpBcl2E1-C	G**A**GGGGAGAGGGAG**A**AAAAATTTTTAAAAA**A**GAGGGAGAGGGG**A**G	Exon 1 +65
HpBcl2I2-T	GAAGGGGG**A**AG**A**AGAGAGAGAAG**A**GAGAGATTTTTAGAGAG**A**GAA GAGAGAGA**A**GA**A**GGGGGAAG	Intron 2 +32279
HpBcl2I2-C	GGGGAGGAGGAAAAGAAGGAAGGAAGAGGTTTTTGGAGAAGGAAG GAAGAAAAGGAGGAGGGG	Intron 2 +112542
Wild-type PPRHs against *Bcl-2*		
HpBcl2E1-C WT	G**C**GGGGAGAGGGAG**T**AAAAATTTTTAAAAA**T**GAGGGAGAGGGG**C**G	Exon 1 +65

*Mismatches and its wild-type base are in bold.

Table 5. PPRH,TFO and ASO used in the uptake experiments.

Name	Sequence (5'-3')*
Uptake experiments:	
Hp-F (HpdI3-B)	[F]GGAGGAGGGAGAGGGAGGAGTTTTTGAGGAGGGAGAGGGAGGAGG
TFBO-F	[F]AAAGGATAGAATTAATATAGTTTAGTCATCTCTCGAGTTCATTCACTGTACTCCG G
ASO-F	[F]GTTTAGCGAACCAACCAT

*All the molecules are labeled with FITC at 5'. Incubation with these molecules in Ham's F12 media did not cause cytotoxicity, thus allowing uptake measurement. HpdI3-B has the same sequence as Hp-F but lacks the 5' labeling.

3.2. Methods

3.2.1. Design of PPRHs

The Triplex-Forming Oligonucleotide Target Sequence Search software (spi.mdanderson.org/tfo/, M.D. Anderson Cancer Center, Houston, TX) was used to design PPRHs. This online tool looks for polypurine sequences upon selection of the gene of interest. The output consists of a list of sequences complying with the parameters that have been previously set, i.e, minimum length, %G, maximum number of interruptions. The output also gives the location of the sequence within the gene, either the forward or the reverse strand, its exact starting point in the gene sequence and its location: within the promoter, exonic or intronic. An example of the output is shown in Figure 7. We only selected sequences with a minimum length of 20 nucleotides and with a maximum of 3 pyrimidine mismatches within the polypurine sequence. The PPRH sequences corresponded to the 5'-3' sequence obtained with the bioinformatic tool, plus 5 thymidines at its 3' followed by the same sequence in the antiparallel orientation. We selected sequences from all regions, i.e. promoter, exon and intron, and from either the template or the coding strands, to compare the effect of PPRHs. Once we had selected proper candidates, BLAST analyses were performed to confirm specificity of the designed PPRHs. The candidates with less unintended targets were chosen. PPRHs were synthesized as non-modified, desalted oligodeoxynucleotides by Sigma-Aldrich (0.05 µmol scale). Lyophilized PPRHs were resuspended in sterile Tris-EDTA buffer (1 mM EDTA and 10 mM Tris, pH 8.0) and stored at -20 ºC.

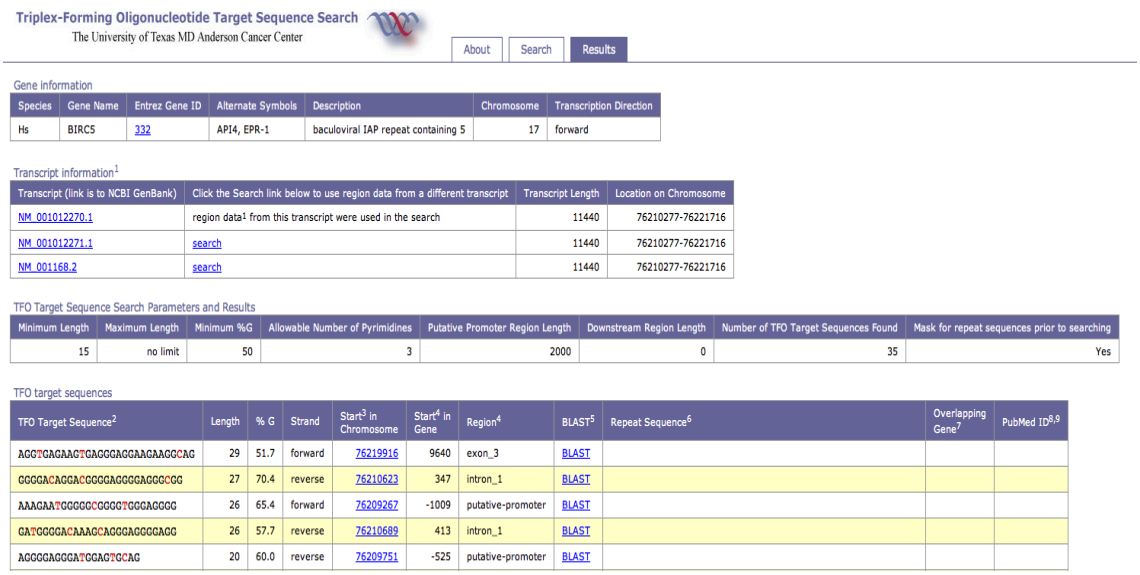

Triplex-Forming Oligonucleotide Target Sequence Search
The University of Texas MD Anderson Cancer Center

About | Search | Results

Gene information

Species	Gene Name	Entrez Gene ID	Alternate Symbols	Description	Chromosome	Transcription Direction
Hs	BIRC5	332	API4, EPR-1	baculoviral IAP repeat containing 5	17	forward

Transcript information[1]

Transcript (link is to NCBI GenBank)	Click the Search link below to use region data from a different transcript	Transcript Length	Location on Chromosome
NM_001012270.1	region data[1] from this transcript were used in the search	11440	76210277-76221716
NM_001012271.1	search	11440	76210277-76221716
NM_001168.2	search	11440	76210277-76221716

TFO Target Sequence Search Parameters and Results

Minimum Length	Maximum Length	Minimum %G	Allowable Number of Pyrimidines	Putative Promoter Region Length	Downstream Region Length	Number of TFO Target Sequences Found	Mask for repeat sequences prior to searching
15	no limit	50	3	2000	0	35	Yes

TFO target sequences

TFO Target Sequence[2]	Length	% G	Strand	Start[3] in Chromosome	Start[4] in Gene	Region[4]	BLAST[5]	Repeat Sequence[6]	Overlapping Gene[7]	PubMed ID[8,9]
AGGTGAGAAGTGAGGGAGGAAGAAGGCAG	29	51.7	forward	76219916	9640	exon_3	BLAST			
GGGGACAGGACGGGGAGGGGAGGGCGG	27	70.4	reverse	76210623	347	intron_1	BLAST			
AAAGAATGGGGGCGGGGTGGGAGGGG	26	65.4	forward	76209267	-1009	putative-promoter	BLAST			
GATGGGGACAAAGCAGGGAGGGGAGG	26	57.7	reverse	76210689	413	intron_1	BLAST			
AGGGGAGGGATGGAGTGCAG	20	60.0	reverse	76209751	-525	putative-promoter	BLAST			

Figure 7. Output information for the *survivin* gene using the TFO Target Sequence Search.

3.2.2. Cellular uptake of PPRHs

To determine the internalization efficiency of PPRHs in different cell lines, uptake experiments were performed using a fluorescent PPRH and flow cytometry analyses. We also determined uptake of a fluorescent TFO and a fluorescent ASO using the same methodology.

For cancer cell lines from solid tumors (PC3, MiaPaCa 2 and HCT116), 200,000 cells were seeded in 55-mm dishes with 2 ml complete F-12 medium. Cells were treated with two different concentrations of FITC-PPRH (Hp-F) either with the transfection reagent DOTAP or without it. The goal of these experiments was to determine the best conditions to use the PPRHs in combination with the liposomal reagent.

For cells growing in suspension, experiments were performed seeding 200,000 cells in 6-well dishes using a final volume of 1 mL of the corresponding medium for each cell line. The goal was to analyze the uptake of the Hp-F and the ASO-F in these cell lines, either naked or using DOTAP.

In all cases, 24 h after transfection, cells were collected, centrifuged at 800 x g at 4°C for 5 minutes, and washed once in PBS. The pellet was resuspended in 500 μl PBS plus Propidium iodide (PI) (final concentration 5 μg/ml, Sigma-Aldrich). Cells were kept on ice for no longer than 30 min. Flow cytometric analyses were performed in a Coulter XL cytometer and data were processed using the software Summit v4.3 (Figure 8). Forward and side scatter parameters were used to select the population to analyze (R1). PI labeling allowed the discard of dead cells (R4), which internalize highly the molecule and could cause a false positive result. Viable cells with the appropriate size and complexity (R1 and R2) were then analyzed for FITC fluorescence. FITC+ IP- cells (R3) were counted as % of fluorescent cells, and their mean ratio was calculated relative to the mean fluorescence of the control without treatment.

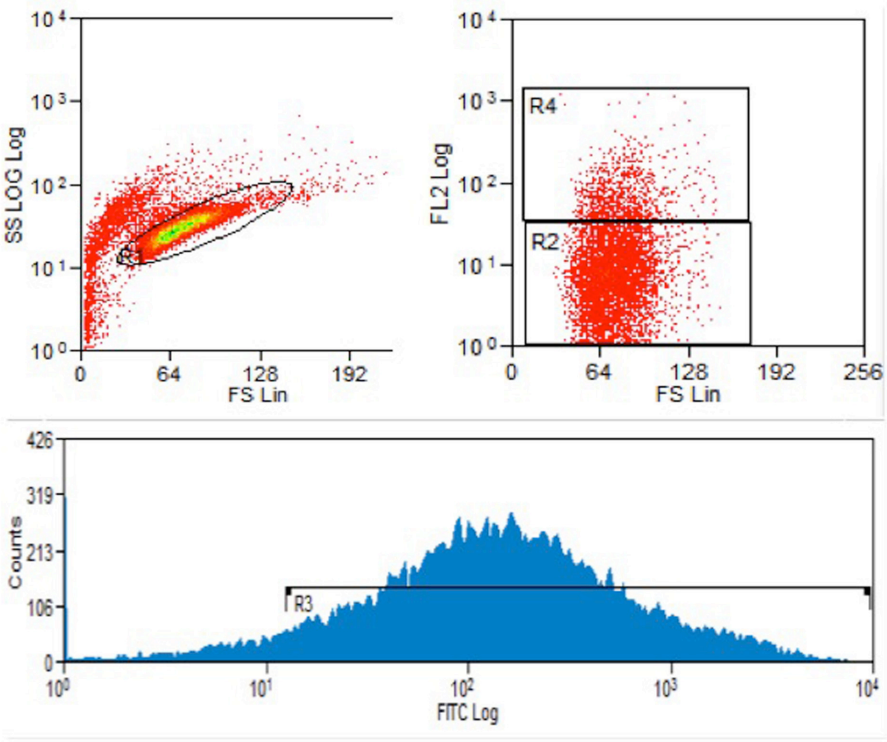

Figure 8. Representative image of the flow cytometry analysis. FS vs SS histogram (above, on the left), FS vs IP labeling (FL2) (above, on the right), Counts (Number of cells) vs FITC (below).

3.2.3. Methodology to study the mechanism of action of PPRHs against promoter sequences

The mechanism of action of the two PPRHs against promoter sequences of the *survivin* gene was performed using *in silico* analyses and EMSA assays, both with HeLa and PC3 nuclear extracts. In the Materials and Methods Section of Article I, the techniques for this study for HeLa nuclear extracts are described. Here there is an in-depth explanation, including PC3 experiments.

3.2.3.1. *In silico* analyses

Using the target sequence for both PPRHs against the promoter sequences of the *survivin* gene (HpsPr-T and HpsPr-C), we performed an *in silico* analysis to predict transcription factors that might bind to these target sequences. We used the MATCH™ software applying a cut-off of 0.95 for matrix similarity and core similarity. The output consisted in different putative transcription factors, with a core and matrix match values between 0.95 and 1.

3.2.3.2. Nuclear extraction

HeLa or PC3 cells were recovered by trypsinization, centrifuged at 800 x g for 5 min and resuspended in hypotonic buffer (15mM NaCl, 60mM KCl, 0,5mM EDTA, 1mM PMSF, 1mM β-mercaptoethanol and 15mM Tris-HCl, pH 8.0) for 5 min. Then, cells were centrifuged again at 800 x g for 5 min and washed with hypotonic buffer containing either 0.05% or 0.1% of Triton to lysate either HeLa or PC3 cells, respectively. After centrifugation for 5 min at 1,200 x g, nuclei were washed with hypotonic buffer once more without triton, and resuspended in hypotonic buffer and KCl at a final concentration of 360mM. Sample tubes were rotated (12 rpm) with a 45º inclination at 4ºC for 45 min. Finally, nuclear extracts were separated from chromatin after centrifugation at 100,000 x g for 30 min.

3.2.3.3. Electrophoretic mobility shift assays (EMSA)

EMSAs were performed to establish the mechanism of action of PPRHs against promoter sequences within the *survivin* gene. The radiolabeled double-stranded target sequences (20,000 cpm) were incubated in 20μl reaction mixtures containing a 1:2 ratio of unspecific DNA:Protein extract (1 μg Herring Sperm (Invitrogen): 2 μg nuclear extract protein), and the following reagents: 5% glycerol, 4 mM $MgCl_2$, 60 mM KCl and 25 mM Tris-HCl, pH 8.0. All the components but the probe were pre-incubated for 15 min in ice, then the probe was added and the mixture was incubated for 15 more minutes. Samples were resolved by gel electrophoresis (5% polyacrylamide/bisacrylamide, 5% glycerol, 1 mM EDTA and 45 mM Tris-borate, pH 8.0).

We performed two different types of experiments to identify the transcription factors involved in the binding: i) competition using the PPRHs and the consensus sequences for specific transcription factors and ii) super-shift assays.

i) In competition experiments, dsDNA consensus sequences (specified in Table 2, Binding experiments) for the putative transcription factors, as well as the different PPRHs, were added in excess (ranging between 100- to 1000-fold relative to the radiolabeled probe) to the reaction mixture.

ii) In the supershift assays, 2 μg or 4 μg of rabbit polyclonal antibody against either Sp1 (PEP-2 X) or Sp3 (D-20X), GATA-2 (H-116X) or GATA-3 (H-48X) (Santa Cruz Biotechnology, Heidelberg, Germany), were added to the reaction mixture 15 min before electrophoresis.

The dried gel was exposed to Europium plates OVN. Radioactive levels were detected by using a Storm 840 Phosphorimager. Quantification of the intensity of the bands was executed with ImageQuant software.

4. RESULTS

4.1. Article I

POLYPURINE REVERSE HOOGSTEEN HAIRPINS AS A GENE THERAPY TOOL AGAINST *SURVIVIN* IN HUMAN PROSTATE CANCER PC3 CELLS *IN VITRO* AND *IN VIVO*

Laura Rodríguez, Xenia Villalobos, Sheila Dakhel, Laura Padilla, Rosa Hervas, Jose Luis Hernández, Carlos J. Ciudad and Véronique Noé

Biochemical Pharmacology, 2013, 86, 1541-1554 (Impact factor: 4.650)

Background

PPRHs are double-stranded DNA molecules formed by two homopurine domains linked by a five-thymidine loop. PPRHs form intramolecular reverse Hoogsteen bonds and are capable of binding to a polypirimidine target sequence by Watson-Crick bonds, thus causing a decrease in gene expression. PPRHs are designed against pyrimidine stretches present mainly in regulatory regions of genes. There are two types of PPRHs depending on the location of their target sequence, either the template or the coding strand of the DNA. Previously in our group, both types of PPRHs against *DHFR* were proved to decrease viability of breast cancer cells by means of decreasing *DHFR* levels (de Almagro et al. 2009; de Almagro et al. 2011).

Objectives

The aim of this work was to establish the proof of principle of PPRHs for their use as gene silencing tool both *in vitro* and *in vivo*, using as a model the *survivin* gene.

Results

PPRHs against different regions (promoter, exon and intron) of the *survivin* gene were designed and their effect was compared in terms of cell viability and apoptosis. The four PPRHs decreased cell viability and increased apoptosis at the range of nanomolar, in PC3 cell line. These PPRHs did not cause a decrease in cell viability in a normal cell line (HUVEC) and two murine cancer cell lines (CT26 and 4T1).

We observed that the most effective PPRHs were a Template- (HpsPr-T) and a Coding-PPRH (HpsPr-C) against two different regions of the *survivin* promoter, and decided to study them in-depth. Both PPRHs decreased *survivin* mRNA and protein levels. To identify their mechanism of action we performed EMSA assays. First, we confirmed their specific binding to their target sequence. Secondly, we hypothesized that the binding of these PPRHs could interfere with the binding of putative transcription factors specific for their target sequences. After an *in silico* analysis and literature mining, we studied the role of Sp1 and Sp3 for the Template-PPRH (HpsPr-T) and GATA for the Coding-PPRH (HpsPr-C). Using EMSA assays with nuclear extracts and competitors, we determined that HpsPr-T and HpsPr-C prevented the binding of Sp1/3 and GATA-3, respectively.

Finally, we conducted two *in vivo* efficacy assays using two different routes of administration, either intratumoral or intravenous, in a subcutaneous xenograft tumor model of PC3 prostate cancer cells. We compared the tumor growth throughout the administration of either HpsPr-C (the most effective one in terms of decrease in cell viability and increase in apoptosis) or Hps-Sc (an scrambled hairpin without target in the human genome). We observed that, independently of the route of administration, the specific Coding-PPRH caused a decrease in tumor volume, in parallel with a decrease in *survivin* protein levels and blood vessel formation. Administration of PPRHs did not cause a decrease in body animal weight, indicating lack of toxicity.

Conclusions:

To sum up, these results constituted the proof of principle of PPRHs as a new gene silencing tool in cancer therapeutics.

Biochemical Pharmacology 86 (2013) 1541–1554

Contents lists available at ScienceDirect

Biochemical Pharmacology

journal homepage: www.elsevier.com/locate/biochempharm

Polypurine reverse Hoogsteen hairpins as a gene therapy tool against *survivin* in human prostate cancer PC3 cells *in vitro* and *in vivo*

Laura Rodríguez [a], Xenia Villalobos [a], Sheila Dakhel [b], Laura Padilla [b], Rosa Hervas [b], Jose Luis Hernández [b], Carlos J. Ciudad [a,*], Véronique Noé [a]

[a] Department of Biochemistry and Molecular Biology, School of Pharmacy, University of Barcelona, 08028 Barcelona, Spain
[b] Biomed Division of LEITAT Technological Center, 08028 Barcelona, Spain

ARTICLE INFO

Article history:
Received 24 July 2013
Accepted 12 September 2013
Available online 23 September 2013

Keywords:
PPRH
Survivin
Gene silencing
Xenograft
Prostate cancer

ABSTRACT

As a new approach for gene therapy, we recently developed a new type of molecule called polypurine reverse Hoogsteen hairpins (PPRHs). We decided to explore the *in vitro* and *in vivo* effect of PPRHs in cancer choosing *survivin* as a target since it is involved in apoptosis, mitosis and angiogenesis, and overexpressed in different tumors. We designed four PPRHs against the *survivin* gene, one of them directed against the template strand and three against different regions of the coding strand. These PPRHs were tested in PC3 prostate cancer cells in an *in vitro* screening of cell viability and apoptosis. PPRHs against the promoter sequence were the most effective and caused a decrease in survivin mRNA and protein levels. We confirmed the binding between the selected PPRHs and their target sequences in the *survivin* gene. In addition we determined that both the template- and the coding-PPRH targeting the *survivin* promoter were interfering with the binding of transcription factors Sp1 and GATA-3, respectively. Finally, we conducted two *in vivo* efficacy assays using the Coding-PPRH against the *survivin* promoter and performing two routes of administration, namely intratumoral and intravenous, in a subcutaneous xenograft tumor model of PC3 prostate cancer cells. The results showed that the chosen Coding-PPRH proved to be effective in decreasing tumor volume, and reduced the levels of survivin protein and the formation of blood vessels. These findings represent the preclinical proof of principle of PPRHs as a new silencing tool for cancer gene therapy.

1. Introduction

Nowadays, modulation of gene expression by nucleic acids has become a routine tool for laboratory research. Different molecules are used as gene modulating tools, such as antisense oligonucleotides (aODNs) or small-interference RNAs (siRNAs). In addition, we have recently described the development of a new type of molecules named polypurine reverse Hoogsteen hairpins (PPRHs), capable of decreasing gene expression.

PPRHs are non-modified DNA molecules formed by two antiparallel polypurine stretches linked by a five-thymidine loop [1,2]. The intramolecular linkage consists of reverse Hoogsteen bonds between adenines and guanines. Then, PPRHs bind to their polypyrimidine target sequence by Watson–Crick bonds forming a triplex structure and displacing the fourth strand of the dsDNA [2].

To design a PPRH, it is essential to find polypyrimidine/polypurine stretches within the gene sequence. These sequences are more common in the genome than it was predicted by random models [3]; they are mostly located in non-coding sequences, including promoters and introns, although they can also be found in coding regions at low frequency. The target sequences do not have to be pure stretches of polypyrimidines and may contain a small number of purine interruptions, since the usage of adenines as a wild card in the PPRH overcomes the instability caused by the interruptions, thus maintaining a functional binding to the target [4].

In previous studies, we described two types of PPRHs with the ability to bind to a target sequence located either in the template DNA strand, Template-PPRHs [4] or in the coding DNA strand, Coding-PPRHs [5]. Each of these molecules is able, through different mechanisms, to decrease gene expression. On the one hand, Template-PPRHs interfere with the transcription

Abbreviations: aODN, antisense oligonucleotide; CRPC, castration-resistant prostatic cancer; DOTAP, *N*-[1-(2,3-dioleoyloxy)propyl]-*N*,*N*,*N*-trimethylammonium methylsulfate; EMSA, electrophoretic mobility shift assay; MTT, (3-(4,5-dimethylthiazol-2-yl)-2,5-diphenyltetrazolium bromide; NE, nuclear extract; PPRHs, Polypurine Reverse Hoogsteen hairpins.

* Corresponding author. Tel.: +34 93 403 4455; fax: +34 93 402 4520.
E-mail addresses: laura.rodriguez@ub.edu (L. Rodríguez), xvillalobos@ub.edu (X. Villalobos), sdakhel@leitat.org (S. Dakhel), lpadilla@leitat.org (L. Padilla), rhervas@leitat.org (R. Hervas), jlhernandez@leitat.org (J.L. Hernández), cciudad@ub.edu, cjciudad@gmail.com (C.J. Ciudad), vnoe@ub.edu (V. Noé).

0006-2952/$ – see front matter © 2013 Elsevier Inc. All rights reserved.
http://dx.doi.org/10.1016/j.bcp.2013.09.013

process, thus decreasing the mRNA and protein levels of the target gene. On the other hand, Coding-PPRHs are able to bind, not only to the coding strand of the DNA but also to the mRNA, because both have the same sequence and orientation. A Coding-PPRH against an intron sequence of the *dhfr* gene caused a splicing alteration by preventing the binding of U2AF65, a pre-mRNA splicing factor, ultimately decreasing gene expression [5]. We proved the efficacy of different Template-PPRHs against genes related to proliferation in breast cancer: *dhfr*, *telomerase* and *survivin* [4].

We decided to further explore the *in vitro* and *in vivo* effects of PPRHs against *survivin*, since it is an anti-apoptotic protein, also involved in mitosis and angiogenesis [6]. Survivin is overexpressed in different tumors, such as prostate [7], lung [8], breast [9], colon [10,11] stomach [12], esophagus [13], pancreas [14], bladder [15], uterus [16], ovary [17], large-cell non-Hodgkin's lymphoma [18], leukemias [19], neuroblastoma [20], melanoma [21] and non-melanoma skin cancers [22]. However, survivin levels are undetectable in most differentiated normal tissues, with the exception of thymus [7], CD34+ bone-marrow-derived stem cells at low levels [23], and the basal colonic epithelium [24]. Moreover, survivin expression correlates to shorter survival [8–10,13,17,18], resistance to chemotherapy [13,25], worse disease progression [18,20], and higher rates of recurrence [15]. All of the above reasons make survivin a good anticancer target and prognosis marker [26].

We focused on prostate cancer, the second cause of death related to cancer in men in the Western world. Given that the treatment options for this disease are limited and barely effective, targeted-therapy has been under development [27]. Examples of this type of therapy are either small molecules or antibodies against tyrosine kinase receptors, such as IGF-1R, EGFR and FGFR or against genes involved in important hallmarks for cancer, such as anti-apoptotic (*survivin*) or proangiogenic proteins (VEGFR) [27].

Survivin is considered a good target to inhibit in prostate cancer for its association with androgen resistance and with aggressive phenotypes. In fact, several Phase-II clinical trials using either small-molecule inhibitors – YM155 – or antisense therapy – LY2181308 – have been conducted for castration-resistant prostatic cancer (CRPC), after showing apoptosis in prostate cancer cell lines and in xenografts [11,28]. However, these two molecules showed modest or lack of activity in Phase II clinical trials, and are currently under investigation in combination with docetaxel [29,30].

Therefore, the aim of this work was to assess the efficacy of PPRHs as a preclinical proof of principle for its application as a new gene therapy approach using a subcutaneous xenograft tumor model of PC3 prostate cancer cells.

2. Materials and methods

2.1. Design and usage of PPRHs

Both Template and Coding-PPRHs were used in these experiments. To find polypyrimidine sequences in the target gene, we used the Triplex-Forming Oligonucleotide Target Sequence Search software (spi.mdanderson.org/tfo/, M.D. Anderson Cancer Center, Houston, TX). Once we had selected proper candidates, BLAST analyses were performed to confirm specificity of the designed PPRHs and the ones with less unintended targets were chosen. PPRHs were synthesized as non-modified oligodeoxynucleotides by Sigma-Aldrich (Madrid, Spain) (0.05 mmol scale). Lyophilized PPRHs were resuspended in sterile Tris-EDTA buffer (1 mM EDTA and 10 mM Tris, pH 8.0; AppliChem, Barcelona, Spain) and stored at −20 °C.

2.2. Preparation of polypurine/polypyrimidine duplexes

The duplexes to be targeted by the hairpins were formed by mixing 25 μg of each single-stranded (ss) polypurine and polypyrimidine oligodeoxynucleotides with 150 mM NaCl (AppliChem, Barcelona, Spain) and incubated at 90 °C for 5 min as described in de Almagro et al. [4].

2.3. Oligodeoxynucleotide labeling

One hundred nanograms of PPRHs or double stranded (ds) oligodeoxynucleotides was 5′-end-labeled with T4 polynucleotide kinase (New England Biolabs, Beverly, MA) and [γ-^{32}P]ATP (3000 Ci/mmol, Perkin Elmer, Madrid, Spain) as described in de Almagro et al. [4].

2.4. DNA–PPRH binding analysis

Binding of PPRHs to their target sequence was analyzed using two approaches: (a) by incubation of the radiolabeled PPRHs (20,000 cpm) in the presence or absence of unlabelled ds target sequence, or (b) by incubation of the radiolabeled ds target sequence with the unlabelled PPRH. In both cases, a buffer containing 10 mM $MgCl_2$, 100 mM NaCl, and 50 mM HEPES, pH 7.2 was used (AppliChem, Barcelona, Spain). Binding reactions (20 μl) were incubated for 30 min at 37 °C before electrophoresis, which was performed on non denaturing 12% polyacrylamide gels (PAGE) containing 10 mM $MgCl_2$, 5% glycerol, and 50 mM HEPES, pH 7.2 (AppliChem, Barcelona, Spain). Gels were electrophoresed for 3–4 h at 10 V/cm at 4 °C, dried, exposed to Europium plates OVN and analyzed using a Storm 840 Phosphorimager (Molecular Dynamics, Sunnyvale, CA). Binding specificity was tested by addition of 1 μg of poly-dI-dC (Sigma-Aldrich, Madrid, Spain) to the binding reaction.

2.5. Electrophoretic mobility shift assay (EMSA)

To analyze the binding of transcription factors to the target sequences of the chosen PPRHs within the *survivin* promoter, EMSA was performed using HeLa nuclear extracts. HeLa cells were harvested by trypsinization, centrifuged at 800 × *g* for 5 min and resuspended in hypotonic buffer (15 mM NaCl, 60 mM KCl, 0.5 mM EDTA, 1 mM PMSF, 1 mM β-mercaptoethanol and 15 mM Tris–HCl, pH 8.0; AppliChem, Barcelona, Spain) for 5 min. Then, cells were centrifuged again at 800 × *g* for 5 min and washed with hypotonic buffer containing 0.05% Triton (Sigma-Aldrich, Madrid, Spain) to lysate the cells. After centrifugation for 5 min at 1200 × *g*, nuclei were washed with hypotonic buffer once more without triton, and resuspended in hypotonic buffer containing a final concentration of 360 mM KCl (AppliChem, Barcelona, Spain). Sample tubes were rotated (12 rpm) with a 45° inclination at 4 °C for 45 min. Finally, nuclear extracts were separated from chromatin after centrifugation at 100,000 × *g* for 30 min.

The radiolabeled ds target sequences (20,000 cpm) were incubated in 20 μl reaction mixtures also containing 1 μg Herring Sperm DNA (Invitrogen, Barcelona, Spain) as unspecific competitor, 2 μg nuclear extract protein, 5% glycerol, 4 mM $MgCl_2$, 60 mM KCl and 25 mM Tris–HCl, pH 8.0 (AppliChem, Barcelona, Spain). After a pre-incubation of 15 min, the probe was added for 15 more minutes. Then samples were resolved by gel electrophoresis (5% polyacrylamide/bisacrylamide, 5% glycerol, 1 mM EDTA and 45 mM Tris-borate, pH 8.0; AppliChem, Barcelona, Spain). In competition experiments, ds DNA consensus sequences (Sp1: 5′-ATTCGATCGGGGCGGGGCGAGC-3′; GATA: 5′-CACTTGATAACA-GAAAGTGATAACTCT-3′; non-related: 5′-AGGAACTCGCGTCC-CAGCCA-3′) for the putative transcription factors determined by

the MATCH™ software, as well as the different PPRHs, were added in excess (ranging between 10- and 200-fold relative to the radiolabeled probe) to the reaction mixture. In the supershift assays, 2 μg of rabbit polyclonal antibodies against either Sp1 (PEP-2X) or Sp3 (D-20X), GATA-2 (H-116X) or GATA-3 (H-48X) (Santa Cruz Biotechnology, Heidelberg, Germany), was added to the reaction mixture 15 min before the electrophoresis. The dried gel was exposed to Europium plates OVN and analyzed using a Storm 840 Phosphorimager (Molecular Dynamics, GE Healthcare Life Sciences, Barcelona, Spain).

2.6. Cell culture

PC3 prostate adenocarcinoma cells (ECACC) and HeLa cervical cancer cells (ATCC) were grown in Ham's F-12 medium supplemented with 7% fetal bovine serum (FBS, GIBCO, Invitrogen, Barcelona, Spain) and incubated at 37 °C in a humidified 5% CO_2 atmosphere. Human Umbilical Vein Endothelial Cells (HUVECs, Lonza, Barcelona, Spain) were cultured in Endothelial cell Basal Medium EBM (Lonza, Barcelona, Spain), supplemented with hEGF, hydrocortisone, brain bovine extract and gentamicine (EGM, Lonza, Barcelona, Spain), and 10% FCS (Invitrogen, Barcelona, Spain). 4T1 breast cancer and CT26 colon cancer cell lines (ECACC), both from mouse, used as negative controls, were also cultured in F-12 medium and 7% FBS.

2.7. Transfection

Cells were plated in 35-mm-diameter dishes. The transfection procedure consisted in mixing the appropriate amount of PPRH and *N*-[1-(2,3-dioleoyloxy)propyl]-*N*,*N*,*N*-trimethylammonium methylsulfate (DOTAP) (Roche, Barcelona, Spain) for 15 min at room temperature, followed by the addition of the mixture to the cells.

2.8. MTT assay

Cells (10,000) were plated in 35-mm-diameter dishes in F12 medium. After 6 days, 0.63 mM of 3-(4,5-dimethylthiazol-2-yl)-2,5-diphenyltetrazolium bromide and 18.4 mM of sodium succinate (both from Sigma-Aldrich, Madrid, Spain) were added to the culture medium and incubated for 3 h at 37 °C. After incubation, the medium was removed and the solubilization reagent (0.57% acetic acid and 10% sodium dodecyl sulfate in dimethyl sulfoxide) (Sigma-Aldrich, Madrid, Spain) was added. Cell viability was measured at 570 nm in a WPA S2100 Diode Array spectrophotometer (Biochrom Ltd., Cambridge, UK).

2.9. mRNA analysis

Total RNA from 60,000 PC3 cells was extracted using Trizol (Life Technologies, Madrid, Spain) following the manufacturer's specifications. Quantification of RNA was conducted measuring its absorbance (260 nm) at 25 °C using a Nanodrop ND-1000 spectrophotometer (Thermo Scientific, Wilmington, DE).

2.10. Reverse transcription

cDNA was synthesized in a 20 μl reaction mixture containing 500 ng of total RNA, 12.5 ng of random hexamers (Roche, Barcelona, Spain), 10 mM dithiothreitol, 20 units of RNasin (Promega, Madrid, Spain), 0.5 mM each dNTP (AppliChem, Barcelona, Spain), 4 μl of buffer (5×), and 200 units of Moloney murine leukemia virus reverse transcriptase (RT) (Invitrogen, Barcelona, Spain). The reaction was incubated at 37 °C for 1 h. 3 μl of the cDNA mixture was used for Real-Time PCR amplification.

2.11. Real-timePCR

The StepOnePlus™ Real-Time PCR Systems (Applied Biosystems, Barcelona, Spain) was used to perform these experiments. Survivin (BIRC5) (HS04194392_S1), adenine phosphoribosyltransferase (APRT) (HS00975725_M1) and 18S rRNA (HS99999901_S1) mRNA Taqman probes were used (Applied Biosystems). The final volume of the reaction was 20 μl, containing 1× TaqMan Universal PCR Mastermix (Applied Biosystems, Barcelona, Spain), 1× TaqMan probe (Applied Biosystems, Barcelona, Spain) and 3 μl of cDNA and H_2O mQ. PCR cycling conditions were 10 min denaturation at 95 °C, followed by 40 cycles of 15 s at 95 °C and 1 min at 60 °C. The mRNA amount of the target gene was calculated using the $\Delta\Delta C_T$ method, where C_T is the threshold cycle that corresponds to the cycle where the amount of amplified mRNA reaches the threshold of fluorescence. APRT and 18S mRNA levels were used as endogenous controls. To analyze the off-target effects of PPRHs we used TaqMan probes for the following unrelated genes: APOA1 (HS00163641_M1), Bcl2 (HS00608023_M1), DHFR (HS00758822_S1), S100A4 (HS00243202_M1) and PDK1 (HS01561850_M1).

2.12. Western analysis

Cells (60,000) were plated in 35-mm-diameter dishes and treated with PPRHs at 100 nM. At different times after transfection (3, 6, 9 h) total protein extracts were obtained and Western blot analyses were performed to detect the levels of survivin protein.

Cells were collected by tripsinization and after a PBS wash, RIPA buffer (50 Tris–HCl pH 7,4, 1% Igepal CA630, 1 mM EDTA, 150 mM NaCl, supplemented with 100 μg/ml of PMSF and Protease Inhibitor Mixture by Sigma-Aldrich, Madrid, Spain) was added to lyse the cells. The extracts were maintained at 4 °C for 30 min, vortexing every 10 min. Cell debris was removed by centrifugation (13,500*g* for 10 min). The Bio-Rad protein assay (Bio-Rad, Barcelona, Spain), based on the Bradford method, was used to determine the protein concentrations using bovine serum albumin as a standard (Sigma-Aldrich, Madrid, Spain).

Total protein cell extracts (100 μg) were electrophoresed on SDS-polyacrylamide gels (15%/7%), and transferred to a polyvinylidene fluoride membrane (Immobilon P, Millipore, Madrid, Spain) using a semidry electroblotter. The membranes were probed with antibodies against survivin (1/250 dilution; 614701, Biolegends, San Diego, CAand AF886, R&D systems, Minneapolis, MN) and tubulin (1/800 dilution; CP06, Calbiochem, Merck, Darmstadt, Germany). Signals were detected by secondary HRP-conjugated antibodies: anti-rabbit (1:2500 dilution; P0399, Dako, Denmark) for survivin, anti-mouse (1/5000 dilution; sc-2005, Santa Cruz Biotechnology, Heidelberg, Germany) for tubulin and enhanced chemiluminiscence using ECL™ Prime Western Blotting Detection Reagent, as recommended by the manufacturer (GE Healthcare, Barcelona, Spain). Tubulin and total protein loading were both used to normalize the results. Quantification was performed using ImageQuant LAS 4000 Mini (GE Healthcare, Barcelona, Spain).

2.13. Cellular uptake of PPRHs

200,000 cells were plated in 55-mm dishes with 2 ml complete F-12 medium and treated with different concentrations of FITC PPRH (HpdI3-F). 24 h after transfection, cells were collected,

centrifuged at 800 × *g* at 4 °C for 5 min, and washed once in PBS. The pellet was resuspended in 500 μl PBS plus Propidium iodide (PI) (final concentration 5 μg/ml) (Sigma-Aldrich, Madrid, Spain). Cells were kept on ice for no longer than 30 min before flow cytometry analysis performed in a Coulter XL cytometer. Different ratios of PPRH:DOTAP were tested to determine the most appropriate to ensure internalization of the molecule.

2.14. Apoptosis

Apoptosis was determined by two different methodologies: Rhodamine method and Caspase 3/7 assay.

Rhodamine method: PC3 cells (120,000) were plated in 55-mm dishes with 2 ml complete F-12 medium and treated with 100 nM of each PPRH. 24 h after treatment, Rhodamine (final concentration 5 ng/μl) (Sigma-Aldrich, Madrid, Spain) was added for 30 min and the cells were collected as previously described for the cellular uptake experiments. Flow-cytometry data were analyzed using the software Summit v4.3. The percentage of Rho-negative, IP-negative cells, corresponded to the apoptotic population.

Caspase-Glo 3/7 assay: 5,000 cells (PC3, HUVEC, 4T1 and CT26) were plated in a 96-well plate in 50 μl F12-complete medium. After 24 h, 100 nM of each PPRH was transfected, and 24 h after transfection, 50 μl of Caspase-Glo 3/7 reagent (Promega, Madrid, Spain) was added. After 1 h of incubation, luminiscence was measured using a Modulus™ Microplate luminometer (Turner Biosystems, Promega, Madrid, Spain). F12-complete medium and the reagent were considered the blank control and untreated cells as background.

2.15. In vivo studies

Tumor growth studies were performed on female athymic mice of 5 weeks old (Hsd:Athymic Nude-Foxn1^{nu}). Mice were purchased from Harlan Interfauna Iberica S.L. (Barcelona, Spain) and maintained in the facilities of the PCB-UB. *In vivo* procedures were approved by the institutional ethical committee and by the local authorities according to the Catalonian and Spanish guidelines governing experimental animal care.

Human PC3 cell line growing in exponential phase was used to implant xenografts in mice. 2×10^6 cells were subcutaneously injected in the right dorso-lateral side of these mice. Tumor growth was measured using calipers twice a week and its volume was calculated using the formula: volume = $(D \times d^2)/2$, in which D is the longest axis of the tumor and d is the shortest.

Those animals with a tumor of approximately 100 mm^3 were selected to conduct the experiments, using a minimum of 10 animals for the intratumoral administration and 6 for the intravenous one.

Mice were administered with either a scramble PPRH (Hps-Sc) or with the anti-*survivin* PPRH (HpsPr-C) using as a vehicle in vivo-jetPEI® (Polyplus transfection, France) at a *N*/*P* ratio of 8 in a buffer containing 5% glucose. Two types of administration were used: Intratumoral administration of 10 μg of PPRH (volume of administration 20 μl) and intravenous administration (via tail vein) of 50 μg of PPRH (volume of administration 200 μl). In both cases, the administration of PPRHs and the measurement of body weight and tumor volume were performed twice a week. Treatments were continued for 3 weeks, after which animals were killed.

2.16. Immunodetection of survivin in tumor samples

At the end of the *in vivo* intratumoral experiment, subcutaneous tumors from PC3 cells were processed for survivin detection, both by Western Blot and Immunofluorescence in histological sections. For protein extraction from tumor samples, frozen tissue was disrupted in ice cold Cell Lysis Buffer (150 mM NaCl, 1% IGEPAL CA630, 5 mM EDTA, 100 μg/ml PMSF, 1 mM Na_3VO_4, 1 mM NaF and 50 mM Tris–HCL, pH 7.4) (AppliChem, Barcelona, Spain) with the aid of a mixer. After centrifugation, protein concentration was determined with the Bradford Reagent. Total extracts (60 μg) were solved in SDS-polyacrylamide gels using the same conditions as described in section 2.12. The following antibodies were used: rabbit polyclonal antibody anti-survivin (1:2000 dilution, AF886, R&D systems, Minneapolis, MN); monoclonal anti-beta actin peroxidase conjugate (1:25,000 dilution, A3854, Sigma-Aldrich, Madrid, Spain); goat anti-rabbit (1:25,000 dilution, A0545, Sigma-Aldrich, Madrid, Spain) was used as secondary antibodies. For immunofluorescence detection, five micrometer-thick sections from the tumor blocks were deparaffinised, rehydrated in grade alcohols and processed. Briefly, antigen retrieval was performed in a microwave oven for 15 min in 10 mM sodium citrate pH 6.0 with 0.05% Tween-20 (AppliChem, Barcelona, Spain). The slides were incubated in 5% normal goat serum for 60 min to prevent nonspecific staining. Then, they were incubated OVN at 4 °C with rabbit polyclonal anti-human survivin (5 μg/ml, AF886, R&D systems, Minneapolis, MN). Thereafter the sections were incubated with Alexa Fluor 488 goat anti-rabbit IgG (H + L) (Invitrogen, Barcelona, Spain) at 2 μg/ml in PBS 1× for 60 min. The slides were kept in a dark environment, washed three times with PBS 1× for 5 min each and mounted with mounting solution (Mowiol, Sigma-Aldrich, Madrid, Spain). Five pictures per tumor were taken using a Leica DM IRBE microscope.

2.17. Immunohistochemical CD31 staining

At the end of the *in vivo* intratumoral experiment, subcutaneous tumors from PC3 cells were OCT (Tissue-Tek®, Sakura, Barcelona, Spain) embedded and frozen. One cryosection (5 μm) corresponding to 3 tumors of each group were analyzed. Sections were fixed in acetone/chloroform (1:1) at −20 °C for 5 min, dried overnight at room temperature, washed with PBS and treated for 10 min at 4 °C in a dark chamber with H_2O_2 (0.03%) in PBS. Then, sections were washed with PBS and blocked for 20 min using PBS-BSA (2%) plus rabbit serum (5%) (Vector, Burlingame, CA) and with Avidin-biotin blocking solution (Dako, Denmark) for 10 min at 4 °C. Samples were incubated for 1 h at room temperature with the monoclonal rat anti-mouse primary antibody directed against CD31 (dil 1:200, BD PharMingen, Belgium) diluted in blocking buffer. Afterwards, sections were incubated with a polyclonal biotinylated anti-rat antibody as secondary antibody (dil 1:500, Vector, Burlingame, CA) for 30 min at room temperature and then the ABC reagent (Pierce, Rockford, IL) was added for 30 min at room temperature. Finally, sections were incubated with NovaRed (Vector, Burlingame, CA) for 20 min at 4 °C and mounted using DPX non-aqueous mounting medium (Sigma-Aldrich, Madrid, Spain). Angiogenesis quantification was measured using two criteria:

M.V.D (v.p./mm^2) = $10^6 \times$ (sum of vessels of each tumor (image A + image B + . . .image N))/(area of one tumor in μm^2(area A + area B + . . . + area N))

A.A.(fractional area of vessels) = (area of vessels of each tumor (image A + image B + . . .image N))/(area of one tumor in μm^2(area A + area B + . . . + area N))

More than 10 pictures per slice, depending on the size of tumors, were taken and analyzed using the NIH ImageJ imaging software.

2.18. Statistical analysis

The *in vitro* data are presented as the mean ± SE values. Statistical analysis was performed using Student's *t* test using SPSS

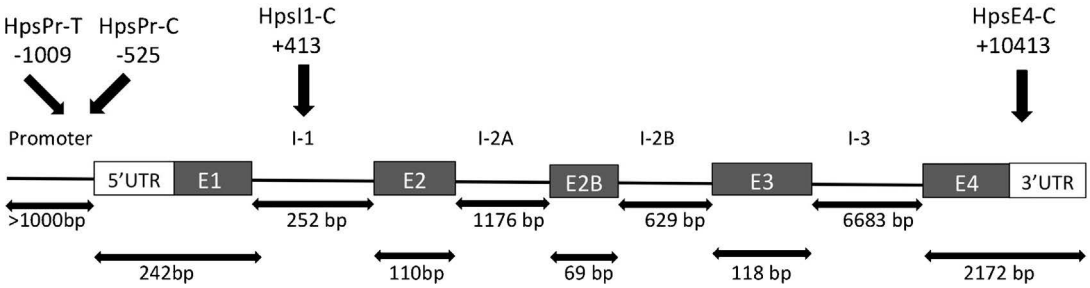

Fig. 1. *Scheme representing the target sequences of the PPRHs used against the survivin gene.* Four PPRHs were designed against the *survivin* gene. Two were directed toward the promoter, one template (HpsPr-B) and one Coding (HpsPr-C), and two other coding-PPRHs against intron 1 (HpsI1-C) and the 3′UTR within exon 4 (HpsE4-C). Nomenclature used was Hp (Hairpin), s (*survivin*), Pr (promoter), I (intron), E (exon). The numbering below the PPRHs corresponds to the start of the target sequence location in the gene referred to the transcriptional start site. The arrows indicate the length of each gene element.

(Chicago, IL) version 20 software for Mac OS X (Apple Computer, Cupertino, CA). In the *in vivo* experiments comparison between groups were performed using the two-tailed nonparametric Mann Whitney *U* test. Results were considered significant if $p < 0.05$ (*), $p < 0.01$ (**), or $p < 0.005$ (***).

3. Results

3.1. Design of PPRHs

We designed four PPRHs against the *survivin* gene, one of them directed against the template strand and three against different regions of the coding strand. We selected polypyrimidine stretches in the promoter, intron 1 and 3′UTR of the gene (Fig. 1). All the sequences have 2 or 3 purine interruptions and therefore adenines were included in the PPRHs at those positions to maintain the binding to the target sequence [4]. The PPRH sequences are listed in Table 1. As negative controls we used a PPRH with a scrambled sequence (Hps-Sc) and a PPRH with intramolecular Watson–Crick bonds instead of Hoogsteen bonds (Hps-WC), which is not able to form triplexes.

3.2. Cellular uptake of PPRHs in PC3 cells

The demonstration of the cellular uptake of PPRHs in PC3 cells was carried out using flow cytometry. Specifically, we measured the percentage of fluorescent cells and their mean fluorescence intensity 24 h after transfection with a fluorescent PPRH (Fig. 2). Given the intrinsic apoptotic effect of the PPRHs against *survivin*, we decided to use a fluorescent PPRH designed against the *dihydrofolate reductase (dhfr)* gene (HpdI3-F) for the uptake experiments, previously tested in SKBR3 cells [4]. This model is useful for this purpose because the incubation of the cells in F12-complete medium -containing the final products of the DHFR enzyme-avoids PPRHs cytotoxicity.

As shown in Fig. 2, 90–95% of cells were FITC-positive at the concentrations tested (100 nM and 1 μM). Surprisingly, the mean fluorescence was 5-times higher at 100 nM than at 1 μM. This can be explained because the best PPRH:DOTAP ratio was 1:100 [4], achieved by mixing 100 nM of PPRH and a fixed concentration of 10 μM of DOTAP which is the maximum concentration of vehicle with no toxicity; when using 1 μM PPRHs this ratio was not longer maintained. Therefore, the chosen concentration to conduct further experiments was 100 nM.

3.3. Effects of PPRHs on cell viability

To compare the effects of PPRHs against different regions of the *survivin* gene in PC3 cells, dose response studies were performed. The resulting cell viabilities are shown in Fig. 3A. The two PPRHs designed against the promoter – HpsPr-T and HpsPr-C – caused the greatest effect at 100 nM with more than 90% decrease in viability. HpsI1-C was highly cytotoxic at 30 nM although its effect was partially reversed at 100 nM; and HpsE4-C showed the lowest effect. We also determined the cytotoxicity caused by the negative controls –Hps-WC and Hps-Sc- observing 101.9% and 83.3% survival, respectively, at the maximum concentration assayed. PPRHs were also tested in HeLa cells, to demonstrate that they are effective in other cancer cell lines and to validate the usage of HeLa nuclear extracts to conduct further mechanism analyses (Fig. 3B). Furthermore, the two most cytotoxic PPRHs against *survivin* were assayed in normal, non-tumoral cells (HUVEC), which do not express the survivin protein (Fig. 3C). We did not observed a decrease in survival in this cell line at 100 nM, indicating that these PPRHs are harmless to cells whose proliferation is not related with *survivin* expression. We also tested both PPRHs in murine cell lines, namely, CT26 (colorectal cancer) and 4T1 (breast cancer) which express murine *survivin* and have been used as a model to test the antitumor effect of dominant-negative mutants of survivin [31,32]. These cell lines were not sensitive to PPRHs designed against the human *survivin* promoter (Fig. 3C).

3.4. Effects of PPRHs on apoptosis

To associate the effect of PPRHs with *survivin* gene function, we measured the apoptotic effect of the PPRHs at 100 nM after 24 h of incubation using two different methodologies, the rhodamine

Table 1
PPRH sequences.

Name	Sequence (5′–3′)	Location
HpsPr-T	GGGGAGGGAGGGGAGGGGGAAAGAAATTTTTAAAGAAAGGGGGAGGGGAGGGAGGGG	Promoter −1009
HpsPr-C	AGGGGAGGGAAGGAGAGAAGTTTTTGAAGAGAGGAAGGGAGGGGA	Promoter −525
HpsI1-C	GGGGAAAAAGAAGGGAGGGGAGGTTTTTGGAGGGGAGGGAAGAAAAAGGGG	Intron 1 +413
HpsE4-C	AAGAAAGGGAGGAGGGAGAATTTTTAAGAGGGAGGAGGGAAAGAA	3′UTR +10413
Hps-WC	CCCCTCCCTCCCCTCCCCCTTTCTTTTTTTTAAAGAAAGGGGGAGGGGAGGGAGGGG	
Hps-Sc	AAGAGAAAAAGAGAAAGAAGAGAGGGTTTTTGGGAGAGAAGAAAGAGAAAAAGAGAA	
HpdI3-F	[F]GGAGGAGGGAGAGGGAGGAGTTTTTGAGGAGGGAGAGGGAGGAGG	

List of the PPRHs sequences used in this study, including their target location in the *survivin* gene. T, template; C, coding; WC and Sc, negative controls; F, fluorescent.

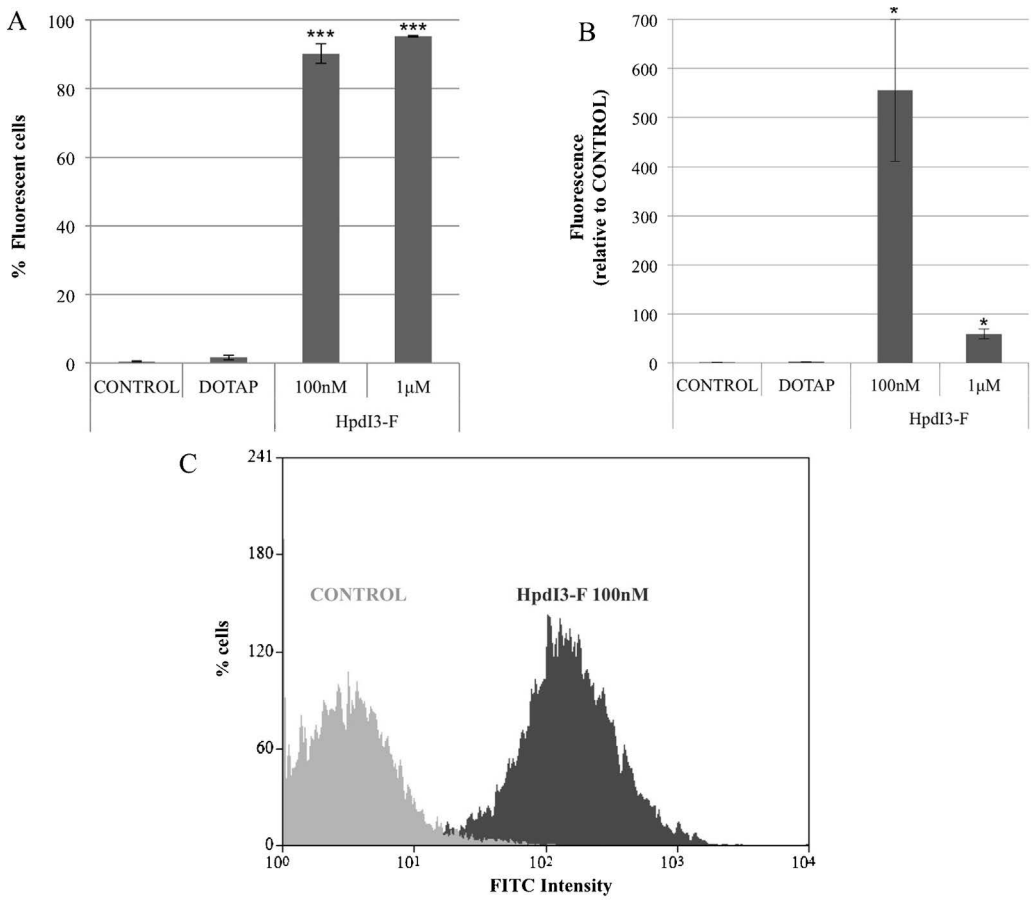

Fig. 2. *Uptake of PPRHs in PC3 cells.* Cells were incubated with 100 nM and 1 μM of fluorescent-PPRH with DOTAP for 24 h and uptake was measured by flow cytometry. (A) Percentage of fluorescent cells determined as FITC-positive and IP-negative cells. Data represent the mean ± SE of four experiments. $^{***}p < 0.005$. (B) Mean intensity of fluorescence of FITC-positive cells. Data represent the mean ± SE of three experiments. $^{*}p < 0.05$. (C) Representative image showing an overlay of control cells and cells treated with 100 nM of fluorescent-PPRH. DOTAP was used at the maximum concentration of 10 μM, resulting in a PPRH:DOTAP ratio of 1:100 and 1:10 for the concentrations of 100 nM and 1 μM of PPRH, respectively.

method (Fig. 4A) and the caspase-3 activity assay (Fig. 4B). The concentration chosen caused the greatest effect on cell viability. HpsPr-C produced the highest apoptotic effect, provoking apoptosis in 50% of the cell population as determined by flow cytometry and inducing a 1.65-fold increase in caspase-3 activity. Surprisingly, HpsPr-T caused a smaller but significant effect than HpsPr-C in apoptosis, even though the decrease in viability was almost as high as that provoked by HpsPr-C (Fig. 4C). The apoptosis produced by HpsE4-C and HpsI1-C was lower than that of HpsPr-C in accordance to the lower decrease in cell viability. The apoptotic levels produced by the most effective PPRHs (HpsPr-T and HpsPr-C) were determined by a caspase-3 assay in control cells (HUVEC, 4T1 and CT26) and no significant changes relative to untreated cells were observed.

3.5. Effects of PPRHs on survivin mRNA levels

Given that both PPRHs against the *survivin* promoter sequence were the most effective in decreasing cell viability, we further explored the ability of those PPRHs to decrease *survivin* expression. Both, HpsPr-T and HpsPr-C were able to decrease *survivin* mRNA levels up to 2-fold (Fig. 5A). The different controls (Hps-Sc and Hps-WC) did not affect *survivin* mRNA levels.

We checked for off-target effects of HpsPr-T and HpsPr-C at a 100 nM, by determining mRNA levels of a set of 5 non-related genes. As shown in Table 2, there was no decrease in the mRNA levels of these genes. We further confirmed the lack of expression of survivin at the mRNA and protein levels in HUVEC cells (Fig. 5B and C), in which no cytotoxicity was observed when using these PPRHs (Fig. 3C).

3.6. Effects of PPRHs on survivin protein levels

Survivin protein levels were also determined in PC3 cells following incubation with 100 nM of either HpsPr-T or HpsPr-C during different periods of time. The Template-PPRH induced a 5-fold decrease in survivin protein levels at 9 h (Fig. 6A), whereas the Coding-PPRH reached only a 2-fold decrease 6 h after transfection (Fig. 6B).

3.7. Binding of PPRHs to their target sequences

The binding between the selected PPRHs and their target sequences was analyzed either by labelling the double-stranded target sequence or the PPRH themselves.

When labelling the target sequences, we observed a maximum binding of 48% of HpsPr-T and 6% of HpsPr-C at the highest concentration of PPRH used (Fig. 7A). When labelling the PPRHs, we also observed their binding to the target sequences, 50% for the HpsPr-T and 18% for the HpsPr-C, respectively, when using 1 μM of the target sequences (Fig. 7B). As seen in Fig. 7B, HpsPr-C presented different electrophoretic structures and to ensure that those conformations belonged to a unique molecular species, the samples were run in a denaturing PAGE obtaining a single band in each case (data not shown).

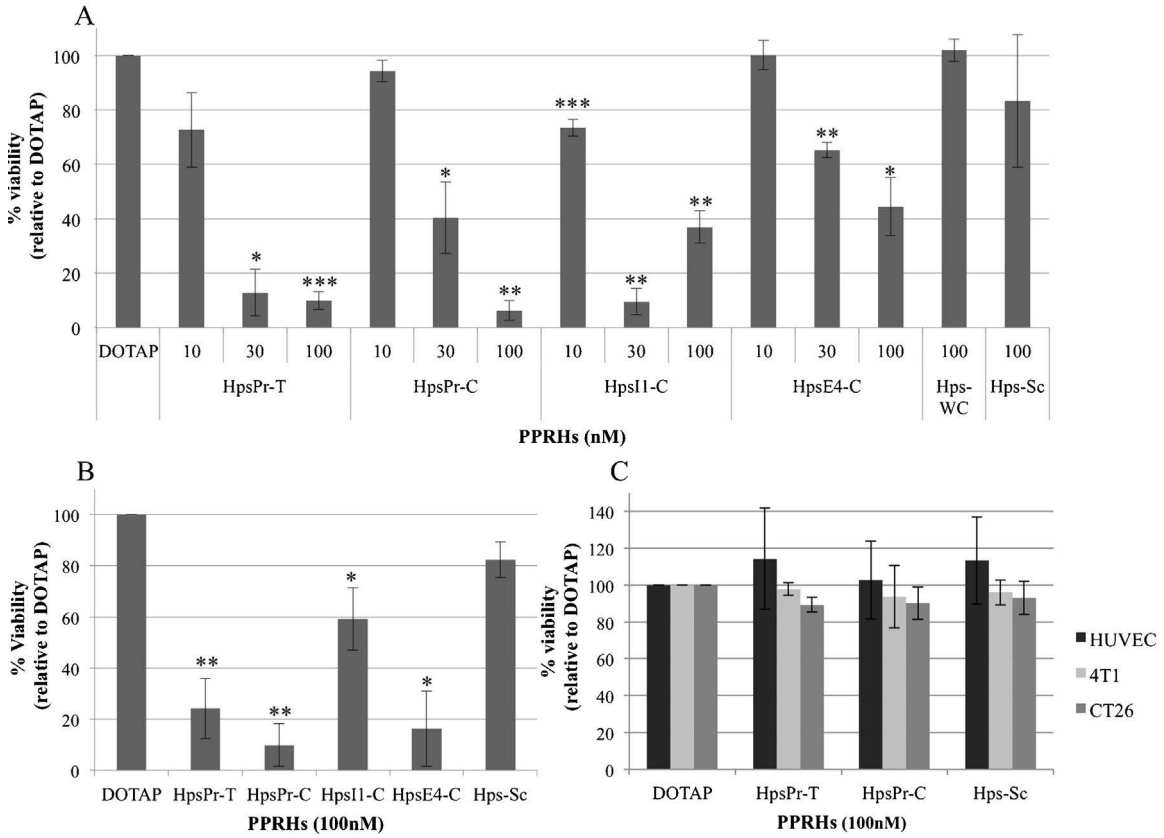

Fig. 3. *Effect of PPRHs against survivin on cell viability.* MTT assays to determine cell survival were performed 6 days after transfection. (A) Dose response of the four designed PPRHs against the *survivin* gene in PC3 cells. DOTAP was used at 5 μM to transfect the PPRHs at 10 and 30 nM, and at 10 μM when transfecting 100 nM PPRH. (B) Cell viability upon transfection of 100 nM PPRHs in HeLa cells. (C) Cell viability upon transfection of 100 nM of PPRHs against the promoter sequence in HUVEC, 4T1 and CT26. Data are mean ± SE values of at least three experiments. $^{*}p < 0.05$, $^{**}p < 0.01$, $^{***}p < 0.005$.

3.8. EMSA analyses

The targets of the two PPRHs that worked more efficiently are located within the *survivin* promoter; the target sequence for HpsPr-T is located at −1009 and the one for HpsPr-C at −525, both relative to the transcriptional initiation site. To study the mechanism of action of these PPRHs, we started analyzing the putative transcription factors that might bind to the target sequences of the PPRHs. We performed an *in silico* search using the MATCH™ software applying a cut-off of 0.95 for both, matrix similarity and core similarity. After literature mining of the found transcription factors, we decided to further explore the role of Sp1 when using HpsPr-T [33] and GATA when using HpsPr-C [34], because of their well-characterized implication in cancer. Moreover, these two transcriptions factors had the highest core similarity and matrix similarity for the target sequence of the corresponding PPRH (1.0 and 1.0 for Sp1 and 1.0 and 0.979 for GATA). Next, we performed EMSA analyses using HeLa nuclear extracts and radiolabeled probes for the double-stranded target sequences of the two PPRHs. The binding pattern for each target sequence is shown in the corresponding lane 2 of Fig. 8A and B.

In both cases, incubation of the radiolabeled target sequence with an excess (100×) of the respective PPRH induced a decrease in the intensity of the binding pattern of nuclear proteins. Incubation with HpsPr-T produced a 52% decrease in the binding (Fig. 8A, lane 3). Incubation with HpsPr-C produced a decrease of 15% that induced a visible release of the free probe (Fig. 8B, lane 3). These results indicated that the specific PPRHs and proteins present in the nuclear extract were competing for the binding to the probe. To identify these proteins, we performed competition assays using the consensus binding sequences for either Sp1 [33] or GATA [35].

In the case of the template-PPRH (HpsPr-T), three bands were identified using competition (Fig. 8A, lanes 4 and 5) and super-shift assays (Fig. 8A, lanes 6 and 7). We observed a decrease in the intensity of three bands in the EMSA in the presence of the Sp1/3-consensus binding sequence as a competitor. When using a 5-fold excess of the Sp1/3-consensus sequence, the band corresponding to Sp1 decreased by 98%, and those corresponding to Sp3 by 85% and 72% (Fig. 8A, lane 4). Using specific antibodies against Sp1 and Sp3 we determined that the upper band corresponded to the binding of Sp1 (Fig. 8A, lane 6), and that two lower bands corresponded to the binding of Sp3 (Fig. 8A, lane 7). Interestingly, the band in-between the two Sp3 bands increased its intensity after the incubation with the antibodies against Sp1 or Sp3, but was decreased in the presence of the Sp1/3 consensus binding sequence. This band might correspond to a factor whose binding sequence overlaps with that for Sp1/3; then, when these two factors are sequestered by antibodies, that other factor – probably Pax4 according to the *in silico* analysis – has a better access to the probe.

In the case of the coding-PPRH (HpsPr-C), a prominent band was observed when incubating the target sequence with the nuclear extract. Competition assays using the GATA consensus sequence were performed confirming the *in silico* prediction (Fig. 8B, lanes 4 and 5). While the GATA consensus sequence at 5 and 50-fold excess produced a decrease in the intensity of the band of 74% and 92%, respectively (Fig. 8B, lanes 4 and 5), the non-related sequence did not cause a significant change in intensity (Fig. 8B, lane 6).

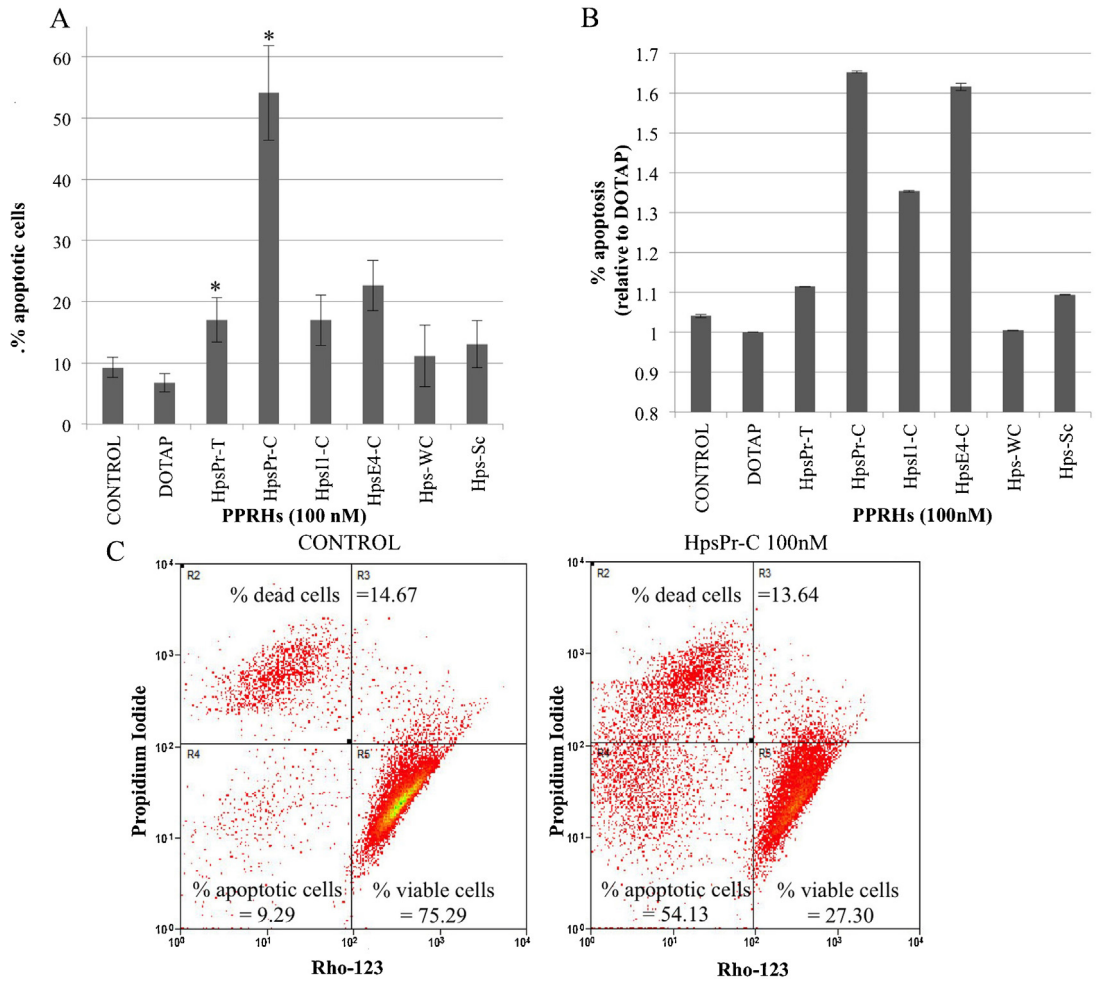

Fig. 4. *Effect of PPRHs on apoptosis.* PC3 cells were transfected with 100 nM of HpsPr-T, HpsPr-C, HpsE4-C and HpsI1-C against the *survivin* gene and two negative controls −Hps-Sc and Hps-WC. 24 h after transfection, apoptosis was measured by two methods. (A) Rhodamine method: Cells Rho123-negative and IP-negative were considered as apoptotic cells. Data represent the mean ± SE of at least three experiments. $^{*}p < 0.05$. (B) Caspase-3/7 assay: Fold change in RLU relative to DOTAP. (C) Representative flow cytometer histograms displaying the cell population treated with 100 nM HpsPr-C and the control sample.

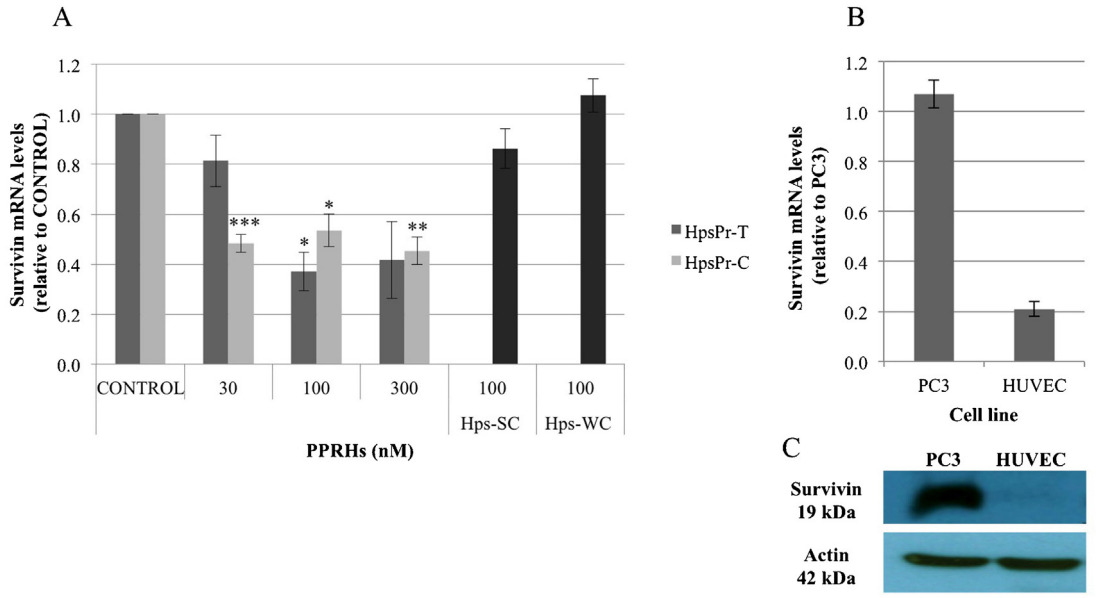

Fig. 5. *Survivin mRNA levels.* (A) RNA was extracted from PC3 cells treated with increasing concentrations of either HpsPr-T for 72 h or HpsPr-C for 24 h. mRNA levels were determined using qRT-PCR and referred to the levels of endogenous controls. Data represent the mean ± SE of at least three experiments. $^{*}p < 0.05$, $^{**}p < 0.01$, $^{***}p < 0.005$. (B) Survivin mRNA levels were analyzed in HUVEC cells and referred to the mRNA levels in PC3 cells. (C) Representative image of a Western blot showing comparatively survivin protein levels in PC3 and HUVEC cell lines.

Table 2
Off-target effects.

	Survivin	APOA1	Bcl2	DHFR	PDK1	S100A4
CONTROL	1	1	1	1	1	1
HpsPr-T	0.37 ± 0.08	1.39 ± 0.16	1.27 ± 0.22	0.93 ± 0.06	1.38 ± 0.25	1.26 ± 0.62
HpsPr-C	0.54 ± 0.07	1.06 ± 0.13	1.05 ± 0.15	0.90 ± 0.04	0.89 ± 0.11	0.93 ± 0.13

mRNA levels of unrelated genes were determined by qRT-PCR after incubation with 100 nM of PPRHs (HpsPr-T and HpsPr-C) against the *survivin* gene.

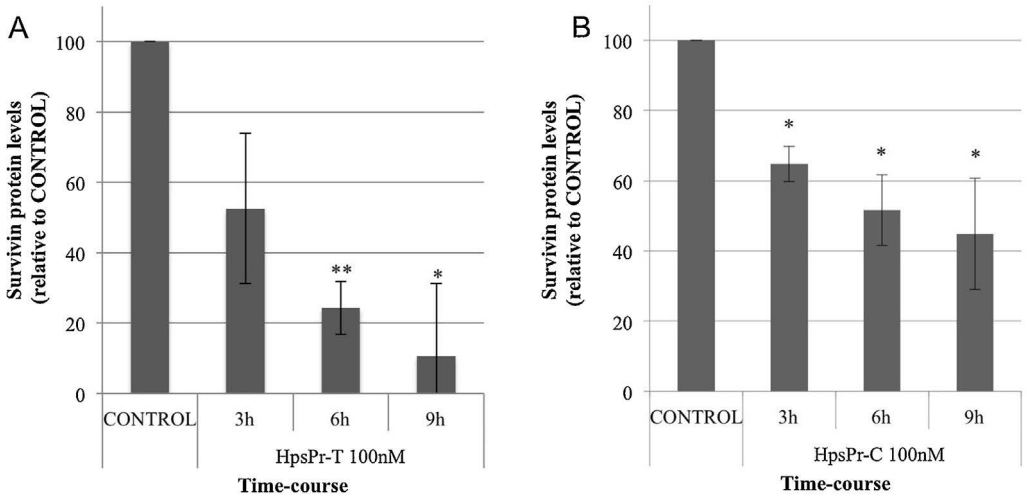

Fig. 6. *Survivin protein levels.* 60,000 PC3 cells were incubated with 100 nM of either HpsPr-T (A) or HpsPr-C (B) for different periods of time. Total protein extracts were obtained and analyzed by Western Blot. Protein levels were normalized using tubulin. Data represent the mean ± SE of at least three experiments. $^{*}p < 0.05$, $^{**}p < 0.01$.

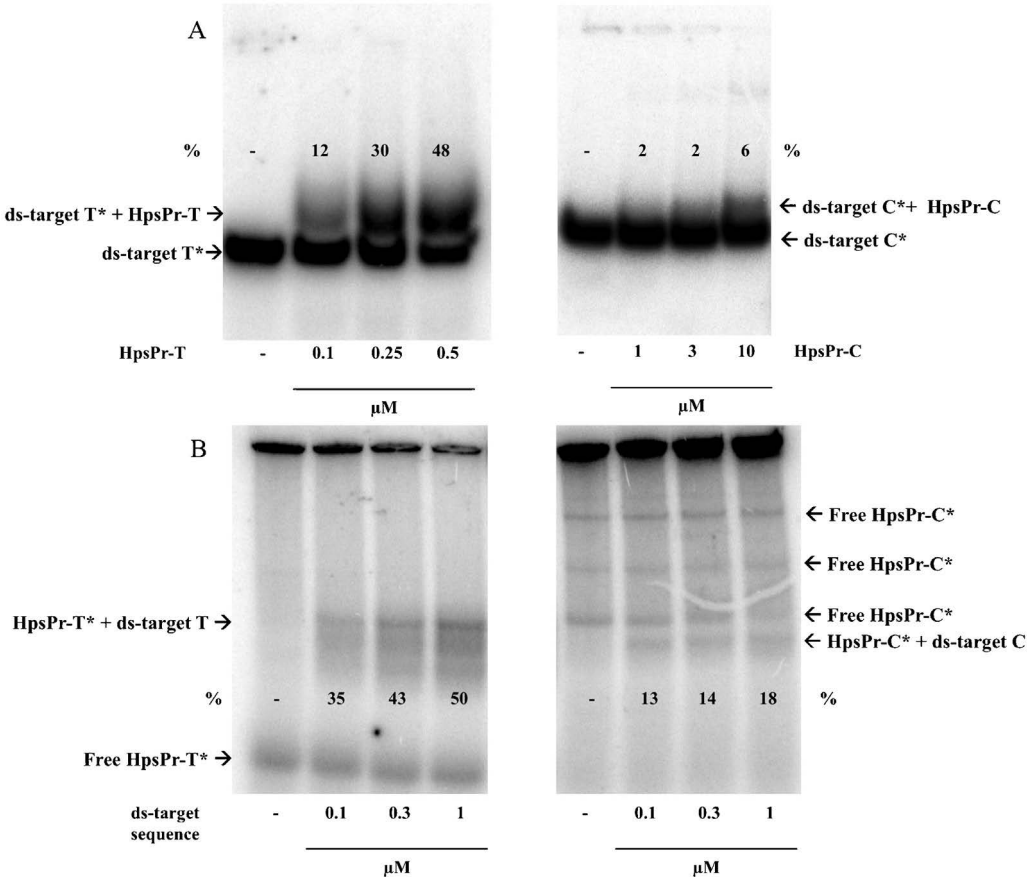

Fig. 7. *PPRHs binding to their target sequence.* (A) Binding of increasing concentrations of the Template-PPRH (HpsPr-T) or the Coding-PPRH (HpsPr-C) after incubation with their radiolabelled ds-target sequences (20,000 cpm). (B) Binding of the radiolabelled Template-PPRH (HpsPr-T) or the radiolabelled Coding-PPRH (HpsPr-C) after incubation with increasing concentrations of their ds-target sequences. 1 µg of poly-dI-dC as non-specific DNA was added to all the binding reactions. * indicates the radiolabelled probes. Binding experiments were performed at least three times. Quantification was performed by phosphorimaging and referred to the total radioactivity. The numbers over (A) or underneath (B) the bands represent the percentage of binding referred to the control (NE).

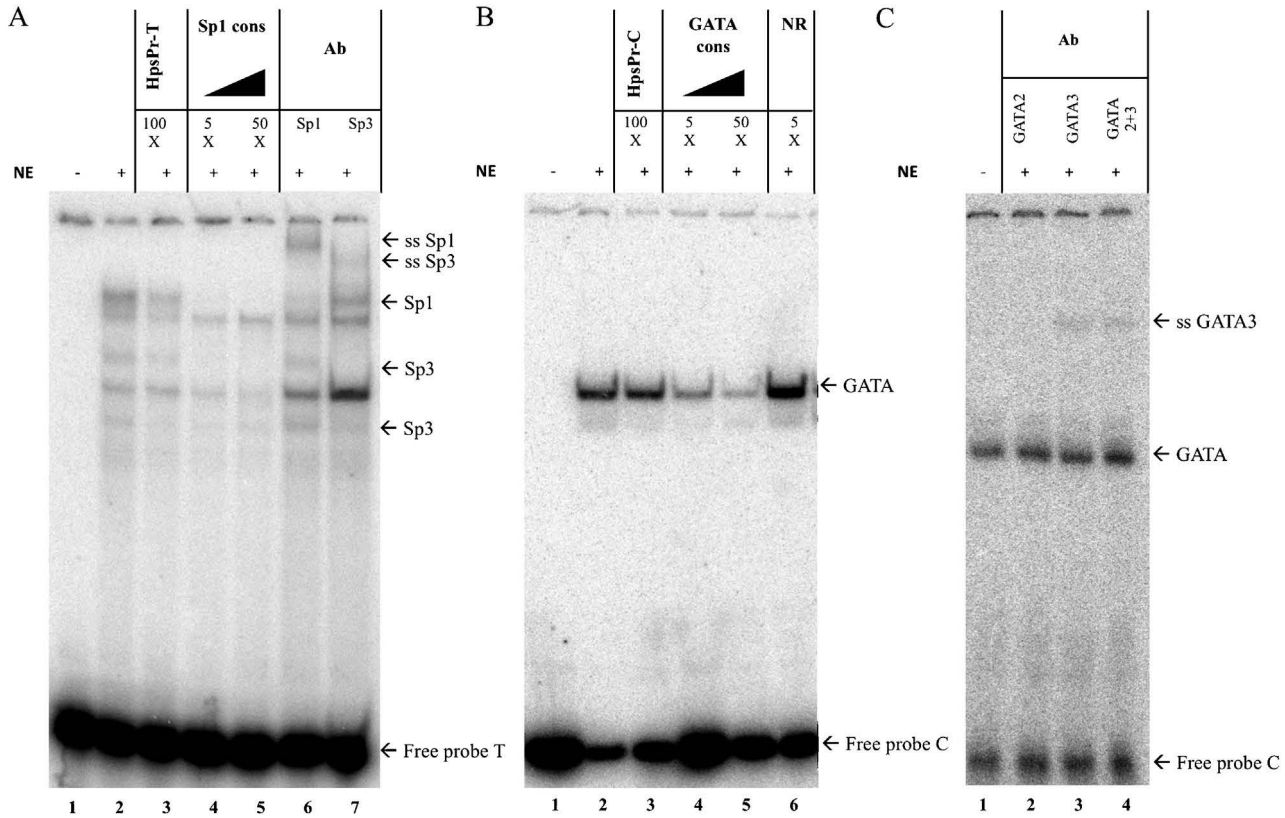

Fig. 8. *Binding of transcription factors to PPRH target sequences.* EMSA assays were conducted using radiolabelled target sequence (20,000 cpm), Herring Sperm DNA as non-specific competitor and HeLa nuclear extracts as the protein source. (A) Bindings obtained using radiolabelled ds-target sequence for HpsPr-T. The binding pattern using HeLa nuclear extracts is shown in lane 2. Competition assays were performed using a 100-fold excess of HpsPr-T (lane 3) or a 5 to 50-fold excess of Sp1/3 consensus sequence (lanes 4 and 5). Supershift assays were performed four times in the presence of antibodies against Sp1 (lane 6) or Sp3 (lane 7). Shifted and supershifted (ss) bands are indicated by arrows. (B) Bindings obtained using radiolabelled ds-target sequence for HpsPr-C. The binding pattern using HeLa nuclear extracts is shown in lane 2. Competition assays were performed using a 100-fold excess of HpsPr-C (lane 3), a 5 to 50-fold excess of GATA consensus sequence (lanes 4 and 5) and a 50-fold excess of a non-related sequence (lane 6). Shifted bands are indicated by arrows. (C) Supershift assays were performed four times in the presence of antibodies against GATA-2 (lane 2), GATA-3 (lane 3) and both antibodies (lane 4). The supershifted (ss) band is indicated by an arrow.

Supershift assays were performed using GATA-2 and GATA-3 antibodies, the GATA family members most abundant in prostate tissue [34]. As shown in Fig. 8C, incubation with GATA-3 antibody produced a supershifted band indicating that this specific factor is binding to the target sequence of HpsPr-C.

3.9. Effects of PPRHs in vivo

Two types of administration, intratumoral and intravenous, were performed using PC3 subcutaneous xenograft tumor model in athymic mice. Two groups were compared, one mock-injected with a scrambled PPRH-Hps-Sc-, and the other injected with the most effective PPRH tested *in vitro*, HpsPr-C (Figs. 2 and 3). Depending upon the route of administration, the dosage of the PPRH varied from 10 μg/injection in the case of intratumoral, and 50 μg/injection for the intravenous. Administration was performed twice a week during 3 weeks and results are presented as tumor volume.

3.9.1. Intratumoral

In the case of intratumoral administration (Fig. 9A), we observed that the PPRH targeting *survivin* (HpsPr-C) produced a delay in tumor growth compared with the scrambled PPRH. At the end of the experiment, the mean relative tumor volume (RTV) of the control group (scrambled-PPRH) was 663.1% with respect to the initial volume, whereas the treated group (HpsPr-C) showed a mean RTV of 396.6%. Taking into account all this data, we calculated the Treatment/Control (*T*/*C*) ratio, which compares the difference in the mean RTV or tumor weight between treated and control groups. These values showed a statistically significant reduction of 40% in tumor volume and almost 30% in tumor weight. The doubling time of the control group was 7.45 days, whereas tumors of the treated group had a doubling time of 9.43, which translates into an absolute growth delay of almost 2 days caused by the administration of the PPRH against *survivin*.

3.9.2. Intravenous

When injecting the PPRHs through the tail vein, the dosage was increased five times to diminish problems associated with whole body distribution or degradation in the bloodstream. As it is shown in Fig. 9B, the PPRH against *survivin* was able to decrease tumor growth *in vivo*, thus producing a delay in tumor growth. In fact, the delay in tumor growth administering HpsPr-C intravenously was higher than intratumorally. This was reflected in the RTV mean which in the treated group was 200% inferior to the control group, meaning a *T*/*C* ratio of 49.6%. Accordingly, the doubling time of the tumor treated with the specific PPRH was almost 2 times higher (19.3 *vs* 10.6) than that of the control group (scramble-PPRH), which means that the cells treated with HpsPr-C took twice the time to double.

In both types of administration, the body weight loss was approximately 2%, indicating lack of toxicity (Fig. 9C and D).

3.9.3. Survivin protein levels and blood vessel formation

To explore the potential correlation between the inhibition of tumor growth and the silencing of *survivin*, we selected tumors

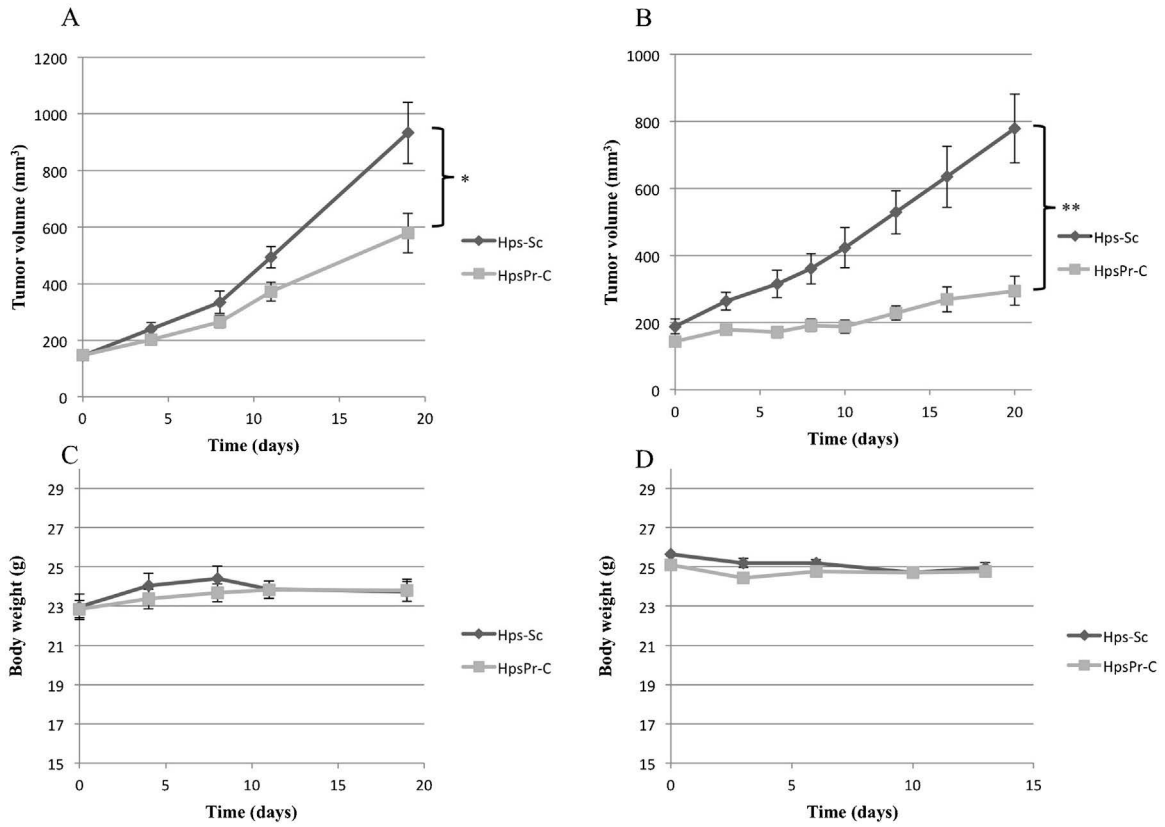

Fig. 9. *PPRH effect on tumor growth and body weight in a PC3 subcutaneous xenograft tumor model.* (A) Progression of tumor volume throughout time when Hps-Sc (negative control) or HpsPr-C were administered by i.t. route twice a week (1001000). Tumor volume is represented as the mean ± SE; $^{*}p < 0.05$. (B) Progression of tumor volume throughout time when Hps-Sc (negative control) or HpsPr-C were administered by i.v. route twice a week (1001000). Tumor volume is represented as the mean ± SE; $^{**}p < 0.01$. (C) and (D) Evolution of body weight of the animals throughout time corresponding to the intratumoral and intravenous administrations, respectively. Data represent the mean ± SE.

from the intratumoral study to perform Western blot and immunofluorescence analyses. We measured the protein levels of survivin in a minimum of 4 tumors from both the control and the treated groups, from samples of the center part and in the tip of the tumor. In both cases, we observed a decrease in survivin protein levels, 52% in the center part and 71% in the tip of the tumor, respectively (Fig. 10A). In addition, we determined survivin expression by immunofluorescence analysis in histological sections, observing a decrease in expression in tumors treated with HpsPr-C, as shown in Fig. 10B.

We also investigated the role of *survivin* in angiogenesis by performing histological analyses of murine CD31 staining for three tumor samples from each group to evaluate blood vessel formation. A representative image is shown in Fig. 11A. Quantification of microvessel density and the fraction area of the vessels revealed a decrease in the vasculature, with a *T*/*C* ratio of 25%, for both microvessel density (Fig. 11B) and fractional area of vessels (Fig. 11C).

4. Discussion

The objectives of this work were to get further knowledge of the effects of PPRHs as new silencing tools and their possibilities to be used as therapeutic agents in *in vivo* approaches. As a model we inhibited the *survivin* gene, since its overexpression in cells promotes the evasion of apoptosis, one of the six hallmarks of cancer [36]. *Survivin* has been used as a suitable target in several experimental settings to decrease cell proliferation using antisense oligonucleotides [37], siRNAs [6,38] or small molecules [29,39,40]. Since we had previously described PPRHs as an alternative gene silencing tool in breast cancer cells (SKBR3, MCF7) [4,5], we decided to design a set of four PPRHs, three Coding- and one Template-PPRH against *survivin* to test the efficacy of PPRHs in prostate cancer cells (PC3) *in vitro* and *in vivo*.

A conclusion of this work is that after comparing the PPRHs against different regions of the *survivin* gene, those against its promoter sequence (HpsPr-T and HpsPr-C) were the most effective in decreasing cell viability in PC3 cells. We previously described the ability of a template-PPRH against the *dhfr* gene to decrease mRNA and protein levels. In this work, we corroborate the action of a template-PPRH against another target, *survivin*. In addition, we observed that the coding-PPRH, HpsPr-C, was also able to decrease mRNA and protein levels of the targeted protein. This was unforeseen since a coding-PPRH against intron 3 of the *dhfr* gene was able to decrease viability without showing a great decrease in mRNA levels [5]. The difference between those two coding-PPRHs is the location of their target sequences, one in an intron (HpdI3-A-TA) and the other within the promoter (HpsPr-C). The effect of the PPRH against *dhfr* intron 3 was due to its interference with the binding of the splicing factor U2AF65, thus altering the splicing process [5]. PPRHs against the *survivin* promoter worked through a different mechanism by inhibiting transcription, thus decreasing gene expression. Specifically, we demonstrated that these PPRHs decreased the binding of transcription factors, such as Sp1 (using HpsPr-T) and GATA (using HpsPr-C), which have binding sites within the PPRHs target sequences. Other authors have proved that both Sp1 and Sp3 regulate the *survivin* promoter via several Sp1-boxes [33,41] and that degradation of Sp1 is related to a decrease in *survivin* expression [42]. Regarding GATA transcription factors, although

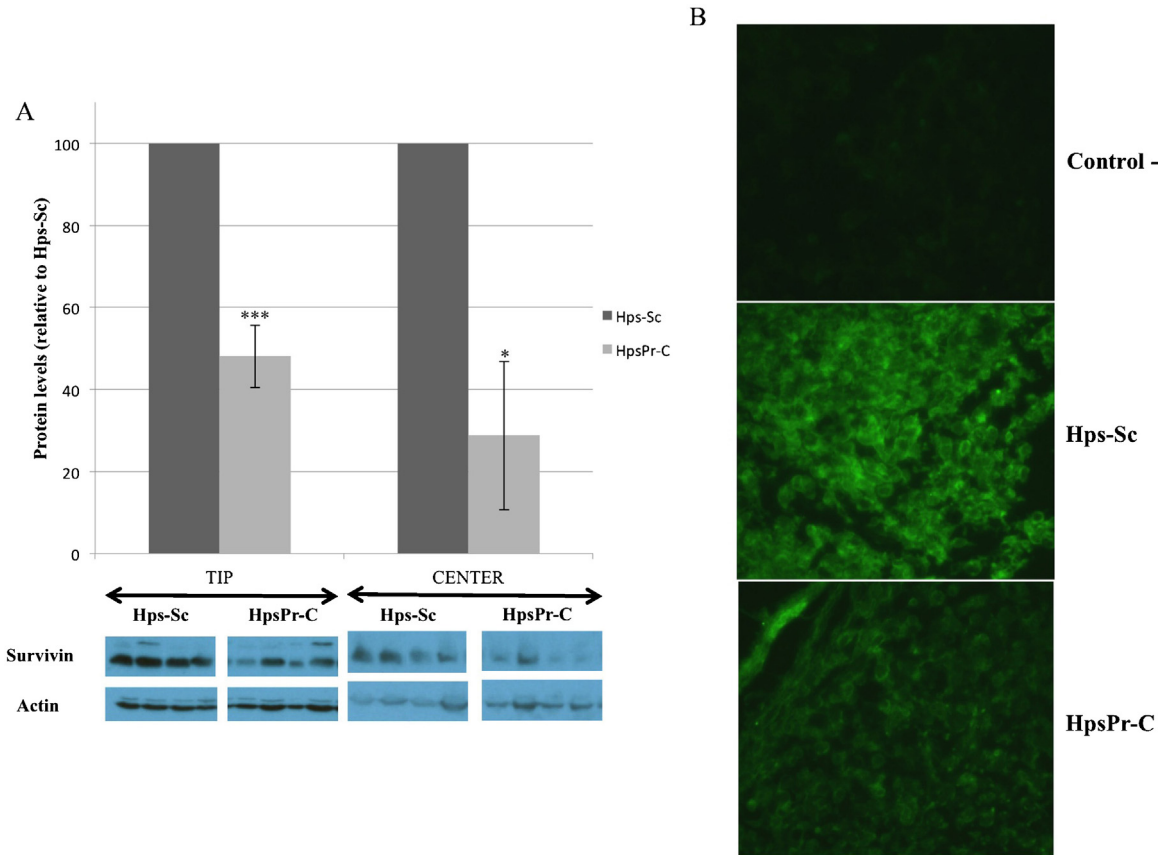

Fig. 10. *Survivin protein levels after intratumoral administration of PPRHs.* (A) Quantification of survivin protein levels in the tip and the center of tumors after administration of either Hps-Sc or HpsPr-C. Total protein extracts were obtained and analyzed by Western Blot. Protein levels were normalized using actin. Data represent the mean ± SE of at least four tumors. $^{*}p < 0.05$, $^{***}p < 0.005$. (B) Representative image of the immunofluorescent analysis of tumors after the administration of either Hps-Sc or HpsPr-C. The negative control corresponds to the fluorescence background given by Alexa Fluor 488. Original magnification: 40×.

they are mainly expressed in hematopoietic cells, GATA-2 and -3 are the predominant family members expressed in the prostate tissue [34] that might be playing a role in *survivin* expression in this tissue. From our work, we can conclude that prevention of the binding of GATA-3 to the *survivin* promoter by HpsPr-C might cause a decrease in *survivin* expression.

There are different Sp1- and GATA-binding sites within the *survivin* promoter. However, upon comparison by multiple alignment analysis of those binding sites, only the core of the binding site is conserved, while the flanking sequences are different enough so that the PPRH will be specific only for its target sequence. In fact, the promoters of the genes selected to study off-target effects all presented binding sites for both GATA and Sp1 and none of those genes were downregulated by the treatment (Table 2).

Regarding the *in vitro* effects, our observations corroborate the extensively reported involvement of *survivin* in the mitochondrial apoptotic pathway and how the decrease in its levels produces an increase in apoptosis [11,37,39]. To decrease mRNA and protein levels of survivin as a therapeutic approach, several molecules have been used such as aODNs [6,37], locked nucleic acids (LNAs) [43], siRNAs[6] and small molecules like the Ras inhibitor farnesylthiosalicylic acid (FTS) [39], YM155 [29] or FL118 [40]. However, the LNA SPC3042 and FL118 presented lack of specificity, by down-regulating or modulating other genes in the IAP or Bcl-2 family [40,43], while others required higher dosages to induce a proper effect, ranging from 200 nM to 1 μM [6,37,38] or even higher (75 μM) when using FTS [39].

As an alternative, we present PPRHs, a new gene silencing tool that work at nanomolar concentrations, a lower range compared to aODNs, and similar to the concentrations of siRNAs used in *in vitro* experiments [6]. We observed a maximum decrease in viability at 100 nM for each one of the PPRHs against the *survivin* promoter sequence. This concentration assured the optimal PPRH uptake in PC3 cells when transfected with DOTAP. Other advantages of PPRHs are their high stability, without the need of modifying residues, and their low cost [4]. To prove their specificity and possible toxicities, we tested our best PPRHs (HpsPr-T and HpsPr-C) in human normal cells. Other authors have used HUVEC cells as normal cells [44,45]. In our case, this cell line was an ideal negative control because it does not express *survivin* and, in consequence, treatment with the selected PPRHs at 100 nM is innocuous. In addition, the species selectivity of these PPRHs against human *survivin* was tested in murine cancer cell lines, where no decrease in viability was observed due to the difference in the *survivin* sequences. To further discard off-target effects, we studied the expression of several genes after treatment with either HpsPr-T or HpsPr-C, not observing decreases in their mRNA levels. It is worth noting that Bcl-2 was one of those genes, thus proving that *survivin* silencing produced apoptosis by itself and not by changing the expression levels of another gene with a similar antiapoptotic function. However, we cannot dismiss other off-target effects due to the binding of the PPRH to unintended targets.

We aimed to explore the usage of PPRHs *in vivo* using a subcutaneous xenograft tumor model of prostate cancer. Using two different types of administration, intratumoral and intravenous, the coding-PPRH against *survivin* promoter was able to decrease the volume of the tumor, demonstrating the efficacy of this PPRH in this model. The delay in tumor growth caused by the administration of HpsPr-C may be related to the decrease in

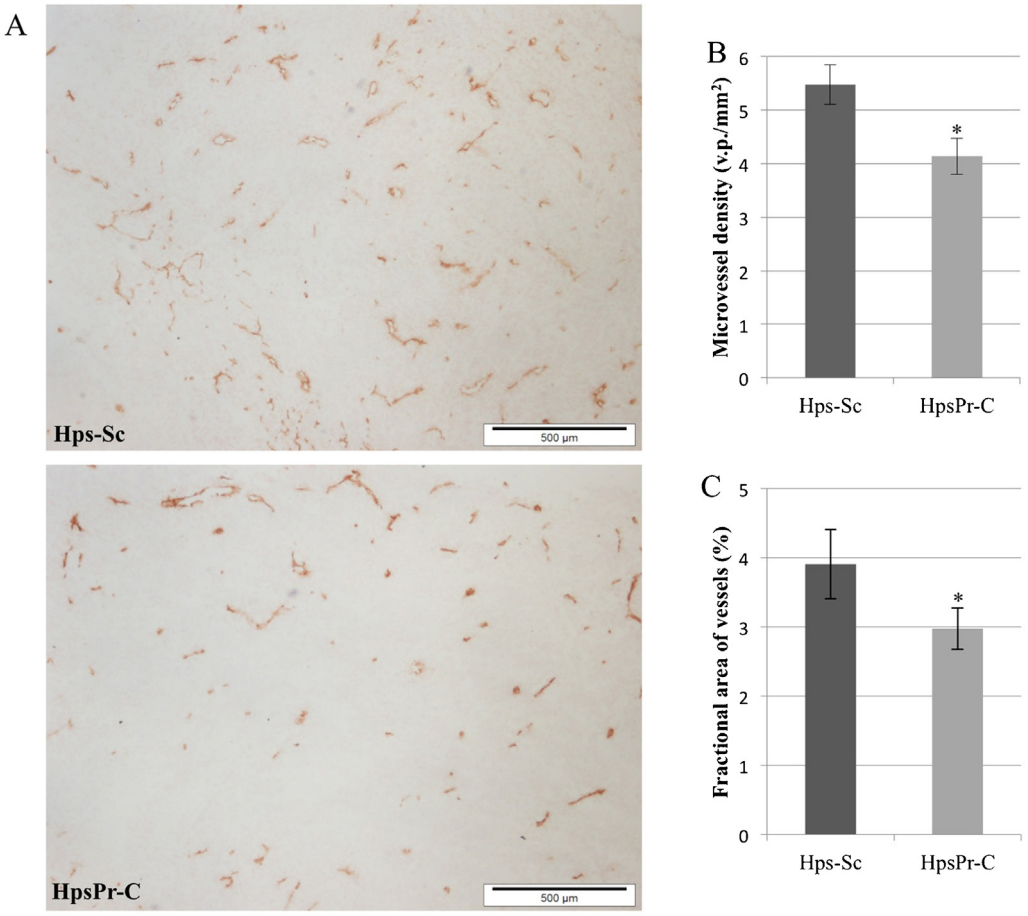

Fig. 11. *Blood vessel formation after intratumoral administration of PPRHs.* (A) Representative image of the immunohistochemical analysis in tumors after administration of either Hps-Sc or HpsPr-C, using anti-CD31 antibody that recognises endothelial cells. (B) Microvessel density and (C) fractional area of vessels of the tumors after administration of either Hps-Sc or HpsPr-C. Data represent the mean ± SE of three tumors. $^{*}p < 0.05$.

the levels of survivin and to a lower degree of blood vessel formation.

The reason for including the intravenous injection as a second route of administration was to overcome the possible drawbacks of the intratumoral administration such as aggressiveness – thus causing loss of tumor structure and alterations in the measurement- and poor-distribution within the tumor – because of the high interstitial fluid pressure and the stiffness of the extracellular matrix [46].

In an aging society with growing life expectancy, diseases such as prostate cancer are going to increase its incidence and effective therapeutic approaches are needed. Up until now, treatment options are limited to surveillance in early stage, surgery or radiotherapy when a radical treatment is needed, hormone therapy in HRPC and chemotherapy in case of metastasis [27]. Currently, different targeted-directed therapies against *survivin* are undergoing clinical trials, such as small molecules – YM155 – and antisense oligonucleotide LY2181308, proving that inhibition of *survivin* is a cutting-edge target for anticancer treatments. However, YM155 have showed modest activity and therefore combination therapies have been suggested for new trials [29]. LY2181308 inhibited growth in subcutaneous xenografted tumors [11], but showed no significant increase in toxicity in Phase II clinical trials in combination with docetaxel in castrate-resistant prostate cancer [30]. Our results are encouraging, but it is important to note that pre-clinical models, such as xenografts, are far from useful to extrapolate results to humans, so there is need to improve the models and test in other organisms.

In summary, this work represents the preclinical proof of principle for the *in vivo* application of PPRHs, opening the possibility to use this technology as a new therapeutic approach.

Acknowledgements

The work was supported by Grant SAF2011-23582 from "Plan Nacional de Investigación Científica" (Spain). Our group holds the Quality Mention from the "Generalitat de Catalunya" SGR2009-118. LR is the recipient of a fellowship (FI) from the "Generalitat de Catalunya".

References

[1] Avino A, Frieden M, Morales JC, Garcia de la Torre B, Guimil Garcia R, Azorin F, et al. Properties of triple helices formed by parallel-stranded hairpins containing 8-aminopurines. Nucleic Acids Res 2002;30:2609–19.
[2] Coma S, Noe V, Eritja R, Ciudad CJ. Strand displacement of double-stranded DNA by triplex-forming antiparallel purine-hairpins. Oligonucleotides 2005;15:269–83.
[3] Goni JR, de la Cruz X, Orozco M. Triplex-forming oligonucleotide target sequences in the human genome. Nucleic Acids Res 2004;32:354–60.
[4] de Almagro MC, Coma S, Noe V, Ciudad CJ. Polypurine hairpins directed against the template strand of DNA knock down the expression of mammalian genes. J Biol Chem 2009;284:11579–89.
[5] de Almagro MC, Mencia N, Noe V, Ciudad CJ. Coding polypurine hairpins cause target-induced cell death in breast cancer cells. Hum Gene Ther 2011;22:451–63.
[6] Coma S, Noe V, Lavarino C, Adan J, Rivas M, Lopez-Matas M, et al. Use of siRNAs and antisense oligonucleotides against survivin RNA to inhibit steps leading to tumor angiogenesis. Oligonucleotides 2004;14:100–13.
[7] Ambrosini G, Adida C, Altieri DC. A novel anti-apoptosis gene, survivin, expressed in cancer and lymphoma. Nat Med 1997;3:917–21.

[8] Monzo M, Rosell R, Felip E, Astudillo J, Sanchez JJ, Maestre J, et al. A novel anti-apoptosis gene: Re-expression of survivin messenger RNA as a prognosis marker in non-small-cell lung cancers. J Clin Oncol 1999;17:2100–4.
[9] Tanaka K, Iwamoto S, Gon G, Nohara T, Iwamoto M, Tanigawa N. Expression of survivin and its relationship to loss of apoptosis in breast carcinomas. Clin Cancer Res 2000;6:127–34.
[10] Kawasaki H, Altieri DC, Lu CD, Toyoda M, Tenjo T, Tanigawa N. Inhibition of apoptosis by survivin predicts shorter survival rates in colorectal cancer. Cancer Res 1998;58:5071–4.
[11] Carrasco RA, Stamm NB, Marcusson E, Sandusky G, Iversen P, Patel BK. Antisense inhibition of survivin expression as a cancer therapeutic. Mol Cancer Ther 2011;10:221–32.
[12] Lu CD, Altieri DC, Tanigawa N. Expression of a novel antiapoptosis gene, survivin, correlated with tumor cell apoptosis and p53 accumulation in gastric carcinomas. Cancer Res 1998;58:1808–12.
[13] Kato J, Kuwabara Y, Mitani M, Shinoda N, Sato A, Toyama T, et al. Expression of survivin in esophageal cancer: correlation with the prognosis and response to chemotherapy. Int J Cancer 2001;95:92–5.
[14] Satoh K, Kaneko K, Hirota M, Masamune A, Satoh A, Shimosegawa T. Expression of survivin is correlated with cancer cell apoptosis and is involved in the development of human pancreatic duct cell tumors. Cancer 2001;92:271–8.
[15] Swana HS, Grossman D, Anthony JN, Weiss RM, Altieri DC. Tumor content of the antiapoptosis molecule survivin and recurrence of bladder cancer. N Engl J Med 1999;341:452–3.
[16] Saitoh Y, Yaginuma Y, Ishikawa M. Analysis of Bcl-2, Bax and Survivin genes in uterine cancer. Int J Oncol 1999;15:137–41.
[17] Yoshida H, Ishiko O, Sumi T, Matsumoto Y, Ogita S. Survivin, bcl-2 and matrix metalloproteinase-2 enhance progression of clear cell- and serous-type ovarian carcinomas. Int J Oncol 2001;19:537–42.
[18] Adida C, Haioun C, Gaulard P, Lepage E, Morel P, Briere J, et al. Prognostic significance of survivin expression in diffuse large B-cell lymphomas. Blood 2000;96:1921–5.
[19] Adida C, Recher C, Raffoux E, Daniel MT, Taksin AL, Rousselot P, et al. Expression and prognostic significance of survivin in de novo acute myeloid leukaemia. Br J Haematol 2000;111:196–203.
[20] Adida C, Berrebi D, Peuchmaur M, Reyes-Mugica M, Altieri DC. Anti-apoptosis gene, survivin, and prognosis of neuroblastoma. Lancet 1998;351:882–3.
[21] Grossman D, McNiff JM, Li F, Altieri DC. Expression and targeting of the apoptosis inhibitor, survivin, in human melanoma. J Invest Dermatol 1999;113:1076–81.
[22] Grossman D, McNiff JM, Li F, Altieri DC. Expression of the apoptosis inhibitor, survivin, in nonmelanoma skin cancer and gene targeting in a keratinocyte cell line. Lab Invest 1999;79:1121–6.
[23] Carter BZ, Milella M, Altieri DC, Andreeff M. Cytokine-regulated expression of survivin in myeloid leukemia. Blood 2001;97:2784–90.
[24] Gianani R, Jarboe E, Orlicky D, Frost M, Bobak J, Lehner R, et al. Expression of survivin in normal, hyperplastic, and neoplastic colonic mucosa. Hum Pathol 2001;32:119–25.
[25] Sarela AI, Guthrie JA, Seymour MT, Ride E, Guillou PJ, O'Riordain DS. Non-operative management of the primary tumour in patients with incurable stage IV colorectal cancer. Br J Surg 2001;88:1352–6.
[26] Altieri DC. The molecular basis and potential role of survivin in cancer diagnosis and therapy. Trends Mol Med 2001;7:542–7.
[27] Ramsay AK, Leung HY. Signalling pathways in prostate carcinogenesis: potentials for molecular-targeted therapy. Clin Sci (Lond) 2009;117:209–28.
[28] Nakahara T, Takeuchi M, Kinoyama I, Minematsu T, Shirasuna K, Matsuhisa A, et al. YM155, a novel small-molecule survivin suppressant, induces regression of established human hormone-refractory prostate tumor xenografts. Cancer Res 2007;67:8014–21.
[29] Tolcher AW, Quinn DI, Ferrari A, Ahmann F, Giaccone G, Drake T, et al. A phase II study of YM155, a novel small-molecule suppressor of survivin, in castration-resistant taxane-pretreated prostate cancer. Ann Oncol 2012;23:968–73.
[30] Wiechno PJCP, Smok-Kalwat J, Pikilel J, Henry DH, Christianson DF, et al. Interim results of a randomized phase II study with window-design to evaluate antitumor activity of the survivin antisense oligonucleotide (ASO) LY2181308 in combination with docetaxel for first-line treatment of castrate-resistant prostate cancer (CRPC). J Clin Oncol 2011;29:abstr 4592.
[31] Li HX, Zhao XY, Wang L, Wang YS, Kan B, Xu JR, et al. Antitumor effect of mSurvivinThr34–>Ala in murine colon carcinoma when administered intravenously. Med Oncol 2010;27:1156–63.
[32] Peng XC, Yang L, Yang LP, Mao YQ, Yang HS, Liu JY, et al. Efficient inhibition of murine breast cancer growth and metastasis by gene transferred mouse survivin Thr34–>Ala mutant. J Exp Clin Cancer Res 2008;27:46.
[33] Li F, Altieri DC. Transcriptional analysis of human survivin gene expression. Biochem J 1999;344(Pt 2):305–11.
[34] Perez-Stable CM, Pozas A, Roos BA. A role for GATA transcription factors in the androgen regulation of the prostate-specific antigen gene enhancer. Mol Cell Endocrinol 2000;167:43–53.
[35] Boidot R, Vegran F, Jacob D, Chevrier S, Cadouot M, Feron O, et al. The transcription factor GATA-1 is overexpressed in breast carcinomas and contributes to survivin upregulation via a promoter polymorphism. Oncogene 2010;29:2577–84.
[36] Hanahan D, Weinberg RA. The hallmarks of cancer. Cell 2000;100:57–70.
[37] Olie RA, Simoes-Wust AP, Baumann B, Leech SH, Fabbro D, Stahel RA, et al. A novel antisense oligonucleotide targeting survivin expression induces apoptosis and sensitizes lung cancer cells to chemotherapy. Cancer Res 2000;60:2805–9.
[38] Kappler M, Bache M, Bartel F, Kotzsch M, Panian M, Wurl P, et al. Knockdown of survivin expression by small interfering RNA reduces the clonogenic survival of human sarcoma cell lines independently of p53. Cancer Gene Ther 2004;11:186–93.
[39] Blum R, Jacob-Hirsch J, Rechavi G, Kloog Y. Suppression of survivin expression in glioblastoma cells by the Ras inhibitor farnesylthiosalicylic acid promotes caspase-dependent apoptosis. Mol Cancer Ther 2006;5:2337–47.
[40] Ling X, Cao S, Cheng Q, Keefe JT, Rustum YM, Li F. A novel small molecule FL118 that selectively inhibits survivin, Mcl-1, XIAP and cIAP2 in a p53-independent manner, shows superior antitumor activity. PLoS One 2012;7:e45571.
[41] Xu R, Zhang P, Huang J, Ge S, Lu J, Qian G. Sp1 and Sp3 regulate basal transcription of the survivin gene. Biochem Biophys Res Commun 2007;356:286–92.
[42] Sankpal UT, Abdelrahim M, Connelly SF, Lee CM, Madero-Visbal R, Colon J, et al. Small molecule tolfenamic acid inhibits PC-3 cell proliferation and invasion in vitro, and tumor growth in orthotopic mouse model for prostate cancer. Prostate 2012;72:1648–4858.
[43] Hansen JB, Fisker N, Westergaard M, Kjaerulff LS, Hansen HF, Thrue CA, et al. SPC3042: a proapoptotic survivin inhibitor. Mol Cancer Ther 2008;7:2736–45.
[44] Kitano T, Yoda H, Tabata K, Miura M, Toriyama M, Motohashi S, et al. Vitamin K3 analogs induce selective tumor cytotoxicity in neuroblastoma. Biol Pharm Bull 2012;35:617–6123.
[45] Mukherjee A, Huber K, Evans H, Lakhani N, Martin S. A cellular and molecular investigation of the action of PMX464, a putative thioredoxin inhibitor, in normal and colorectal cancer cell lines. Br J Pharmacol 2007;151:1167–75.
[46] Holback H, Yeo Y. Intratumoral drug delivery with nanoparticulate carriers. Pharm Res 2011;28:1819–30.

4.1.1. Additional results Article I

4.1.1.1. Mechanism of action of PPRHs in the PC3 cell line

MATCH software

The input of the target sequence for the PPRHs into the MATCH ™ software gave an output consisting in different putative transcription factors, with a core and matrix match values between 0.95 and 1. The output for both ds-T (double stranded target sequence for HpsPr-T) and ds-C (double stranded target sequence for HpsPr-C) are shown in Figure 9 and 10, respectively.

After literature mining of the putative transcription factors, we selected Sp1 for HpsPr-T and GATA for HpsPr-C because they were the factors with a higher core and matrix similarity and their implication in cancer (Li & Altieri 1999; Perez-Stable et al. 2000).

matrix identifier	position (strand)	core match	matrix match	sequence (always the (+)-strand is shown)	factor name
V$CAP_01	1 (+)	0.971	0.970	CCACCcct	cap
V$IK2_01	4 (-)	1.000	0.952	ccccTCCCAccc	Ik-2
V$PAX4_03	5 (+)	1.000	0.985	ccctccCACCCc	Pax-4
V$CAP_01	10 (+)	0.971	0.968	CCACCccg	cap
V$GC_01	10 (-)	1.000	0.968	ccaccCCGCCccca	GC box
V$SP1_Q6	11 (-)	1.000	0.988	caccCCGCCccca	Sp1
V$SP1_01	12 (-)	1.000	1.000	accCCGCCcc	Sp1
V$CAP_01	21 (+)	0.984	0.984	CCATTctt	cap

Figure 9. Output information for the target sequence of the Template-PPRH (HpsPr-T) using the MATCH ™ software

matrix identifier	position (strand)	core match	matrix match	sequence (always the (+)-strand is shown)	factor name
V$P300_01	3 (-)	1.000	0.961	gctgcACTCCatcc	p300
V$CAP_01	6 (+)	0.987	0.984	GCACTcca	cap
V$GATA1_01	9 (-)	1.000	0.979	ctCCATCcct	GATA-1
V$GATA2_01	9 (-)	0.987	0.976	ctCCATCcct	GATA-2
V$GATA3_01	9 (-)	0.969	0.961	ctCCATCcc	GATA-3
V$CAP_01	11 (+)	0.971	0.970	CCATCcct	cap
V$MZF1_01	18 (-)	1.000	0.977	TCCCCtgt	MZF1

Figure 10. Output information for the target sequence of the Coding-PPRH (HpsPr-C) using the MATCH ™ software

EMSA assays

Once we had resolved the mechanism of action of both PPRHs against promoter sequences of the *survivin* gene using HeLa nuclear extracts, we thought it was important to study the mechanism of action in the PC3 cell line used in the *in vitro* and *in vivo* experiments. Therefore, we prepared nuclear extracts from PC3 cells as described in Materials and Methods section 3.2.3.2 and used them to conduct

EMSA assays, using the radiolabeled double-stranded target sequences (ds-T and ds-C) for both PPRHs (HpsPr-T and HpsPr-C).

Figure 11 shows a representative EMSA assay for the Template-PPRH. In Figure 11A we analyzed the binding pattern and performed competition with the PPRH. Incubation of PC3 nuclear extracts with the double-stranded sequence (ds-T) generated a pattern (lane 2) similar to the pattern observed with HeLa extracts (Figure 8A, Article I). Incubation with increasing concentrations of HpsPr-T caused a 50% decrease in the intensity of the bands corresponding to the proteins bound to the target sequence. In Figure 11B, we performed competition assays with the Sp1/3-consensus binding sequence. In lane 3 where the competitor was at 100X-fold excess, a mean decrease of 38% in the intensity of the 3 upper bands was observed, while in lane 4, at 500X-fold excess, those 3 bands almost disappeared, reaching a mean decrease in intensity of around 82%. To further identify which transcription factor corresponded to which band we performed supershift assays, shown in Figure 11C. Using antibodies against Sp1 (lane 1), Sp3 (lane 2), and both of them in combination (lane 3), we determined that the upper band corresponded to Sp1, and the two lower bands corresponded to Sp3. There was an additional band that did not disappear neither incubating with the consensus sequence, nor using the antibodies, that could correspond to another putative transcription factor not yet determined. As suggested in Article I, there might be another factor binding to a similar sequence to Sp1/3.

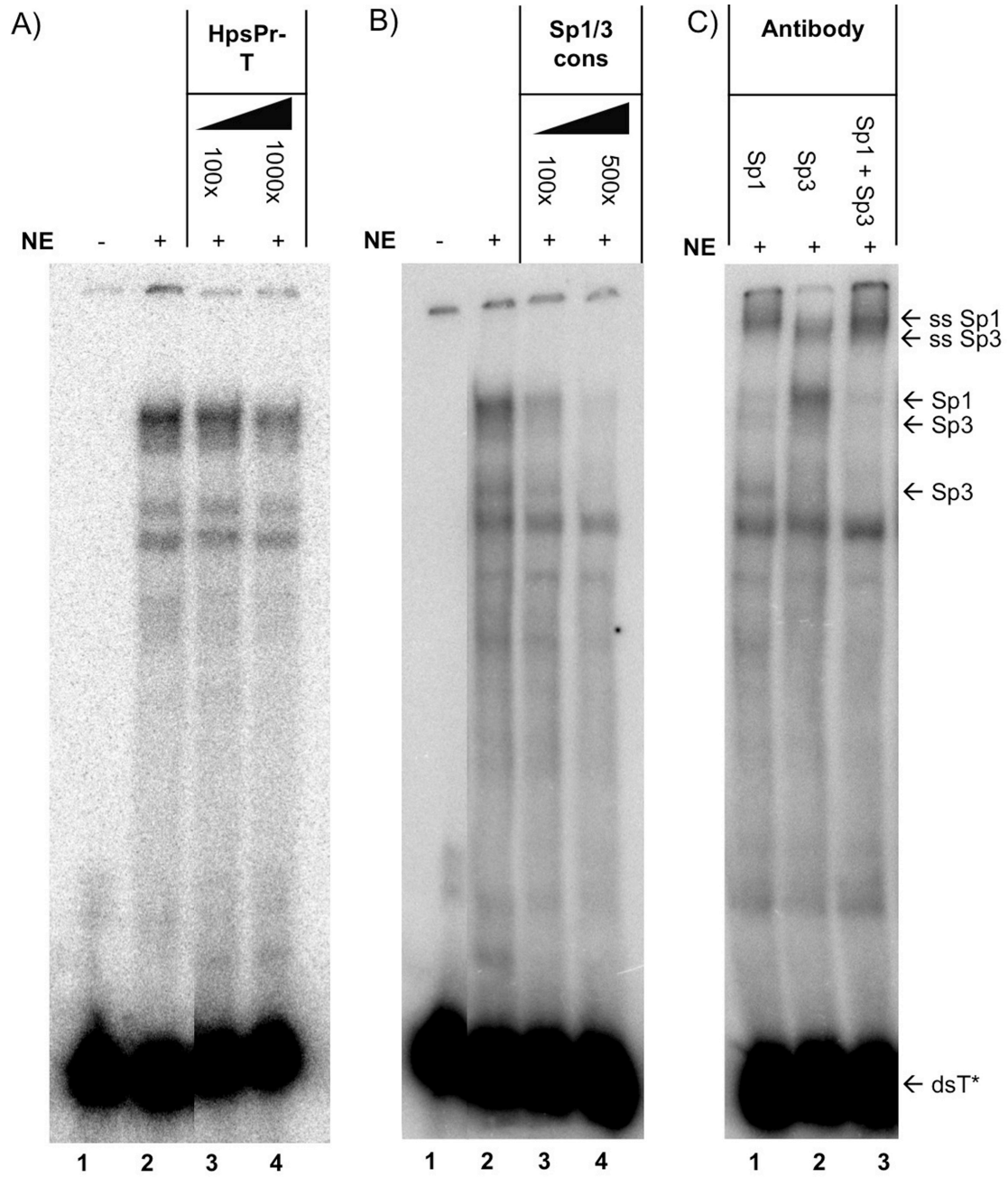

Figure 11. Binding of transcription factors to HpsPr-T target sequence. EMSA assays were conducted using radiolabeled target sequence ds-T (20,000 cpm), Herring Sperm DNA as non-specific competitor and PC3 nuclear extracts. A) The binding pattern using PC3 nuclear extracts is shown in lane 2. Competition assays were performed using a 100 and 1000-fold excess of HpsPr-T (lane 3 and 4) B) Competition assays with the Sp1/3 consensus sequence using 100 and 500-fold excess (lane 3 and 4). C) Supershift assays in the presence of 2 µg of antibodies against Sp1 (lane 1), Sp3 (lane 2) or both (lane 3). Shifted and supershifted (ss) bands are indicated by arrows.

A representative EMSA for the Coding-PPRH is shown in Figure 12. In lane 2 we observed that the binding pattern with PC3 nuclear extracts was also similar to the one obtained with HeLa nuclear extracts (Figure 8B, Paper I). Competition between PC3 nuclear extract and HpsPr-C for the binding to the target sequence was observed, HpsPr-C produced a 22% decrease in the binding at 100X (lane 3) and 42% at 500X-fold excess (lane 4). It is worth mentioning the appearance of a band in the lowest part of the electrophoresis when using the PPRH (lanes 3 to 5), probably corresponding to the binding between the PPRH and its target sequence, which presented a faster mobility because of its lower molecular weight. We performed competition assays using the GATA-consensus sequence (lanes 6 to 8) to determine that the main band observed when incubating with PC3 nuclear extracts corresponded to the binding of the GATA transcription factor. A decrease of around 60% in the intensity of the band was observed at the maximum concentration. As the GATA family is composed of various members, we performed supershift assays using antibodies against GATA-2 and GATA-3, because they were the most abundant members in prostate tissue (Perez-Stable et al. 2000). Using the GATA-2 antibody we did not observe any supershift (lane 9 and 10), while in lane 11, 12 and 13, where the antibody against GATA-3 was used, a weak upper band corresponding to the binding of the antibody was observed, proving GATA-3 was implicated in the binding.

These results corroborated those obtained using HeLa nuclear extracts, and demonstrated that the mechanism of action of PPRHs is independent of cell line. PPRHs against promoter sequences might prevent binding of transcription factors specific for their target sequences in a sequence-specific manner.

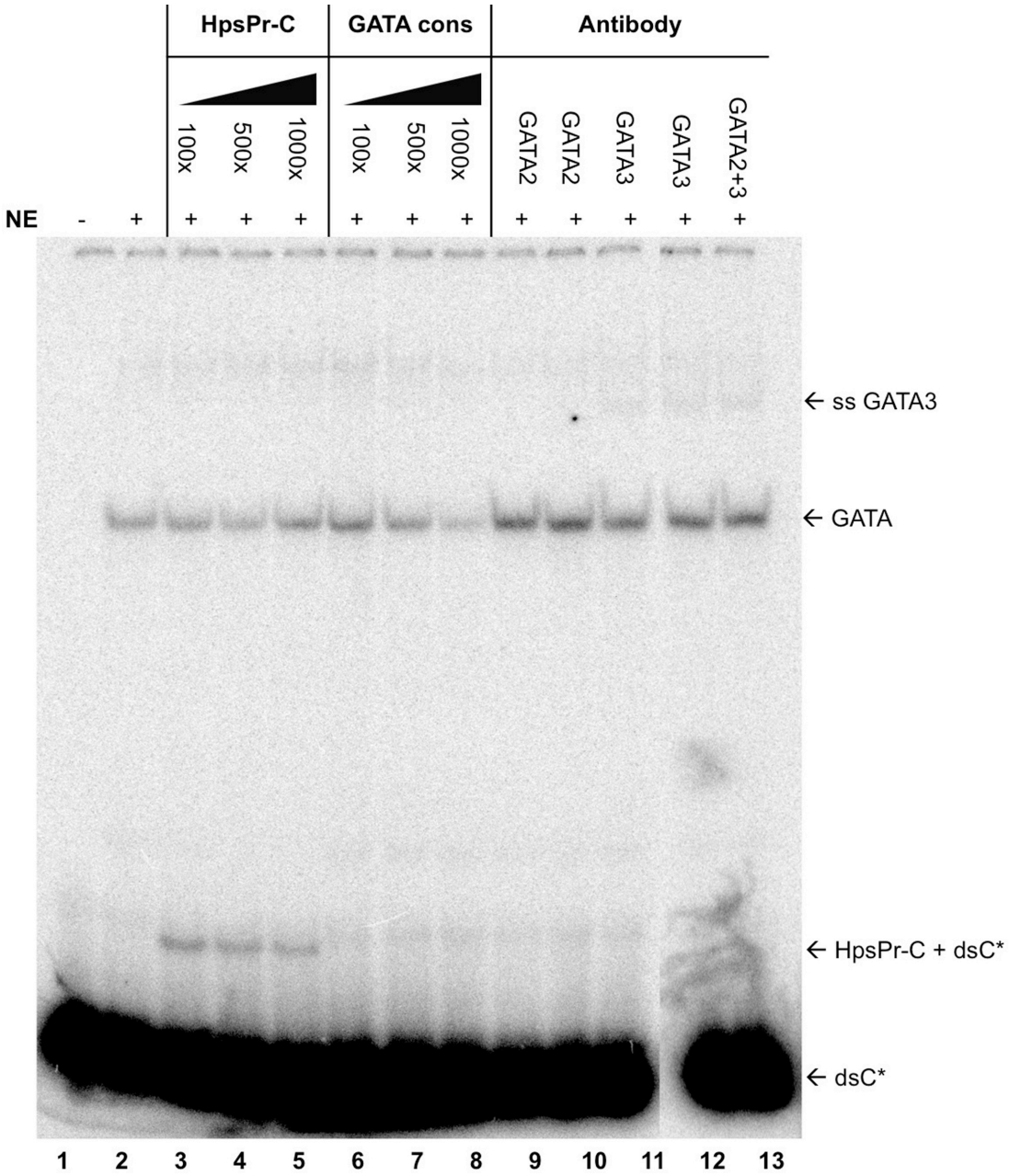

Figure 12. Binding of transcription factors to HpsPr-C target sequence. EMSA assays were conducted using the radiolabeled target sequence ds-C (20,000 cpm), Herring Sperm DNA as non-specific competitor and PC3 nuclear extracts. The binding pattern using PC3 nuclear extracts is shown in lane 2. Competition assays were performed using 100, 500 and 1000-fold excess of HpsPr-C (lane 3-5) or 100, 500 and 1000-fold excess of GATA consensus sequence (lanes 6-8). Supershift assays in the presence of two different amounts of antibodies against GATA-2 (2 µg, lane 9 and 4 µg, lane 10), GATA-3 (2 µg, lane 11 and 4 µg, lane 12) and 2 µg of each antibody (lane 13). Shifted and supershifted (ss) bands are indicated by arrows.

4.1.1.2. Broadening the application of *survivin* PPRHs to other cancer types

Cellular uptake of PPRHs in HCT116 and MiaPaCa 2 cells

We also studied the uptake of PPRHs in HCT116 and MiaPaCa 2 by flow cytometry. In Table 6 are displayed the percentage of FITC+ cells and the mean intensity of the cells, 24 after transfection with a fluorescent PPRH, either using DOTAP or without vehicle (with the intention to compare, we added the values of PC3 cells to the table). We used the best ratio to transfect PPRHs, corresponding to 1:100 (100nM PPRH with 10μM DOTAP), previously determined in PC3 cells (Rodriguez et al. 2013). At this ratio and concentration, we observed around 90% of fluorescent cells in the 3 cell lines. However, the mean intensity value varied from one cell line to another, indicating a different efficiency of transfection. Relative to MiaPaCa 2 cell line, which is the cell line with less mean intensity of fluorescence, PC3 internalized 9.7-fold more PPRH and HCT116 4-fold more PPRH. A low percentage of cells displayed a very low value of mean fluorescence when incubating the FITC-PPRH without DOTAP, indicating almost none PPRH entered the cells without vehicle.

Table 6. Percentage (%) FITC+ cells and Mean intensity of FITC fluorescence of PC3, HCT116 and MiaPaCa 2 cells. Cells were analyzed by flow cytometry 24 after transfection of a fluorescent PPRH, either using 10μM DOTAP or without vehicle. Data represent the mean ± SE of at least three experiments.

	PC3		HCT116		MiaPaCa 2	
SAMPLE	**%FITC+ CELLS**	**MEAN INTENSITY**	**%FITC+ CELLS**	**MEAN INTENSITY**	**%FITC+ CELLS**	**MEAN INTENSITY**
CONTROL	0.45 ± 0.13	1.00 ± 0.00	0.29 ±0.14	1.00 ±0.00	1.62 ±0.89	1.00 ±0.00
HpF 100nM +DOTAP	90.18 ±2.86	555.33 ±166.94	90.80 ±6.15	241.05 ±81.06	85.05 ±6.32	57.14 ±24.84
HpF 100nM	4.27 ±1.13	3.11 ±0.63	5.53 ±4.53	10.60 ±7.11	18.77 ±15.09	1.52 ±1.17

Figure 13 shows an overlay of the mean intensity of fluorescence for the 3 cells lines. Populations of fluorescent cells were displaced towards the right part of the x-axis, thus indicating a higher FITC intensity caused by internalization of the fluorescent PPRH. It is worth mentioning that this displacement was higher for

PC3 than for HCT116, and the one with the lower intensity corresponded to MiaPaCa 2.

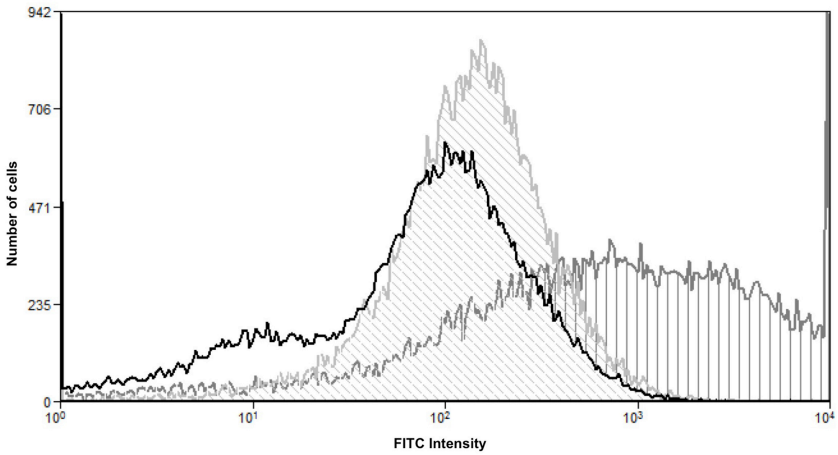

Figure 13. Representative image of the uptake showing an overlay of the 3 cell lines. MiaPaCa 2 (black line), HCT116 (light grey) and PC3 (dark grey) cells treated with 100 nM of FITC-PPRH and 10μM of DOTAP.

Effects of PPRHs on cell viability

As we have previously stated in the introduction section, *survivin* is a good antitumoral target in different types of cancers, including prostate, pancreas and colon. For this reason, we decided to reproduce the experiments of cell viability and apoptosis in cancer cell lines from these tissues. We tested the different PPRHs designed against *survivin* in HCT116 from colon cancer and MiaPaCa 2 from pancreatic cancer.

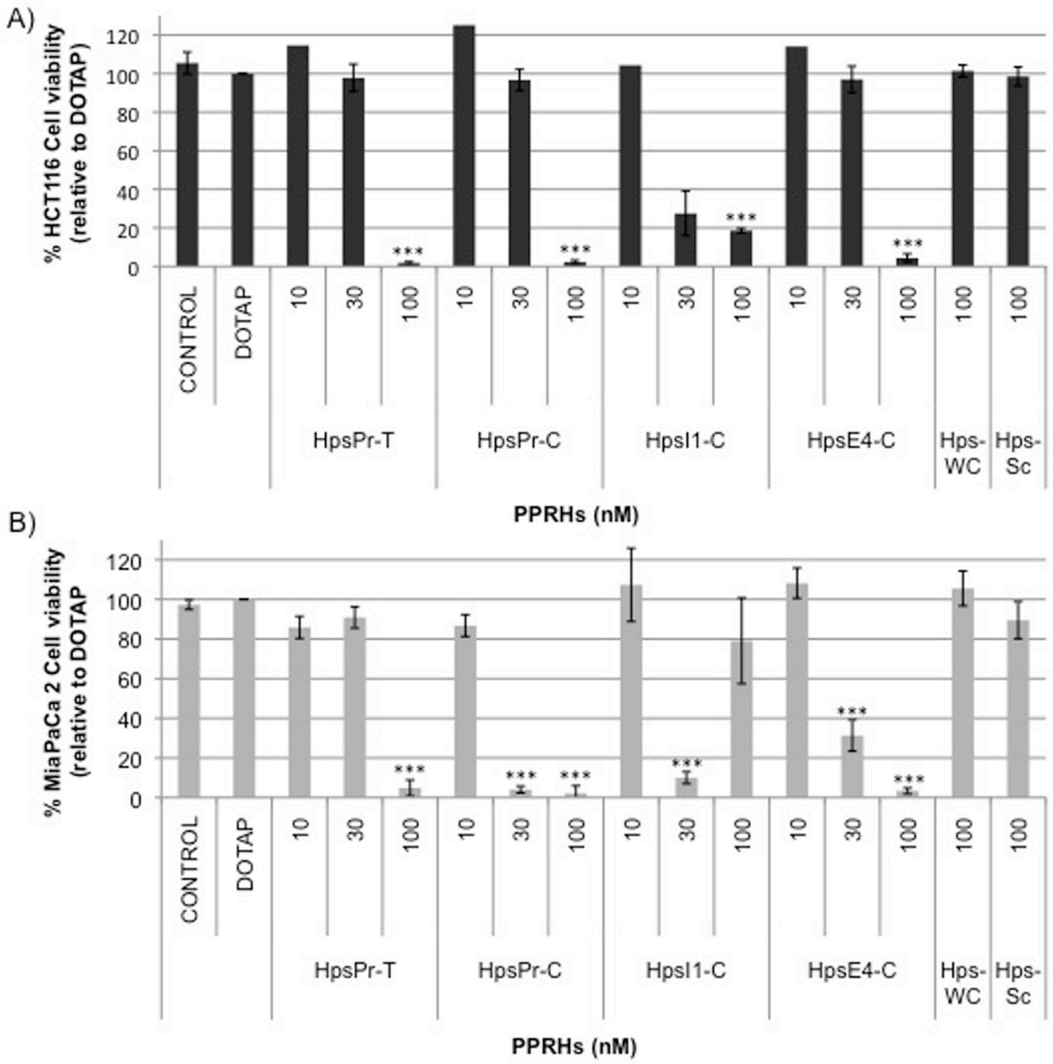

Figure 14. Effect of PPRHs against *survivin* on the viability of HTC116 and MiaPaCa 2 cells. MTT assays to determine cell survival were performed 6 days after transfection. A) Dose response of the four designed PPRHs against the *survivin* gene and negative controls -Hps-WC and Hps-Sc- in HCT116 cells. B) Dose response of the four designed PPRHs against the *survivin* gene and the negative controls -Hps-WC and Hps-Sc- in MiaPaCa 2 cells. DOTAP was used at 5μM to transfect the PPRHs at 10 and 30 nM, and at 10μM to transfect 100 nM PPRH. Data are mean ±SE values of at least three experiments. *p<0.05, **p<0.01, ***p<0.005.

Figure 14 shows the effect on cell viability of these PPRHs. A dose-response effect was observed for all PPRHs with the exception of HpsI1-C, which caused more death at 30nM than 100nM in MiaPaCa 2 (also observed in PC3 cells). The effect varied between cell lines, but the PPRHs with a more similar behavior in the three cell lines were those against the promoter sequences, HpsPr-T and HpsPr-C, which caused a decrease of almost 100% in cell viability at 100nM in the 3 cell lines. For HpsE4-C, the effect was higher in HCT116 and MiaPaCa 2 than in PC3. The negative controls, Hps-WC and Hps-Sc, did not cause a decrease in cell viability at 100nM in any of the cell lines tested.

Effects of PPRHs on apoptosis

Figure 15 represents the results using flow cytometry to determine apoptosis, 24h after transfection with the different PPRHs against *survivin* in HCT116 (Fig. 15A) and MiaPaCa 2 cells (Fig. 15B). The most significant increase in the percentage of apoptotic cells was obtained upon transfection of HpsPr-C in both cell lines, reaching values of 53% HCT116 apoptotic cells and 41% MiaPaCa 2 apoptotic cells. This correlated with the results obtained in PC3 cells, with 54% of apoptotic cells with this PPRH (Fig.4, Article I). HpsE4-C also caused an increase in apoptosis (39% in HCT116 and 20% in MiaPaCa 2, respectively), similar to that caused in PC3 (22% of apoptotic cells). On the other hand, HpsPr-T and HpsI1-C caused a very slight increase in apoptosis in all cell lines. It is worth mentioning that the percentage of apoptotic cells using MiaPaCa 2 was lower than using HCT116, and that might be related to the different uptake of PPRHs previously observed.

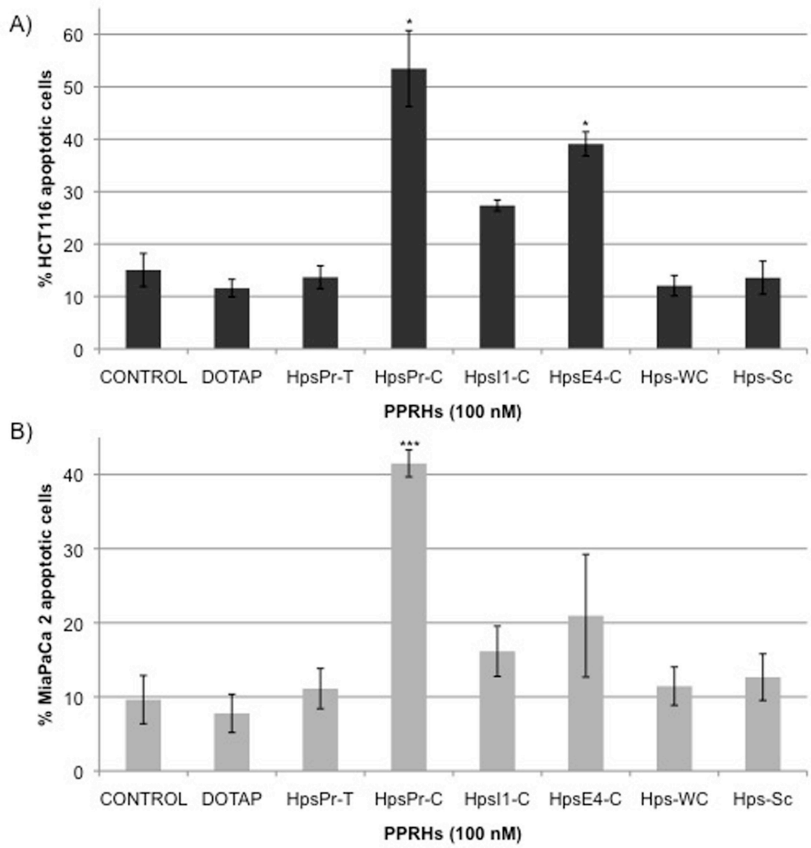

Figure 15. Effect of PPRHs against *survivin* on apoptosis. Cells were transfected with 100 nM of HpsPr-T, HpsPr-C, HpsE4-C and HpsI1-C against the *survivin* gene and two negative controls –Hps-WC and Hps-Sc. 24 hours after transfection, apoptosis was measured by the rhodamine method. Cells Rho123-negative and IP-negative were considered as apoptotic cells. A) HCT116 apoptotic cells B) MiaPaCa 2 apoptotic cells. Data represent the mean ± SE of at least three experiments. *p<0.05, **p<0.01, ***p<0.005.

4.1.1.3. Bcl-2 as another anti-apoptotic target in solid tumors

Design of PPRHs against Bcl-2

We designed Template and Coding-PPRHs against *Bcl-2* to conduct a comparison study. Specifically, HpBcl2Pr-C was directed against the promoter, HpBcl2E1-C against exon 1 and the other two PPRHs against intron 2, one against the template (HpBcl2I2-T) and one against the coding strand (HpBcl2I2-C). The PPRHs sequences are listed in Table 4, in the Materials and Methods section 3.1.3. The location of their target sequences within the *Bcl-2* gene is depicted in Figure 16.

Figure 16. Scheme representing the target sequences of the PPRHs against the *Bcl-2* gene. Four PPRHs were designed against the *Bcl-2* gene, one directed toward the promoter (HpBcl2Pr-C), one against exon 1, specifically the 5'UTR (HpBcl2E1-C) and two other PPRHs against intron 2, one template (HpBcl2I2-T) and one coding (HpBcl2I2-C). Nomenclature used was Hp (Hairpin), Bcl2 (*Bcl2*), Pr (promoter), I (intron), E (exon). The numbering below the PPRHs corresponds to the start of the target sequence location in the gene referred to the transcriptional start site. The arrows indicate the length of each gene element.

Effects of PPRHs on cell viability

Dose-response studies using the four designed PPRHs and negative controls were performed in three different cell lines: PC3 (prostate cancer), MiaPaCa 2 (pancreatic cancer) and HCT116 (colon cancer). The resulting cell viabilities are shown in Figure 17. In PC3 cells (dark grey bars), the four PPRHs caused a significant effect, but the most effective were two Coding-PPRHs, one directed against the promoter sequence, HpBcl2Pr-C, and one against exon 1, HpBcl2E1-C, with more than 80% decrease in cell viability at 30nM. These two PPRHs were also the most effective in the other two cell lines, causing more than 95% of cell death already at 30nM in MiaPaCa 2 (light grey bars) and HCT116 (black bars) cells. The two PPRHs directed against intron 2 did not show a great effect in any cell line.

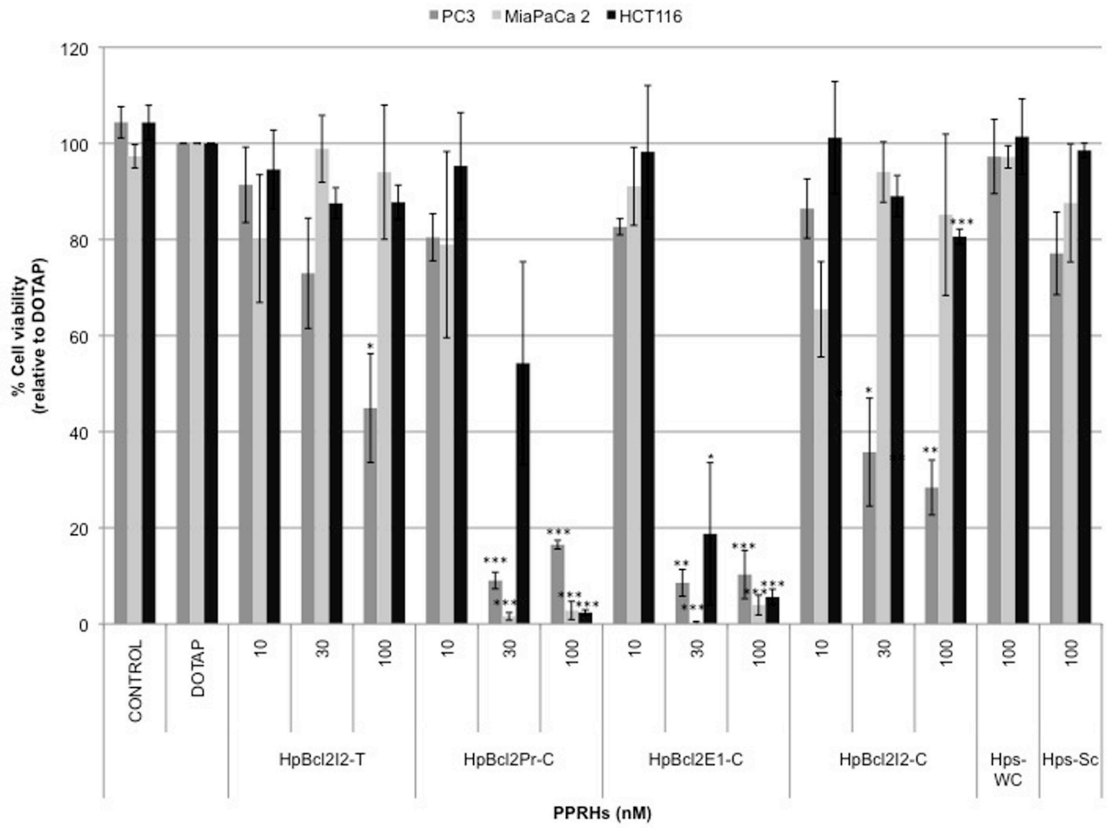

Figure 17. Effect of PPRHs against *Bcl-2* on cell viability. MTT assays to determine cell survival were performed 6 days after transfection. Dose response of the four designed PPRHs against the *Bcl-2* gene and the negative controls-Hps-WC and Hps-Sc- in PC3, MiaPaCa 2 and HCT116 cells. DOTAP was used at 5μM to transfect the PPRHs at 10 and 30 nM, and at 10μM for 100 nM PPRH. . Data represent the mean ± SE of at least three experiments. *p<0.05, **p<0.01, ***p<0.005.

PPRHs against *Bcl-2* were also tested in CT26 cells at the most effective concentration, 100nM. CT26 cells were used as a negative control because they express murine *Bcl-2* and should not be sensitive to PPRHs designed against the human gene. Figure 18 shows no decrease in this murine cell line viability upon transfection of the four PPRHs against human *Bcl-2*.

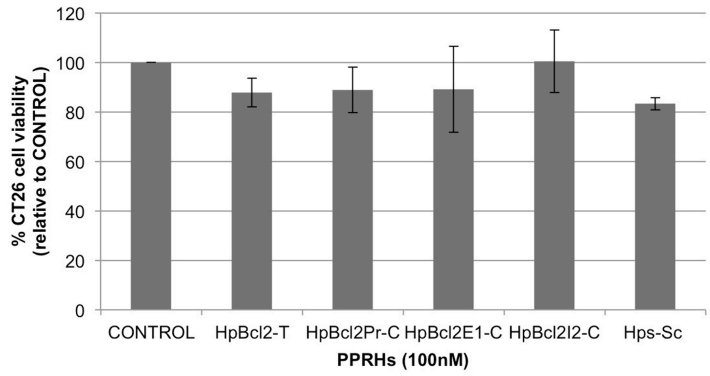

Figure 18. Effect of PPRHs against *Bcl-2* on cell viability. MTT assays to determine cell survival were performed 6 days after transfection. Cell viability upon transfection of 100nM of PPRHs in CT26. DOTAP was used at 10μM. Data are mean ±SE values of at least three experiments.

Effects of PPRHs on apoptosis

Apoptosis was measured by two methodologies: the rhodamine method (Figure 19A) and the caspase-3 activity assay (Figure 19B) as detailed in Materials and Methods, section 2.14, Article I. These assays were used to establish a connection between inhibition of *Bcl-2* and its anti-apoptotic function. Both approaches showed a similar pattern for the PPRHs tested, which can be correlated with the effect on cell viability. The PPRHs that caused a higher decrease in cell viability were those causing a higher increase in apoptosis, namely HpBcl2Pr-C and HpBcl2E1-C. Using flow cytometry, transfection at 100nM of PPRHs induced apoptosis up to 30-50% of the cell population in the three cell lines. Using the caspase-3 assay, these two PPRHs caused a 2-fold increase in PC3 cells (dark grey bars), a 4-fold increase in MiaPaCa 2 cells (light grey bars) and reached 5-fold (HpBcl2Pr-C) and 7-fold (HpBcl2E1-C) in HCT116 cells (black bars). It is important to note that the higher values for both assays were obtained with the HCT116 cell line, probably indicating a higher susceptibility of these cells to apoptosis through silencing of *Bcl-2* (HCT116 had the highest expression of *Bcl-2*, compared to the two other cell lines, as determined by qRT-PCR (data not shown)).

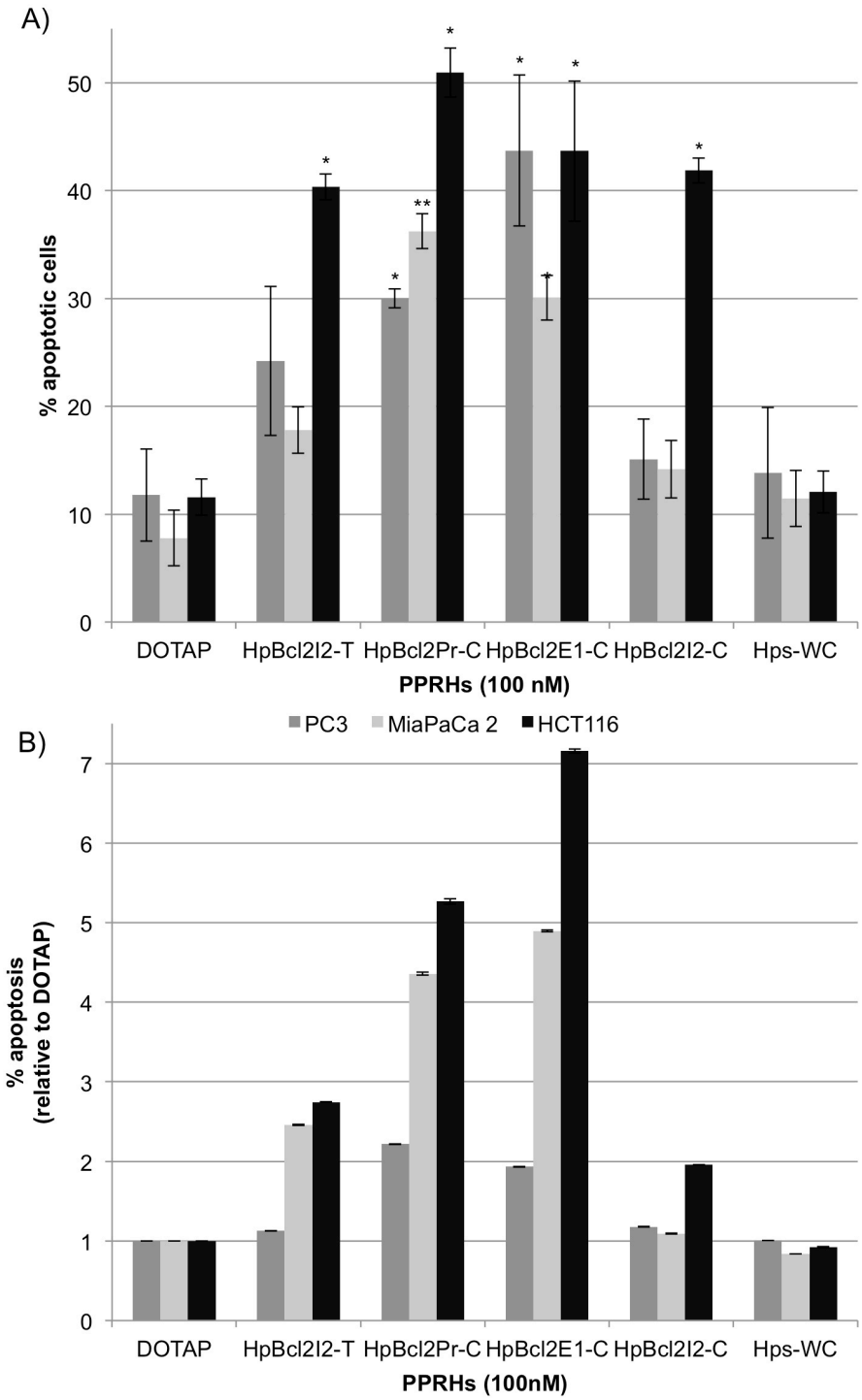

Figure 19. Effect of PPRHs against *Bcl-2* on apoptosis. PC3 cells were transfected with 100 nM of PPRHs against *Bcl-2* and the negative control- Hps-WC. 24 hours after transfection, apoptosis was measured by two methods. A) Rhodamine method: Cells Rho123-negative and IP-negative were considered as apoptotic cells. Data represent the mean ± SE of at least three experiments. *p<0.05, *p<0.01. B) Caspase-3/7 assay: Fold change in RLU relative to DOTAP.

Effects of PPRHs on Bcl-2 mRNA and protein levels

We evaluated the effect of a dose-response of HpBcl2E1-C on *Bcl-2* mRNA levels in PC3 cells (Figure 20A).

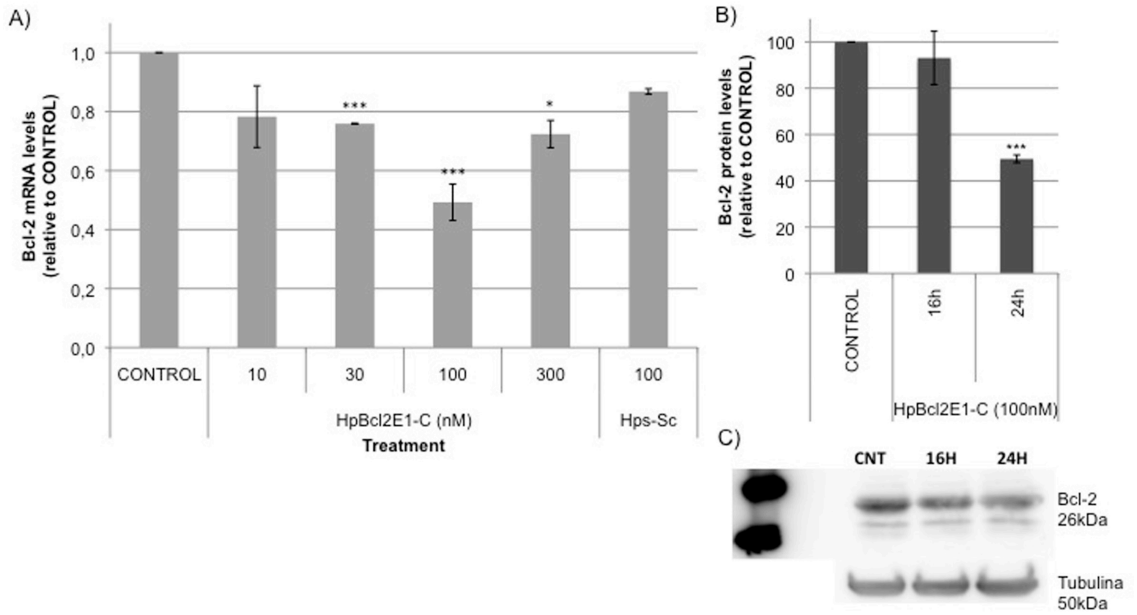

Figure 20. *Bcl-2* mRNA and protein levels. A) RNA was extracted from PC3 cells after treatment with increasing concentrations of HpBcl2E1-C. mRNA levels were determined using qRT-PCR and referred to the levels of endogenous controls. B) PC3 cells were incubated with 100nM of HpBcl2E1-C for 16 and 24h. Total protein extracts were obtained and analyzed by Western Blot. Protein levels were normalized using tubulin. C) Representative image of a Western blot showing Bcl-2 and tubulin (endogenous control) protein levels in PC3 after incubation with HpBcl2E1-C. Data represent the mean ± SE of at least three experiments. *p<0.05, **p<0.01, ***p<0.005.

At a concentration of 100nM, HpBcl2E1-C caused a 2-fold decrease of *Bcl-2* mRNA levels, 24h after transfection (Figure 20A), that was reflected in a 2-fold decrease of Bcl-2 protein levels (Figure 20B and C). Even though the decrease in mRNA levels at 300nM was significant, it was inferior to 100nM. This could be explained by the fact that the best ratio to complex the PPRH with DOTAP is 1:100 (PPRH:DOTAP) but the maximum concentration for DOTAP without causing toxicity is 10µM. Therefore, this best ratio is only applicable when using 100nM, because at 300nM, the ratio is 1:33.

4.1.1.4 Mechanism of action of a Template-PPRH against an intronic sequence of the *DHFR* gene

Previously in our group, it was suggested that a Template-PPRH against an intronic sequence of the DHFR gene (HpdI3-B) caused a decrease in gene expression by inhibition of mRNA elongation, the same mechanism as TFOs (de Almagro et al. 2009). Nevertheless, further proof was needed to affirm the mechanism of action for this template PPRH. We rationalize that if the decrease in expression caused by the PPRH was due to a decrease in transcription, this effect would be observed after the site where the PPRH was bound to the DNA target. Therefore, PCR amplification of a sequence upstream of the PPRH target would not decrease in the presence of the PPRH, whereas amplification of a downstream sequence would decrease in these conditions.

To address that issue, we tested the effect of HpdI3-B in PC3 cells through the analysis of *DHFR* mRNA levels with three different sets of primers.

- DHFR exon3-exon 4 primers: complementary to the mRNA sequence.
- pre-PPRH primers: complementary to the pre-mRNA sequence.
- post-PPRH primers: complementary to the pre-mRNA sequence.

Table 7. Primer sequences for *DHFR* mRNA and pre-mRNA amplification.

Primers		Sequence (5'-3')
DHFR	Forward	GAAGACCTGGTTCTCCATTCC
	Reverse	TGCCACCAACTATCCAGACC
Pre-PPRH	Forward	ACCTGGTCCCTGTAACTGC
	Reverse	CAGGCTGGAAAAAGACATGGTG
Post-PPRH	Forward	GGGAGGAGGCAATCAAGAGA
	Reverse	GTCAAGTTTTTAGCCTGGTGC

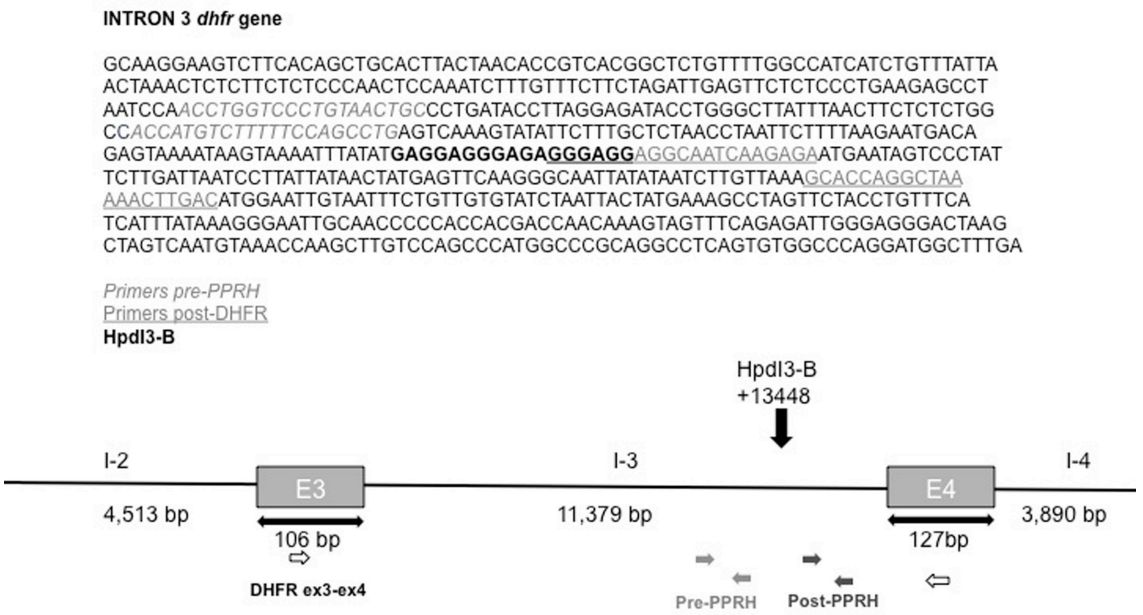

Figure 21. Sequence and design of the PPRH and primers used to study the mechanism of action.

We analyzed mRNA levels 3h after transfection of the PPRH, in order to see a decrease in pre-mRNA levels, which were meant to occur early than the normal timing for mRNA analysis (24 or 48h). We also analyzed the cytotoxicity caused by HpdI3-B in PC3 cells, using the selective medium -GHT. DHFR inhibition in these culture conditions will cause cell death, due to the lack of the final products of DHFR enzymatic activity, and thus, the inability of cells to synthesize DNA.

In Figure 22, we observed that this PPRH caused a reduction in cell viability at 100nM and was able to decrease *DHFR* mRNA levels 1.4-fold, 3 hours after transfection. The analysis of the pre-mRNA levels upstream and downstream of the PPRH binding site showed a decrease in pre-mRNA levels when using the primers post-PPRH, indicating that the presence of the PPRH prevent elongation of the mRNA from the sequence where the PPRH was bound.

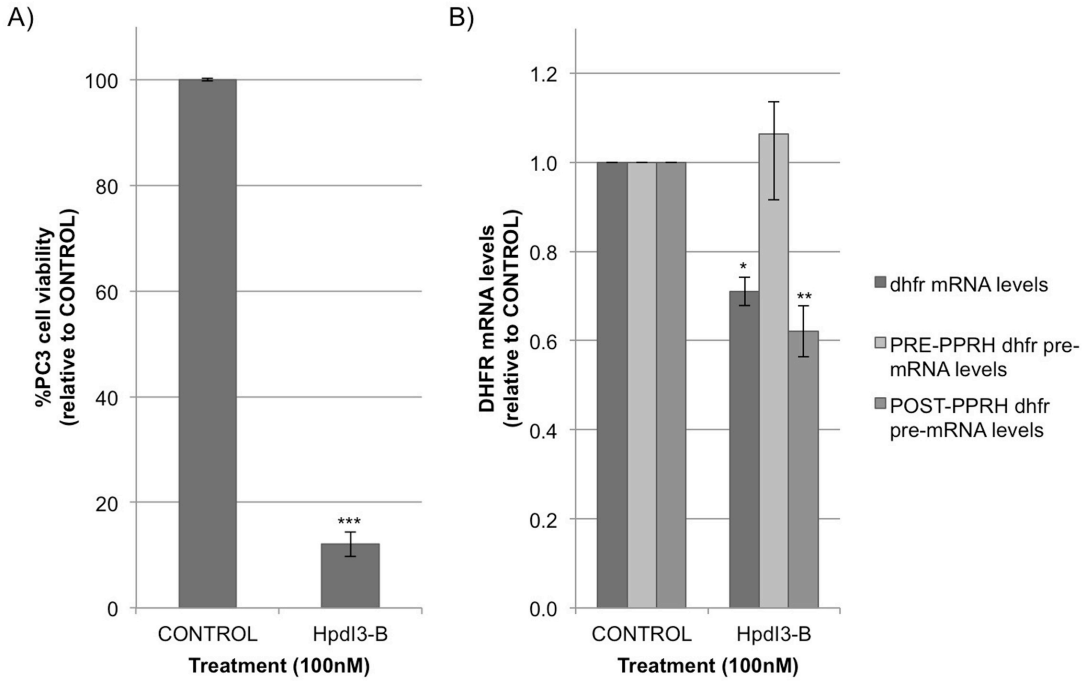

Figure 22. Effect of HpdI3-B on cell viability and *DHFR* mRNA and pre-mRNA levels. A) 100nM of HpdI3-B was transfected in PC3 cells. DOTAP was used at 10μM. MTT assays to determine cell survival were performed 6 days after transfection. B) RNA was extracted from PC3 cells 3 hours after treatment with 100nM of HpdI3-B. mRNA and pre-mRNA levels were determined using qRT-PCR and referred to the levels of endogenous controls. Data represent the mean ± SE of at least three experiments. *p<0.05, **p<0.01, ***p<0.005.

4.2. Article II:

IMPROVED DESIGN OF PPRHs FOR GENE SILENCING

Laura Rodríguez, Xenia Villalobos, Anna Solé, Carolina Lliberós,
Carlos J. Ciudad and Véronique Noé

Molecular Pharmaceutics, 2015, doi: 10.1021/mp5007008 (impact factor **4.787**)

Background

In a previous work, we studied in-depth the mechanism of action and efficacy of PPRHs against promoter sequences of the *survivin* gene. Despite these PPRHs worked efficiently without causing known off-target effects, the use of PPRHs carrying adenines confronting the purine interruptions in the polypyrimidine target could raise some concern on specificity. Previous studies in our group had shown that when a single interruption occurred, the usage of an adenine in front of the interruption in both domains of the PPRH, maintained the binding to the target while keeping the homopurine nature of the PPRH (Coma et al. 2005). That is, adenines can be used as wild cards at the time of designing PPRHs. Later, a functional study of PPRHs against *DHFR* was performed in terms of cell viability and mRNA determination. PPRHs carrying adenines in front of the purine interruptions proved to be efficient (de Almagro et al. 2009). It is important to bear in mind that target sequences usually have more than one interruption, and the higher the number, the higher the possibility of off-target effects.

Objectives

In this work, we studied different characteristics of PPRHs, namely length and interruptions, with the aim to improve their applicability as gene silencing tools. We also compared PPRHs to non-modified TFOs, and designed a new molecule, the Wedge-PPRH, based on PPRHs.

Results

First, we compared PPRHs with different lengths (20, 25 and 30 nt) against an intronic sequence of the *TERT* gene, in terms of binding and cell viability. We

observed that even though all of them were able to bind to the target sequence, the longer the PPRH, the higher the effect in terms of decrease in cell viability.

Secondly, we conducted a comparison between PPRHs and non-modified TFOs. TFOs are polypurine single-stranded oligonucleotides with gene silencing capabilities. We proved that the presence of the hairpin structure provided PPRHs with the advantages of higher affinity of binding and higher efficacy.

To avoid possible off-target effects, we explored the possibility of using Wild-type PPRHs, which carry the complementary base of the interruption in both strands of the PPRH. Comparison with the regular PPRHs showed that Wild-type PPRHs had a higher binding affinity to their target sequence and produced a higher decrease in cell viability.

Finally, we developed a new molecule called Wedge-PPRH based on PPRHs but with a 5' extension that made possible the formation of a locked structure with the double-stranded DNA. This molecule proved to decrease cell viability in prostate and breast cancer cell lines.

Conclusions

As a summary, we established different properties to be considered when designing PPRHs, such as length and mismatch substitution. We also proved PPRHs to be more efficient than TFOs, and designed a brand new molecule.

molecular pharmaceutics

Article

pubs.acs.org/molecularpharmaceutics

Improved Design of PPRHs for Gene Silencing

Laura Rodríguez, Xenia Villalobos, Anna Solé, Carolina Lliberós, Carlos J. Ciudad, and Véronique Noé*

Department of Biochemistry and Molecular Biology, School of Pharmacy, University of Barcelona, 08028 Barcelona, Spain

ABSTRACT: Nowadays, the modulation of gene expression by nucleic acids has become a routine tool in biomedical research for target validation and it is also used to develop new therapeutic approaches. Recently, we developed the so-called polypurine reverse Hoogsteen hairpins (PPRHs) that show high stability and a low immunogenic profile and we demonstrated their efficacy both in vitro and in vivo. In this work, we explored different characteristics of PPRHs to improve their usage as a tool for gene silencing. We studied the role of PPRH length in the range from 20 to 30 nucleotides. We also proved their higher affinity of binding and efficacy on cell viability compared to nonmodified TFOs. To overcome possible off-target effects, we tested wild-type PPRHs, which proved to be capable of binding to their target sequence with more affinity, displaying a higher stability of binding and a higher effect in terms of cell viability. Moreover, we developed a brand new molecule called Wedge-PPRH with the ability to lock the ds-DNA into the displaced structure and proved its efficacy in prostate and breast cancer cell lines.

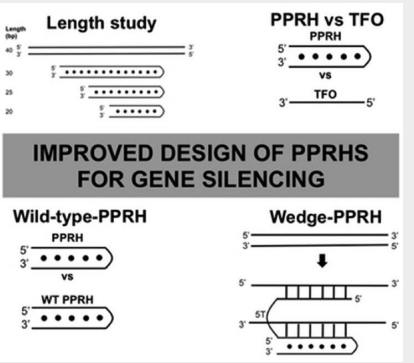

KEYWORDS: *gene silencing, PPRH, wild-type, Wedge-PPRH, nucleic acid*

INTRODUCTION

In 1957, Felsenfeld described the existence of triple-stranded nucleic acids[1] and K. Hoogsteen justified triplex formation with the finding of Hoogsteen bonds.[2] These discoveries prompted the development of a gene-silencing tool called triplex forming oligonucleotides (TFOs), capable of binding to the purine strand in the major groove of the double helix by hydrogen bonds. The study of their mechanism of action concluded that TFOs interfered with the transcription process.[3−5] Purine TFOs have several advantages over pyrimidine TFOs because they bind to their target sequence in a pH-independent manner, with higher affinity and faster kinetics.[6] Kool and colleagues found out that purine sequences in a hairpin or a circular structure could form triplexes with their single-stranded pyrimidine target sequence with a higher binding affinity.[7]

All these studies led us to develop the polypurine reverse Hoogsteen hairpins (PPRHs), which are composed of two antiparallel polypurine domains, which form intramolecular reverse-Hoogsteen bonds linked by a five-thymidine loop, therefore forming a hairpin structure. PPRHs are capable of binding to polypyrimidine stretches in the DNA, causing strand displacement.[8] Template-PPRHs are directed against the template strand and cause inhibition of transcription.[9] Coding PPRHs are directed against the coding strand and can also bind to the mRNA. Depending on the location of the target sequence, either in introns or promoters, PPRHs act through different mechanisms. A coding-PPRH against an intronic sequence in the *dhfr* gene caused a splicing alteration by preventing the binding of the splicing factor U2AF65 to its target sequence.[10] PPRHs against promoter sequences, both a template-PPRH (HpsPr-T) and a coding-PPRH (HpsPr-C) directed against two different regions of the *survivin* promoter, prevented the binding of transcription factors specific for the corresponding target sequences -Sp1, Sp3 and GATA-3-, causing a decrease in *survivin* expression.[11]

The main limitation for the design of either TFOs or PPRHs would be the presence of polypurine/polypyrimidine stretches. However, their rate of occurrence in the genome has been proved to be higher than predicted by random models,[12,13] which opens the possibility to design sequence-specific molecules against genes that play important roles in cancer, such as *survivin* or *TERT*.

We have previously studied the role of *survivin* in cancer using siRNAs and ODNs,[14] and more recently, we used PPRHs against *survivin* to validate this new technology both in vitro and in vivo. This approach allowed us to confirm their efficacy in terms of decrease in mRNA and protein levels, resulting in a decrease in cell viability and increase in apoptosis in vitro. Using a xenografted model of prostate cancer we proved that the administration of a PPRH against a promoter sequence in the *survivin* gene caused a reduction in tumor growth, through the decrease in survivin levels and in blood vessel formation, thus establishing the proof of principle for PPRHs usage in vivo.[11]

We have also studied important properties of PPRHs and concluded that they are less immunogenic and much more stable than siRNAs.[15] Even though these advantages make PPRHs an attractive tool for gene silencing, there is room for improvement.

The aim of this work was to further improve PPRHs in terms of affinity and specificity and to compare them with nonmodified TFOs. To do so, we studied the influence of length and

Received: October 17, 2014
Revised: December 16, 2014
Accepted: January 15, 2015

DOI: 10.1021/mp5007008
Mol. Pharmaceutics XXXX, XXX, XXX−XXX

pyrimidine interruptions within the PPRHs and developed the Wedge-PPRH, a brand new molecule based on PPRHs.

MATERIALS AND METHODS

Design and Usage of PPRHs. PPRHs of different length against an intronic sequence of the *telomerase* gene (Table 1) and

Table 1. DNA Oligonucleotides Sequences and PPRHs of Different Lengths against the *Telomerase* Gene

Name*	Sequence (5′-3′)
TERT target sequence	5′ CAGGCAGGACAAGGAAGCGGGAGGAAGGCAGGAGGCTCTT 3′ 3′ GTCCGTCCTGTTCCTTCGCCCTCCTTCCGTCCTCCGAGAA 5′
HptI10-T	5′ AGGAAAAGGAAGAGGGAGGAAGGAAGGAGG 3′ 3′ AGGAAAAGGAAGAGGGAGGAAGGAAGGAGG 5′ 5T
HptI10-T2	5′ AAGGAAGAGGGAGGAAGGAAGGAGG 3′ 3′ AAGGAAGAGGGAGGAAGGAAGGAGG 5′ 5T
HptI10-T3	5′ GAAGAGGGAGGAAGGAAGGA 3′ 3′ GAAGAGGGAGGAAGGAAGGA 5′ 5T

PPRH hairpins against the template strand of intron 10 of the *telomerase* gene (TERT target): HptI10-T, 30 nt carrying three A-substitutions in place of the pyrimidine interruptions in each domain. HptI10-T2, 25 nt carrying two A-substitutions and HptI10-T3, 20 nt carrying two A-substitutions. Interruptions are marked in bold. Bullets represent reverse-Hoogsteen bonds and lines Watson−Crick bonds.

PPRHs and nonmodified TFOs against promoter sequences of the *survivin* gene (Table 2) were used in these experiments. The Triplex-Forming Oligonucleotide Target Sequence Search software (M.D. Anderson Cancer Center, Houston, TX) (www.spi.mdanderson.org/tfo/) was used to find polypurine sequences and BLAST software was carried out to confirm the specificity of the designed molecules. The nomenclature used in this study was: Hp for PPRH hairpin; s for survivin; t for TERT; Pr for promoter; I10 for intron 10; T for template-PPRH; C for coding-PPRH; and WT for wild type. Wedge-PPRHs were designed by extending the 5′ end of HpsPr-T WT, with a pyrimidine sequence complementary to the upper strand that is displaced by the PPRH (Table 3). PPRHs were synthesized as nonmodified oligodeoxynucleotides by Sigma-Aldrich (Madrid, Spain) (0.05 μmol scale; DESALT-unmodified and desalted). Lyophilized PPRHs were resuspended in sterile Tris-EDTA buffer (1 mM EDTA and 10 mM Tris, pH 8.0) and stored at −20 °C.

Preparation of Polypurine/Polypyrimidine Duplexes. The duplexes to be targeted by the hairpins corresponded to the intronic sequence within the *TERT* gene (Table 1) and two promoter sequences of the *survivin* gene (Table 2). The single-stranded molecules were purchased from Sigma and resuspended in Tris-EDTA buffer. To make the duplexes, 25 μg of each single-stranded (ss) polypurine and polypyrimidine oligodeoxynucleotides were incubated with 150 mM NaCl at 90 °C for 5 min as described by de Almagro et al.[9]

Oligodeoxynucleotide Labeling. One hundred nanograms of PPRHs or double stranded (ds) oligodeoxynucleotides were 5′-end-labeled with T4 polynucleotide kinase (New England Biolabs, Beverly, MA) and [γ-^{32}P]ATP as described by de Almagro et al.[9]

Table 2. DNA Oligonucleotides Sequences, PPRHs, and TFOs Directed against the *Survivin* Gene

Name*	Sequence (5′-3′)
Template-PPRHs and Coding-TFO against the *survivin* promoter sequence at -1009	
Target sequence	5′ ATTAAAGAATGGGGGCGGGGTGGGAGGGGTGG 3′ 3′ TAATTTCTTACCCCCGCCCCACCCTCCCCACC 5′
HpsPr-T	5T AAAGAAAGGGGGAGGGGAGGGAGGGG 3′ AAAGAAAGGGGGAGGGGAGGGAGGGG 5′
HpsPr-T WT	5T AAAGAATGGGGGCGGGGTGGGAGGGG 3′ AAAGAATGGGGGCGGGGTGGGAGGGG 5′
TFO-sPr-C	5′ GGGGAGGGAGGGGAGGGGGAAAGAAA 3′
Coding-PPRHs and Template-TFO against the *survivin* promoter sequence at -525	
Target sequence	5′ CTGCTGCACTCCATCCCTCCCCTGTT 3′ 3′ GACGACGTGAGGTAGGGAGGGGACAA 5′
HpsPr-C	5T GAAGAGAGGAAGGGAGGGGA 3′ GAAGAGAGGAAGGGAGGGGA 5′
HpsPr-C WT	5T GACGTGAGGTAGGGAGGGGA 3′ GACGTGAGGTAGGGAGGGGA 5′
TFO-sPr-T	5′ GAAGAGAGGAAGGGAGGGGA 3′
Negative controls	
Hps-WC	5′ CCCCTCCCTCCCCTCCCCCTTTCTTT 3′ 5T 3′ GGGGAGGGAGGGGAGGGGGAAAGAAA
Hps-Sc	5′ AAGAGAAAAAGAGAAAGAAGAGAGGG 3′ 5T 3′ AAGAGAAAAAGAGAAAGAAGAGAGGG
TFO-Sc	5′ GGAAAAAGGAGGA 3′

*PPRH hairpins and TFO against the *survivin* promoter at −1009: HpsPr-T, 26 nt carrying three A-substitutions in place of the pyrimidine interruptions in each domain; HpsPr-T WT 26 nt carrying the corresponding three pyrimidine interruptions in each domain; TFO-sPr-C carrying three A-substitutions in place of the pyrimidine interruptions. PPRH hairpins and TFO against the *survivin* promoter at −525: HpsPr-C, 20 nt carrying three A-substitutions in place of the pyrimidine interruptions in each domain; HpsPr-T WT 20 nt carrying the corresponding three pyrimidine interruptions in each domain; TFO-sPr-T carrying three A-substitutions in place of the pyrimidine interruptions. Negative controls: Hps-WC is a hairpin with intramolecular Watson−Crick bonds; Hps-Sc is a hairpin with intramolecular reverse-Hoogsteen bond and no target in the genome; TFO-Sc is a polypurine sequence and no target in the human genome. Interruptions are marked in bold. Bullets represent reverse-Hoogsteen bonds and lines Watson−Crick bonds.

PPRH and TFO DNA Binding Analyses. Binding studies for PPRHs and TFOs were performed using radiolabeled ds-target sequences (20 000 cpm). The radiolabeled sequences were incubated with increasing concentrations (0.1 μM, 1 μM, and 10 μM) of each PPRH or TFO in a buffer containing 10 mM $MgCl_2$, 100 mM NaCl, and 50 mM HEPES, pH 7.2 and 0.5 μg of poly dI-dC (Sigma-Aldrich) as a nonspecific competitor. Binding reactions (20 μL) were preincubated for 5 min at 65 °C, followed by 30 min at 37 °C and then, loaded in nondenaturing 12% polyacrylamide gels (PAGE) containing 10 mM $MgCl_2$, 5% glycerol and 50 mM HEPES, pH 7.2. Electrophoresis was carried

DOI: 10.1021/mp5007008
Mol. Pharmaceutics XXXX, XXX, XXX−XXX

Table 3. Sequence of Wedge-PPRHs against the *Survivin* Gene*

Name	Sequence (5′-3′)
Target sequence	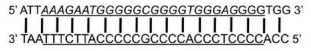
Wedge-PPRH-23	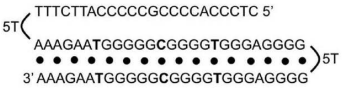
Wedge-PPRH-17	
Wedge-PPRH WC	

*Wedge-PPRH-23 is constituted of HpsPr-T WT with a 23-nt 5′ extension corresponding to the polypyrimidine sequence complementary to the coding strand of the target sequence. Wedge-PPRH-17 is constituted of HpsPr-T WT with a shorter 5′ extension of 17-nt. Wedge-PPRH WC is constituted of Hps-WC with the same 17-nt 5′ extension as Wedge-PPRH-17. Interruptions are marked in bold. Bullets represent reverse-Hoogsteen bonds and lines Watson−Crick bonds.

out for approximately 4 h at 10 V/cm at 4 °C. After drying the gel, it was exposed to Europium plates OVN and analyzed using a Storm 840 Phosphorimager (Molecular Dynamics, Sunnyvale, CA).

UV Absorption Studies. Previous to the analyses, the PPRHs in combination with their single-stranded target sequence (0.5 μM of each strand) were incubated in a buffer containing 100 mM NaCl and 50 mM HEPES, pH 7.2, heated to 90 °C during 5 min, cooled slowly to room temperature, and stored at 4 °C.

Melting experiments were performed using a V-650 Spectrophotometer (Jasco, Madrid, Spain) connected to a temperature controller that increased temperature at a rate of 1 °C/min from 10 to 90 °C. Absorbance of the samples was measured in a 1 cm path length quartz cells.

The MeltWin 3.5 software was used to perform a thermodynamic analysis to calculate melting temperatures (T_m) and free energy values (ΔG) as the mean of two independent melting experiments.

Cell Culture. PC3 prostate adenocarcinoma cells (ECACC), SKBR3 breast adenocarcinoma cells (ATCC) and MiaPaCa-2 pancreas carcinoma cells (ATCC) were cultivated in Ham's F-12 medium supplemented with 7% fetal bovine serum (GIBCO, Invitrogen, Barcelona, Spain) and incubated at 37 °C in a humidified 5% CO_2 atmosphere.

Transfection. The transfection procedure consisted in mixing the appropriate amount of either PPRH or TFO and the transfection reagent DOTAP (Roche, Mannheim, Germany or Biontex, Germany) for 20 min in a volume of 200 μL of medium at room temperature, followed by the addition of the mixture to the cells plated in 35 mm-diameter dishes in a total volume of 1 mL.

MTT Assay. MiaPaCa 2 (5000), PC3 (10 000), or SKBR3 (10 000) cells were plated in 35 mm-diameter dishes in F12 medium and treated with the appropriate concentration of each molecule. After 6 days, MTT assay was performed as described by Rodríguez et al.[11]

mRNA Analyses. A total of 60 000 PC3 or MiaPaCa 2 cells were plated in 35 mm-diameter dishes in F12 medium and total RNA was extracted 48 or 72 h after transfection, using Ultraspec (Biontex) or Trizol (Life Technologies, Madrid, Spain), following the manufacturer's specifications. Quantification of RNA was performed measuring its absorbance (260 nm) at 25 °C using a Nanodrop ND-1000 spectrophotometer.

Reverse Transcription. cDNA was synthesized using 1 μg of total RNA, as described by Rodríguez et al.[11] for *TERT* mRNA levels determination.

For *survivin* mRNA levels, 500 ng were used in a total volume of 20 μL of reaction containing 2 μL of Buffer 10x (500 mM Tris-HCl pH 8.3, 750 mM KCl, 30 mM $MgCl_2$, 100 mM DTT) (Lucigen, Middleton, Wisconsin), 12.5 ng of random hexamers (Roche), 0.5 mM each dNTP (AppliChem, Barcelona, Spain), 20 units of NxGen RNase inhibitor (Lucigen) and 200 units of NxGen M-MuLV reverse transcriptase (Lucigen). The reaction was incubated at 37 °C for 1 h and 3 μL of the cDNA per sample were used for qRT-PCR.

Real Time-PCR. The StepOnePlus Real-Time PCR Systems (Applied Biosystems, Barcelona, Spain) was used to perform these experiments.

SYBR was used to determine *TERT* mRNA levels. Primer sequences were: TERT-Fw, 5′-GCGGAAGACAGTGGTGAACT-3′; TERT-Rv, 5′-AGCTGGAGTAGTCGCTCTGC-3′; and the endogenous control, APRT-Fw, 5′-AAGGCTGAGCTGGAGATTCA-3′; APRT-Rv, 5′-GGTACAGGTGCCAGCTTCTC-3′.

The final volume of the reaction was 20 μL, containing 10 μL of Biotools Mastermix (2X) (Biotools, Madrid, Spain), 1 μL of SYBR (dilution 1/1000, Life technologies), 0.25 μM of each primer, 3 μL of cDNA and H_2O mQ. PCR cycling conditions were 2 min at 50 °C, 10 min denaturation at 95 °C, followed by 35 cycles of 15 s at 95 °C and 1 min at 60 °C.

To determine *survivin* mRNA levels, the following TaqMan probes were used: Survivin (BIRC5) (HS04194392_S1), and adenine phosphoribosyl-transferase (APRT) (HS00975725_M1) and 18S rRNA (HS99999901_S1), as endogenous controls. The reaction contained 1x TaqMan Universal PCR Mastermix (Applied Biosystems), 1x TaqMan probe (Applied Biosystems), 3 μL of cDNA and H_2O mQ to a final volume of 20 μL. PCR cycling conditions were 10 min denaturation at 95 °C, followed by 40 cycles of 15 s at 95 °C and 1 min at 60 °C.

The mRNA quantification was calculated using the $\Delta\Delta C_T$ method, where C_T is the threshold cycle that corresponds to the cycle where the amount of amplified mRNA reaches the threshold of fluorescence.

RESULTS

Design of PPRHs. Different PPRHs were designed to assess the effect of length, their efficacy compared with TFOs, and how to cope with the presence of purine interruptions in the polypyrimidine target sequence. Furthermore, we tested new designs for improving the effectiveness of the PPRHs. The specific design in each case is described below. To test for specificity, we performed BLAST analyses with all PPRHs using as a database the reference genomic sequence of *Homo sapiens*. In

C
DOI: 10.1021/mp5007008
Mol. Pharmaceutics XXXX, XXX, XXX−XXX

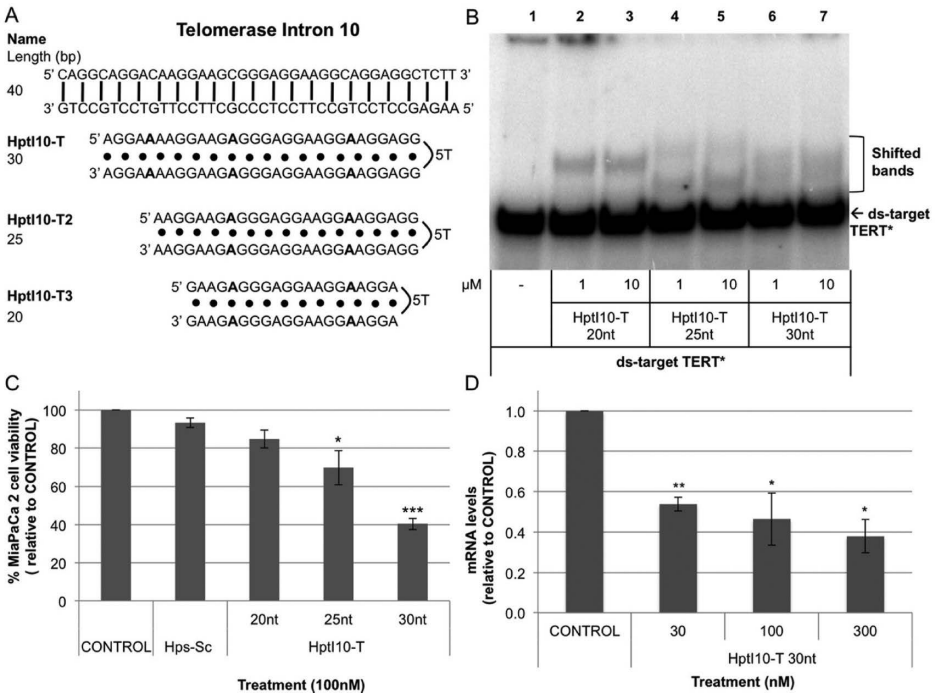

Figure 1. PPRHs of different length: diagram, binding to their target sequence, effect on cell viability, and *TERT* mRNA levels. (A) Representative diagram of the three PPRHs designed against the same intronic sequence of the *TERT* gene, but with different lengths. Bullets represent reverse-Hoogsteen bonds. Interruptions, substituted by adenines, are marked in bold. (B) HptI10-T of different lengths (lane 2 and 3, 20 nucleotides; lane 4 and 5, 25 nucleotides; and lane 6 and 7, 30 nucleotides) was incubated with the radiolabeled ds-target sequence (20 000 cpm) within intron 10 of the *TERT* gene (40 nucleotides). (C) CONTROL cells are untreated MiaPaCa 2 cells. A total of 100 nM of PPRHs against the *TERT* gene were transfected in MiaPaCa 2 cells. DOTAP was used at 10 μM. MTT assays to determine cell survival were performed 6 days after transfection. Data are mean ± SEM values of at least three experiments. *$p < 0.05$, **$p < 0.01$, ***$p < 0.005$. (D) RNA was extracted from MiaPaCa 2 cells treated with increasing concentrations of HptI10-T for 72h. mRNA levels were determined using qRT-PCR and referred to the levels of endogenous controls. Data are mean ± SEM values of at least three experiments. *$p < 0.05$, **$p < 0.01$, ***$p < 0.005$.

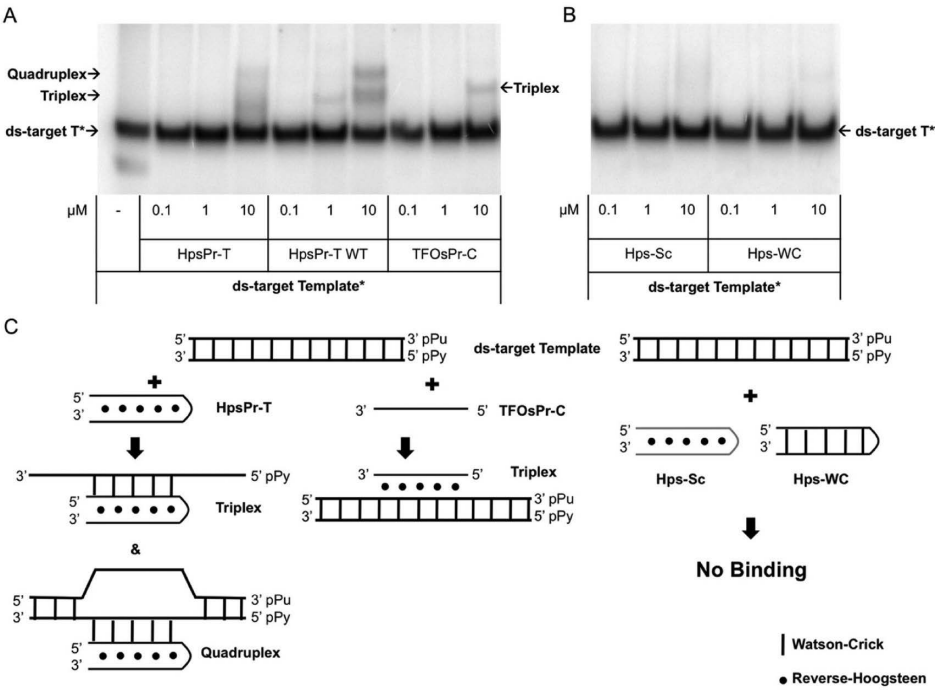

Figure 2. Binding of template-PPRHs and TFO to their target sequence. (A) Binding of the template-PPRH either with adenines in the pyrimidine interruptions (HpsPr-T) or the wild-type version (HpsPr-T WT) and the TFOsPr-C after incubation with increasing concentrations of their radiolabeled ds-target sequence (20 000 cpm). Shifted bands are indicated by arrows. (B) Binding of the negative controls, either Hps-Sc or Hps-WC to the radiolabeled ds-target sequence (20 000 cpm) for the specific PPRHs. (C) Schematic representation of the binding of the different molecules used in this study, including HpsPr-T, HpsPr-T WT, TFOsPr-C, Hps-Sc, Hps-WC.

DOI: 10.1021/mp5007008
Mol. Pharmaceutics XXXX, XXX, XXX−XXX

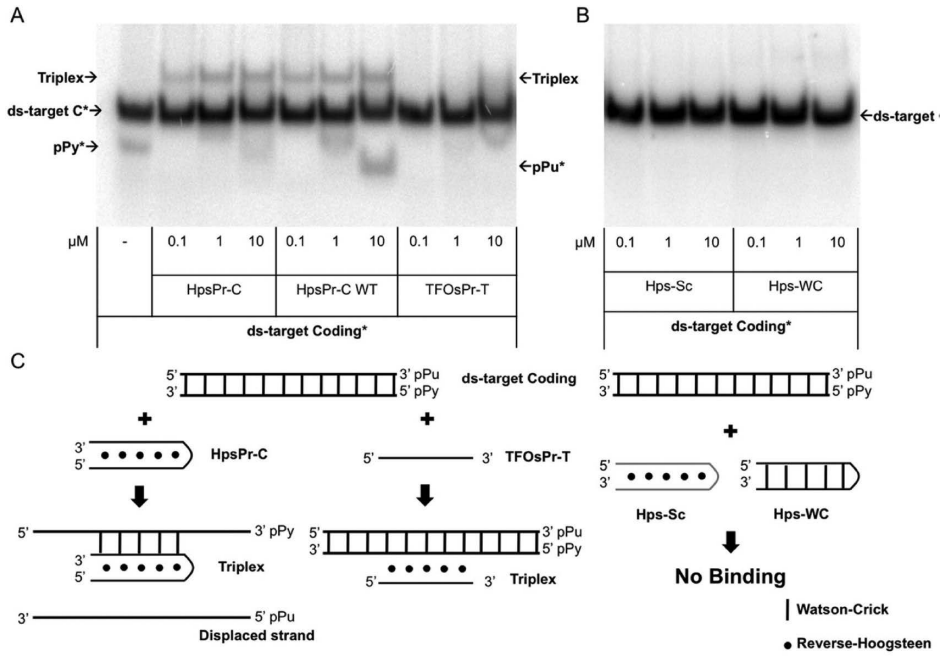

Figure 3. Binding of coding-PPRHs and TFO to their target sequence. (A) Binding of the coding-PPRH either with adenines in the pyrimidine interruptions (HpsPr-C) or the wild-type version (HpsPr-C WT) and the TFOsPr-T after incubation with increasing concentrations of their radiolabeled ds-target sequence (20 000 cpm). Shifted bands are indicated by arrows. (B) Binding of the negative controls, either Hps-Sc or Hps-WC to the radiolabeled ds-target sequence (20 000 cpm) for the specific PPRHs. (C) Schematic representation of the binding of the different molecules used in this study, including HpsPr-C, HpsPr-C WT, TFOsPr-T, Hps-Sc, Hps-WC.

all experiments, we used as negative controls either a PPRH with a scrambled sequence (Hps-Sc) or a PPRH with intramolecular Watson−Crick bonds instead of Hoogsteen bonds (Hps-WC), which is not able to form triplexes with the DNA. We also used as negative control a TFO with a scrambled sequence without target in the human genome (TFO-Sc).

Effect of PPRHs Length on Binding to the Target, Cell Viability and mRNA. To compare the effects of PPRHs with different lengths, we needed to start with a gene containing a polypurine/polypyrimidine stretch long enough to allow the design of PPRHs with different number of nucleotides. We found a 30 nucleotides polypyrimidine sequence within intron 10 of the *TERT* gene that opened the possibility to test PPRHs lengthening 20, 25, or 30 nucleotides against the same target sequence (Table 1, Figure 1A). HptI10-T had 3 three pyrimidine interruptions, whereas HptI10-T2 and HptI10-T3 had two interruptions. For these experiments, we used PPRHs where the pyrimidine interruptions were substituted by adenines in both strands of the PPRH. As shown in Figure 1B the three PPRHs tested were capable of binding to their target sequence at a concentration as low as 1 μM. However, in terms of cell viability, we observed that the longer the sequence, the higher the effect. Specifically, the 20-, 25-, and 30-nucleotide PPRHs decreased cell viability by 15%, 30%, and 60%, respectively (Figure 1C). In the case of TERT inhibitors, reaching 60% decrease in cell viability can be considered a notable effect because a long time is needed for the cell to shorten the telomeres enough to enter senescence. For that reason, inhibitors of TERT are commonly used in combination with other drugs.[16] We also determined the mRNA levels of TERT using the longest PPRH that caused a dose-dependent decrease, reaching 60% at 300 nM (Figure 1D).

Comparison between PPRHs and Nonmodified TFOs. *Binding to Target Sequences.* For the comparative analyses, we used PPRHs against the promoter sequence of *survivin*, which have been previously validated in terms of efficacy in prostate cancer cells and in a xenografted tumor model.[11] Those PPRHs were designed against two different sequences within the promoter, one against a distal region, at-1009, in the template strand of the DNA (Template-PPRH), and another against a more proximal region, at −525, in the coding strand (Coding-PPRH). Thus, the corresponding TFOs that would bind to the same sequence as PPRHs were designed. PPRHs are double-stranded molecules formed by two polypurine strands that bind to the pyrimidine target in the DNA sequence by Watson−Crick bonds, whereas TFOs are single-stranded polypurine molecules that will bind to the purine strand in the DNA by reverse-Hoogsteen bonds forming a triplex structure. Therefore, the TFO that binds to the same region as the template-PPRH will bind to the coding strand, and the TFO that binds to the same region as the coding-PPRH will bind to the template strand. PPRHs and TFOs sequences are listed in Table 2.

The binding was analyzed using the corresponding radiolabeled ds-target sequence for each PPRH either template or coding, shown in Figures 2 and 3.

We observed that both the Template-PPRH (HpsPr-T) and the corresponding TFO (TFOsPr-C) were specific for their target sequence, as indicated by the shifted bands (Figure 2A), whereas the two negative controls, Hps-Sc and Hps-WC, did not bind to the target sequences (Figure 2B). The template-PPRH against the promoter sequence (HpsPr-T) was bound to the target sequence forming a triplex structure-binding of the PPRH to the pyrimidine target sequence- and quadruplex structure-binding of the PPRH to the duplex, whereas the TFO formed a single triplex structure-binding of the TFO to the duplex (Figure 2A and 2C).

Regarding the coding-PPRH, we also observed specificity of both HpsPr-C and TFOsPr-T, as indicated by the shifted band (Figure 3), in contrast to the two negative controls, Hps-Sc and

DOI: 10.1021/mp5007008
Mol. Pharmaceutics XXXX, XXX, XXX−XXX

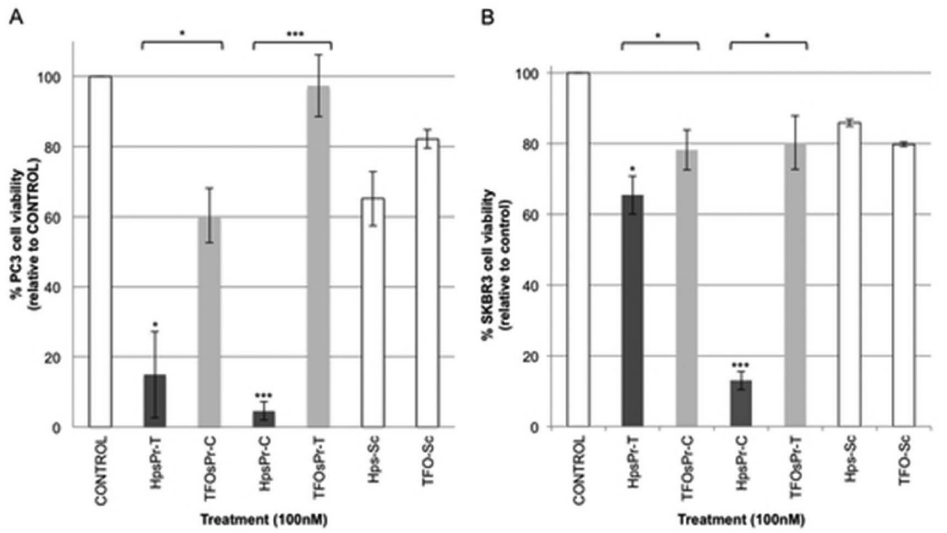

Figure 4. Effect of PPRHs and TFOs against *survivin* on cell viability. (A) Cell viability in PC3 cells upon incubation with 100 nM of the two PPRHs (dark gray) or the two TFOs (light gray) against the *survivin* gene. Negative controls -Hps-Sc and TFO-Sc(blank bars)- were tested at the same conditions. CONTROL cells are untreated PC3 cells. (B) Cell viability in SKBR3 cells upon incubation with 100 nM of the two PPRHs (dark gray) or the two TFOs (light gray) against the *survivin* gene. Negative controls -Hps-Sc and TFO-Sc(blank bars)- were tested at the same conditions. CONTROL cells are untreated SKBR3 cells. MTT assays to determine cell survival were performed 6 days after transfection. DOTAP was used at 10 μM. Data are mean ± SEM values of at least three experiments. $^{*}p < 0.05$, $^{**}p < 0.01$, $^{***}p < 0.005$.

Hps-WC, which did not bind to the target sequence (Figure 3B). HpsPr-C was capable of binding to its target sequence from 100 nM to 10 μM, causing strand displacement at 10 μM. On the other hand, the TFO against the same sequence only showed some binding at 10 μM (Figure 3A), proving that it had less affinity to the target sequence than the coding-PPRH. In Figure 3C there is a representation of the different structures observed in the binding assays. In this case, we only observed the triplex structure because the PPRH was capable of displacing the purine strand completely. The different length of their target sequences might cause the difference of binding between the template- and coding-PPRH. In the case of the coding-PPRH, the target sequence is shorter, and in consequence, easier to displace.

Cell Viability. We compared the effect of PPRHs and TFOs in two cell lines, PC3 from prostate cancer and SKBR3 from breast cancer, upon incubation with 100 nM of the DNA molecules (PPRH or TFO) plus 10 μM of the liposomal reagent DOTAP (Roche). In both cell lines, there was a significant difference between the use of PPRHs vs TFOs; both template- and coding-PPRHs exerted a higher decrease in cell viability than the corresponding TFOs at 100 nM, as shown in Figure 4. Negative controls for each type of molecule -Hps-Sc and TFO-Sc- were used at the same conditions and a rather small effect was observed upon incubation in both cell lines, probably due to the transfection reagent.

It was also observed that PPRHs and TFOs caused a higher decrease in viability in PC3 than in SKBR3 cells. This could be caused by the different transfection efficiency of DOTAP in each cell line. PC3 cells internalize almost four times more PPRH than SKBR3 using the same conditions of transfection, as determined in uptake experiments using flow cytometry and fluorescently labeled PPRHs. Using this methodology, we also compared the uptake of fluorescently labeled PPRH and TFO, observing that 24 h after transfection, more than 90% of PC3 cells showed a similar mean intensity of fluorescence with either molecule (data not shown). This result indicated that the difference in effect of PPRHs and TFOs was due to a different intrinsic efficacy rather than a different uptake.

Comparison between PPRHs Carrying Adenines and Wild-Type Sequences. *Binding to Their Target Sequence.* Once we had compared PPRHs and nonmodified TFOs, we wanted to improve our PPRHs in terms of efficacy and specificity. To do so, we decided to explore the usage of wild-type PPRHs including pyrimidine interruptions in their sequences instead of substituting the interruptions by adenines. We had previously stated that the best base—in terms of binding and cytotoxicity—to substitute a single interruption was adenine;[9] however, it is usual to find polypurine stretches with several interruptions that could compromise the specificity of the molecule. We studied HpsPr-T and HpsPr-C against *survivin*, both of which contained three interruptions substituted by adenines, and their counterparts, HpsPr-T WT and HpsPr-C WT, in which the wild-type sequence was used. PPRHs sequences are listed in Table 2, including a scheme of the molecules. It is important to mention the difference between the two approaches: The A-substitution involved using two adenines in each interruption, one in the Watson−Crick strand (that will bind to the pyrimidine target sequence) and one in the reverse-Hoogsteen strand (that forms the hairpin structure). In the wild-type version, the same pyrimidine (C or T) of the interruption was used in both strands of the PPRH.

When performing BLAST analyses using the wild-type sequences, the first match with the lowest e-value and maximum identity was always the target sequence within the *survivin* gene. However, when using the sequences where the pyrimidines were substituted by adenines, several sequences were found with the same identity but higher e-value, indicating possible off-target effects.

In the binding assays with the *survivin* promoter shown in Figure 2 and 3, there was the general tendency that the wild-type PPRHs were capable of binding to the polypyrimidine target sequences with more affinity and at lower concentrations than the PPRHs with adenines in front of the purine interruptions. In

DOI: 10.1021/mp5007008
Mol. Pharmaceutics XXXX, XXX, XXX−XXX

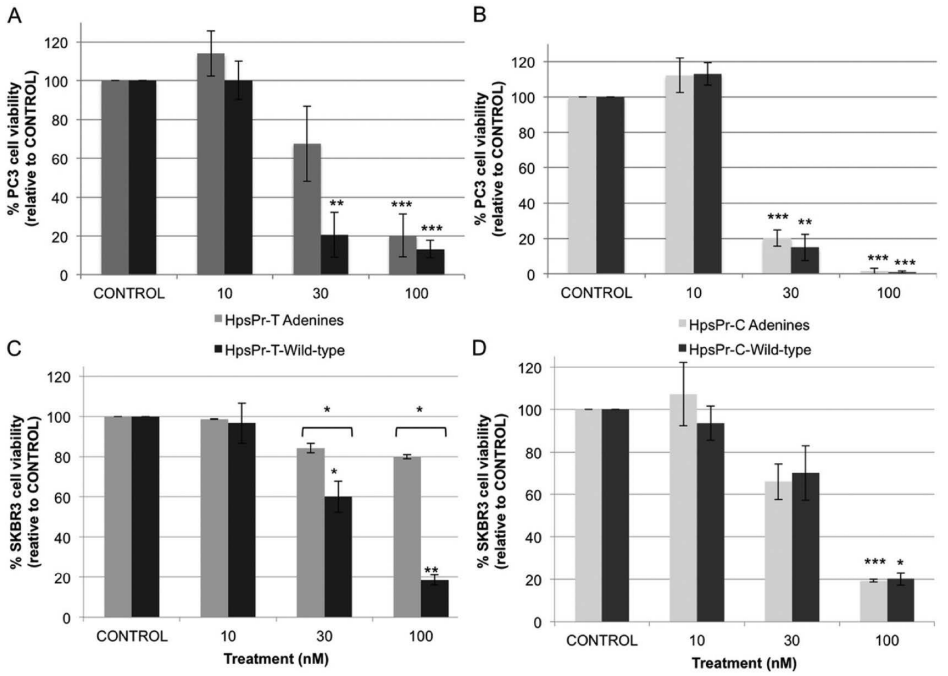

Figure 5. Effect of PPRHs against *survivin* on cell viability. (A) Dose response of template-PPRHs against *survivin* in PC3 cells. (B) Dose response of coding-PPRHs against *survivin* in PC3 cells. (C) Dose response of template-PPRHs against *survivin* in SKBR3 cells. (D) Dose response of coding-PPRHs against *survivin* in SKBR3 cells. DOTAP was used at 5 μM to transfect 10 nM and 30 nM and at 10 μM to transfect 100 nM PPRH. CONTROL cells are untreated cells. MTT assays to determine cell survival were performed 6 days after transfection. Data are mean ± SEM values of at least three experiments. *$p < 0.05$, **$p < 0.01$, ***$p < 0.005$. Light gray corresponds to the adenine version and dark gray to the wild-type version.

the case of the template-PPRH, there was a clear difference in the binding affinity between HpsPr-T and HpsPr-T WT, only the wild-type version bound to its target at concentrations as low as at 1 μM, whereas the other PPRH did not generate a shifted band up until 10 μM (Figure 2A). In the case of the coding-PPRH, both PPRHs originated a band corresponding to the triplex at all concentrations tested (from 0.1 to 10 μM), but the wild-type showed five times more strand displacement upon binding (Figure 3A).

Cell Viability Assays. To compare the effect of PPRHs with or without pyrimidine interruptions, dose response studies in PC3 and SKBR3 were performed and the IC_{50} for each molecule was calculated. The resulting cell viabilities are shown in Figure 5 and the IC_{50}'s in Table 4. Template and coding-PPRHs decreased cell viability in a dose-dependent manner in both cell lines, and in all cases, the wild-type counterpart presented a lower IC_{50}.

Melting Experiments. Melting temperatures and $-\Delta G$ were obtained using the MeltWin 3.5 software[17] and are displayed in Table 5. We measured the changes in absorbance at 260 nm when increasing temperature from 10 to 90 °C; in all cases, sigmoidal curves with a single transition corresponding to the switch from bound complex to random coil were observed, which corresponds to a bimolecular melting curve, previously described in ref 18. Comparison between the PPRH containing interruptions substituted by adenines and the wild-type counterpart showed a clear difference of around 20 °C, the wild-type presenting the higher temperature and the lower ΔG, meaning these PPRHs had a higher affinity for the target sequence. It was also clear that the longer the PPRH, the higher the melting temperature; therefore, the template-PPRH, which is 26 nucleotides long, had a higher temperature than the coding-PPRH that was 20 nucleotides long.

Table 4. IC_{50} Calculated for PPRHs and Wedge-PPRH in PC3 and SKBR3

	PC3	SKBR3
PPRH*	IC_{50} (nM)	IC_{50} (nM)
HpsPr-T A	46.21	346.57
HpsPr-T WT	30.14	40.77
HpsPr-C A	16.50	43.32
HpsPr-C WT	14.44	43.32
Wedge-PPRH-17	21.62	41.17

*A indicates adenines and WT wild-type.

Table 5. Melting Transition Temperatures, T_m, and Free Energies, ΔG, at pH 7.2

complex*	T_m ± std error (°C)	ΔG ± std error (kcal/mol, at 37 °C)
HpsPr-T A + Ppy	54.05 ± 0.23	−12.60 ± 0.13
HpsPr-T WT + Ppy	73.47 ± 0.30	−19.81 ± 0.70
HpsPr-C A + Ppy	37.24 ± 2.42	−9.29 ± 0.53
HpsPr-C WT + Ppy	66.45 ± 0.07	−25.96 ± 2.29

*A indicates adenines and WT wild-type.

Survivin mRNA Levels. Treatment for 48 h of wild-type PPRHs against *survivin* caused a decrease in its expression. Specifically, HpsPr-T WT caused a 2.4-fold decrease and HpsPr-C WT caused a 3-fold decrease in mRNA levels, whereas no effect was observed with the negative control HpsPr-WC (Figure 6).

Wedge-PPRH. *Design.* Concurrently to the study of wild-type PPRHs, we decided to further improve PPRHs by designing a structure that would lock the strand displacement, which may stabilize the PPRH-DNA complex and cause a higher effect. The design consisted in extending the 5′ with the sequence of polypyrimidines complementary to the polypurine strand. The

DOI: 10.1021/mp5007008
Mol. Pharmaceutics XXXX, XXX, XXX−XXX

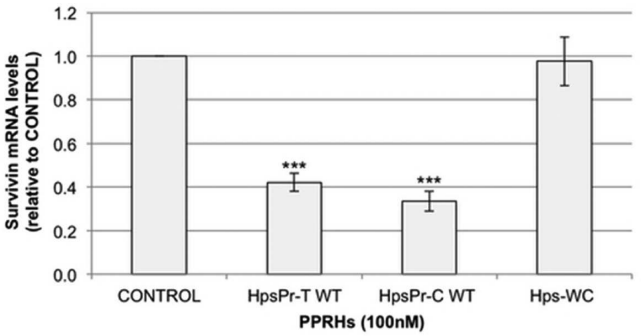

Figure 6. Effect of wild-type PPRHs on *survivin* mRNA levels. RNA was extracted from PC3 cells treated with 100 nM of HpsPr-T WT, HpsPr-C WT and the negative control Hps-WC for 48 h. mRNA levels were determined using qRT-PCR and referred to the levels of *APRT* as an endogenous control. DOTAP was used at 8 μM. Data are mean ± SEM values of at least three experiments. *$p < 0.05$, **$p < 0.01$, ***$p < 0.005$.

rationale was that such PPRH could open the double strand and the extension could bind to the coding strand, as detailed in Figure 7B.

The Template-PPRH was selected to perform this study. We designed two Wedge-PPRHs; one had a 5′ extension of 23 bases complementary to the purine sequence, linked by a 5T loop to give flexibility for the turn, and another with a shorter extension of 17 nucleotides. As a negative control we used Wedge-PPRH WC, which presented the 17-nucleotide complementary sequence followed by a hairpin that formed Watson−Crick bonds instead of reverse-Hoogsteen bonds, a useful control to determine the importance of the PPRH in this structure. All the sequences are listed in Table 3.

Binding to the Target Sequence. We performed binding analyses for the three wedge structures. We observed a similar pattern of binding between the Wedge-PPRH-23 and the HpsPr-T WT (Figure 7A compared to Figure 2A), indicating that the presence of the 5′ extension did not prevent the binding of the PPRH to its target sequence. Wedge-PPRH-23 formed two bands corresponding to a triplex and a quadruplex structure (Figure 7B). We expected to observe an additional band (quintuplex) if the 5′ extension could bind to the displaced polypurine strand which was not seen with the Wedge-PPRH-23. Therefore, we tested a shorter version of the Wedge-PPRH with an extension of only 17 nucleotides, so it could hybridize to the polypurine displaced strand. Using Wedge-PPRH-17 we observed an additional shifted band corresponding to the quintuplex structure (Figure 7B). Moreover, Wedge-PPRH-17 bound to the target sequence at a lower concentration (100 nM) than when using PPRHs and Wedge-PPRH-23. It is important to note that binding with the Wedge-PPRH WC showed a low intensity band that might correspond to the binding of the 17-nucleotide extension to its complementary sequence, no additional bands were observed because of the lack of PPRH structure, indicating the importance of this structure for the opening of the dsDNA.

To really demonstrate the identity of the quintuplex, we performed binding experiments with both the Wedge-PPRH-17 and the duplex and competing with either the coding strand (pPu) (Figure 8A and B), the pyrimidine strand (pPy), or the duplex (dsT) (Figure 8B). In Figure 8A, we observed the competition between the polypurine sequence (at 20×, lanes 3 and 6; or 50×, lanes 4 and 7) and the radiolabeled duplex (20 000 cpm) at different concentrations of Wedge-PPRH-17 (100 nM, lanes 2−4; and 1 μM, lanes 5−7). The disappearance of the

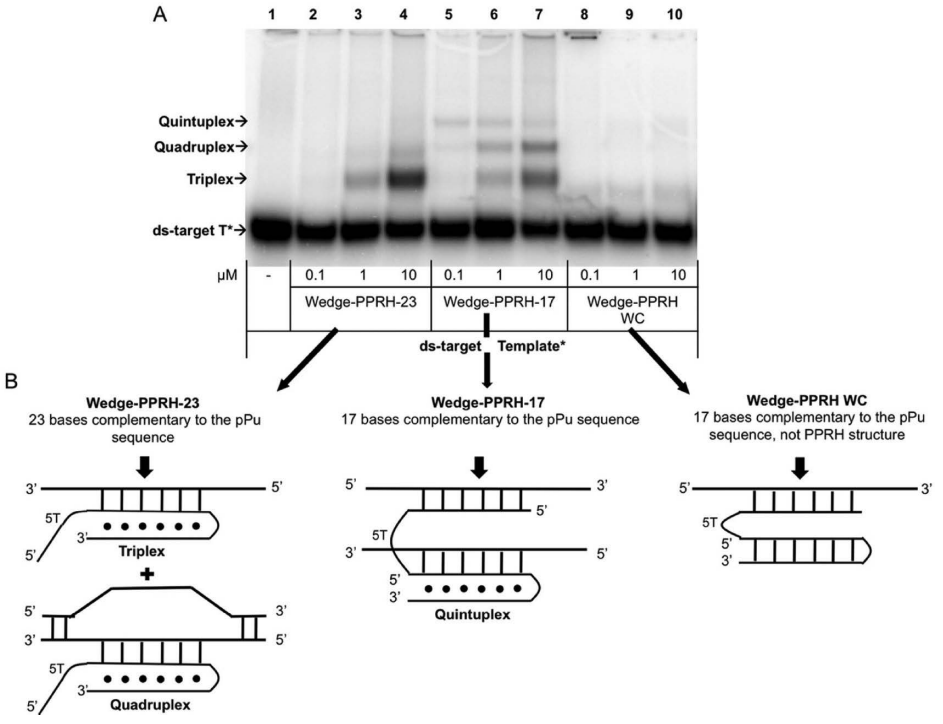

Figure 7. Binding of Wedge-PPRH to its target sequence. (A) Binding of Wedge-PPRH to its radiolabeled ds-target sequence (20 000 cpm). The mobility of the ds-target sequence is shown in lane 1. Binding of Wedge-PPRH-23 is shown in lane 2, 3, and 4. Binding of Wedge-PPRH-17 is shown in lane 5, 6, and 7. The negative control, Wedge-PPRH WC is shown in lane 8, 9, and 10. Shifted bands are indicated by arrows. (B) Schematic representation of the structures corresponding to the different bands observed in the electrophoresis.

DOI: 10.1021/mp5007008
Mol. Pharmaceutics XXXX, XXX, XXX−XXX

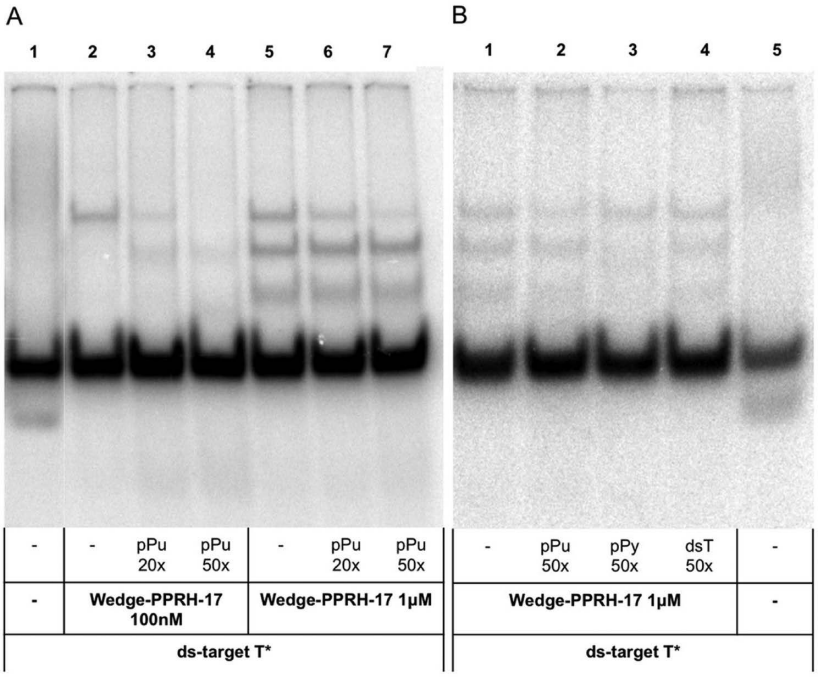

Figure 8. Identification of the shifted bands in the binding assays with Wedge-PPRH-17. (A) Binding of Wedge-PPRH-17 to its radiolabeled ds-target sequence (20 000 cpm). The mobility of the ds-target sequence is shown in lane 1. The binding pattern of the Wedge-PPRH-17 is shown at two different concentrations of Wedge-PPRH: 100 nM (lane 2−4) and 1 μM (lane 5−7); competition assays were performed using 20-fold (lane 3 and 6) and 50-fold (lane 4 and 7) excess of the coding strand of the target sequence. (B) Binding of Wedge-PPRH-17 at 1 μM to its radiolabeled ds-target sequence (20 000 cpm). The mobility of the ds-target sequence is shown in lane 5. The binding pattern of the Wedge-PPRH is shown in lane 1 and competition assays were performed using 50-fold excess of either the coding (lane 2) or the template strand (lane 3) or the ds-target sequence (lane 4).

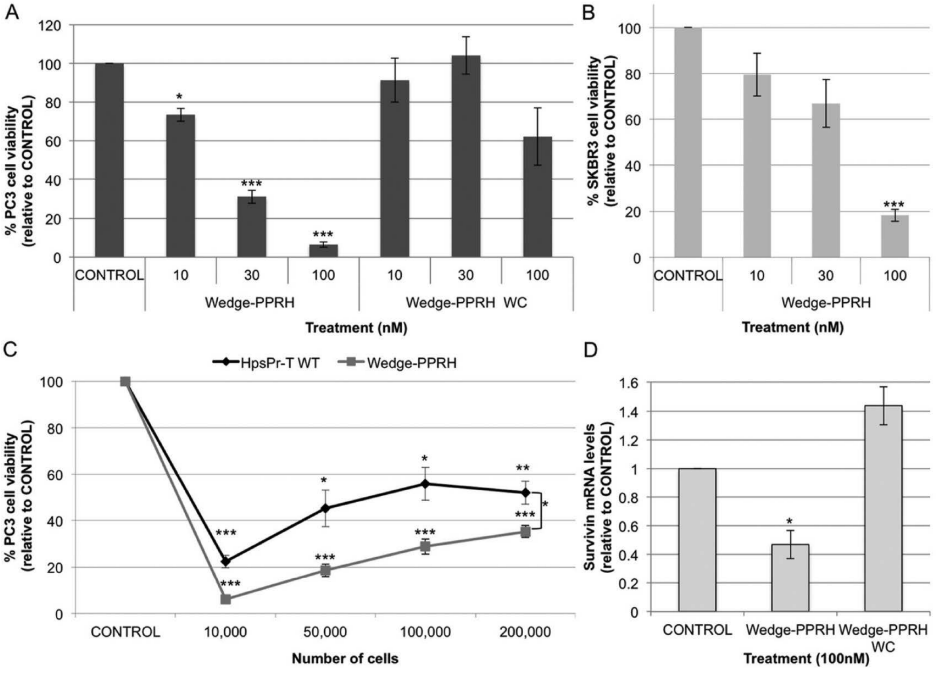

Figure 9. Effect of Wedge-PPRH-17 on cell viability and *survivin* mRNA levels. (A) Effect in PC3 cells. (B) Effect in SKBR3 cells. In both cases, DOTAP was used at 5 μM to transfect 10 nM and 30 nM, and at 10 μM to transfect 100 nM of Wedge-PPRH. CONTROL cells are untreated cells. MTT assays to determine cell survival were performed 6 days after transfection. Data are mean ± SEM values of at least three experiments. *$p < 0.05$, **$p < 0.01$, ***$p < 0.005$. (C) Effect of HpsPr-T WT and Wedge-PPRH-17 on cell viability when scaling-up the number of PC3 cells. (D) RNA was extracted from PC3 cells treated with 100 nM of Wedge-PPRH-17 or Wedge-PPRH WC for 48 h. DOTAP was used at 8 μM. mRNA levels were determined using qRT-PCR and referred to the levels of the endogenous control *18S*. Data are mean ± SEM values of at least three experiments. *$p < 0.05$.

upper band, corresponding to the quintuplex, indicates its high affinity to the polypurine sequence and that the 5′ pyrimidine extension was binding to the displaced polypurine sequence. In fact, when using the lowest concentration of Wedge-PPRH-17

DOI: 10.1021/mp5007008
Mol. Pharmaceutics XXXX, XXX, XXX−XXX

(100 nM), the competition by pPu (20× or 50×) produced the disappearance of the quintuplex while the quadruplex appeared. When the Wedge-PPRH-17 was increased at 1 μM, the competition with pPu also decreased the intensity of the band corresponding to the quintuplex.

In Figure 8B, aside from competing the duplex with pPu (lane 2), we competed with pPy (lane 3) and the duplex (lane 4). Competition with pPy caused a decrease in the intensity of the bands corresponding to the triplex and quadruplex structures, but not the quintuplex, reaffirming the quintuplex was the band most difficult to displace because it had the highest affinity. In lane 4, we observed the decrease of the three shifted bands because the competition was performed with the duplex.

Cell Viability Assays and Survivin mRNA Levels. We decided to further explore the effect of the Wedge-PPRH with the extension of 17-nucleotides in terms of cell viability and mRNA levels because we had shown that it was capable of forming the locked structure.

In PC3 cells, we observed a similar effect on cell viability of the Wedge-PPRH-17 compared to the original or wild-type-PPRHs (Figure 9A compared to Figure 5A). However, when analyzing the data, the Wedge-PPRH-17 presented a lower IC_{50} than HpsPr-T WT (Table 4), indicating that the Wedge-PPRH-17 had a higher efficacy. Wedge-PPRH WC was innocuous at 10 and 30 nM and caused only a slight decrease at 100 nM (Figure 9A). In SKBR3, Wedge-PPRH-17 had a dose-dependent effect (Figure 9B) similar to HpsPr-T WT (Figure 5D) and, as a result, a similar IC_{50} was obtained (Table 4).

We performed a scale-up experiment to figure out the effect of PPRHs when increasing the number of cells. Keeping the concentration of either the PPRH or the Wedge-PPRH (100 nM) unchanged, we observed that there was a slight loss of effect when increasing the number of cells, but both molecules maintained its efficacy up to 200 000 cells. As shown in Figure 9C, Wedge-PPRH-17 maintained its efficacy significantly in a more stable way.

Regarding mRNA levels, Wedge-PPRH-17 caused a 2-fold decrease at 100 nM, whereas Wedge-PPRH WC did not cause a decrease in *survivin* mRNA level. (Figure 9D).

■ DISCUSSION

The purpose of this study was to improve the suitability of the polypurine reverse Hoogsteen hairpins as gene targeting tools by exploring several characteristics. Specifically, we focused on the following properties of PPRHs: (i) nucleotide length to define the optimal range in their design, (ii) affinity and effect compared with nonmodified TFOs, (iii) specificity toward the target sequence by using wild-type-PPRHs, and (iv) development of a new structure termed Wedge-PPRH.

PPRH Nucleotide Length. The possibility to design PPRHs depends on the presence of polypurine/polypyrimidine sequences in the target genes. Goñi et al.[13] reported that triplex target sequences were overrepresented in the human genome, finding them commonly in regulatory regions. This abundance allows the design of PPRHs against almost any gene although each one will present different options of length for targeting. From our study, we can conclude that whenever possible, the longer the PPRH, the greater the effect, starting with a minimum of 20 nucleotides. In the case of the *TERT* gene used in this study, we observed binding of the PPRHs to their target from 20 to 30 nucleotides but the higher effect was obtained with the longest one.

Comparison between PPRHs and Nonmodified TFOs. One difference between PPRHs and TFOs is that PPRHs are double-stranded DNA molecules whereas TFOs are single-stranded. Because of this, their binding differs: PPRHs form intramolecular reverse Hoogsteen bonds and bind by Watson–Crick bonds to their polypyrimidine target sequence, TFOs form Hoogsteen bonds with the purine strand in the double helix. Using the same binding conditions of pH and salt composition, and taking into account that the PPRH and the corresponding TFO have the same sequence, we observed that PPRHs bind at lower concentrations than TFOs to the target sequence, indicating a higher affinity. Moreover, in terms of cell viability, both PPRHs exerted a higher effect in PC3 and SKBR3 cells than TFOs, indicating that PPRHs were more effective.

Kool and colleagues[18] had previously shown that hairpin structures formed by two purine domains could bind to the pyrimidine target sequence in a cooperative fashion and with higher affinity than the two separate strands. Thus, the existence of the hairpin structure represents a clear advantage over single-stranded molecules and proves that the strand that does not interact directly with the DNA contributes to the binding. In our work, we corroborated that the strand that allows the formation of the intramolecular Hoogsteen bonds within the PPRH favors its binding to the target sequence with higher affinity than TFOs. In addition, we prove that the increase in affinity displayed by PPRHs is reflected in a stronger effect in terms of cell viability.

Specificity of PPRHs. In the mismatches study, T_m experiments showed that the presence of mismatches caused a decrease in T_m, indicating less affinity for the target sequence, in accordance with previous results from Kool.[18] In the case of HpsPr-T, 3 mismatches caused a decrease of around 17 °C in the T_m relative to the wild-type, whereas HpsPr-C, which also contained three mismatches, had a melting temperature of 25 °C below its wild-type counterpart. Therefore, T_m is affected not only by the length of the oligonucleotide but also by the presence of mismatches, proving the wild-type version is a better choice. Wang et al.[7] also reported that the presence of a hairpin structure stabilized the binding, then allowing for the presence of mismatches, even though with a lower T_m.

Currently, one of the main problems of gene-silencing technologies is the off-target effects caused by lack of specificity. siRNAs are known to activate TLRs, leading to inflammation and other off-target effects.[19] In this regard, PPRHs avoid off-target effects caused by activation of the immune system as opposed to siRNAs.[15]

Another problem intrinsic to the siRNA pathway is that siRNAs could bind to nontarget genes by acting as miRNAs.[19] Other authors have reported that as few as 11 nucleotides are sufficient to silence nontargeted genes, so although degradation of siRNA is occurring, they can cause off-target effects.[20] Degradation of siRNAs is meant to occur earlier than in the case of PPRHs because their half-life is much shorter.[15]

In this work, we prove that wild-type PPRHs have a higher affinity to their target sequence, and therefore, they are meant to have less off-target effects caused by their binding to nontargeted sequences. That is, the more interruptions substituted by adenines, the lower the T_m and affinity, increasing the possible off-target effects. However, up to 3 mismatches in a sequence of 20 nucleotides has proved to be effective both in vitro and in vivo without known off-target effects.[11] Avoidance of off-target effects using the wild-type version and prevention of activation of the immune response are appreciable advantages of PPRHs over siRNAs.

DOI: 10.1021/mp5007008
Mol. Pharmaceutics XXXX, XXX, XXX–XXX

Wedge-PPRH. As previously stated, PPRHs are highly stable and resistant without the need of chemical modifications, which is another advantage over aODNs, TFOs, or siRNAs. However, there is room for improvement in terms of binding or effect. For this reason, we developed a new molecule called Wedge-PPRH, which binds simultaneously to both strands of the target sequence. Other authors have tested similar strategies based on triplexes capable of binding to adjacent polypyrimidine and polypurine sequences in both strands, using what they called alternate-strand triplex formation.[21,22] A Wedge-PPRH of the adequate length had a slightly better effect than PPRHs in decreasing cell viability and its effect was more constant as the number of incubated cells increases. Considering that the only difference between the Wedge-PPRH and the HpsPr-T WT is the 5′ extension, we can conclude that the formation of the quintuplex structure, which locks the displaced strand of the dsDNA, contributes to the higher effect observed with the Wedge-PPRH.

As a summary, in this work, we investigated characteristics to improve the performance of PPRHs as a gene silencing tool and suggest a number of criteria to take into account when designing these molecules.

■ AUTHOR INFORMATION

Corresponding Author

*E-mail: vnoe@ub.edu. Phone: +34 93 403 4455. Fax: +34 93 402 4520. Address: Department of Biochemistry and Molecular Biology, School of Pharmacy, Av. Diagonal 643, E-08028 Barcelona, Spain.

Notes

The authors declare no competing financial interest.

■ ACKNOWLEDGMENTS

The work was supported by Grant SAF2014-51825-R from "Plan Nacional de Investigación Científica" (Spain). Our group holds the Quality Mention from the "Generalitat de Catalunya" 2014-SGR96. L.R. and A.S. are recipients of FI fellowships from the "Generalitat de Catalunya". X.V. is recipient of APIF fellowship from University of Barcelona. We thank Maria Tintoré and Sonia Pérez from CSIC for their help with T_m experiments and the use of MeltWin 3.5 software.

■ ABBREVIATIONS:

PPRH, polypurine reverse Hoogsteen hairpin; TFO, triplex-forming oligonucletide; WT, wild-type; DOTAP, *N*-[1-(2,3-dioleoyloxy)propyl]-*N*,*N*,*N*-trimethylammonium methylsulfate; MTT, (3-(4,5-dimethylthiazol-2-yl)-2,5-diphenyltetrazolium bromide

■ REFERENCES

(1) Felsenfeld, G.; Rich, A. Studies on the formation of two- and three-stranded polyribonucleotides. *Biochim. Biophys. Acta* **1957**, *26* (3), 457−68.

(2) Hoogsteen, K. The crystal and molecular structure of a hydrogen-bonded complex between 1-methylthymine and 9-methyladenine. *Acta Crystallogr.* **1963**, *16*, 907−916.

(3) Hewett, P. W.; Daft, E. L.; Laughton, C. A.; Ahmad, S.; Ahmed, A.; Murray, J. C. Selective inhibition of the human tie-1 promoter with triplex-forming oligonucleotides targeted to Ets binding sites. *Mol. Med.* **2006**, *12* (1−3), 8−16.

(4) Postel, E. H.; Flint, S. J.; Kessler, D. J.; Hogan, M. E. Evidence that a triplex-forming oligodeoxyribonucleotide binds to the c-myc promoter in HeLa cells, thereby reducing c-myc mRNA levels. *Proc. Natl. Acad. Sci. U.S.A.* **1991**, *88* (18), 8227−31.

(5) Praseuth, D.; Guieysse, A. L.; Helene, C. Triple helix formation and the antigene strategy for sequence-specific control of gene expression. *Biochim. Biophys. Acta* **1999**, *1489* (1), 181−206.

(6) Faucon, B.; Mergny, J. L.; Helene, C. Effect of third strand composition on the triple helix formation: purine versus pyrimidine oligodeoxynucleotides. *Nucleic Acids Res.* **1996**, *24* (16), 3181−8.

(7) Wang, S.; Kool, E. T. Recognition of Single-Stranded Nucleic Acids by Triplex Formation: The Binding of Pyrimidine-Rich Sequences. *J. Am. Chem. Soc.* **1994**, *116* (19), 8857−8858.

(8) Coma, S.; Noe, V.; Eritja, R.; Ciudad, C. J. Strand displacement of double-stranded DNA by triplex-forming antiparallel purine-hairpins. *Oligonucleotides* **2005**, *15* (4), 269−83.

(9) de Almagro, M. C.; Coma, S.; Noe, V.; Ciudad, C. J. Polypurine hairpins directed against the template strand of DNA knock down the expression of mammalian genes. *J. Biol. Chem.* **2009**, *284* (17), 11579−89.

(10) de Almagro, M. C.; Mencia, N.; Noe, V.; Ciudad, C. J. Coding polypurine hairpins cause target-induced cell death in breast cancer cells. *Human Gene Therapy* **2011**, *22* (4), 451−63.

(11) Rodriguez, L.; Villalobos, X.; Dakhel, S.; Padilla, L.; Hervas, R.; Hernandez, J. L.; Ciudad, C. J.; Noe, V. Polypurine reverse Hoogsteen hairpins as a gene therapy tool against survivin in human prostate cancer PC3 cells in vitro and in vivo. *Biochem. Pharmacol.* **2013**, *86* (11), 1541−54.

(12) Goni, J. R.; de la Cruz, X.; Orozco, M. Triplex-forming oligonucleotide target sequences in the human genome. *Nucleic Acids Res.* **2004**, *32* (1), 354−60.

(13) Goni, J. R.; Vaquerizas, J. M.; Dopazo, J.; Orozco, M. Exploring the reasons for the large density of triplex-forming oligonucleotide target sequences in the human regulatory regions. *BMC Genomics* **2006**, *7*, 63.

(14) Coma, S.; Noe, V.; Lavarino, C.; Adan, J.; Rivas, M.; Lopez-Matas, M.; Pagan, R.; Mitjans, F.; Vilaro, S.; Piulats, J.; Ciudad, C. J. Use of siRNAs and antisense oligonucleotides against survivin RNA to inhibit steps leading to tumor angiogenesis. *Oligonucleotides* **2004**, *14* (2), 100−13.

(15) Villalobos, X.; Rodriguez, L.; Prevot, J.; Oleaga, C.; Ciudad, C. J.; Noe, V. Stability and immunogenicity properties of the gene-silencing polypurine reverse Hoogsteen hairpins. *Mol. Pharmaceutics* **2014**, *11* (1), 254−64.

(16) Philippi, C.; Loretz, B.; Schaefer, U. F.; Lehr, C. M. Telomerase as an emerging target to fight cancer–opportunities and challenges for nanomedicine. *J. Controlled Release* **2010**, *146* (2), 228−40.

(17) McDowell, J. A.; Turner, D. H. Investigation of the structural basis for thermodynamic stabilities of tandem GU mismatches: solution structure of (rGAGGUCUC)2 by two-dimensional NMR and simulated annealing. *Biochemistry* **1996**, *35* (45), 14077−89.

(18) Vo, T.; Wang, S.; Kool, E. T. Targeting pyrimidine single strands by triplex formation: structural optimization of binding. *Nucleic Acids Res.* **1995**, *23* (15), 2937−44.

(19) Burnett, J. C.; Rossi, J. J.; Tiemann, K. Current progress of siRNA/shRNA therapeutics in clinical trials. *Biotechnol. J.* **2011**, *6* (9), 1130−46.

(20) Jackson, A. L.; Bartz, S. R.; Schelter, J.; Kobayashi, S. V.; Burchard, J.; Mao, M.; Li, B.; Cavet, G.; Linsley, P. S. Expression profiling reveals off-target gene regulation by RNAi. *Natu. Biotechnol.* **2003**, *21* (6), 635−7.

(21) Balatskaya, S. V.; Belotserkovskii, B. P.; Johnston, B. H. Alternate-strand triplex formation: modulation of binding to matched and mismatched duplexes by sequence choice in the Pu-Pu-Py block. *Biochemistry* **1996**, *35* (41), 13328−37.

(22) Jayasena, S. D.; Johnston, B. H. Oligonucleotide-directed triple helix formation at adjacent oligopurine and oligopyrimidine DNA tracts by alternate strand recognition. *Nucleic Acids Res.* **1992**, *20* (20), 5279−88.

DOI: 10.1021/mp5007008
Mol. Pharmaceutics XXXX, XXX, XXX−XXX

4.2.1. Additional results Article II

4.2.1.1. Determination of the best base to place in front of purine interruptions

It was previously demonstrated in our group that when a purine interruption occurred throughout the polypyrimidine target sequence of a PPRH, substitution by adenines in both strands of the hairpin was the best option to maintain binding while keeping a pure polypurine hairpin sequence (de Almagro et al. 2009). Nevertheless, polypurine/polypyrimidine stretches with a higher number of mismatches in the sequence are abundant in the genome. Designing PPRHs against these targets opened the possibility to use this technology towards more genes, but the presence of mismatches represented an obstacle. We proved that using adenines for up to 3 mismatches in a PPRH sequence maintained the binding to the target sequence and caused effect (Rodriguez et al. 2013). However, an improved version of these PPRHs was possible by using, in the PPRH, the complementary pyrimidine to the purine interruption found in the polypyrimidine target sequence, instead of adenines; therefore avoiding possible off-target effects due to the change of sequence. We decided to compare 3 different approaches, as shown in Figure 23:

1. To use adenines in both PPRH strands to substitute interruptions (HpsPr-T).
2. To use the same pyrimidine interruption (complementary to the purine interruption) in both PPRH strands (HpsPr-T WT).
3. To use the pyrimidine interruption in the PPRH strand that will form Watson-Crick bonds with the target sequence, and its complementary base in the reverse-Hoogsteen domain (HpsPr-T WT 2).

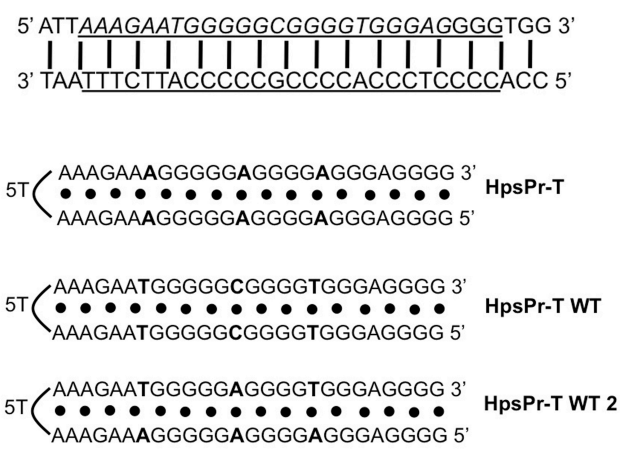

Figure 23. Target sequence and PPRHs designed to determine the best base to use when pyrimidine interruptions occur. Lines represent Watson-Crick bonds and bullets reverse Hoogsteen bonds. The target sequences for the PPRHs are underlined.

In the case of HpsPr-T WT 2 it was not possible to use C and G for the mismatch in the center of the sequence, because the abundance of Gs represented a problem for the synthesis of the oligonucleotide, we used As instead.

We performed binding analyses and cell viability assays using the three options. As shown in Figure 24A, all PPRHs were capable of binding to its target sequence in the same conditions. Binding caused the formation of two extra bands corresponding to the triplex and quadruplex structures. It is important to remark that HpsPr-T WT and HpsPr-T WT 2 bound with a slightly higher intensity to the target sequence than HpsPr-T. Thus PPRHs bearing up to three interruptions substituted by adenines were capable of binding to their target sequences; however, using pyrimidines in the Watson-Crick domain allowed for a better binding. Then PPRHs were transfected in PC3 cells and cell viability was analyzed. In Figure 24B, the results using the three PPRHs are represented. HpsPr-T WT caused a higher decrease in cell viability than HpsPr-T. Surprisingly, HpsPr-T WT 2 caused less effect than the other two PPRHs. For this reason, we conducted further studies with HpsPr-T WT, which are included in Article II.

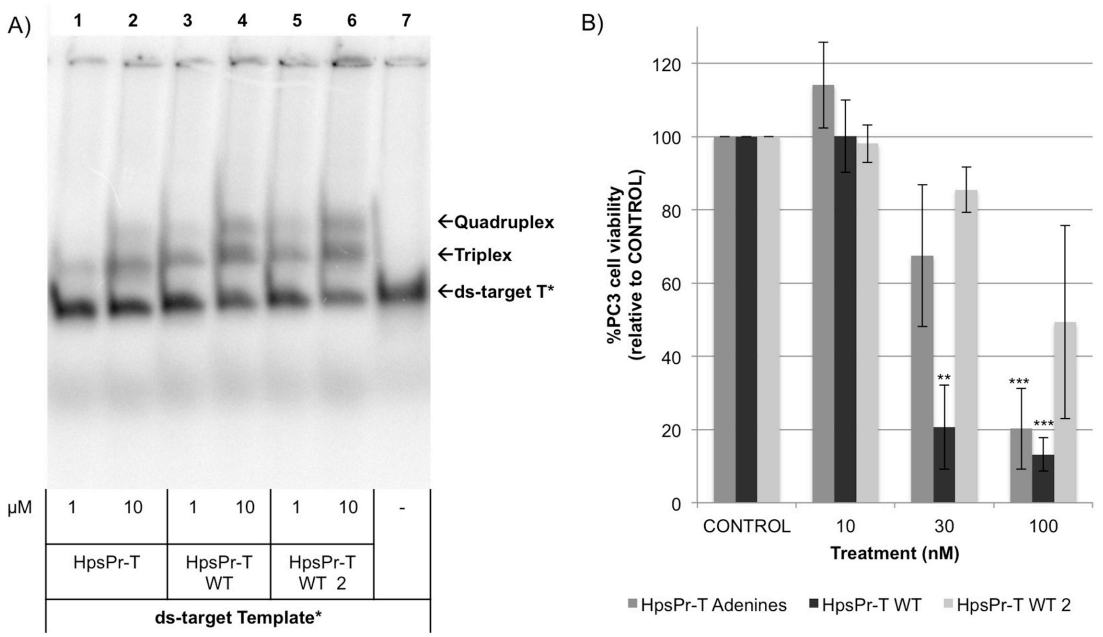

Figure 24. Comparison of the three approaches of Template-PPRHs against the *survivin* gene: binding to their target sequence and effect on cell viability. A) HpsPr-T, HsPr-T WT and HpsPr-T WT 2 were incubated with the radiolabeled ds-target sequence (20,000 cpm) within the promoter sequence at -1009 of the *survivin* gene. B) 100 nM of PPRHs were transfected in PC3 cells. MTT assays to determine cell survival were performed 6 days after transfection. Data are mean ±SEM values of at least three experiments *p<0.05, **p<0.01, ***p<0.005.

4.2.1.2. Effect of a WT-PPRH against Bcl-2

Once it was demonstrated that Wild-type PPRHs against *survivin* had a higher affinity and a higher efficacy than those with Adenine interruptions (Rodriguez 2015), we decided to test this approach in a PPRH targeting another gene. We designed the wild type version of the best PPRH candidate against *Bcl-2*, HpBcl2E1-C, and compared their effect in terms of cell viability and mRNA levels.

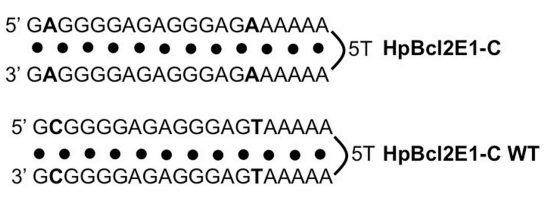

Figure 25. Adenines and Wild-type version of HpBcl2E1-C, against exon 1 of the *Bcl-2* gene.

In Figure 26A, we observed a similar effect between the PPRH using adenines in the interruptions compared to the PPRH with the corresponding pyrimidine interruptions. Analysis of the IC_{50} of both molecules proved that the Wild-type version was more effective, with an IC_{50} of 10.9 nM, compared to 18.7 nM for HpBcl2E1-C. In terms of mRNA levels, HpBcl2E1-C WT decreased around 2-fold *Bcl-2* mRNA levels, reaching a similar value to its counterpart (Figure 26B).

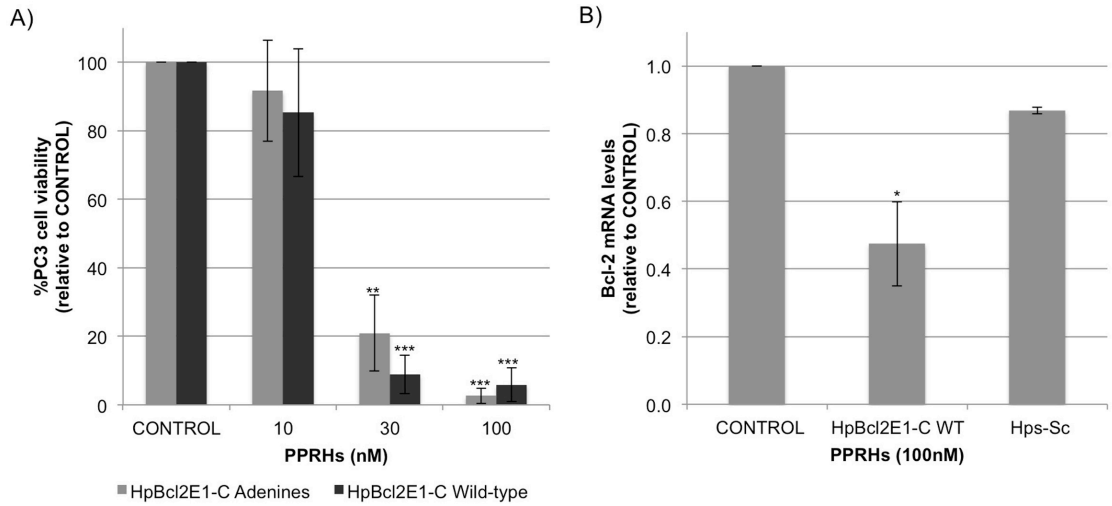

Figure 26. Effect of a Wild-Type PPRH against *Bcl-2* on cell viability and *Bcl-2* mRNA levels. A) MTT assays to determine cell survival were performed 6 days after transfection. Dose response of both molecules in PC3 cells. B) RNA was extracted from PC3 cells 24 hours after treatment with 100nM of HpBcl2E1-C. mRNA levels were determined using qRT-PCR and referred to the levels of APRT. Data are mean ±SEM values of at least three experiments *p<0.05, **p<0.01, ***p<0.005.

4.2.1.3. Uptake of PPRHs and TFOs in PC3 and SKBR3 cells

In the Results section "*Comparison between PPRHs and non-modified TFOs*" in Article II, we analyzed the effect of PPRHs and TFOs in PC3 and SKBR3 cell lines in terms of binding analyses and cell viability. We observed an evident difference between their effect, PPRHs displayed a higher affinity and a higher efficacy than TFOs. Moreover, PPRHs worked better in PC3 cells than in SKBR3 cells. To understand that difference, we performed uptake experiments, which were not included in the manuscript.

On the one hand, we aimed to elucidate the reason why the same PPRH caused a different decrease in viability when using different cell lines. We determined the population of FITC+ IP- cells in both cell lines, 24h after transfection of a fluorescent PPRH. We observed that even though the percentage of fluorescent cells were almost 100% for both cell lines at the tested conditions, the value of the mean fluorescence was 4-times higher for PC3 than for SKBR3 cells. This is reflected in the histogram shown in Figure 27. Therefore, the difference in effect could be due to the different uptake of the PPRH in these cells. The more PPRH entered, the more effect would be caused.

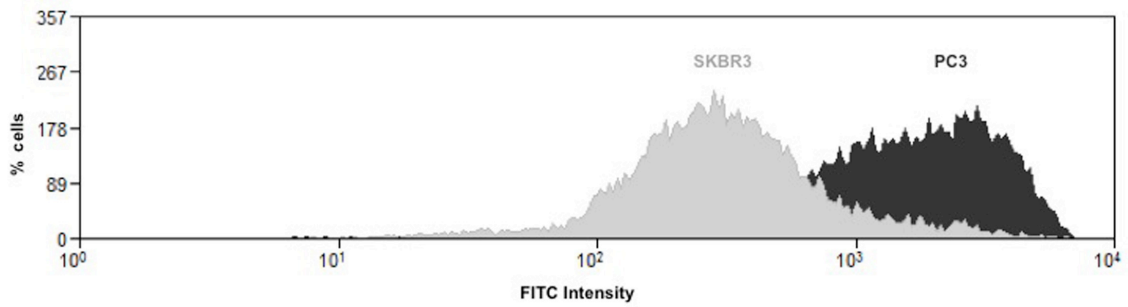

Figure 27. Representative image showing overlays of PC3 and SKBR3 cells. PC3 (dark grey) and SKBR3 cells (light grey) treated with 100nM of fluorescent-PPRH are represented. 100 nM of PPRH was transfected using 10μM DOTAP (PPRH:DOTAP ratio of 1:100).

On the other hand, we wanted to know if the difference in effect between PPRHs and TFOs was due to a difference in the uptake or in the efficacy of these molecules. We performed uptake experiments in PC3 cells using untreated cells as a control and either a fluorescently labeled PPRH (Hp-F) or a fluorescently labeled TFO (TFO-F). In the histogram shown in Figure 28, we observed a similar mean fluorescence using either the PPRH or TFO, as observed in a major overlap of the fluorescent peaks.

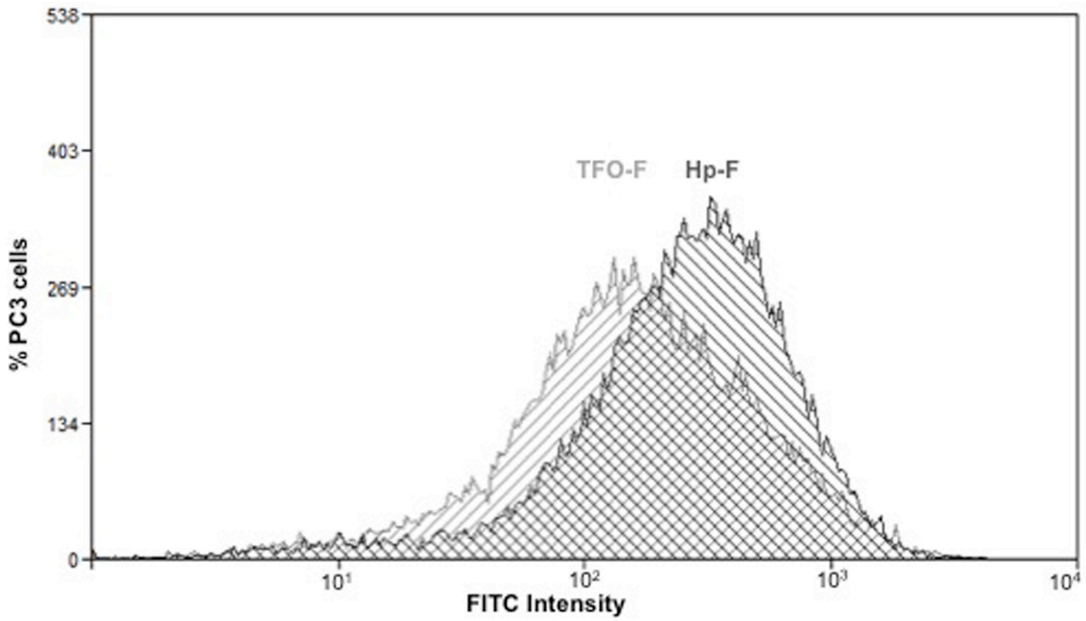

Figure 28. Representative image showing overlays of PC3 and SKBR3 cells. PC3 cells treated with 100 nM of either fluorescent-TFO (light grey) or fluorescent-PPRH (dark grey) are represented. DOTAP was used at 10μM, resulting in a PPRH:DOTAP ratio of 1:100 for both molecules.

4.2.1.4. Uptake of PPRHs into different cell lines: from solid tumors to hematopoietic malignancies

As it was shown in section 4.1.1.2, PPRHs were easily transfected into cancer cell lines from solid tumors, such as PC3, HCT116 and MiaPaCa 2 cells. Usage of the liposomal reagent DOTAP enabled the entry of the molecule into a high percentage of cells and thus favored its gene silencing function. PPRHs are a new technology that could be used against different malignancies, and it was worth exploring their use in other cell lines, representative of other tumors. For this purpose, we explored the uptake in hematopoietic cancer cell lines that grow in suspension and are known to be difficult-to-transfect (Zhao et al. 2012).

On the one hand, we analyzed the different uptake either using DOTAP or without vehicle, in Jurkat, K562 and THP-1 cells, from different types of human leukemia and EL4.BU cells, a mouse lymphoma cell line. Results are shown in Figure 29.

On the other hand, we selected three different cell lines from human B-cell lymphoma such as Granta-519, HBL-2 and WSU-FSCCL cells and determined the uptake of the PPRH in time-course experiments (Figure 30).

A)

% FITC+ Jurkat CELLS		
SAMPLE		MEAN ±STD ERROR
	CONTROL	1.76 ± 0.47
	HpF 100nM	2.46 ± 0.53
DOTAP	HpF 1µM	73.44 ± 7.31
	HpF 100nM	31.04 ± 3.60
NO VEHICLE	HpF 1µM	86.50 ± 2.88 *

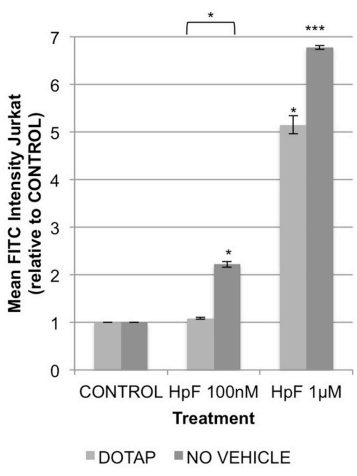

B)

% FITC+ K562 CELLS		
SAMPLE		MEAN ±STD ERROR
	CONTROL	1.23 ± 0.51
	HpF 100nM	82.25 ± 11.86 *
DOTAP	HpF 1µM	97.92 ± 1.67 ***
	HpF 100nM	10.46 ± 5.00
NO VEHICLE	HpF 1µM	38.13 ± 18.04

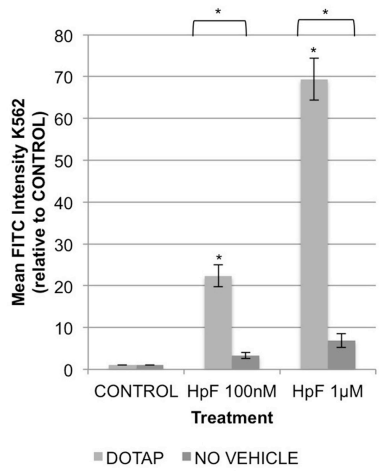

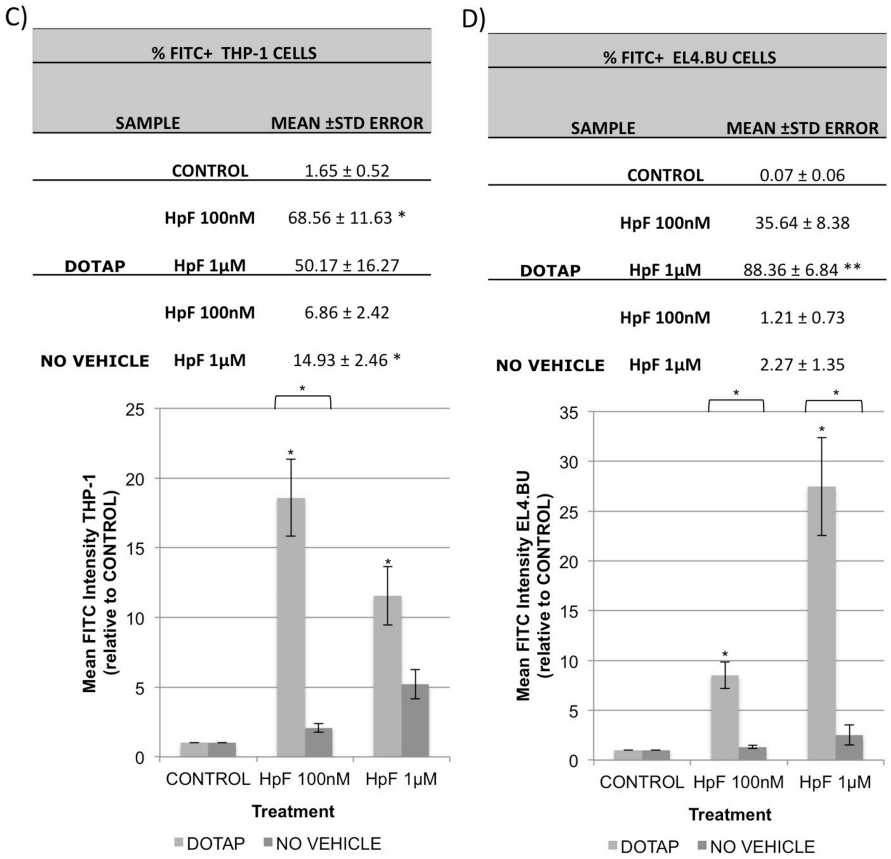

Figure 29. Uptake of PPRHs in different hematological malignancies. Jurkat (A), K562 (B), THP-1 (C) and EL4.BU.OU6 (D) cells were incubated with 100 nM and 1 µM of HpF with (light grey) or without DOTAP (dark grey) for 24 h. Uptake was measured by flow cytometry. Tables show percentage of fluorescent cells determined as FITC-positive IP-negative cells. Graphs represent the mean intensity of fluorescence of cells, relative to the CONTROL (not treated with HpF). Data represent the mean ± SE of a minimum of 3 experiments. *p < 0.05., ***p<0.005. DOTAP was used at the maximum concentration of 10µM, resulting in a PPRH:DOTAP ratio of 1:100 and 1:10 for the concentrations of 100 nM and 1 µM of PPRH, respectively.

As each cell line behaved in a different fashion, it was convenient to analyze them independently.

A) At 100nM, Jurkat cells were more efficiently transfected without vehicle than with DOTAP, whereas at 1µM a population superior to 70% of FITC+ cells displayed a similar intensity in both cases. Despite that these results open the possibility to use PPRHs without vehicle in these cells, it would be important to take into account the low value of fluorescence obtained, compared to cell lines efficiently transfected with liposomes.

B) K562 cells were easily transfected with DOTAP and displayed a dose-response effect, reaching almost 100% of FITC+ cells with a mean of 69.4 at 1µM. However, the PPRH was not able to enter the cell without the liposomal reagent. As a consequence, the difference in the conditions was significant at both concentrations.

C) THP-1 cells were also transfected more efficiently using DOTAP than without it, but in this case, the best condition was 100nM of PPRH with 10µM of DOTAP, reaching 68% of FITC+ cells with a maximum intensity of around 20.

D) The behavior of EL4.BU cell line was similar to K562, the transfection using DOTAP was more efficient than without vehicle, reaching 88% of cells transfected with 27.5 of mean intensity at 1µM.

The same experiments were performed using a fluorescent ASO, instead of the PPRH. We aimed to determine if the different uptake in each cell line was dependent on the molecule used in the study. It is important to take into account that the intrinsic fluorescence of the ASO-F is higher than the Hp-F, which is reflected in higher mean intensities for all cell lines. This is something we cannot control because it depends on the commercial labeling yield of each molecule.

Table 8. Uptake of ASOs in different hematological malignancies. Jurkat (A), K562 (B), THP-1 (C) and EL4.BU.OU6 (D) cells were incubated with 100 nM and 1 µM of ASO-F with or without DOTAP for 24 h. Uptake was measured by flow cytometry. Tables show percentage of fluorescent cells determined as FITC-positive IP-negative cells and mean intensity of fluorescence, relative to the CONTROL (not treated with ASO-F). Data represent the mean ± SE of a minimum of 3 experiments. *p < 0.05., ***p<0.005. DOTAP was used at 5 µM for the concentration of 100 nM and 10µM for 1 µM of ASO, respectively.

A)

Jurkat CELLS			
SAMPLE		% FITC+ ±STD ERROR	MEAN INTENSITY ±STD ERROR
	CONTROL	1.76 ± 0.47	1 ± 0.00
DOTAP	ASO-F 100nM	85.40 ± 13.05	10.51 ± 3.87
	ASO-F 1µM	97.56 ± 0.23	58.40 ± 7.4
NO VEHICLE	ASO-F 100nM	97.43 ± 1.53	26.76 ± 1.78
	ASO-F 1µM	98.30 ± 0.27	57.29 ± 3.23

B)

K562 CELLS			
SAMPLE		% FITC+ ±STD ERROR	MEAN INTENSITY ±STD ERROR
	CONTROL	1.23 ± 0.51	1 ± 0.00
DOTAP	ASO-F 100nM	89.97 ± 6.73	138.38 ± 24.38
	ASO-F 1µM	98.97 ± 0.23	140.22 ± 46.86
NO VEHICLE	ASO-F 100nM	52.63 ± 15.81	20.68 ± 7.48
	ASO-F 1µM	75.40 ± 11.82	33.68 ± 9.54

C)

THP-1 CELLS			
SAMPLE		% FITC+ ±STD ERROR	MEAN INTENSITY ±STD ERROR
	CONTROL	1.65 ± 0.52	1 ± 0.00
DOTAP	ASO-F 100nM	61.34 ± 11.63	98.38 ± 28.39
	ASO-F 1µM	98.88 ± 0.53	70.52 ± 12.55
NO VEHICLE	ASO-F 100nM	58.70 ± 8.87	14.16 ± 2.39
	ASO-F 1µM	98.81 ± 0.44	50.28 ± 7.08

D)

EL4.BU6 CELLS			
SAMPLE		% FITC+ ±STD ERROR	MEAN INTENSITY ±STD ERROR
	CONTROL	0.07 ± 0.06	1 ± 0.00
DOTAP	ASO-F 100nM	85.57 ± 6.84	40.26 ± 7.22
	ASO-F 1µM	99.17 ± 0.54	74.58 ± 10.11
NO VEHICLE	ASO-F 100nM	5.90 ± 3.77	8.31 ± 4.11
	ASO-F 1µM	17.98 ± 6.34	30.55 ± 16.82

Results are shown in Table 8. If we look at the trends of each cell line, we can extract one general conclusion, each cell line behaves the same way either using a PPRH or an ASO. Jurkat cells reached the highest mean intensity without DOTAP at 100nM of ASO, and similar intensities and percentage of FITC+ cells at 1μM, which resembles to the results using the PPRH. For cells easily transfected with DOTAP, such as K562 and EL4, we observed also a high percentage of FITC+ cells with high mean intensity only when using DOTAP. Regarding THP-1 cells, they were also best transfected with DOTAP, and the best conditions were, as well as for PPRHs, 100nM of ASO. It is important to take into account ASOs complexed with DOTAP are used at different ratios than PPRHs; specifically, the best ratio is 1:10, as established previously in our group (Rodriguez 1999). That is why we used different concentrations of DOTAP for the ASO, 5 μM of DOTAP for 100nM and 10μM of DOTAP for 1μM of ASO, reaching ratios of 1:50 and 1:10, respectively.

Regarding B-cell lymphoma derived lines, they are also known to be difficult to transfect. Moreover, ASOs are used in clinical trials against these malignancies without the use of vehicles (O'Brien et al. 2005). Then, the aim of the study was to elucidate if naked PPRHs were also able to enter these cells. To do so, we performed a time and dose-dependent study using naked PPRHs, for Granta-519 (Figure 30A), HBL-2 (Figure 30B), and WSU-FSCCL cells (Figure 30C). In order to compare the results, we also analyzed the internalization of PPRHs using DOTAP as transfection reagent (Figure 30D).

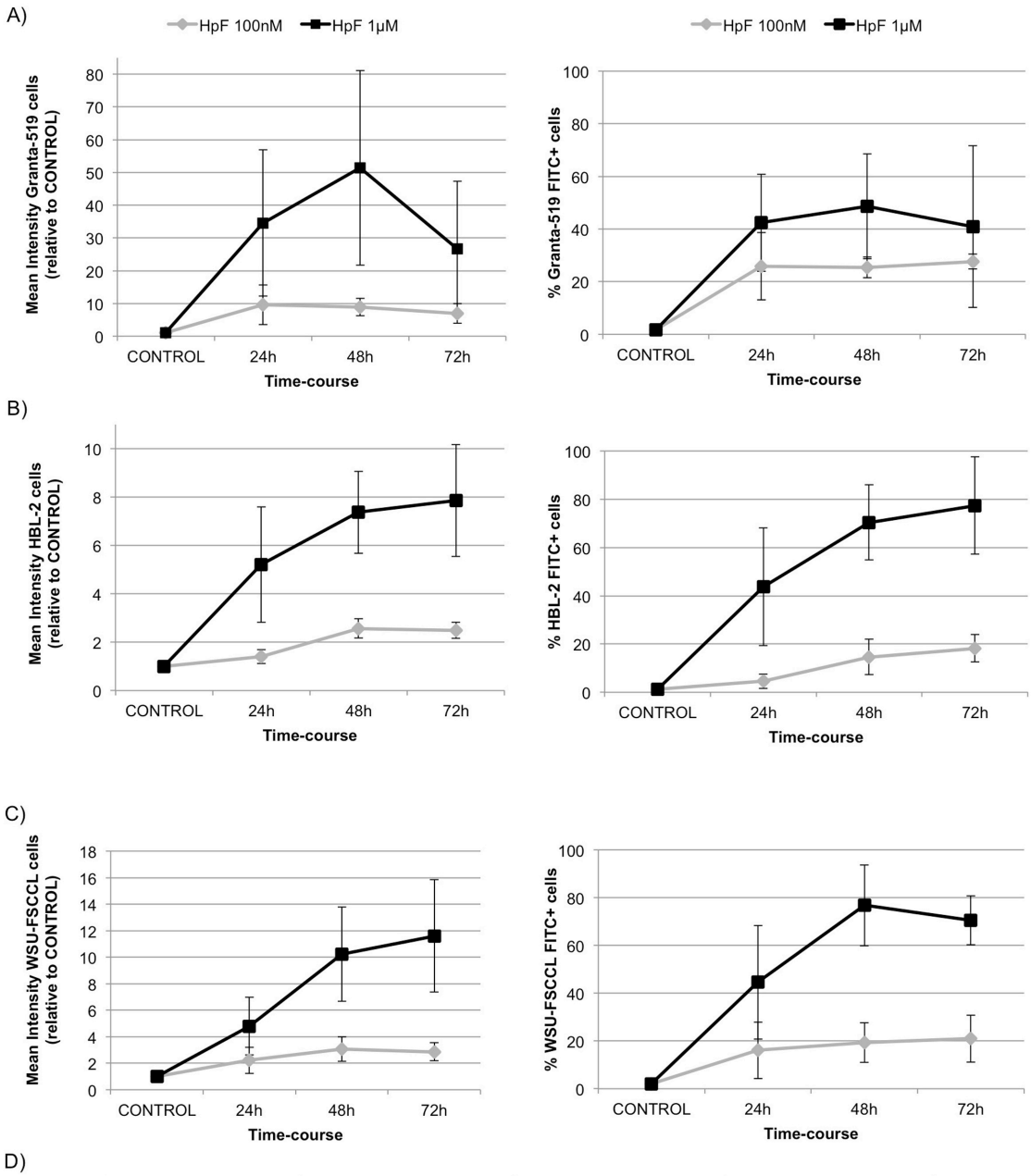

D)

		Granta-519 CELLS		HBL-2 CELLS		WSU-FSCCL CELLS	
SAMPLE		MEAN INTENSITY	% FITC+	MEAN INTENSITY	% FITC+	MEAN INTENSITY	% FITC+
CONTROL		1.00	3.56	1.00	0.76	1.00	1.03
HpF 100nM + DOTAP	24h	21.91	88.08	4.81	58.34	19.36	97.42
	48h	47.85	98.57	11.87	60.22	13.77	73.57

Figure 30. Uptake of PPRHs in different lymphoma cell lines. Granta-519 (A), HBL-2 (B) and WSU-FSCCL(C) cells were incubated with 100 nM and 1 µM of HpF without DOTAP for 24, 48 and 72 h. Uptake was measured by flow cytometry. Mean intensity and %FITC+ cells are represented as the mean ± SE of a minimum of 2 experiments. D) Cells were incubated with 100nM HpF and 10µM of DOTAP. The table shows the mean intensity of fluorescence and the percentage of fluorescent cells determined as FITC-positive and IP-negative cells.

It is also better to analyze these results independently of cell line:

A) Granta-519 cells exhibited the highest mean intensity (around 50, relative to untreated CONTROL) compared to the other lymphoma cell lines. The percentage of fluorescent cells was around 50% from 24h and it did not increase throughout time. The usage of DOTAP increased the percentage of FITC+ cells but the mean intensity was not higher than 50, indicating that the total amount of PPRH inside the cells was similar to the amount obtained without the vehicle.

B) The mean intensity obtained with HBL-2 cells was considerable lower, however, almost 80% of cells were FITC+ after 72 h. In this cell line, neither the intensity nor the percentage of FITC+ cells increased significantly when using DOTAP as a vehicle, therefore, it did not offer any advantage upon transfection. These results were similar to those obtained in Jurkat cells.

C) In WSU-FSCCL cells, incubation with 1 μM of fluorescent PPRH for 72h caused an increase in mean intensity of around 10 units in 70% of the cells. Similar fluorescence and percentage of FITC+ cells were obtained using DOTAP.

5. DISCUSSION

The aims of this work were to expand the applications of PPRHs as gene silencing tools and as promising therapeutic agents. To do so, it was necessary to increase our knowledge about PPRHs. Specifically, it was essential to understand their mechanism of action and to examine their efficacy, both *in vitro* and *in vivo.* Moreover, we tried to improve their properties as much as possible to tackle the concerns related to gene silencing techniques.

5.1. Validation of PPRHs *in vitro* and *in vivo*

To properly validate a technology, the choice of the appropriate gene is of prime importance. Cancer is a heterogeneous disease but several nodal genes involved in the preliminary stages give rise to cancer and allow the maintenance of its proliferative status. Target-directed therapies have been under development since the nineties with the purpose to kill specifically cancer cells by attacking their most important hallmarks.

In our group, Polypurine reverse Hoogsteen hairpins have been under study for the past ten years. From the knowledge gathered about TFOs and purine hairpins, we proved that PPRHs were able to bind to double strand DNA, opening the possibility to use these molecules as gene modulating tools. The next step was to design PPRHs against genes involved in cancer proliferation. In this regard, PPRHs were proved to be useful against *DHFR* in breast cancer cell lines. In this work, we wanted to extend their use against targets involved in important cancer pathways, such as *survivin* and *Bcl-2*.

Survivin and *Bcl-2* are good therapeutic targets because they are important players in resisting cell death due to their anti-apoptotic activity and to their overexpression in different malignancies. In fact, various strategies to target *survivin* and *Bcl-2* are presently under clinical trials. These strategies are mainly based on antisense oligonucleotides (LY2181308 for *survivin* and oblimersen for *Bcl-2*) or small molecules (YM155 for *survivin* and ABT-derivatives for *Bcl-2*). So far, none of the above-mentioned drugs have been approved by the regulatory agencies.

To study the efficacy of PPRHs against these anti-apoptotic targets, we designed molecules against different regions within these genes and evaluated their effect in terms of cell viability and apoptosis.

5.1.1. *In vitro* validation

5.1.1.1 *Survivin*

To ensure that gene silencing molecules exert their function, internalization must be achieved. We used the liposomal reagent DOTAP and tested its suitability as a vehicle for PPRHs in the three cell lines used in this work (PC3, HCT116 and MiaPaCa 2). Despite each cell line has a different efficiency of transfection, all of them were sensitive to PPRHs against *survivin* in the nanomolar range. Indeed, 30 nM of PPRHs was enough to induce a response. Specifically, we observed that the most effective PPRHs were those directed towards promoter sequences of the *survivin* gene (HpsPr-T and HpsPr-C). These PPRHs caused a powerful decrease in cell viability in all cell lines tested and the Coding-PPRH (HpsPr-C) also caused a considerable increase in apoptosis in only 24 h. Carrasco et al. also proved the relation between the antisense inhibition of *survivin* and the increase of apoptosis (Carrasco et al. 2011). Therefore, we can conclude that the effect caused by PPRHs correlated with the well-known implication of *survivin* in apoptosis.

We studied the gene silencing capacity of these molecules by measuring *survivin* mRNA levels upon transfection with 100nM of the most effective PPRHs. HpsPr-T and HpsPr-C induced a dose-response decrease in *survivin* mRNA levels and caused a decrease in protein levels.

Once we selected the PPRHs against promoter sequences as the best candidates, we explored in-depth their mechanism of action. Previously in our group, a Template and a Coding-PPRH against intron 3 of the *DHFR* gene were studied and different mechanisms of action were proposed. Whereas the Template-PPRH (HpdI3-B) inhibited transcription (de Almagro et al. 2009), the Coding-PPRH (HpdI3-A-TA) caused a splicing alteration by prevention of binding of U2AF65 (de Almagro et al. 2011). In fact, we performed experiments to add extra proof of the inhibition of transcription exerted by HpdI3-B when bound to its target sequence.

In this work, we studied PPRHs against promoter sequences and proposed a different mechanism of action. Using EMSA assays with HeLa and PC3 nuclear extracts, we proved that the binding of these molecules to their target sequences prevented the binding of transcription factors specific for these target sequences, which may ultimately cause the observed decrease in *survivin* expression. Specifically, HpsPr-T prevented the binding of Sp1 and Sp3 to their GC-box at -

1009 in the *survivin* promoter, and HpsPr-C prevented the binding of GATA-3 to its binding sequence at -525. Figure 31 shows a representation of the mechanism of action of both PPRHs. On the one hand, various authors have found Sp1 boxes in the *survivin* promoter that were responsible for its basal expression, and established a relation between binding of both Sp1 and Sp3 to these boxes and *survivin* expression (Li & Altieri 1999; Xu et al. 2007). On the other hand, GATA transcription factors act as key regulators in a variety of tissues. GATA-2 and GATA-3 are the majority members in prostate tissue and play an important role in urogenital development (Perez-Stable et al. 2000). In fact, GATA-2 was found highly expressed in a proportion of prostate cancer patients, and this was related to poor outcome (Böhm et al. 2009). Nevertheless, it is important to take into account that both Sp1 and GATA are common transcription factors and there might be off-target effects due to interference with the binding boxes present in other genes. In this regard, we compared different binding sites for these transcription factors and verified that whereas the core is highly conserved, the flanking sites are different enough. Thus, bearing in mind that the binding sequences for PPRHs are 20 or more base pairs in length, which are much longer than the core site, PPRHs can be specific enough for their target sequence. In fact, the lack of variation in the mRNA levels of different genes carrying binding boxes for these transcription factors in their promoters proved that point. Moreover, preliminary studies using whole genome analysis showed that incubation with PPRHs did not alter the expression of unintended targets (data not shown).

To assess off-target effects in a functional way, we assayed the most effective PPRHs in a normal cell line (HUVEC) and in two murine cell lines (CT26 and 4T1). The lack of effect observed in these cell lines demonstrated that these PPRHs were innocuous for cell lines that did not overexpress *survivin* such as HUVEC, or for cell lines expressing murine *survivin*, with a clustal score of 19.7 upon alignment of *survivin* human and murine sequences. In conclusion, these PPRHs were not toxic for normal cells and were species-specific.

From these results we can deduce that the mechanism of action is common for different cell lines, but that each PPRH will exert their silencing effect by a different mechanism according to the location of their target region.

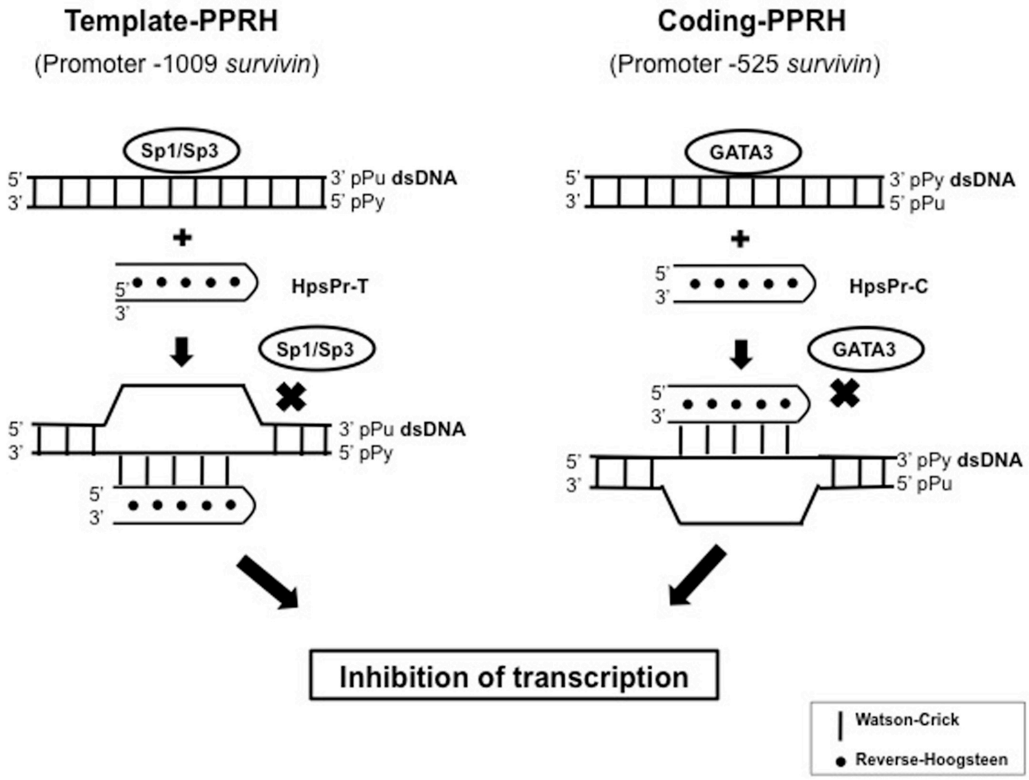

Figure 31. Mechanism of Action of Template- and Coding-PPRHs against promoter sequences.

5.1.1.2. *Bcl-2*

To widen the application of PPRHs against anti-apoptotic targets, we designed and compared four different PPRHs against *Bcl-2* in the aforementioned cell lines. In this case, the most effective PPRHs were HpBcl2Pr-C, directed against the *Bcl-2* promoter and HpBcl2E1-C, directed against exon 1. All the PPRHs against Bcl-2 were also proved to be harmless in a murine cancer cell line (CT26), which reinforced the statement that these PPRHs were specific for the human sequences. Silencing of *Bcl-2* caused a decrease in cell viability and an increase in apoptosis, the latter effect observed in just 24h, in agreement with Bcl-2 being an anti-apoptotic target. This effect correlated with the results from the *survivin* PPRHs, and proved that when the target is involved in an important pathway, the effect is quite fast. Additional studies performed with HpBcl2E1-C proved its capacity to decrease *Bcl-2* mRNA and protein levels. All of these results also support the conclusions from de Almagro et al., 2011, that stated that the activity of a Coding-PPRH against *DHFR*, an enzyme involved in nucleotide synthesis, was observed in

only 48h (de Almagro et al. 2011). Apart from oblimersen, which is under clinical trials, there are other gene silencing molecules under development against *Bcl-2*; recently, another ASO against the 5' region of the *Bcl-2* gene displayed anti-proliferative effects in a panel of cancer cell lines and xenografts using liposomes and other nanoparticle platforms (Rodrigueza et al. 2014).

Exploring PPRHs against two independent anti-apoptotic targets and reaching similar conclusions proved PPRHs to be a robust technology.

5.1.2. *In vivo* validation

After all the *in vitro* studies conducted in this work, we decided to take the next step toward *in vivo* studies. Subcutaneous xenograft models are widely used to test efficacy of new anticancer agents as they can provide valuable preliminary information about efficacy and toxicity. Moreover, it is a technique that allows easy monitoring and measurement of tumor growth, and that is reproducible. However, we must keep in mind the limitations of the method: the tumor is not located in its native tissue hence it might behave differently. Moreover, these tumors do not develop metastases (Simeoni et al. 2013). A retrospective analysis from NCI using data from xenograft models and Phase II clinical trials, found that 45% of the molecules tested in xenograft models were predictive of responsiveness in clinical settings. Therefore, tests of the activity of new agents in various xenograft models increase the probability of clinical activity (Johnson et al. 2001).

We performed two *in vivo* studies to determine the efficacy of the most effective PPRH *in vitro* (HpsPr-C) compared with a scrambled PPRH (Hps-Sc). We monitored tumor growth throughout administration via two routes, namely intratumoral and intravenous, in a subcutaneous xenograft tumor model of prostate cancer. In both settings, the specific PPRH was able to induce a significant decrease in tumor volume, without induction of toxicity to the animals. Tumors administered intratumorally with HpsPr-C exhibited a lower content of *survivin* and a lower degree of vasculature. The decrease in *survivin*, although modest, may be related with the delay in tumor growth observed in these tumors. It is not the first time a modest silencing activity in protein expression using a xenograft model produced a good antitumoral effect. Carrasco et al. reported that a chemically modified ASO against *survivin* decreased its levels for 48h in two xenografts

models. However, evaluation of the average *survivin* content by immunoblotting showed a slight effect (Carrasco et al. 2011). A possible explanation was an uneven distribution of the silencing molecule in the tumor. Since the Western blot were performed using the homogenized tumor, the sample would include cells that internalized the molecules and cells that were intact, thus the effect detected might be diluted. Moreover, *survivin* expression is tightly regulated with a quite short half-life of around 30 min (Zhao et al. 2000), hampering detection of expression changes.

Intratumoral and intravenous injections present obvious differences. Intratumoral administration is aggressive, and disaggregation of the tumor could induce to artifacts when measuring the tumor. Moreover, distribution inside the tumor is poor (Holback & Yeo 2011). In fact, even though both types of administration showed a delay in tumor growth, intravenous administration displayed a greater effect. All in all, use of two different routes of administration and accomplishment of the same results reflects the reliability and robustness of the technology.

It is noteworthy that, despite the PPRH delayed tumor growth, it did not stop completely the development of the tumor, indicating either more dose would be necessary or that inhibition of *survivin* was not enough to stop cancer from spreading. Although target-directed therapy is an attractive approach for its specificity, targeting only one gene might not be enough to eradicate cancer. The main reason is the capability of cancer cells to develop resistance by redundant pathways (Hanahan & Weinberg 2011). For that reason, most trials in the current days are based on combination therapies. Accordingly, a combination between PPRHs and other molecules might be a good idea and studies in this direction should be performed in the future.

To sum up, a PPRH against *survivin* was demonstrated to decrease tumor growth *in vivo*, which is the first preclinical proof of principle of this technology for their use as a new therapeutic approach.

5.2. Other applications of PPRHs as silencing tools:

One of the goals of this work was to broaden the applications of PPRHs as a technology for gene validation. In this regard, I have collaborated in two scientific articles to apply these molecules in two different experimental settings.

5.2.1.Functional validation of Sp1 targets ((Oleaga et al. 2012), Appendix)

Sp1 is a transcription factor that regulates genes related to development of tissues and organs, cell cycle and cancer.

The aim of this work was to determine new genes regulated by Sp1 *in vivo*. To do so, microarray experiments were performed after treatment with a siRNA against Sp1 in HeLa cells. After data analysis using GeneSpring GX software and literature mining, 11 genes were validated as Sp1 targets. Among these genes were RAB20, FGF21 and IHPK2. RAB20 belongs to the RAS oncogene family and is overexpressed in different tumors. FGF21 is a member of the fibroblast growth factor family and is involved in cellular processes such as growth and metabolism. Inositol hexaphosphate kinase 2 (IHPK2) is an enzyme that might intervene in regulation of cell death.

I was involved in the validation of the above-mentioned genes regulated by Sp1. PPRHs against these 3 genes were designed to validate their role in cancer proliferation. Transfection of these PPRHs caused a decrease in cell viability of around 97% for HpRAB20 and HpFGF21, and 52% for HpIHPK2, whereas the negative controls showed no effect. These results confirmed that these three genes, which were regulated by Sp1, were involved in proliferation and cancer.

5.2.2. PPRHs against GSTs in MTX resistance. ((Barros et al. 2013), Appendix)

Resistance to chemotherapeutics, such as methotrexate (MTX), is a main drawback for cancer treatments. Elucidation of drug resistance mechanisms is of utmost importance to tackle the genes responsible for the appearance and maintenance of resistance.

The aim of this work was to establish whether there was a relationship between cytochrome *c* and resistance to methotrexate. It was proved that the reduced state of cytochrome *c*, achieved by using exogenous reducing agents (TMPD or ascorbate) or reduced glutathione (GSH), protected cells from MTX-induced

apoptosis. Whole genome expression microarray data from MCF-7 sensitive and resistant cells revealed that isoforms of the Glutathione S-transferases (GSTs) family were overexpressed in different resistant cells in contrast to sensitive cells. To explore the implication of these enzymes in GSH levels and reduction of cytochrome *c*, their increased levels were validated both at the mRNA and protein levels and functional assays were performed. PPRHs were used to decrease the levels of GSTM1 and GSTM4 and we tested if that decrease sensitized MCF-7 cells to MTX.

The contribution I made in this project was to use PPRHs against different GSTs in MCF-7 resistant cells and SaOs2 resistant cells to determine if the decrease in GST levels induced sensitization to MTX in terms of cell viability and apoptosis. Treatment of both sensitive and resistant cells with PPRHs against GSTs prior to administration of MTX, sensitized cells, hence inducing an increase in cell death caused by MTX.

The conclusion of this work was that overexpression of GSTs and increased GSH levels are related to a more reduced state of cytochrome *c*, which prevent the cells from MTX-induced apoptosis.

5.3. Improvements of PPRHs

5.3.1. Comparison between gene silencing molecules

Nowadays, the modulation of gene expression by nucleic acids has become a routine tool for laboratory research. However, gene silencing as a therapeutic strategy needs to overcome several technical problems previously stated in the introduction.

Despite ASOs and siRNAs have similarities because both are nucleic acids and they both target mRNA, they have also differences in terms of cost, stability, and delivery. However, several studies have compared the activity of these two molecules and no clear choice has become apparent, much to the contrary, they argued that the choice would always depend upon the application - *in vitro* or *in vivo*-, type of administration and delivery system -systemically or locally-. Modifications such as locked nucleic acids (LNA) or 2-O-methoxyethyl (2' MOE)-RNA, among others, have increased the affinity and potency of ASOs and siRNAs while reducing undesirable responses (Watts & Corey 2012).

We have previously demonstrated in our group the higher stability of PPRHs compared to non-modified siRNAs. We also analyzed the immune response after transfection of either a scrambled PPRH or an unspecific siRNA and concluded that PPRHs are less immunogenic than siRNAs (Villalobos et al. 2014). These results are encouraging because PPRHs display better attributes than siRNAs, without the need of modifications. However, other properties needed to be studied to prove the suitability of PPRHs as gene targeting tools.

Previously in our group, a comparison of the effect of a PPRH, an ASO and a siRNA against the same target was conducted in MCF-7 resistant cells. Results showed that a Template-PPRH against *DHFR* was more effective than an ASO and a siRNA against the same gene (de Almagro et al. 2009). It is important to bear in mind that PPRHs follow the antigene strategy, which presents several advantages compared to the antisense effect exerted by antisense oligonucleotides (ASOs) or small interfering RNAs (siRNAs). First, when targeting the gene, there are only two targets per cell corresponding to the two alleles, compared to the multiple copies of mRNA. Secondly, inhibition of transcription avoids formation of mRNA, while molecules that inhibit translation do not stop formation of the mRNA and are meant to act in a more transient fashion. Finally, targeting DNA might impair DNA-

binding proteins that might be important for gene expression (Praseuth et al. 1999).

In this work, we compared PPRHs with TFOs designed against the same region (two promoter regions within the *survivin* gene). Comparison of these two molecules provides valuable information because of their similarities. First, both molecules are directed towards the same region but to complementary sequences: the PPRH is directed against the pyrimidine strand and the TFO against the purine strand. Moreover, both molecules have the same composition of purines, except that the PPRH is double-stranded by formation of a hairpin structure and the TFO is single-stranded. Finally, both molecules form triplexes with the DNA, whereas the PPRH forms Watson-Crick bonds with the target sequence and intramolecular reverse-Hoogsteen bonds, the TFO forms reverse-Hoogsteen bonds with the purine strand of the double-stranded target sequence. This study corroborated that the presence of the hairpin structure in the PPRH have several advantages: i) the binding affinity is higher for the PPRH than for the TFO, i.e the PPRH binds to the target sequence at lower concentrations. ii) At equal conditions, PPRHs are more potent than TFOs in terms of decrease in cell viability. iii) The difference in effect is due to the intrinsic efficacy of the molecule because the uptake is similar for both molecules. Our results are in agreement with Kool (Vo et al. 1995), indicating that the presence of the reverse-Hoogsteen strand in the PPRH, even though it does not interact with the double-stranded DNA sequence, provides an advantage for PPRHs over TFOs.

5.3.2. Important properties upon design

We explored important properties of PPRHs, such as length and specificity, to establish some recommendations upon design of PPRHs.

For any target gene, the TFO target sequence search tool supplies different possibilities of purine sequences, susceptible to be used to design PPRHs. These sequences vary in length, percentage of Guanines, strand (forward or reverse) and location (promoter, intron, exon) within the gene. Up until this moment, we have proved that both Template- and Coding-PPRHs against a particular gene decreased the levels of the targeted gene, although with different mechanisms of action depending on the location of the target sequence.

It is known that polypurine/polypyrimidine sequences are more abundant in regulatory regions, such as introns and promoters (Goñi et al. 2006). Both Template and Coding-PPRHs against either introns or promoters have been demonstrated to be effective. PPRHs against intronic sequences of the *DHFR* gene decreased cell viability of breast cancer cell lines. Two PPRHs against promoter sequences of the *survivin* gene and a Coding-PPRH against an exonic sequence of *Bcl-2* decreased cell viability and increased apoptosis of cancer cell lines from prostate, colon and pancreas, through the decrease in the levels of the targeted genes.

5.3.2.1. Length

Regarding the length, our results conclude that whenever possible, the longer the PPRH, the higher the effect. In our hands, PPRHs from 20-nucleotide length were able to bind with high affinity to their target sequence, show effect and maintain specificity (Rodriguez et al. 2013). When the sequence of the gene allows for longer target sequences, such as in the case of the *TERT* gene, a longer PPRH was demonstrated to cause a higher decrease in cell viability than their shorter versions. It was previously stated that upon design of ASOs and TFOs, a 17-nucleotide long sequence should find one single target in the genome (François et al. 1999). Naturally, the longer the sequence, the less probability the molecule would bind to unintended targets.

Other authors proved that when using pyrimidine TFOs, length also played an important role. They observed that the triplex was more stabilized with longer molecules (Shindo et al. 1993). However, a similar study using G,T-TFOs showed that the optimal length was 12-mer. They explained the difference between these two molecules in the capability of G-rich oligonucleotides to self-associate, thus avoiding triplex formation. Despite that, they did not found a correlation between the formation of tetraplexes and the inability to form triplexes (Cheng & Van Dyke 1997). Arimondo et al. studied the importance of length in G,A-TFOs. They stated that longer TFOs bound to the target sequence with a lower K_d, meaning a higher stability of the triplex. They also studied the importance of sequence polarity, reaching to the conclusion that presence of Guanines in 3' reflected in a higher

stability due to its role in the nucleation step during triplex formation (Arimondo et al. 1998).

There has been also studies regarding length of polypyrimidine PNAs which form triplexes with its target sequence. Bentin et al. proved that PNAs of 12 and 15-mer displayed more complexity in terms of structures than 10-mer PNAs, but displayed a similar efficiency of binding (Bentin et al. 2006). Other authors proved that a 19-mer PNA inhibited expression while 15-mer and 17-mer against the same target did not, proving inhibition of gene expression is sensitive to PNA length (Liu et al. 2004).

Bhagat et al. studied the gene silencing activity of RNA and DNA oligonucleotides ranging from 15- to 25-mer, and found that the 19-mer DNA and RNA oligonucleotides were the most efficient ones in decreasing mRNA levels (Bhagat et al. 2011).

siRNAs length has also been explored. Kim et al. studied a set of dsRNAs ranging from 21 to 45-bp against different targets and determined that the best candidate was the 27-mer duplex, while longer duplexes lost RNAi activity (Kim et al. 2005). Hu et al. studied siRNAs against *huntingtin* ranging from 15 to 21-nucleotides and concluded that when using siRNAs below 17-nt, the potency decreased (Hu et al. 2014).

All in all, length is an important property to take into consideration when designing gene silencing molecules, although the best length will depend on the type of molecule.

5.3.2.2. Specificity

In regard to specificity, and with the goal to address concerns about off-target effects, we decided to explore the possibility to use PPRHs carrying pyrimidine interruptions, the so-called Wild-type PPRHs.

Up until now, when a pyrimidine target sequence had purine interruptions, the designed PPRH contained adenines in the place of the interruption in both domains of the PPRH. This approach was previously studied in our group and it was confirmed that PPRHs carrying adenines maintained the binding while keeping the pure purine sequence of the PPRH. Below there is the reasoning for the choice of this approach.

Coma et al. studied the effect of one interruption on an 11-nt hairpin by EMSA and T_m assays. They substituted the pyrimidine interruption (C) for either adenine or guanine (hairpin1-AA or hairpin1-GG) in both strands of the PPRH or used the pyrimidine of the interruption (C) in the Watson-Crick domain and its complementary base (G) in the reverse-Hoogsteen domain of the hairpin (hairpin1-CG). EMSA assays showed that the three molecules were able to bind to their double-stranded target sequence, but hairpin1-AA had the higher binding affinity, followed closely by hairpin1-CG, while hairpin1-GG displayed the lowest affinity. These results were corroborated using melting experiments, in which hairpin1-AA and hairpin1-CG had a T_m of 45ºC, while hairpin1-GG had a T_m of 40.7ºC. Using the approach of adenines, the hairpin was elongated to 20-nucleotides, which then contained 3 mismatches substituted by adenines in both strands of the molecule. Binding of this hairpin was checked in EMSA assays and they proved that in spite of interruptions, the binding occurred in just 10 minutes and with high affinity (Coma et al. 2005).

Afterward, de Almagro et al. tested the effect of interruptions not only in terms of binding but also in functional assays. They tested two PPRHs against *DHFR*: A 20-nt PPRH carrying one interruption (T), which was substituted in both strands by either adenines (HpdI3-misTA), guanines (HpdI3-misTG) or thymidines (HpdI3-misTT); and another PPRH of 21-nt carrying one interruption (C) substituted by adenines in both strands (HpdI3-misCA). They observed that all the PPRHs bound to their target sequence, but the PPRH using thymidines (HpdI3-misTT) was the one with the lowest affinity. Upon transfection of these PPRHs in breast cancer cells, those carrying adenines in the interruptions worked better than the others, but all of them less efficiently than the PPRH without interruptions. They concluded that adenine was the best base to use in front of the interruption to diminish the effect on instability in triplex formation (de Almagro et al. 2009).

So far, when one pyrimidine interruption occurred in the PPRH sequence, adenine was the base to use. It is obvious to deduce that the longer the target sequence, the more interruptions is meant to have. In this work we have demonstrated that PPRHs of 20 (HpsPr-C), 26 (HpsPr-T) and 30 (HptI10-T) nucleotides carrying 3 interruptions substituted by adenines in both strands of the

PPRH were able to bind to their target sequence with high affinity and cause a reduction of the targeted gene levels. However, the more interruptions are substituted by adenines, the more probability that some binding to unintended targets may occur. To enlarge the options to design PPRHs against regions carrying interruptions without penalizing their specificity, we decided to test whether the use of the pyrimidine interruptions was detrimental for the binding affinity of the PPRH. We tested three approaches using a 26-nt PPRH against *survivin* carrying 3 interruptions: using adenines in both strands as the positive control (HpsPr-T), using the pyrimidine interruptions in both strands of the PPRH (HpsPr-T WT) or using the pyrimidine interruption in the Watson-Crick domain and its complementary base in the reverse-Hoogsteen domain. (HpsPr-T WT 2). In EMSA assays we observed that the three PPRHs were able to bind to their target sequence, thus corroborating the results from Coma and de Almagro (Coma et al. 2005; de Almagro et al. 2009). Moreover, the three PPRHs produced the same binding pattern, suggesting that the change of bases did not alter their structure. In cell viability assays, the PPRH that caused a higher decrease in cell viability was the one carrying pyrimidine interruptions in both strands of the PPRH (HpsPr-T WT) and it was the chosen approach for the follow-up experiments. This result is different from those by de Almagro, in which the best candidate was the one carrying adenines. It is worth mentioning that HpdI3-misTT – the more similar approach to WT- showed low affinity of binding, and it was not further tested *in vitro.* In our case, using the best PPRHs against *survivin*, we designed their Wild-type counterparts and compared their effect in terms of binding, melting experiments, cell viability and analyzed their gene silencing capacity. We proved that Wild-type PPRHs bound with better affinity to their target sequences, exhibited by a higher intensity of binding, a higher T_m and a lower ΔG. Regarding efficacy, WT-PPRHs had a lower IC_{50} than the regular PPRHs and were able to decrease *survivin* mRNA levels. Analysis of cell viability and mRNA levels using the best candidate for *Bcl-2*, HpBcl2E1-C, in comparison with its Wild-type counterpart, showed the same behavior.

Other authors have tried to tackle the problem of interruptions in triplex binding by using either natural or synthetic analogues within the TFO sequence (Gowers & Fox 1999). As an example, Aviñó et al. used parallel-hairpins with 8-

aminopurines to increase affinity (Aviñó et al. 2002). Newer approaches included using triplex intercalators, such as neomycin, to enhance affinity (Arya 2011). In our approach, nor synthetic bases nor intercalators were necessary, however, it would be interesting to study in-depth the chemical binding that takes place between this WT-PPRH and its specific target sequence. The effect of mismatches in TFOs has been studied, and the results pointed out the importance in the location of the mismatch. Specifically, interruption at the 3' end of purine TFOs destabilized the triplex because this sequence is important for the nucleation during triplex formation (Arimondo et al. 1998).

5.3.2.3. Wedge-PPRH

We developed a new molecule, the so-called Wedge-PPRH, able to bind to both strands of the DNA in a locked structure. It was composed of a PPRH (HpsPr-T WT) that bound to its pyrimidine target sequence and a 5' extension complementary to the displaced polypurine sequence in the complementary strand of the target DNA. The extension with the appropriate length (17-nt) allowed for the formation of a quintuplex structure at low concentrations, proving the new structure had a slightly higher affinity. The effect in terms of cell viability was also slightly better than that of the Wild-type PPRH and it was maintained when increasing the number of cells. Other authors have tested similar approaches using TFOs with two consecutive target sequences in the two strands of the DNA, but the approach was only tested *in vitro* by EMSA assays (Jayasena & Johnston 1992; Balatskaya et al. 1996). In our case, we further tested this idea in cells.

5.3.2.4. Uptake

PPRHs designed against anti-apoptotic targets such as *survivin* and *Bcl-2* complexed with DOTAP are able to enter cell lines from solid tumors and exert their effect. To extend the application of these PPRHs, we performed a screening of the uptake of PPRHs into different cell lines derived from hematological malignancies using flow cytometry. This was quite a challenge taking into account that most of these cell lines are known to be hard-to-transfect (Zhao et al. 2012).

Flow cytometry is a technique widely used to study the uptake of molecules. The advantage of using fluorescein-labeled molecules and to dye cells with

propidium iodide is the possibility to discard dead cells and have the certainty to analyze only alive cells with the proper size and complexity. Dead cells tend to accumulate polyanions (such as DNA molecules), and could induce false positive results. Regarding the possible interaction between fluorescein and lipid membranes due to its hydrophobicity, competition experiments between non-labelled and 5'-fluorescently labeled oligonucleotides proved both molecules behave in a similar way, hence the presence of the fluorophore may not alter the results (Tonkinson & Stein 1994).

We decided to evaluate two approaches: the uptake using DOTAP and without the aid of a vehicle.

On the one hand, taking into account all the uptake results using DOTAP, from both solid tumor cell lines and hematological malignancies, we could extract a trend. In general, the values for the mean intensity of cell lines from solid tumors were higher than the mean obtained using hematopoietic cell lines. Therefore, DOTAP is a good transfection reagent for solid tumors, but there is need to find other approaches to internalize PPRHs in hematological malignancies. This conclusion corroborates the known complexity associated with using gene-silencing technologies in hematological malignancies. Other authors have tested polymer nanocomplexes to deliver plasmid DNA in Jurkat cells and reported a maximum of 27% transfection rate (Zhao et al. 2012). However, it is worth mentioning that MiaPaCa 2, which is the cell line with a lower efficiency of transfection, had a mean intensity similar to that obtained for K562 and Granta-519, using DOTAP. As we observed an effect in MiaPaCa 2 cells, there would be interesting to test the effect in these other cell lines.

On the other hand, we tried the naked strategy because oligonucleotides in clinical trials for leukemia, such as oblimersen, were administered without vehicle, either alone (O'Brien et al. 2005) or in combination with other chemotherapeutic agents (NCI 2002). In fact, the study of the uptake mechanism of oligonucleotides into cells have found that uptake depends on concentration; whereas at low concentration, ASOs interact with membrane receptors that mediate their internalization (Loke et al. 1989), at higher than 1 μM, ASOs enter by fluid phase endocytosis (Yakubov et al. 1989). Therefore, cells can internalize oligonucleotides without the aid of a vehicle, and we hypothesized that as PPRHs were also DNA

molecules, they might enter without vehicle as well. Nonetheless, it is worth mentioning that positive internalization is not an unequivocal sign of a reliable effect. Although entrance is promising, oligonucleotides can be trapped in endosomes or lisosomes where they cannot exert their function, as it was demonstrated in HL60 cells for a phosphorothioate ASO (Tonkinson & Stein 1994). Nevertheless, uptake studies in K562 cells found that internalization of a phosphorothioate ASO took place via the endosomal pathway to be then translocated into the nucleus (Beltinger et al. 1995). Hartmann et al. found that localization of an ASO varied upon via of internalization, when entering naked, the ASO localized in vesicles whereas when using lipofectin, the ASO localized in the nucleus (Hartmann et al. 1998). All of these studies reflect the great amount of variables needed to take into account in uptake experiments.

From our results we can conclude that uptake depends on the cell line, as each one displays different transfection efficiencies, but does not depend on the molecule, as comparison between a PPRH and an ASO demonstrated the same tendency for both molecules in each cell line. Zhao et al. have also observed a heterogeneous uptake depending on the cell type. They reported that myeloid cells, and specifically monocytes, internalized more fluorescently labeled ASO than B or T-cells. They also found that leukemic cells internalized more ASO than normal cells from the same patient and that activated cells, by means of using proliferative inducers, internalized more ASO than non-activated cells. This proved that different uptake between cell lines might be related to different proliferative rate (Zhao et al. 1996).

We also observed that 100nM was not enough to produce an increase in fluorescence, while at 1μM there was an increase both in mean intensity and in the percentage of fluorescent cells, meaning the spontaneous uptake is concentration dependent, as previously suggested by other authors (Loke et al. 1989; Yakubov et al. 1989).

Altogether, use of PPRHs in hematological malignancies remains a challenge although some advances have been made. We now know that while some cell lines could be tested with naked PPRHs (Jurkat and WSU-FSCCL), others could be transfected with DOTAP or other reagents (K562 and Granta-519). However, of crucial importance is the development of vehicles to enhance internalization.

6. CONCLUSIONS

1. Both Template- and Coding-PPRHs against anti-apoptotic targets decrease cell viability and increase apoptosis in cancer cell lines from prostate, colon and pancreas (PC3, HCT116 and MiaPaCa 2).

2. PPRHs have a rapid effect and work at nanomolar range, like siRNAs, and at lower concentration than that needed for ASOs or TFOs to exert their effect.

3. PPRHs against human *survivin* do not cause decrease in cell viability of either a human normal cell line or murine cancer cell lines. Therefore, PPRHs proved to be target-specific and species-specific.

4. The PPRHs against promoter sequences within the *survivin* gene, HpsPr-T and HpsPr-C, decrease both mRNA and protein levels of the targeted gene.

5. HpsPr-T and HpsPr-C prevent the binding of transcription factors specific for their target sequences, thus causing a decrease in gene expression. Specifically, HpsPr-T prevents the binding of Sp1 and Sp3, and HpsPr-C prevents the binding of GATA-3.

6. The *in vivo* administration, both intratumorally and intravenously, of a Coding-PPRH against a promoter sequence of the *survivin* gene, HpsPr-C, cause a decrease in tumor growth of a PC3 xenograft compared to administration of a scrambled molecule (Hps-Sc), which constitutes the proof of principle of this technology. This PPRH also causes a decrease in *survivin* protein levels and a decrease in blood vessel formation.

7. PPRHs can be used as a tool to validate genes in proliferation and cancer. PPRHs can be used to target genes related to resistance, as chemosensitizers.

8. Using the *TERT* gene as a model, we concluded that when designing PPRHs, the longer the PPRH, the greater the effect, starting with a minimum of 20 nucleotides for specificity.

9. PPRHs display higher efficacy in terms of binding and effect than TFOs.

10. Wild-type PPRHs have a higher affinity and thermal stability of binding than regular PPRHs, and this reflects on a lower IC_{50} in PC3 and SKBR3 cells.

11. Wedge-PPRH, a further development derived from the PPRHs, also caused an effect *in vitro* against a prostate and a breast cancer cell line, showing a slightly higher binding and efficacy.

12. PPRHs are efficiently transfected into cancer cell lines from solid tumors using DOTAP as a vehicle. For hematopoietic malignancies, study of uptake lead to conclude that each cell line must be explored separately. Use of naked PPRHs can be tested but development of an optimal vehicle is essential.

BIBLIOGRAPHY

Adams, J.M. & Cory, S., 2007. The Bcl-2 apoptotic switch in cancer development and therapy. *Oncogene*, 26(9), pp.1324–1337.

De Almagro, M.C. et al., 2011. Coding polypurine hairpins cause target-induced cell death in breast cancer cells. *Human gene therapy*, 22(4), pp.451–63.

De Almagro, M.C. et al., 2009. Polypurine hairpins directed against the template strand of DNA knock down the expression of mammalian genes. *The Journal of biological chemistry*, 284(17), pp.11579–89.

Altieri, D.C., 2003a. Survivin, versatile modulation of cell division and apoptosis in cancer. *Oncogene*, 22(53), pp.8581–9.

Altieri, D.C., 2003b. Validating survivin as a cancer therapeutic target. *Nature reviews. Cancer*, 3(1), pp.46–54.

Ambrosini, G., Adida, C. & Altieri, D.C., 1997. A novel anti-apoptosis gene, survivin, expressed in cancer and lymphoma. *Nat Med*, 3(8), pp.917–921.

Arimondo, P.B. et al., 1998. Triple Helix Formation by (G , A) -Containing Oligonucleotides : Asymmetric Sequence Effect †. *Biochemistry*, 37(47), pp.16627–16635.

Arya, D.P., 2011. New approaches toward recognition of nucleic acid triple helices. *Accounts of Chemical Research*, 44, pp.134–146.

Astellas Pharma Inc, 2007. An Open-Label Study of YM155 + Docetaxel in Subjects With Advanced Hormone Refractory Prostate Cancer and Other Solid Tumors. *Clinicaltrials.Gov*, pp.5/1/2007–3/1/2010.

Aviñó, A. et al., 2002. Properties of triple helices formed by parallel-stranded hairpins containing 8-aminopurines. *Nucleic Acids Res*, 30(12), pp.2609–2619.

Azmi, A.S. et al., 2011. Emerging Bcl-2 inhibitors for the treatment of cancer. *Expert Opin Emerg Drugs*, 16(1), pp.59–70.

Balatskaya, S. V, Belotserkovskii, B.P. & Johnston, B.H., 1996. Alternate-strand triplex formation: modulation of binding to matched and mismatched duplexes by sequence choice in the Pu-Pu-Py block. *Biochemistry*, 35(41), pp.13328–13337.

Barros, S. et al., 2013. The Redox State of Cytochrome C Modulates Resistance to Methotrexate in Human MCF7 Breast Cancer Cells. *PLoS ONE*, 8(5).

Beltinger, C. et al., 1995. Binding, uptake, and intracellular trafficking of phosphorothioate-modified oligodeoxynucleotides. *The Journal of clinical investigation*, 95(4), pp.1814–23.

Bentin, T., Hansen, G.I. & Nielsen, P.E., 2006. Structural diversity of target-specific homopyrimidine peptide nucleic acid-dsDNA complexes. *Nucleic acids research*, 34(20), pp.5790–9.

Bhagat, L. et al., 2011. Novel oligonucleotides containing two 3′-ends complementary to target mRNA show optimal gene-silencing activity. *Journal of Medicinal Chemistry*, 54, pp.3027–3036.

Bodur, C. et al., 2013. Pramanicin Analog Induces Apoptosis in Human Colon Cancer Cells: Critical Roles for Bcl-2, Bim, and p38 MAPK Signaling. *PLoS ONE*, 8(2).

Böhm, M. et al., 2009. A role for GATA-2 in transition to an aggressive phenotype in prostate cancer through modulation of key androgen-regulated genes. *Oncogene*, 28(43), pp.3847–56.

Bold, R.J. et al., 1999. Prognostic factors in resectable pancreatic cancer: p53 and bcl-2. *J Gastrointest Surg*, 3, pp.263–277.

Burnett, J.C., Rossi, J.J. & Tiemann, K., 2012. Current progress of siRNA/shRNA Therapeutics in Clinical Trails. *Biotechnol J*, 6(9), pp.1130–1146.

Carrasco, R. a et al., 2011. Antisense inhibition of survivin expression as a cancer therapeutic. *Mol Cancer Ther*, 10(2), pp.221–232.

Carter, B.Z. et al., 2001. Cytokine-regulated expression of survivin in myeloid leukemia. *Blood*, 97(9), pp.2784–2790.

Cheng, A.J. & Van Dyke, M.W., 1997. Oligodeoxyribonucleotide length and sequence effects on intramolecular and intermolecular G-quartet formation. *Gene*, 197, pp.253–260.

Chi, K.N., 2005. Targeting Bcl-2 with oblimersen for patients with hormone refractory prostate cancer. *World journal of urology*, 23(1), pp.33–7.

Coma, S. et al., 2005. Strand displacement of double-stranded DNA by triplex-forming antiparallel purine-hairpins. *Oligonucleotides*, 15(4), pp.269–283.

Coma, S. et al., 2004. Use of siRNAs and antisense oligonucleotides against survivin RNA to inhibit steps leading to tumor angiogenesis. *Oligonucleotides*, 14(2), pp.100–113.

Dohi, T. et al., 2004. Mitochondrial survivin inhibits apoptosis and promotes tumorigenesis. *Journal of Clinical Investigation*, 114(8), pp.1117–1127.

Duca, M. et al., 2008. The triple helix: 50 years later, the outcome. *Nucleic Acids Res*, 36(16), pp.5123–5138.

Elbashir, S.M. et al., 2001. Duplexes of 21 ± nucleotide RNAs mediate RNA interference in cultured mammalian cells. *Nature*, 411, pp.1–5.

Faucon, B., Mergny, J.L. & Helene, C., 1996. Effect of third strand composition on the triple helix formation: purine versus pyrimidine oligodeoxynucleotides. *Nucleic Acids Res*, 24(16), pp.3181–3188.

Felgueiras, J., Silva, J.V. & Fardilha, M., 2014. Prostate cancer: the need for biomarkers and new therapeutic targets. *Journal of Zhejiang University. Science. B*, 15(1), pp.16–42.

Felsenfeld, G. & Rich, A., 1957. Studies on the formation of two- and three-stranded polyribonucleotides. *Biochim Biophys Acta*, 26(3), pp.457–468.

Ferreira, C.S.M. et al., 2008. DNA aptamers against the MUC1 tumour marker: design of aptamer-antibody sandwich ELISA for the early diagnosis of epithelial tumours. *Anal Bioanal Chem*, 390(4), pp.1039–1050.

François, J. et al., 1999. Design of antisense and triplex-forming oligonucleotides. *methods in enzymology*, 313(1997), pp.74–95.

Furuya, Y. et al., 1996. Expression of bcl-2 and the progression of human and rodent prostatic cancers. *Clin Cancer Res*, 2, pp.389–398.

Gall, J.G. et al., 1998. RNA as a target of double-stranded RNA-mediated genetic interference in Caenorhabditis elegans. *Proc Natl Acad Sci U S A*, 95, pp.15502–15507.

Gianani, R. et al., 2001. Expression of survivin in normal, hyperplastic, and neoplastic colonic mucosa. *Hum Pathol*, 32(1), pp.119–125.

Goni, J.R. et al., 2004. Triplex-forming oligonucleotide target sequences in the human genome. *Nucleic acids research*, 32(1), pp.354–60.

Goñi, J.R. et al., 2006. Exploring the reasons for the large density of triplex-forming oligonucleotide target sequences in the human regulatory regions. *BMC genomics*, 7, p.63.

Gowers, D.M. & Fox, K.R., 1999. Towards mixed sequence recognition by triple helix formation. *Nucleic Acids Res*, 27(7), pp.1569–1577.

Grillone, L.R. & Lanz, R., 2001. Fomivirsen. *Drugs of Today*, 37, pp.245–255.

Hair, P., Cameron, F. & McKeage, K., 2013. Mipomersen sodium: First global approval. *Drugs*, 73, pp.487–493.

Hall, C. et al., 2013. Bcl-2 family of proteins as therapeutic targets in genitourinary neoplasms. *Clinical genitourinary cancer*, 11(1), pp.10–9.

Hanahan, D. & Weinberg, R. a, 2011. Hallmarks of cancer: the next generation. *Cell*, 144(5), pp.646–74.

Hanahan, D. & Weinberg, R.A., 2000. The hallmarks of cancer. *Cell*, 100(1), pp.57–70.

Hartmann, G. et al., 1998. Spontaneous and Cationic Lipid-Mediated Uptake of Antisense Oligonucleotides in Human Monocytes and Lymphocytes 1. *The Journal of pharmacology and experimental therapeutics*, 285(2), pp.920–928.

Hewett, P.W. et al., 2006. Selective inhibition of the human tie-1 promoter with triplex-forming oligonucleotides targeted to Ets binding sites. *Mol Med*, 12(1-3), pp.8–16.

Holback, H. & Yeo, Y., Intratumoral drug delivery with nanoparticulate carriers. *Pharm Res*, 28(8), pp.1819–1830.

Hoogsteen, K., 1963. The crystal and molecular structure of a hydrogen-bonded complex between 1-methylthymine and 9-methyladenine. *Acta Crystallographica*, 16, pp.907–916.

Hu, J. et al., 2014. Exploring the effect of sequence length and composition on allele-selective inhibition of human huntingtin expression by single-stranded silencing RNAs. *Nucleic acid therapeutics*, 24(3), pp.199–209.

Jackson, A.L. et al., 2003. Expression profiling reveals off-target gene regulation by RNAi. *Nat Biotechnol*, 21(6), pp.635–637.

Jayasena, S.D. & Johnston, B.H., 1992. Oligonucleotide-directed triple helix formation at adjacent oligopurine and oligopyrimidine DNA tracts by alternate strand recognition. *Nucleic acids research*, 20(20), pp.5279–88.

Jiang, K., 2013. Biotech comes to its “antisenses” after hard-won drug approval. *Nature medicine*, 19(3), p.252.

Johnson, J.I. et al., 2001. Relationships between drug activity in NCI preclinical in vitro and in vivo models and early clinical trials. *British journal of cancer*, 84(10), pp.1424–1431.

Kawasaki, H. et al., 1998. Inhibition of apoptosis by survivin predicts shorter survival rates in colorectal cancer. *Cancer Res*, 58(22), pp.5071–5074.

Kim, D.-H. et al., 2005. Synthetic dsRNA Dicer substrates enhance RNAi potency and efficacy. *Nature biotechnology*, 23(2), pp.222–6.

Kleinman, M.E. et al., 2008. Sequence- and target-independent angiogenesis suppression by siRNA via TLR3. *Nature*, 452, pp.591–597.

Krajewska, M. et al., 1996. Immunohistochemical Analysis of bcl-2 , bax , bcl-X , and mcl-1 Expression in Prostate Cancers. *AJP*, 148(5), pp.1567–1576.

Li, F. & Altieri, D.C., 1999. Transcriptional analysis of human survivin gene expression. *Biochem J*, 344 Pt 2, pp.305–311.

Liu, Y. et al., 2004. Efficient and isoform-selective inhibition of cellular gene expression by peptide nucleic acids. *Biochemistry*, 43(7), pp.1921–7.

Loke, S.L. et al., 1989. Characterization of oligonucleotide transport into living cells. *Proc Natl Acad Sci U S A*, 86(May), pp.3474–3478.

McDonnell, T.J. & Korsmeyer, S.J., 1991. Progression from lymphoid hyperplasia to high-grade malignant lymphoma in mice transgenic for the t(14; 18). *Nature*, 349, pp.254–256.

Mohammad, R.M. et al., 1993. *A unique EBV-negative low-grade lymphoma line (WSU-FSCCL) exhibiting both t(14;18) and t(8;11).*,

Nakahara, T. et al., 2007. YM155, a novel small-molecule survivin suppressant, induces regression of established human hormone-refractory prostate tumor xenografts. *Cancer Res*, 67(17), pp.8014–8021.

NCI, 2002. Oblimersen, Cytarabine, and Daunorubicin in Treating Older Patients With Acute Myeloid Leukemia. *Clinicaltrials.Gov*, p.4/1/2002.

O'Brien, S.M. et al., 2005. Phase I to II multicenter study of oblimersen sodium, a Bcl-2 antisense oligonucleotide, in patients with advanced chronic lymphocytic leukemia. *Journal of Clinical Oncology*, 23(30), pp.7697–702.

O'Connor, D.S., Grossman, D., et al., 2000. Regulation of apoptosis at cell division by p34 cdc2 phosphorylation of survivin. *PNAS*, 97(24), pp.10–14.

O'Connor, D.S., Schechner, J.S., et al., 2000. Short Communication Control of Apoptosis during Angiogenesis by Survivin Expression in Endothelial Cells. *American Journal of Pathology*, 156(2), pp.393–398.

Oleaga, C. et al., 2012. Identification of novel Sp1 targets involved in proliferation and cancer by functional genomics. *Biochem Pharmacol*, 84(12), pp.1581–1591.

Osser, C.H.J.R. et al., 2003. Bcl-2 is significantly overexpressed in localized radio-recurrent prostate carcinoma , compared with localized radio-naive prostate carcinoma. *Int. J. Radiation Oncology Biol. Phys.*, 56(1), pp.1–6.

Peng, H.W. et al., 1985. Establishment and characterization of a new human lymphoma-derived cell line--HBL-2. *Chinese journal of microbiology and immunology*, 18, pp.79–85.

Perez-Stable, C.M., Pozas, A. & Roos, B.A., 2000. A role for GATA transcription factors in the androgen regulation of the prostate-specific antigen gene enhancer. *Mol Cell Endocrinol*, 167(1-2), pp.43–53.

Postel, E.H. et al., 1991. Evidence that a triplex-forming oligodeoxyribonucleotide binds to the c-myc promoter in HeLa cells, thereby reducing c-myc mRNA levels. *Proc Natl Acad Sci U S A*, 88(18), pp.8227–8231.

Praseuth, D., Guieysse, a L. & Hélène, C., 1999. Triple helix formation and the antigene strategy for sequence-specific control of gene expression. *Biochimica et biophysica acta*, 1489(1), pp.181–206.

Ramsay, A.K. & Leung, H.Y., 2009. Signalling pathways in prostate carcinogenesis: potentials for molecular-targeted therapy. *Clin Sci (Lond)*, 117(6), pp.209–228.

Robbins, M., Judge, A. & MacLachlan, I., 2009. siRNA and innate immunity. *Oligonucleotides*, 19(2), pp.89–102.

Rodriguez, L., 2015. Improved design of PPRHs for gene silencing. *Molecular Pharmaceutics*. doi 10.1021/mp5007008

Rodriguez, L. et al., 2013. Polypurine reverse Hoogsteen hairpins as a gene therapy tool against survivin in human prostate cancer PC3 cells in vitro and in vivo. *Biochem Pharmacol*, 86(11), pp.1541–1554.

Rodriguez, M., 1999. Effects of anti-sense oligonucleotides directed toward dihydrofolate reductase RNA in mammalian cultured cells. *Int J Cancer*, 81, pp.785–792.

Rodríguez, M. et al., 2002. Development and effects of immunoliposomes carrying an antisense oligonucleotide against DHFR RNA and directed toward human breast cancer cells overexpressing HER2. *Antisense Nucleic Acid Drug Dev*, 12(5), pp.311–325.

Rodrigueza, W. V et al., 2014. Development and antitumor activity of a BCL-2 targeted single-stranded DNA oligonucleotide. *Cancer chemotherapy and pharmacology*, 74(1), pp.151–66.

Satoh, K. et al., 2001. Expression of survivin is correlated with cancer cell apoptosis and is involved in the development of human pancreatic duct cell tumors. *Cancer*, 92(2), pp.271–278.

Scarfò, L. & Ghia, P., 2013. Reprogramming cell death: BCL2 family inhibition in hematological malignancies. *Immunology letters*, 155(1-2), pp.36–9.

Shariat, S.F. et al., 2004. Survivin expression is associated with features of biologically aggressive prostate carcinoma. *Cancer*, 100(4), pp.751–7.

Shindo, H., Torigoe, J.H. & Sara, A., 1993. Thermodynamic and Kinetic Studies of DNA Triplex Formation of an Oligohomopyrimidine and a Matched Duplex by Filter Binding Assay. *Biochemistry*, 32, pp.8963–8969.

Simeoni, M. et al., 2013. Modeling of human tumor xenografts and dose rationale in oncology. *Drug discovery today: Technologies*, 10(3), pp.e365–72.

Siomi, H. & Siomi, M.C., 2009. On the road to reading the RNA-interference code. *Nature*, 457(7228), pp.396–404.

Sternberg, C.N. et al., 2009. Docetaxel plus oblimersen sodium (Bcl-2 antisense oligonucleotide): an EORTC multicenter, randomized phase II study in patients with castration-resistant prostate cancer. *Annals of oncology*, 20(7), pp.1264–9.

Tolcher, a W. et al., 2012. A phase II study of YM155, a novel small-molecule suppressor of survivin, in castration-resistant taxane-pretreated prostate cancer. *Annals of oncology*, 23(4), pp.968–73.

Tonkinson, J.L. & Stein, C.A., 1994. Patterns of intracellular compartmentalization , trafficking and acidification of 5 '-fluorescein labeled phosphodiester and phosphorothioate oligodeoxynucleotides in HL60 cells oligodeoxynucleotides in HL60 cells. *Nucleic Acids Res*, 22(20), pp.4268–4275.

Villalobos, X. et al., 2014. Stability and immunogenicity properties of the gene-silencing polypurine reverse Hoogsteen hairpins. *Mol Pharm*, 11(1), pp.254–264.

Vo, T., Wang, S. & Kool, E.T., 1995. Targeting pyrimidine single strands by triplex formation: structural optimization of binding. *Nucleic Acids Res*, 23(15), pp.2937–2944.

Watts, J.K. & Corey, D.R., 2012. Silencing disease genes in the laboratory and the clinic. *The Journal of pathology*, 226(2), pp.365–79.

Wells, R.D. & Collier, D.A., 1988. The chemistry and biology of unusual DNA structures adopted by oligopurine.oligopyrimidine sequences. *The FASEB Journal*, 2, pp.2939–2949.

WHO, 2012. Globocan 2012 International Agency for Research on Cancer (IARC). *2012*, p.4.

Wiechno, P. et al., 2014. A randomised phase 2 study combining LY2181308 sodium (survivin antisense oligonucleotide) with first-line docetaxel/prednisone in patients with castration-resistant prostate cancer. *European urology*, 65(3), pp.516–20.

Willis, S.N. & Adams, J.M., 2005. Life in the balance : how BH3-only proteins induce apoptosis. *Curr Opin Cell Biol.*, 17(6), pp.617–625.

Wu, H. et al., 2004. Determination of the role of the human RNase H1 in the pharmacology of DNA-like antisense drugs. *The Journal of biological chemistry*, 279(17), pp.17181–9.

Xu, R. et al., 2007. Sp1 and Sp3 regulate basal transcription of the survivin gene. *Biochem Biophys Res Commun*, 356(1), pp.286–292.

Yakubov, L. a et al., 1989. Mechanism of oligonucleotide uptake by cells: involvement of specific receptors? *Proc Natl Acad Sci U S A*, 86(September), pp.6454–6458.

Zhang, M. et al., 2005. Survivin mediates resistance to antiandrogen therapy in prostate cancer. *Oncogene*, 24(15), pp.2474–82.

Zhao, J. et al., 2000. The ubiquitin-proteasome pathway regulates survivin degradation in a cell cycle-dependent manner. *Journal of cell science*, 113, pp.4363–71.

Zhao, N. et al., 2012. Transfecting the hard-to-transfect lymphoma/leukemia cells using a simple cationic polymer nanocomplex. *J Control Release*, 159(1), pp.104–110.

Zhao, Q. et al., 1996. Oligonucleotide uptake in human hematopoietic cells is increased in leukemia and is related to cellular activation. *Blood*, 88, pp.1788–1795.

Zielinski, R.R., Eigl, B.J. & Chi, K.N., 2013. Targeting the apoptosis pathway in prostate cancer. *Cancer J*, 19(1), pp.79–89.

APPENDIXES

Article III:

IDENTIFICATION OF NOVEL SP1 TARGETS INVOLVED IN PROLIFERATION AND CANCER BY FUNCTIONAL GENOMICS

Carlota Oleaga, Sabine Welten, Audrey Belloc, Anna Solé, Laura Rodriguez, Núria Mencia, Elisabet Selga, Alicia Tapias, Veronique Noé and Carlos J. Ciudad

Biochemical Pharmacology 84 (2012) 1581-1591. (Impact factor: 4.650)

Biochemical Pharmacology 84 (2012) 1581–1591

Contents lists available at SciVerse ScienceDirect

Biochemical Pharmacology

journal homepage: www.elsevier.com/locate/biochempharm

Identification of novel Sp1 targets involved in proliferation and cancer by functional genomics

Carlota Oleaga [1], Sabine Welten [1], Audrey Belloc [1], Anna Solé, Laura Rodriguez [3], Núria Mencia [2], Elisabet Selga, Alicia Tapias, Veronique Noé, Carlos J. Ciudad [1,*]

Department of Biochemistry and Molecular Biology, School of Pharmacy, University of Barcelona, Barcelona, Spain

ARTICLE INFO

Article history:
Received 20 June 2012
Accepted 17 September 2012
Available online 25 September 2012

Keywords:
Sp1
Target
Genomics
Proliferation
Cancer

ABSTRACT

Sp1 is a transcription factor regulating many genes through its DNA binding domain, containing three zinc fingers. We were interested in identifying target genes regulated by Sp1, particularly those involved in proliferation and cancer. Our approach was to treat HeLa cells with a siRNA directed against Sp1 mRNA to decrease the expression of Sp1 and, in turn, the genes activated by this transcription factor. Sp1-siRNA treatment led to a great number of differentially expressed genes as determined by whole genome cDNA microarray analysis. Underexpressed genes were selected since they represent putative genes activated by Sp1 and classified in six Gene Onthology categories, namely proliferation and cancer, mRNA processing, lipid metabolism, glucidic metabolism, transcription and translation. Putative Sp1 binding sites were found in the promoters of the selected genes using the Match™ software. After literature mining, 11 genes were selected for further validation. Underexpression by qRT-PCR was confirmed for the 11 genes plus Sp1 in HeLa cells after Sp1-siRNA treatment. EMSA and ChIP assays were performed to test for binding of Sp1 to the promoters of these genes. We observed binding of Sp1 to the promoters of RAB20, FGF21, IHPK2, ARHGAP18, NPM3, SRSF7, CALM3, PGD and Sp1 itself. Furthermore, the mRNA levels of RAB20, FGF21 and IHPK2 and luciferase activity for these three genes related to proliferation and cancer, were determined after overexpression of Sp1 in HeLa cells, to confirm their regulation by Sp1. Involvement of these three genes in proliferation was validated by gene silencing using polypurine reverse hoogsteen hairpins.

1. Introduction

The Sp1 transcription factor which belongs to the Sp family of transcription factors (TF) is characterized by three Cys2His2 zinc fingers required for the sequence-specific DNA binding to GC-rich promoter elements. Sp1 is ubiquitously expressed in mammalian cells and regulates the transcriptional activity of multiple target genes involved in many cellular processes such as cell differentiation, cell cycle progression and oncogenesis [1–3]. Sp1 encodes a 105 kDa protein containing two glutamine-rich transactivation subdomains that stimulate transcription. Next to the glutamine-rich domains there are serine/threonine subregions involved in posttranslational modifications, such as glycosylation, acetylation, phosphorylation and sumoylation, which regulate Sp1 activity [4]. Single or multiple Sp1-binding sites have been mapped in promoters of genes involved in almost all cellular processes. In these promoters, Sp1 is usually a transcriptional activator, whereas Sp3, another TF that belongs to the Sp family, can act as an activator as well as a repressor. Since both transcription factors bind to the same binding site, the Sp1/Sp3 ratio in a cell will determine the activation state of the promoter [3].

Previously, we investigated the regulation of Sp1 by cloning the 5′ region of this gene, determining its transcriptional start site, and analyzing its promoter for putative TF binding sites [5]. The Sp1 promoter is regulated by Sp1, Sp3, NF-Y and E2F [5,6]. Sp1-dependent transcription can also be influenced by changes in Sp1 abundance, as it increases during the G1-phase of the cell cycle, by DNA binding activity and by interaction with other nuclear factors [1], such as the interaction of Sp1 with retinoblastoma protein in a complex that enhances the transcriptional activation of Sp1 [7].

Abbreviations: FDR, false discovery rate; GEO, gene expression omnibus; GO, gene ontology; MTT, 3-(4,5-dimethylthiazol-2-yl)-2,5-diphenyltetrazolium bromide; NE, nuclear extract; NP-40, nonyl phenoxypolyethoxylethanol; PPRHs, polypurine reverse hoogsteen hairpins; RMA, robust multichip average; siNR, siRNA non related; siSp1, siRNA directed against Sp1; TF, transcription factor.

* Corresponding author. Tel.: +34 93 403 4455; fax: +34 93 402 4520.
E-mail addresses: coleaga@ub.edu (C. Oleaga), s.m.j.welten@lumc.nl (S. Welten), didiodr@hotmail.com (A. Belloc), anna_sfer@hotmail.com (A. Solé), laura.rodriguez@ub.edu (L. Rodriguez), nuriamencia@ub.edu (N. Mencia), eselga@gencardio.com (E. Selga), atapias@fli-leibniz.de (A. Tapias), vnoe@ub.edu (V. Noé), cciudad@ub.edu (C.J. Ciudad).

[1] Contributed equally to the work.
[2] Recipient of a fellowship (APIF) from the University of Barcelona (UB).
[3] Recipient of a fellowship (FI) from the "Generalitat de Catalunya".

0006-2952/$ – see front matter © 2012 Elsevier Inc. All rights reserved.
http://dx.doi.org/10.1016/j.bcp.2012.09.014

Sp1 also interacts with CDK4, SKP2, Rad51, BRCA2 and p21, and these proteins are also able to activate the Sp1 promoter. Furthermore, Sp1 mRNA expression is increased upon transient overexpression of CDK4, Rad51, E2F, p21 or Stat3, whereas its mRNA levels are decreased upon overexpression of NF-κB and p53 [8].

Sp1 knockout embryos are retarded in development, show a broad range of abnormalities and die around day 11 of gestation whereas mice lacking Sp3 are postnatal lethal and show cardiac malformations. Knocking out Sp1 and Sp3 is lethal, and heterozygous Sp1/Sp3 mice show embryonic lethality accompanied by a range of developmental abnormalities such as morphological alterations of the lung, impaired ossification, anemia, and placental defects [9]. It can be concluded that the Sp family plays an important role in the normal development of tissues and organs.

Deregulation of Sp1 and Sp3 can be seen in many cancers and diseases. Genes associated to Sp1 such as Rb, p53 and E2F have been found to play important roles in cancer hallmarks [10]. Angiogenesis is an important aspect in the growth and metastasis of cancers and tumor cells are able to produce their own angiogenic factors. Of these angiogenic factors, VEGF is considered to be one of the most potent factors. The expression of the VEGF gene is stimulated by TNF-α, through the action of Sp1 [11]. Transfection of cells with Sp1 decoy oligonucleotides suppressed the expression of VEGF and reduced the invasiveness and proliferation of A459 lung adenocarcinoma and U251 glioblastoma cells [12]. Sp1 protein was found to be highly expressed in the nuclei of gastric tumor cells, whereas minimal levels of Sp1 protein were detected in stromal or normal glandular cells within or surrounding the tumor [13,14]. Furthermore, the survival of patients with high Sp1 protein levels was significantly decreased when compared to patients with low to non-detectable Sp1 protein levels [13].

siRNAs against Sp1, Sp3 and Sp4 have been used to investigate the role of these TFs in angiogenesis and cell growth in Panc-1 cells. siRNAs for Sp3, but not for Sp1 or Sp4, inhibited the phosphorylation of retinoblastoma protein, blocked transition to the G1/S phase and upregulated p27 promoter activity in pancreatic cells [15].

The aim of this work was to identify Sp1 targets, with special emphasis in those involved in proliferation and cancer. It is known that Sp1 is able to regulate a large number of genes through its DNA binding domain, but not much is known about which genes this TF actually regulates *in vivo*. We determined changes in gene expression in HeLa cells upon treatment with a siRNA against Sp1 by using whole human genome microarrays and show evidence for 8 genes newly described to be regulated by Sp1.

2. Materials and methods

2.1. Cell culture

HeLa human cervical carcinoma cells were grown in Ham's F-12 medium containing 7% fetal bovine serum (FBS) (Gibco-Invitrogen-Life Technologies SA, Madrid, Spain). Cell cultures were maintained at 37 °C in a humidified 5% CO_2 environment.

2.2. Sp1 knockdown and overexpression

Sp1 siRNA (siSp1) was designed using the iRNAi 2.1 software (Alexander Griekspoor & Tom Groothuis) and synthesized by Thermo (Thermo Fisher Scientific SL, Madrid, Spain), against the following sense sequence in the Sp1 mRNA: 5′-AACAGCGTTTCTG-CAGCTACC-3′ (GC content: 47.8% and ΔG3′: 7.5; ΔG5′: 7.8; Dif: −0.3). Non-related siRNAs (siNR) were purchased from Ambion (Life Technologies SA, Madrid, Spain).

Transfection with siSp1 was performed using Metafectene (Biontex, Martinsried/Planegg, Germany). For each 35 mm well, 2 μl of metafectene in 100 μl of serum-free F-12 medium were added to 100 nM of the siRNAs in 100 μl of serum-free F-12. Complexes were incubated 20 min at room temperature and were added to the cells for 48 h.

Overexpression of Sp1 was accomplished by transient transfection (48 h) of 1 μg of an expression vector for Sp1 (pCMV-Sp1) using Fugene 6® (Roche, Barcelona, Spain) following the manufacturer's instructions. Briefly, 3 μl of Fugene in 100 μl of serum-free medium was incubated at room temperature for 5 min. The vector was added to the mixture and incubated at room temperature for 20 min before its addition to the cells.

2.3. Real time RT-PCR (qRT-PCR)

Total RNA was extracted from HeLa cells (30,000), either control or treated with siSp1 or pCMV-Sp1, using the Ultraspec™ RNA reagent (Biotecx, Ecogen, Barcelona, Spain) in accordance with the manufacturer's instructions. Complementary DNA was synthesized from 1 μg of total RNA as described in [16]. Sp1 mRNA levels were determined in an ABI Prism 7000 Sequence Detection System (Applied Biosystems, Life Technologies SA, Madrid, Spain) using 3 μl of the cDNA mixture and the assays-on-demand Hs00412720_m1 for Sp1 and Hs99999901_s1 for 18S RNA (Applied Biosystems, Life Technologies SA, Madrid, Spain). 18S RNA was used as endogenous control. The reaction was performed following the manufacturer's recommendations.

RAB20, FGF21, IHPK2, ARHGAP18, NPM3, SFRS7, CALM3, PGD, SLC2A3, CEBPδ and CBFβ mRNA levels were determined by SYBR-Green qRT-PCR (Applied Biosystems, Life Technologies SA, Madrid, Spain) and the pairs of primers listed below (Table 1) using 18S RNA as endogenous control. Fold-changes in gene expression were calculated using the standard ΔΔCt method.

2.4. Western blot analysis

Whole extracts were obtained from control or siSp1 treated cells (30,000) for 48 h according to [17]. Total extracts (40 μg) were resolved on a SDS-7%-polyacrylamide gels (AppliChem, Ecogen, Barcelona, Spain) and transferred to PVDF membranes (Immobilon P, Millipore, Madrid, Spain) using a semidry electroblotter. The membranes were probed with anti-Sp1 antibody (sc-59) (Santa Cruz Biotechnology Inc., Heidelberg, Germany) 1:100 dilution, OVN at 4 °C. Signals were detected with anti-rabbit secondary horseradish peroxidase–conjugated antibody (P0399) (Dako, Barcelona, Spain) 1:5000 dilution, for 1 h at room temperature, and enhanced chemiluminescence, as recommended by the manufacturer (Amersham, GE Healthcare Life Sciences, Barcelona, Spain). To normalize the results blots were reprobed with an antibody against tubulin (Cp06) (Calbiochem, Millipore, Merck, Madrid, Spain) 1:500 dilution, OVN at 4 °C and detected with anti-mouse (NIF 824) (Amersham, GE Healthcare Life Sciences, Barcelona, Spain) 1:2500 dilution, for 1 h at room temperature.

2.5. Cell survival studies

Cell survival was measured by the MTT test as described in [18] (Sigma–Aldrich Quimica S.A., Madrid, Spain). Results were expressed as the percentage of survival with respect to the control.

2.6. Microarrays

Gene expression was analyzed by hybridization to GeneChip® Human Genome U133 PLUS 2.0 Affymetrix microarrays, containing

Table 1
Primers used for mRNA determination by qRT-PCR. The sequences and product sizes for each of the selected genes are indicated.

Gene	Forward primer	Reverse primer	Size (bp)
18S	5′-gcgaaagcatttgccaagaa-3′	5′-catcacagacctgttattgc-3′	508
RAB20	5′-cgccttctacctgaagcagtg-3′	5′-gccggtgattcacatcatag-3′	140
FGF21	5′-cttgaagccgggagttattc-3′	5′-gcttcggactggtaaacattg-3′	162
IHPK2	5′-ccaagggaacatcagttctac-3′	5′-gagtgaatttgcgcatctcag-3′	55
ARHGAP18	5′-cactgaatcgcagtcacttag-3′	5′-gggatcagcttctcttcacc-3′	93
NPM3	5′-ggcaccagattgttacgatg-3′	5′-gaaacttgtcagggaacagg-3′	191
SRSF7	5′-gattgtcatcgttacagccg-3′	5′-cttgatcgtcgaggagatgc-3′	140
CALM3	5′-gatcaatgaggtggatgcag-3′	5′-catctccatcgatgtcagcc-3′	248
PGD	5′-gacatcatcattgacggagg-3′	5′-cacagcagggttctccagttc-3′	229
SLC2A3	5′-gtcaacctgttggctgtcac-3′	5′-ggaaggatggtaaaacccag-3′	293
CEBPδ	5′-ctgcgagagaagctaaacgtg-3′	5′-cttagctgcatcaacaggag-3′	91
CBFβ	5′-gaacagcgacaaacacctag-3′	5′-cccataccatccagtctttg-3′	143

54,675 transcripts and variants. Total RNA for cDNA arrays was prepared from triplicate samples from both control and siSp1-treated cells using RNAeasy Mini kit (Qiagen, Barcelona, Spain) following the recommendations of the manufacturer. The integrity of the RNA species was checked using the Bioanalyzer 2100 system (Agilent Technologies, Madrid, Spain). Labeling, hybridization and detection were carried out following the manufacturer's specifications. Microarray data are available from GEO as series accession number GSE37935.

2.7. Microarray data analysis

Quantification was carried out with GeneSpring GX 11.5.1 software (Agilent Technologies, Madrid, Spain), which allows multi-filter comparisons using data from different experiments to perform the normalization, generation of lists and the functional classification of the differentially expressed genes. The input data was subjected to preprocess baseline transformation using the RMA summarization algorithm using the median of control samples. After grouping the triplicates of each experimental condition, lists of differentially expressed genes could be generated by using volcano plot analysis. Unpaired *t*-Test was applied using asymptotic *p*-value computation and multiple testing correction of Benjamini–Hochberg FDR. The expression of each gene was reported as the ratio of the value obtained for each condition relative to the control condition after normalization and statistical analysis of the data. The corrected *p*-value cut-off applied was of <0.01; then the output of this statistical analysis was filtered by fold expression, selecting specifically those genes that had a differential expression of at least 2-fold. Finally, the obtained gene list was classified according to gene ontology biological processes. After data mining, the selected genes could be grouped into the categories of (i) proliferation and cancer; (ii) mRNA processing; (iii) lipid metabolism; (iv) glucidic metabolism; (v) transcription; and (vi) translation.

2.8. Database searching

Searching for the different promoter sequences analyzed was performed using human BLAT (UCSC Genome Bioinformatics Site). The presence of putative Sp1 binding sites in the promoters was analyzed using the Match™ 1.0 software [19] that uses a library of mononucleotide weight matrices from TRANSFAC® 6.0. The values of the settings for core and matrix were changed depending on the stringency required for the search.

2.9. Electrophoretic mobility shift, supershift and competition assays

Nuclear extracts were prepared as described in [5] from exponentially growing HeLa cells or HeLa cells (5×10^5) transiently transfected (48 h) with 1 μg of an expression vector for Sp1 (pCMV-Sp1) using Fugene 6® (Roche, Barcelona, Spain). The probes were constructed by annealing commercially synthesized complementary single-stranded oligodeoxynucleotides corresponding to putative Sp1 DNA binding sites (underlined) present in the RAB20 (5′-CCCCGCCCCCGCCCCCGGGCC-3′), FGF21 (5′-GGGTGATTGGGCGGGCCTGTC-3′) or IHPK2 (5′-GCGGGACTCCGCCCATGCCAC-3′) gene promoters. Each ds oligonucleotide was gel-purified, end-labeled with T4 polynucleotide kinase (New England Biolabs, Barcelona, Spain) and [γ-^{32}P]-ATP (3000 Ci/mmol, Perkin Elmer, Madrid, Spain), and used as the probe in gel shift experiments. DNA/Protein binding assays were performed as described [20] using 2 μg of nuclear extract, 20,000 cpm of the radioactive probes and 1 μg of poly[d(I-C)] (Sigma–Aldrich Quimica S.A., Madrid, Spain) as unspecific competitor. After electrophoresis in 5% polyacrylamide and 5% glycerol native gels, the bindings were visualized using a PhosphorImager with ImageQuant software v 5.2 (Molecular Dynamics, GE Healthcare Life Sciences, Barcelona, Spain).

In the supershift experiments, 2 μg of rabbit polyclonal antibody PEP-2 (sc-59) (Santa Cruz Biotechnology Inc., Heidelberg, Germany) against Sp1 or 2 μg of rabbit polyclonal antibody (D-20) (Santa Cruz Biotechnology Inc., Heidelberg, Germany) against Sp3 were added to the reaction mixture and incubated on ice for 15 min after addition of the probe.

Competition assays where performed incubating the FGF21 radioactive probe with increasing fold excess (5, 20, 50 and 100×) of competitor ds probes corresponding to RAB20, IHPK2 and FGF21 itself. The addition of the cold probes was performed 15 min before the labeled probe.

2.10. Chromatin immunoprecipitation (ChIP analysis)

HeLa cells were washed twice with phospate-buffered saline (PBS) and subsequently incubated with 1% formaldehyde for 10 min, at room temperature. The crosslinking reaction was terminated by addition of 0.125 M glycine dissolved in PBS. Cells were washed three times with ice-cold PBS, scraped off the culture dish in 2 ml PBS containing 1 mM PMSF and centrifuged at 4 °C for 10 min. The pellet was resuspended in lysis buffer (5 mM Pipes pH 8.0, 85 mM KCl, 0.5% NP40 and protease inhibitors) and after 30 min incubation on ice, cells were dounced on ice to aid nuclei release. After centrifugation at 4 °C for 10 min, the pellet was resuspended in sonication buffer (50 mM Tris–HCl pH 8.0, 10 mM EDTA, 0.1% SDS, 0.5% deoxycholic acid and protease inhibitors). All previous chemical reagents where purchase from AppliChem (Ecogen, Barcelona, Spain). Cells were sonicated in an ice-water bath to obtain chromatin fragments of an average length of 500–1500 bp. This was usually achieved by sonicating the chromatin 8 rounds for 20 s, with 30 s between each round of sonication (cycle was set at 1, amplitude at 50) in a Ultrasonic processor UP 200 S (GmbH, Valladolid, Spain). Sonicated chromatin was then either processed immediately or stored at −80 °C.

For immunoprecipitation, 100 μl of sonicated chromatin was diluted in 900 μl ChIP dilution buffer (16.7 mM Tris–HCl pH 8.1, 1.2 mM EDTA, 0.01% SDS, 1.1% Triton X-100, 167 mM NaCl and protease inhibitors leupeptin and PMSF) and pre-cleared with 20 μl pre-washed protein A/agarose (sc-2001) (Santa Cruz Biotechnology Inc., Heidelberg, Germany) by incubating for 2 h at 4 °C on a rotating wheel. Samples were centrifuged 13,000 rpm for 2 min at 4 °C and the supernatant was then incubated overnight (4 °C, on a rotating wheel) with 5 μg of rabbit polyclonal anti-Sp1 antibody (sc-59 X) (Santa Cruz Biotechnology Inc., Heidelberg, Germany), mouse IgG1 negative control (x0931) (Dako, Barcelona, Spain), or no antibody (beads-only control). After immunoprecipitation, 40 μl of pre-washed protein A/agarose (pre-blocked overnight with 1 μg/μl herring sperm DNA) was added per sample, and incubation continued for 1 h at 4 °C with rotation. The chromatin-antibody-protein A/agarose complexes were collected by centrifugation (13,000 rpm, 2 min, 4 °C). Supernatant from the beads-only control was collected and saved as input. Samples were sequentially washed with 1 ml of low salt buffer (0.1% SDS, 1% Triton X-100, 2 mM EDTA, 20 mM Tris–HCl pH 8.1, 150 mM NaCl, twice for 10 min), high salt buffer (0.1% SDS, 1% Triton X-100, 2 mM EDTA, 20 mM Tris–HCl pH 8.1, 500 mM NaCl, once for 10 min), LiCl buffer (0.25 M LiCl, 0.5% NP40, 0.5% deoxycholic acid, 10 mM Tris–HCl pH 8.1, 1 mM EDTA, once for 5 min) and TE (10 mM Tris–HCl, 1 mM EDTA, pH 8.0, three times for 5 min). The protein/DNA complexes were then eluted from the protein A/agarose by incubation with 250 μl elution buffer (1% SDS, 0.1 M $NaHCO_3$) for 15 min at room temperature. Elution was repeated and eluates were combined. Crosslinking was reversed by addition of 20 μl 5 M NaCl to the eluates and 500 μl of the saved input DNA and overnight heating of the samples to 65 °C. The next day, all samples were digested with 5 μl proteinase K (10 mg/ml) for 1 h at 55 °C. DNA was recovered by phenol/chloroform extraction. DNA precipitation was carried out by addition of 1 ml of absolute ethanol to each sample plus 5 μl of glycogen blue. The resulting pellets were resuspended in TE (in 60 μl TE for the immunoprecipitations and 200 μl TE for the input) and stored at −20 °C until needed for PCR.

PCR was performed to amplify the immunoprecipitated and input DNAs. Primers were designed in the promoter regions for each of the selected genes with PrimerBLAST tool; in such a way that the region amplified contained at least one Sp1 transcription factor binding-site. Table 2 contains primer sequences and information for each of the selected genes.

1–2 μl of immunoprecipitated DNA was used for amplification of the selected genes. PCR reaction mix contained 5% DMSO to facilitate DNA strand separation and to improve PCR efficiency. The reactions were performed in a MJ Research Thermocycler (Ecogen, Barcelona, Spain) under standard conditions in a final volume of 50 μl for at least 32 cycles.

For each sample, 10 μl of the PCR products was electrophoresed in a 5% acrylamide gel. The gel was run at 160 V in TBE 1x, and the amplified fragments were visualized after ethidium bromide staining.

2.11. Luciferase constructs, cotransfections and luciferase assay

Luciferase constructs RAB20.LUC, FGF21.LUC or IHPK2.LUC were engineered by unidirectional cloning of the dsDNA sequence containing the same Sp1 DNA binding sites (underlined) present in the RAB20, FGF21 or IHPK2 gene promoters as those used in the EMSA experiments, between the Mlu I and the Xho I sites of the reporter luciferase vector pGL3-basic (Promega, Madrid, Spain). Hybridization of the following specific primer pairs including the overhang terminus of the restriction enzymes Mlu I and Xho I (highlighted): RAB20-MX-FW (5′-**CGCGT**CCCCGCCCCCGCCCCCGGGCC**C**-3′) & RAB20-MX-RV (5′-**TCGAG**GGCCCGGGGGCGGGGGCGGGG**A**-3′), FGF21-MX-FW (5′-**CGCGT**GGGTGATTGGGCGGGCCTGTC**C**-3′) & FGF21-MX-RV (5′-**TCGAG** GACAGGCCCGCCCAATCACCC**A**-3′) or IHPK2-MX-FW (5′-**CGCGT** GCGGGACTCCGCCCATGCCAC**C**-3′) & IHPK2-MX-RV (5′-**TCGAG** GTGGCATGGGCGGAGTCCCGC**A**-3′) was performed to obtain the inserts.

For luciferase assays, 2.5×10^5 HeLa cells were plated in 6-well dishes the day before transfection. The medium (2 mL) was renewed before transfection that was performed with Fugene 6® (Promega, Madrid, Spain). For each well, the transfection reagent was incubated for 5 min with 100 μL of serum & antibiotic-free medium, followed by the addition of plasmid DNA and incubated for 20 min (ratio of 3:1 (μL of transfection reagent:μg of plasmid DNA), all at room temperature. 500 ng of either RAB20.LUC, FGF21.LUC or IHPK2.LUC and 500 ng of the Sp1 expression vector pCMV-Sp1 [21] were mixed before the addition of the transfection reagent. Luciferase activity was determined 30 h after transfection. Cell extracts were prepared by lysing the cells with 200 μL of freshly diluted 1× Reporter Lysis Buffer (25 mM Tris–Phosphate pH7.8, 2 mM DTT, 2 mM EDTA, 10% glycerol, 1% Triton X_100). The lysate was centrifugated at 12,000 × *g* for 2 min (4 °C) to pellet the cell debries. The supernatants were transferred to a fresh tube. 15 μL of the extract was added to 15 μL of the luciferase assay substrate (Promega, Madrid, Spain) at room temperature. Luminescence of the samples was measured 2 s after mixture in the Glomax™ (Promega, Madrid, Spain) 20/20 Luminometer, in which the light production (relative luminescence units; RLU) was measured with 5 s integration during 10 s. Three different experiments were performed for each transfection.

Luciferase results were corrected by total protein concentration, which was determined with the Bio-Rad protein assay reagent Bradford (Bio-Rad, Barcelona, Spain) according to the manufacturer's protocol.

Table 2
ChIP analysis primer sequences. The sequences of the primers to detect the immunoprecipitated promoters bound to Sp1 are indicated as well as the PCR product sizes.

Gene	Forward primer	Reverse primer	Size (bp)
Sp1	5′-cggacaccaggcacgcaact-3′	5′-gaggcaagcgaacccggacc-3′	216
GAPDH	5′-atggttgccactggggatct-3′	5′-tgccaaagcctaggggaaga-3′	174
RAB20	5′-ggagctcaagagaggaagcgc-3′	5′-ctcggctggagaactcggatg-3′	228
FGF21	5′-ctgtagctcctgccaaatgg-3′	5′-gtggtttagaattggtgccag-3′	217
IHPK2	5′-gttcgaagtagcgtgggaag-3′	5′-cctgcctgtctgcatctaac-3′	181
ARHGAP18	5′-gcgatcctgacacagagaag-3′	5′-cttcgcctcctttaaccaaag-3′	222
NPM3	5′-gctgtaagagccttcttcaaac-3′	5′-gagacactcttccgacacag-3′	297
SRSF7	5′-gcggaaggaactgaagagac-3′	5′-gattgttaaggctgagggtcc-3′	217
CALM3	5′-ccaattcctgtgcagggtg-3′	5′-gagcacggggatcaaggttc-3′	283
PGD	5′-gtcctgcgtgagttgctatg-3′	5′-cgacgcctgttagaccatc-3′	206
SLC2A3	5′-gcaatcttgtgatctctcgg-3′	5′-cctccaggcttttctggtag-3′	233
CEBPδ	5′-ctctgcgtccaagcgaggc-3′	5′-ggcaccctcctgcaacgtg-3′	253
CBFβ	5′-ggagttgtgaatggtgcgtc-3′	5′-cgttccggggagtctgag-3′	245

Table 3
PPRHs against Sp1 targets. The sequences of PPRHs hairpins to knock down Sp1 selected target genes are indicated.

PPRH name	Sequence
Hp-RAB20	5′-aagggagagaggaagagagaagggggttttgggggaagagagaaggaga gagggaa-3′
Hp-FGF21	5′-agggaggaagggaaggaggggggttttgggggaggaagggaaggaggga-3′
Hp-IHPK2	5′-gagggaaagaggagaggaaaagaggaagttttgaaggagaaaaggagagga gaaagggag-3′
Hp-sc	5′-aaaagaagaagaagaagaagaagaagaaggtttttggaagaagaagaagaaga agaagaagaaaa-3′
Hp-nr	5′-cctccttccttcctccctcttccttttccttttttaggaaaaggaagagggaggaagg aaggagg-3′

2.12. PPRH design to knock down RAB20, FGF21 and IHPK2 expression

PPRHs hairpins (Hp) against RAB20, FGF21 and IHPK2 genes were designed as described in de Almagro et al. [22] in order to functionally validate these targets. Non-related (Hp-nr) and scrambled (Hp-sc) PPRHs were assessed as negative controls. Table 3 describes PPRHs sequences used. HeLa cells (10,000) were plated in 35-mm plates and PPRHs transfection (100 nM) was performed using 10 μM DOTAP reagent (Roche, Barcelona, Spain) as in de Almagro et al. [22]. Five days after transfection cell survival was analyzed as previously described in this section. Results were expressed as the percentage of survival with respect to control cells.

3. Results

3.1. Effects of siRNA against Sp1 on its mRNA and protein levels, and on cell survival

Exponentially growing HeLa cells were treated with siSp1 or with a siNR, both at a concentration of 100 nM. After 48 h, Sp1 mRNA levels were measured by qRT-PCR and cell survival was determined by the MTT assay. Sp1 mRNA levels were decreased by 90% in cells treated with siSp1 when compared to cells treated with siNR (Fig. 1A). Knockdown of Sp1 after siSp1 treatment was confirmed by Western blot analysis. Sp1 protein was decreased in cells treated with siRNA against Sp1 when compared to cells treated with siNR and cells treated with no siRNA as a control (Fig. 1B). Cell survival decreased by 50% in cells treated with siSp1, whereas survival of cells treated with siNR was unaffected (Fig. 1C). On the other hand, transient overexpression of Sp1 using a eukaryotic expression vector (3 μg) for this protein caused an increase in cell proliferation of 40%. These results are in accordance with previous studies showing decreased cell growth upon inhibition of Sp-family members [12,15,23].

3.2. Functional genomics upon cell incubation with siSp1

Affymetrix whole genome arrays were used to determine genes that were differentially expressed upon knocking down Sp1 by siSp1 treatment. Genomic analysis was processed using the GeneSpring GX software. Fig. 2 shows a volcano plot of the genes differentially expressed upon Sp1 knockdown. Genes that were underexpressed by at least 2-fold, at a cut-off of $p < 0.01$, were selected for further analysis, since they represent those genes that are putatively activated by Sp1. The underexpressed genes were classified in six GO categories (Table 4).

3.3. Search of Sp1 sites within the promoters of the underexpressed genes

All 36 genes in Table 4 with the exception of one, the lamin B receptor, showed putative Sp1 binding sites when using values for Core > 0.9 and Matrix > 0.8 in the Match™ analyses. Then, a more stringent search for Sp1 binding sites was performed using values of Core = 1 and Matrix > 0.9, shortening the list down to 21 genes. This list was subjected to literature mining to finally select a total of 11 genes according to their bibliographic interest. The 11 selected genes were grouped in 4 GO categories (proliferation, mRNA processing, glucidic metabolism and transcription), which included 3 genes (SLC2A3, C/EBPδ, and CBFβ) already reported as regulated by Sp1 [24–26]. These 3 genes and Sp1 itself [5,6] were taken as positive controls. Additionally, the accuracy of Match™ was positively checked by running this software using the

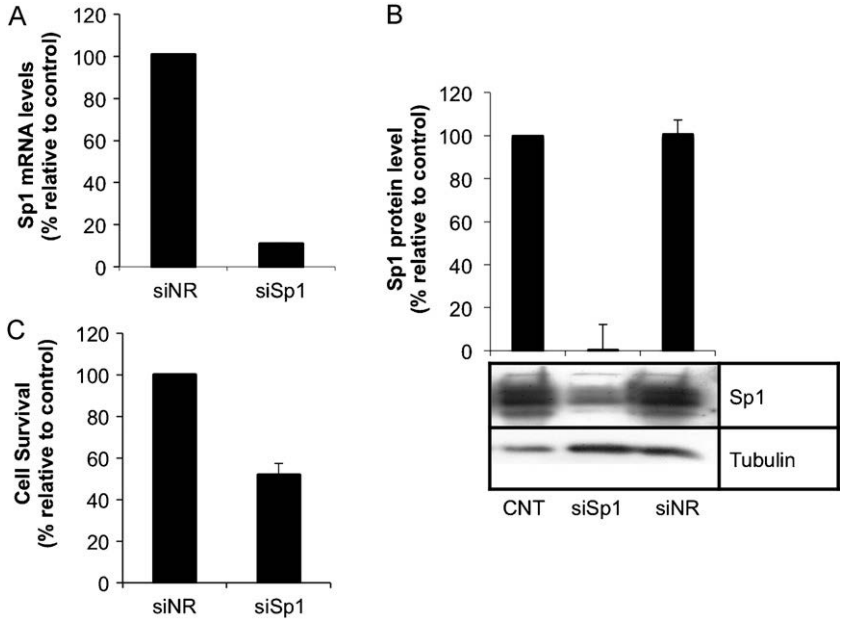

Fig. 1. Cell survival and Sp1 mRNA and protein levels upon siSp1 incubation. Exponentially growing HeLa cells were treated with 100 nM of either siRNA against Sp1 RNA (siSp1) or control (siNR). (A) Sp1 mRNA levels were determined by qRT-PCR. (B) Sp1 protein was determined by Western blot using PEP-2 antibody. (C) Cell survival was assessed by the MTT assay 48 h after the siRNA treatment. Values are the mean ± SE of three independent experiments.

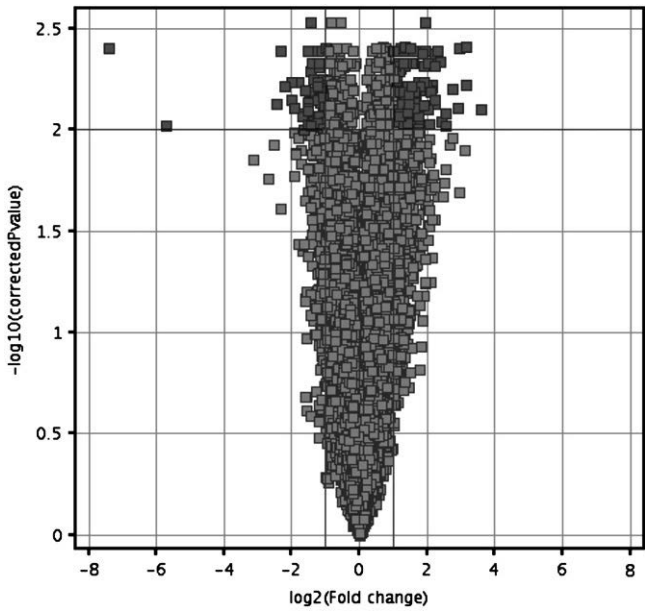

Fig. 2. Identification of genes differentially expressed upon knocking down Sp1. Affymetrix complete genome microarrays (HG U133 PLUS 2.0) were used to identify the changes in gene expression in HeLa cells after treatment with siSp1. Lists of genes differentially expressed in siSp1-treated cells were generated using GeneSpring GX v11.5.1. The image shows a volcano plot representation and the genes differentially expressed by 2-fold with a *t*-test *p*-value of <0.01 are shown in red. Overexpressed genes are located in the upper-right side and underexpressed genes in the upper-left side. (grey scale for printed version).

sequences corresponding to the binding motifs extracted from ChIP-seq technology for the transcription factors STAT1 [27], NF-κβ [28], NRSF [29] and HSF [30]. The sequences of the Sp1 sites of the 11 selected genes, along with the Sp1-box core position, are shown in Table 5.

3.4. Validation at the RNA level of the effects caused by siSp1

Validation of the underexpression caused by siSp1 was determined by qRT-PCR for 11 genes (RAB20, FGF21, IHPK2, ARHGAP18, NPM3, SRSF7, CALM3, PGD, SLC2A3, C/EBPδ and CBFβ). Underexpression was confirmed for all the 11 genes as well as Sp1 (Fig. 3).

3.5. Sp1 regulates RAB20, FGF21 and IHPK2 mRNA levels

To confirm the role of Sp1 in the regulation of the selected genes, the effect of overexpression of Sp1 on the putative targets involved in proliferation and cancer was determined by transfecting HeLa cells with an expression vector for Sp1. After 48 h, RNA was extracted and mRNA levels were determined by qRT-PCR. Sp1 overexpression caused an increase in the mRNA levels of RAB20, FGF21 and IHPK2 genes (Fig. 4).

3.6. Sp1 binds to RAB20, FGF21 and IHPK2 promoters

To test that the putative Sp1-boxes were indeed susceptible to be bound by transcription factor Sp1, we performed EMSA using double stranded 21-nucleotide length probes corresponding to the natural sequence of the Sp1 binding sites within the RAB20, FGF21 and IHPK2 gene promoters. Nuclear extracts were prepared from control HeLa cells or cells transfected with an expression vector for Sp1 (pCMV-Sp1). Fig. 5 shows the binding pattern for the different probes analyzed. The major band corresponds to Sp1 binding and two minor bands correspond to Sp3 binding, as determined in the supershift experiments using Sp1 and Sp3 antibodies. The binding corresponding to Sp1 was increased for the RAB20 (42%), IHPK2 (12%) and FGF21 (9%) gene promoters when using nuclear extracts from cells transfected with pCMV-Sp1.

3.7. Similarity of RAB20, FGF21 and IHPK2 Sp1 binding sequences vs the consensus

Sp1 consensus sequence (G/T)(G/A)GG(C/A)G(G/T)(G/A)(G/A) contains 3 binding subsites for the union of the three zinc fingers of Sp1 [31]. Sequence comparison among RAB20, FGF21 and IHPK2 Sp1 binding sequences and the consensus for this TF was carried out to explain the different Sp1 binding to each promoter when overexpressing Sp1. RAB20 matches with higher similarity with the Sp1 consensus sequence than FGF21 and IHPK2 (Fig. 6A). Competition binding assays between RAB20, FGF21 and IHPK2 Sp1 binding sequences demonstrates that RAB20 sequence shows the highest affinity for Sp1 (Fig. 6 B and C). This observation correlates with its higher similarity with the consensus.

3.8. Sp1 binds to RAB20, FGF21, IHPK2, ARHGAP18, NPM3, SFSR7, CALM3 and PGD in vivo

To investigate whether Sp1 binds *in vivo* to the promoters of the selected genes, ChIP experiments were performed with chromatin from HeLa cells and a specific antibody against Sp1. The promoter regions of the selected genes were amplified from the immunoprecipitated DNA to check for Sp1 binding to these regions. Fig. 7 shows the PCR products from the immunoprecipitations with Sp1 and mouse IgG1 antibodies, in relation to the input. Sp1 protein was found to bind to the promoters of RAB20, FGF21, IHPK2, ARHGAP18, NPM3, SRSF7, CALM3, and PGD. Sp1 promoter was used as positive control.

3.9. Luciferase activity of RAB20, FGF21 and IHPK2 Sp1 binding sites upon Sp1 overexpression

To analyze whether RAB20, FGF21 and IHPK2 promoters could be regulated by transcription factor Sp1, transient transfection assays with the luciferase reporter vectors containing the selected Sp1 binding sequence for each gene (RAB20.LUC, FGF21.LUC and IHPK2.LUC) were performed in HeLa cells. As shown in Fig. 8, overexpression of Sp1 induced luciferase activity of the three genes by more than 2-fold compared to the controls.

3.10. Functional validation of Sp1 proliferation and cancer targets using PPRHs silencing methodology

In order to functionally validate RAB20, FGF21 and IHPK2 as proliferation and cancer target genes we knocked down these genes using specific PPRHs. The evaluation of cell survival was performed afterwards by the MTT assay and a cytoxicity of 40% for IHPK2 and $>95\%$ for RAB20 and FGF21 in HeLa cells was observed (Fig. 9). These effects were specific since cytotoxicity was not induced by the non-related and scrambled PPRHs. Thus, our results confirm the implication of these three genes regulated by Sp1, in proliferation and cancer.

4. Discussion

The main objective of this work was to identify gene targets activated *in vivo* by Sp1. HeLa cells were treated with a siRNA against Sp1 and expression microarrays were carried out to identify changes in gene expression. Since Sp1 is a general transcription factor, there were a substantial number of differentially expressed genes that can be observed by accessing the

Table 4
Gene ontology classification of genes underexpressed by 2-fold. GeneSpring GX was used to classify the genes underexpressed by 2-fold with a *t*-test *p*-value of <0.01 by gene ontology (biological process). The ratio column corresponds to the expression of each gene after Sp1-siRNA treatment relative to the control. The Match™ software and the TRANSFAC® database were used to search for putative Sp1 binding sites in the promoters of the classified genes. R indicates that a reference exists of Sp1 binding to the gene, and the genes selected for further studies are marked with a √.

GOntology biological process	Ratio	Gene symbol	Gene title	Sp1 box Core > 0.9 Matrix > 0.8	Stringent Sp1 box Core = 1 Matrix > 0.9	Ref.	Choice
Proliferation and cancer	0.20	GLULD1	Glutamate-ammonia ligase (glutamine synthetase) domain containing 1	+			
	0.35	RAB20	RAB20, member RAS oncogene family	+	+		√
	0.36	FGF21	Fibroblast growth factor 21	+	+		√
	0.37	INHBE	Inhibin, beta E	+			
	0.44	LBR	Lamin B receptor				
	0.45	ZNF364	Zinc finger protein 364	+	+		
	0.45	IHPK2	Inositol hexaphosphate kinase 2	+	+		√
	0.49	GADD45B	Growth arrest and DNA-damage-inducible, beta	+			
	0.49	ZNRF1	Zinc and ring finger 1	+	+		
	0.42	OSMR	Oncostatin M receptor	+			
	0.44	IPO5	Importin 5	+			
	0.42	ARHGAP18	Rho GTPase activating protein 18	+	+		√
mRNA processing	0.26	SFRS1	Splicing factor, arginine/serine-rich 1 (splicing factor 2, alternate splicing factor)	+			
	0.49	NPM3	Nucleophosmin/nucleoplasmin, 3	+	+		√
	0.49	SFRS7	Splicing factor, arginine/serine-rich 7, 35kDa	+	+		√
	0.49	SFRS12	Splicing factor, arginine/serine-rich 12	+			
Lipid metabolism	0.36	ACSL3	Acyl-CoA synthetase long-chain family member 3	+			
	0.46	LEPROTL1	Leptin receptor overlapping transcript-like 1	+	+		
	0.50	ELOVL5	ELOVL family member 5,elongation of long chain fatty acids (FEN1/Elo2,SUR4/Elo3-like,yeast)	+			
Glucidic metabolism	0.32	AGXT2L1	Alanine-glyoxylate aminotransferase 2-like 1	+	+		
	0.37	PDE7B	Phosphodiesterase 7B	+			
	0.39	RPE	Ribulose-5-phosphate-3-epimerase	+	+		
	0.47	GFPT2	Glutamine-fructose-6-phosphate transaminase 2	+	+		
	0.47	CALM3	Calmodulin 3 (phosphorylase kinase, delta)	+	+		√
	0.47	ENO3	Enolase 3 (beta, muscle)	+			
	0.50	PGD	Phosphogluconate dehydrogenase	+	+		√
	0.25	SLC2A3	Solute carrier family 2 (facilitated glucose transporter), member 3	+	+	R	C
Transcription	0.31	SNAPC3	Small nuclear RNA activating complex, polypeptide 3, 50kDa	+	+		
	0.35	LOC57228	Small trans-membrane and glycosylated protein	+			
	0.38	ATF7	Activating transcription factor7	+			
	0.49	PNN	Pinin, desmosome associated protein	+	+		
	0.35	PSIP1	PC4 and SFRS1 interacting protein 1	+	+		
	0.36	CEBPD	CCAAT/enhancer binding protein (C/EBP), delta	+	+	R	C
	0.38	CBFB	Core-binding factor, beta subunit	+	+	R	C
Translation	0.42	FNBP1	Formin binding protein 1	+	+		
	0.50	GFM1	G elongation factor, mitochondrial 1	+			

microarray data deposited in GEO. In our approach, we focused on those underexpressed genes that displayed a high statistical significance ($p < 0.01$) upon knockdown of Sp1, since they represent genes activated *bona fide* by Sp1. From the original 36 genes that met these criteria, a further selection was made of those containing stringent putative binding sites (Sp1 boxes) in their promoters, gathering 21 genes that could be bound by Sp1 with high probability. This selection of genes susceptible to be activated by Sp1 was subjected to literature data mining, leading to a limited list of 11 interesting genes that fell within the categories of proliferation, mRNA processing, glucidic metabolism and transcription. We found in our list 3 genes (SLC2A3, C/EBPδ, and CBFβ) already reported as regulated by Sp1 [24–26], leaving a list of 8 genes newly described to be under the regulation of Sp1.

Confirmation of mRNA underexpression for the 11 selected genes was carried out by qRT-PCR. Furthermore, ChIP assays were performed to verify binding of Sp1 to the promoters of these genes. The results of the ChIP assays confirmed that Sp1 binds to the promoter regions of RAB20, FGF21, IHPK2, ARHGAP18, NPM3, SRSF7, CALM3 and PGD, in addition of the Sp1 gene itself. Functional validation was achieved by determining that the endogenous mRNA levels of the three Sp1 gene-targets within the category of proliferation, RAB20, FGF21 and IHPK2, were increased upon Sp1 overexpression. Binding by Sp1 to the promoters of these three genes was verified by gel shift analyses, which was increased by Sp1 overexpression. Among these three genes, the Sp1 binding sequence in the RAB20 promoter showed the highest affinity for Sp1 according to the competition experiments. This site shows the highest similarity for the consensus Sp1 binding site reported in Marco et al. [31]. This affinity for RAB20 may explain the higher response in terms of Sp1 binding and mRNA levels when Sp1 is overexpressed. Luciferase assays using specific constructs containing the same endogenous Sp1 boxes for each of these 3 genes as those used in the EMSA experiments, confirmed that Sp1 was responsible for the activation of these genes, which complement the binding analysis studies.

RAB20 belongs to the family of RAS oncogenes and its overexpression has previously been characterized in exocrine pancreatic carcinoma [32], in colorectal adenomas by a process of gene amplification [33] and in triple negative breast cancers [34]. The binding of Sp1 to the promoter of RAB20 indicates that it might play a role in the activation of this gene. An interesting observation

Table 5
Sp1-box sequences in the promoters of selected genes. It is presented 33 nt of the sequences of the promoters of the selected genes with the Sp1-boxes (in bold and underlined) and the position of the core with respect to the translational start site. (*) Sequences reported as the complementary strand of the Sp1 binding site.

Gene	Sp1 box core position	5′-3′ Sequence of Sp1 boxes
RAB20	−264*	CCCCGCCCCC**GCCCCCGCCCCCG**GGCCCTTTCA
FGF21	−210	AGGGAGGGTG**ATTGGGCGGGCCTG**TCTGGGTAT
IHPK2	−252	GTTCTTGCGG**GACTCCGCCCATG**CCACCCACCT
	−231	CTATGAGCTC**ATGGGGCGGGGTT**AGATGCAGAC
ARHGAP18	−133	TTCACACGGG**GAGGGGCGGGGTC**TGTCCAGGGA
NPM3	−26	GCCTTCTTCA**AACTCCGCCCCCG**ACACGCACAA
	−73	GGCCAGTTCC**GGCCCCGCCCATT**AAAGGAGACG
SFRS7	−256	ACACGCGGGT**CATGGGCGGAGGG**ATACGTTTCT
	−326	TTCCCCATGC**TGTCCCGCCCCCT**CCTCTCCCCG
CALM3	−141	TGAGGGACCG**TTGGGGCGGGAGG**CGGCGGCGGC
	−193 and −178	GG**GTGGGGCGGGGCC**GA**GCGAGGCGGGGCG**CGC
	−369	AAGTGGGCCC**GGGAGGCGGGGCG**CGCGGCGAGG
PGD	−203	GGCCCCCGGG**GGTGGGCGGGCAC**GTTTGCCTCG
	−279	AAGCTCTGCG**CGTGGGCGGGGAG**CCCGGAGCCT
SLC2A3	−302* and −308*	CAGAACT**ACCCCCGCCCCCGCCCCAC**AGACAAT
CEBPδ	−97*	CTGACGTGCA**CGCCCCGCCCCGA**CTCCGGCACC
	−146	GCCGCGGGGG**AAGGGGCGGGGGC**GCCCTGGGAG
	−175	GGAGCCCCCC**GGAGCCGCCCCGA**GCCTTCCCGG
	−472	TCCTGTCGCC**GGAGGGCGGGGGG**TGGAGACCCG
CBFβ	−7	GGCCGGCCGGCGCGGCC**TCAGGGCGGGAAG**ATG
	−134	CGGGAGCCCA**CGCGGGCGGGCGC**CTGAAACAAA
	−175	GTTGGGCTCG**AGCGGGCGGCGGC**GCCTCAGACT
	−260	CGGCGGCGGC**CGGGGGCGGTGAG**CGCTGGGGCT
	−304 and −313	GGCCGG**CGGGGGCGGGGTGGGCGGTGAG**AGGAA
	−349	CGGAGTTGGA**GGCGGGCGGGCGC**GCGAGGAGGA
	−421	CCGCTCCGCC**AGCGGGCGGGTGG**CGCATGCGCG

from our results is that Sp1 overexpression leads to overexpression of RAB20. Thus, Sp1 may play a role in the development of the abovementioned types of cancer.

The protein encoded by FGF21 is a member of the fibroblast growth factor (FGF) family, involved in a wide range of biological

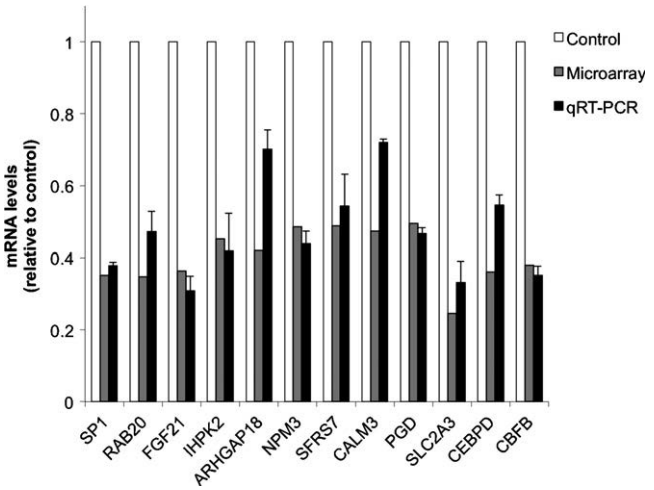

Fig. 3. Validation of downregulated genes. Underexpression of selected genes was confirmed by qRT-PCR (black bars). Values are the mean ± SE of three independent experiments of the changes in the mRNA levels relative to control (white bars). For comparison purposes the values found in the microarray (grey bars) are also represented.

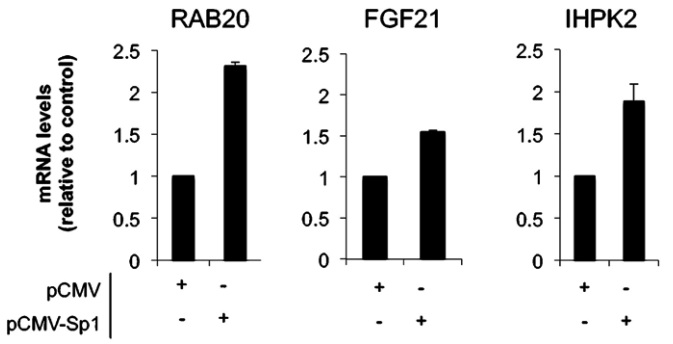

Fig. 4. Sp1 regulates gene expression. Exponentially growing HeLa cells were treated either with the expression vector for Sp1 (pCMV-Sp1) or with an empty vector. Forty-eight hours later, RNA was extracted and mRNA levels for RAB20, FGF21 and IHPK2 were determined. Values are the mean ± SE of three independent experiments.

processes including embryonic development, cell growth, morphogenesis, tissue repair, tumor growth and invasion. Recently, it has been reported to play a role as a metabolic regulator [35], and it causes an increase in ERK1/2 phosphorylation in mouse liver *in vivo* [36].

Inositol hexaphosphate kinase 2 (IHPK2) encodes a protein considered to be involved in the conversion of inositol hexakisphosphate (InsP6) to diphosphoinositol pentakisphosphate (InsP7/PP-InsP5) and 1,3,4,5,6-pentakisphosphate (InsP5) to PP-InsP4. Overexpression of IHPK2 sensitized ovarian carcinoma cell lines to the growth-suppressive and apoptotic effects of interferon beta (IFN-β), IFN-α2, and γ-irradiation [37,38]. According to our results, Sp1, which binds to the promoter of IHPK2, could play a role in IHPK2 gene expression and its effects on IFN-β in ovarian cancers.

For both, FGF21 and IHPK2, we also studied the effect of Sp1 overexpression, resulting in increased mRNA levels.

ARHGAP18 is a Rho-GTPase activating protein, which modulates cell signaling [39]. Recently, ARHGAP18 has been identified as a putative oncogene which expression in murine mammary gland cells altered their growth kinetics and caused their morphological transformation [40]. The results of ChIP analysis confirmed that Sp1 binds to its promoter. Further research is needed to determine the effects of Sp1 on this gene.

NPM3 and SRSF7 are both classified as mRNA processing genes. NPM3 likely functions as a molecular chaperone in the cell nucleus and it has been associated with mitogenesis in tumors and enhanced activator-dependent transcription, suggesting that its overexpression might lead to uncontrolled cell proliferation [41]. For instance, diffuse large B-cell lymphoma (DLBCL) is a more aggressive tumor with a higher cell growth fraction than follicular lymphoma (FL) and it has been shown that NPM3 levels were higher in DLBCL than in FL [42]. SRSF7 is a member of the serine/arginine (SR)-rich protein family involved mainly in pre-mRNA splicing [43]. SRSF7 is believed to be involved in both constitutive splicing and alternative splicing of many pre-mRNAs. In addition, it helps mRNA export to the cytoplasm and enhances the expression of unspliced mRNA [44]. A recent study has demonstrated that splicing misregulation of adult-specific exon 10 of microtubule-associated protein tau results in expression of abnormal ratios of tau isoforms, leading to frontotemporal dementia with Parkinsonism. SRSF7 strongly inhibits inclusion of tau exon 10 indicating that it plays a key role in regulation of exon 10 splicing and implying a pathogenic role for this factor in neurodegenerative diseases [45,46].

CALM3 is a calmodulin involved in differentiation and maturation of specific brain or muscle regions [47]. It has been

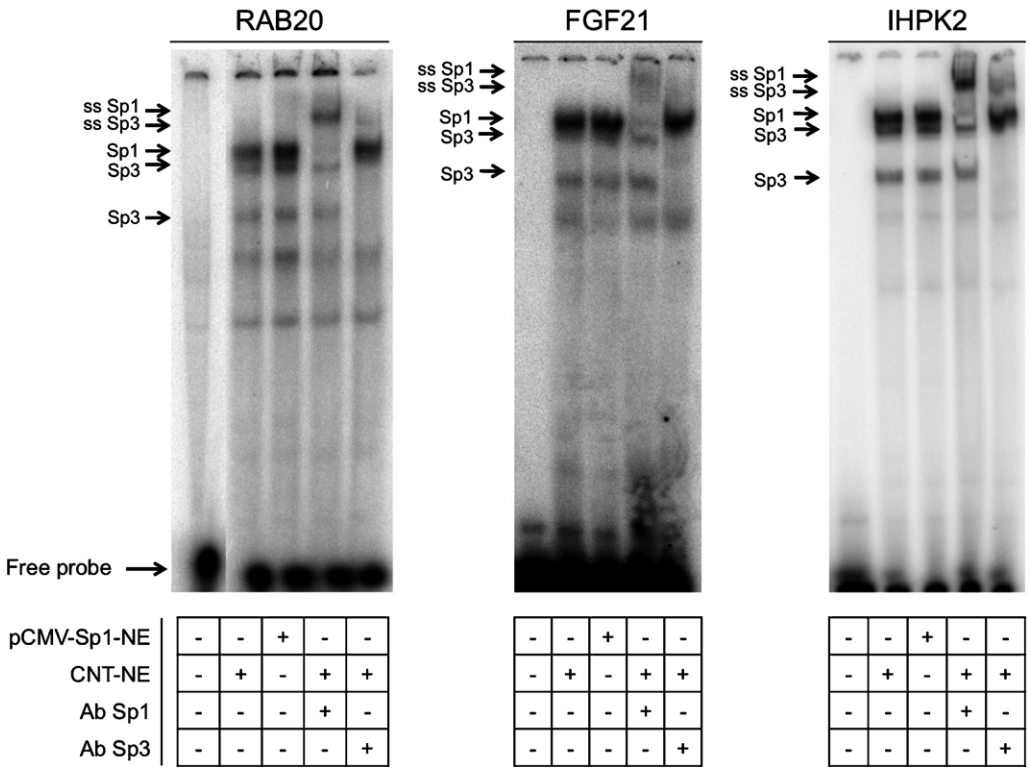

Fig. 5. Characterization of Sp1 binding to RAB20, FGF21 and IHPK2 promoters. EMSA were performed using sequences corresponding to Sp1 sites within the RAB20, FGF21 and IHPK2 promoter and nuclear extracts (NE) from either exponentially growing parental HeLa cells or transfected with an expression vector for Sp1 (pCMV-Sp1). Binding reactions were performed with 20,000 cpm of [γ-^{32}P]ATP-labeled ds probes, 2 μg of NE and 1 μg of poly[d(I-C)] used as nonspecific competitor. Supershift mobility assays were performed in the presence of specific antibodies against Sp1 or Sp3. Shifted and supershifted (ss) bands are indicated by arrows.

shown that the CALM3 transcript increases in proliferating human teratoma cells as well as in differentiating of neuroblastoma cells [48,49]. PGD, which is also classified as playing a role in the glucidic metabolism, is a phosphogluconate dehydrogenase and is the second enzyme in the pentose phosphate pathway. A reduction in the activity of PGD has been reported to induce cell death in the hepatoma cell line HA22T/VGH by interfering with redox state regulation [50]. The malignant transformation of oval

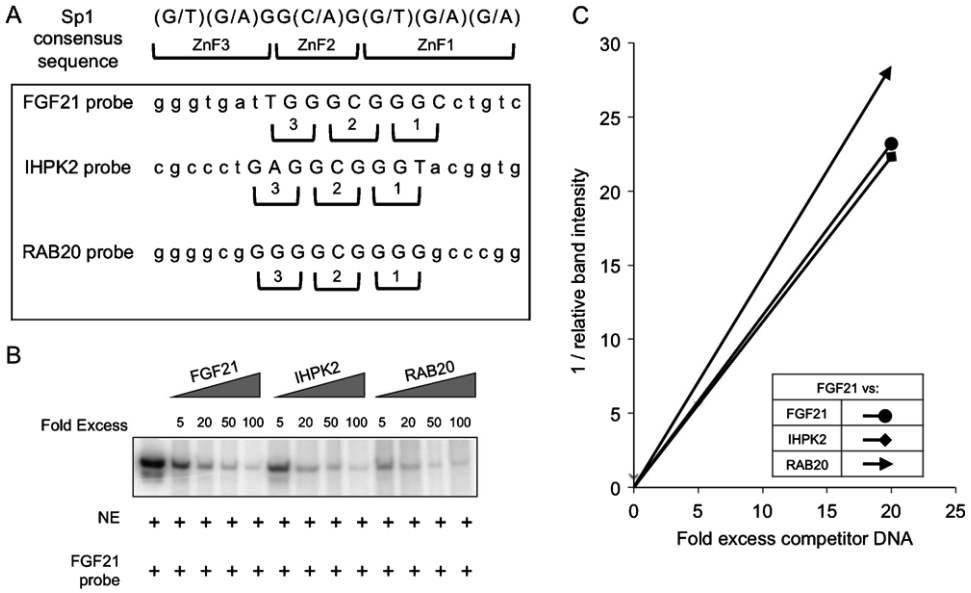

Fig. 6. Sp1 binding sites affinity for the RAB20, FGF21 and IHPK2 promoters. (A) Sequence comparison among RAB20, FGF21 and IHPK2 Sp1 binding sequences with the consensus sequence for Sp1. The position of the 3 zinc finger (ZnF) binding sites are also shown. (B) Competition analysis between FGF21 labeled probe and increasing fold excess (5, 20, 50 and 100×) of FGF21, IHPK2 and RAB20 cold probes. Binding reactions were performed with 20,000 cpm of each [γ-^{32}P]ATP-labeled ds probe, 2 μg nuclear extracts (NE) from exponentially growing HeLa cells and 1 μg of poly[d(I-C)] used as nonspecific competitor. (C) The reciprocal of the relative amount of bound probe (the value in the absence of competitor taken as one) is plotted *versus* the fold excess of the competitor DNA, with a best fit straight line fitted to the points by regression analysis. The slope of this line is proportional to the relative binding affinity of the competitor DNA. The slopes for each promoter are: RAB20: 1.42, FGF21: 1.16 and IHPK2: 1.12.

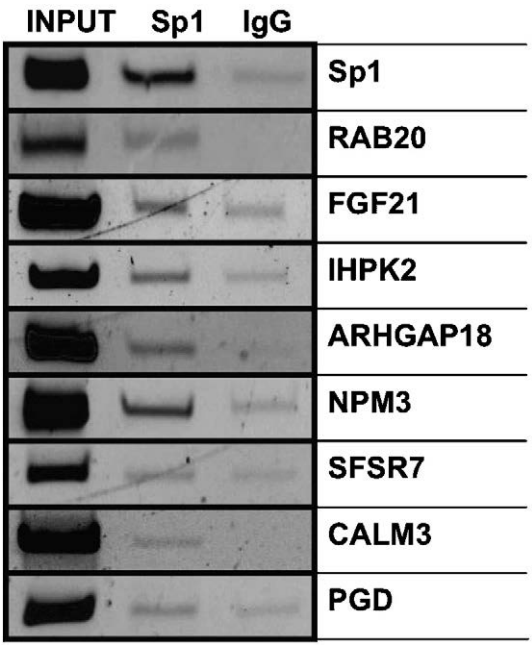

Fig. 7. ChIP analysis of the selected promoters. ChIP analysis of Sp1 binding to the selected promoters was performed using HeLa cells subjected to Sp1 and IgG immunoprecipitation. DNA bound to the immunoprecipitated Sp1 using specific antibody, was amplified by PCR. Mouse IgG was used as negative control. Representative images of the PCR products corresponding to the amplification of RAB20, FGF21, IHPK2, ARHGAP18, NPM3, SRSF7, CALM3, PGD and Sp1 (specific primers are described in Table 2) promoter fragments are shown. The input lane corresponds to the whole (non immunoprecipitated) DNA and the Sp1 and IgG lanes correspond to the immunoprecipitations with Sp1 and IgG, respectively.

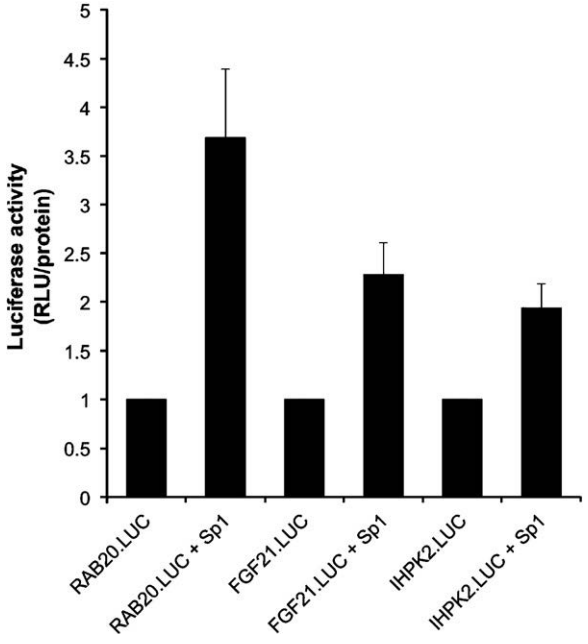

Fig. 8. Luciferase activity of RAB20, FGF21 and IHPK2 promoters upon Sp1 overexpression. 500 ng of either RAB20.LUC, FGF21.LUC or IHPK2.LUC constructs in the presence or in the absence of the Sp1 expression vector (500 ng) were cotransfected in HeLa cells. Luciferase activity (relative light units, RLU) was determined 30 h after transfection and the values for each sample were normalized by total protein concentration (mg/mL). Luciferase activity is expressed as fold change between the values obtained in the presence *vs.* the absence of Sp1. Values correspond to the mean ± SE of three independent experiments.

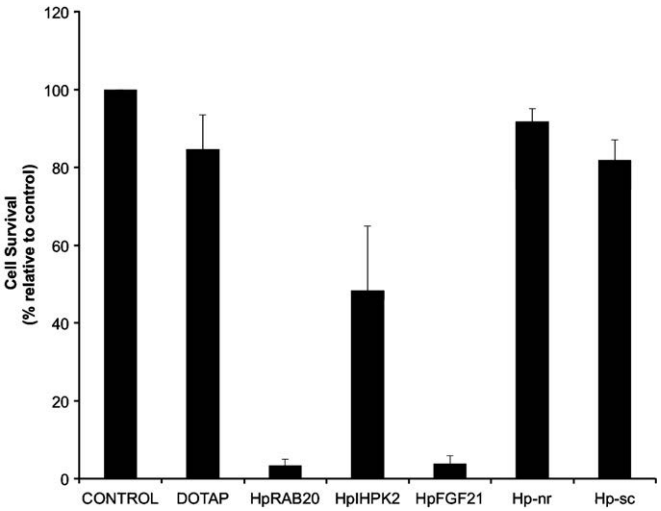

Fig. 9. Effect of knocking down RAB20, FGF21 and IHPK2 using PPRHs. 100 nM of Hp-RAB20, Hp-FGF21 and Hp-IHPK2 and the negative controls Hp-wc and Hp-sc were transfected using 10 μM DOTAP in HeLa cells. Five days after transfection, the MTT assay was carried out. Values are referred as % to control and correspond to the mean ± SE of three independent experiments.

cells, a type of liver epithelial cells that proliferate during the early stages of hepatocarcinogenesis, was accompanied by an increase in the activity of 6-phosphogluconate dehydrogenase [51]. In a genome wide association study to identify susceptibility variants for hepatitis B virus related to hepatocellular carcinoma, the 1p36.22 locus was found to be highly associated with this type of carcinoma. The 1p36.22 locus contains the PGD gene, in addition to two other genes [52]. Altogether, these findings suggest a role for PGD-related pathways in the pathogenesis of hepatocarcinomas.

In conclusion, we identified 8 new gene targets whose expression can be activated by the binding of Sp1 protein to their promoter regions. Four of them, RAB20, FGF21, IHPK2 and ARHGAP18 are involved in proliferation and cancer, NPM3, SRSF7 are related to mRNA processing, and CALM3 and PGD play a role in glucidic metabolism. Further extensive studies are needed to generalize the results since the data obtained in HeLa cells may be cell type specific. However, the findings of this work open now the possibility to explore the role of these Sp1-activated genes in their specific pathways. The effects observed by silencing RAB20, FGF21 or IHPK2 genes using PPRHs hairpins confirm the role of these three genes in proliferation.

Conflict of interest

The authors declare no potential conflicts of interest.

Acknowledgements

The work was supported by grants SAF08-043, SAF2011-23582 from "Plan Nacional de Investigación Científica" (Spain). Our group holds the quality mention from the "Generalitat de Catalunya" SGR2009-118.

References

[1] Li L, He S, Sun JM, Davie JR. Gene regulation by Sp1 and Sp3. Biochem Cell Biol 2004;82:460–71.
[2] Li L, Davie JR. The role of Sp1 and Sp3 in normal and cancer cell biology. Ann Anat 2010;192:275–83.
[3] Lania L, Majello B, De Luca P. Transcriptional regulation by the Sp family proteins. Int J Biochem Cell Biol 1997;29:1313–23.

[4] Spengler ML, Brattain MG. Sumoylation inhibits cleavage of Sp1 N-terminal negative regulatory domain and inhibits Sp1-dependent transcription. J Biol Chem 2006;281:5567–74.
[5] Nicolas M, Noe V, Jensen KB, Ciudad CJ. Cloning and characterization of the 5′-flanking region of the human transcription factor Sp1 gene. J Biol Chem 2001;276:22126–32.
[6] Nicolas M, Noe V, Ciudad CJ. Transcriptional regulation of the human Sp1 gene promoter by the specificity protein (Sp) family members nuclear factor Y (NF-Y) and E2F. Biochem J 2003;371:265–75.
[7] Noe V, Alemany C, Chasin LA, Ciudad CJ. Retinoblastoma protein associates with SP1 and activates the hamster dihydrofolate reductase promoter. Oncogene 1998;16:1931–8.
[8] Tapias A, Ciudad CJ, Roninson IB, Noe V. Regulation of Sp1 by cell cycle related proteins. Cell Cycle 2008;7:2856–67.
[9] Kruger I, Vollmer M, Simmons DG, Elsasser HP, Philipsen S, Suske G. Sp1/Sp3 compound heterozygous mice are not viable: impaired erythropoiesis and severe placental defects. Dev Dyn 2007;236:2235–44.
[10] Hanahan D, Weinberg RA. The hallmarks of cancer. Cell 2000;100:57–70.
[11] Ryuto M, Ono M, Izumi H, Yoshida S, Weich HA, Kohno K, et al. Induction of vascular endothelial growth factor by tumor necrosis factor alpha in human glioma cells. Possible roles of SP-1. J Biol Chem 1996;271:28220–28.
[12] Ishibashi H, Nakagawa K, Onimaru M, Castellanous EJ, Kaneda Y, Nakashima Y, et al. Sp1 decoy transfected to carcinoma cells suppresses the expression of vascular endothelial growth factor, transforming growth factor beta1, and tissue factor and also cell growth and invasion activities. Cancer Res 2000;60:6531–6.
[13] Wang L, Wei D, Huang S, Peng Z, Le X, Wu TT, et al. Transcription factor Sp1 expression is a significant predictor of survival in human gastric cancer. Clin Cancer Res 2003;9:6371–80.
[14] Zhang J, Zhu ZG, Ji J, Yuan F, Yu YY, Liu BY, et al. Transcription factor Sp1 expression in gastric cancer and its relationship to long-term prognosis. World J Gastroenterol 2005;11:2213–7.
[15] Abdelrahim M, Smith 3rd R, Burghardt R, Safe S. Role of Sp proteins in regulation of vascular endothelial growth factor expression and proliferation of pancreatic cancer cells. Cancer Res 2004;64:6740–9.
[16] Mencia N, Selga E, Rico I, de Almagro MC, Villalobos X, Ramirez S, et al. Overexpression of S100A4 in human cancer cell lines resistant to methotrexate. BMC Cancer 2010;10:250.
[17] Selga E, Oleaga C, Ramirez S, de Almagro MC, Noe V, Ciudad CJ. Networking of differentially expressed genes in human cancer cells resistant to methotrexate. Genome Med 2009;1:83.
[18] Mosmann T. Rapid colorimetric assay for cellular growth and survival: application to proliferation and cytotoxicity assays. J Immunol Methods 1983;65 :55–63.
[19] Kel AE, Gossling E, Reuter I, Cheremushkin E, Kel-Margoulis OV, Wingender E. MATCH: a tool for searching transcription factor binding sites in DNA sequences. Nucleic Acids Res 2003;31:3576–9.
[20] Noe V, Alemany C, Nicolas M, Ciudad CJ. Sp1 involvement in the 4beta-phorbol 12-myristate 13-acetate (TPA)-mediated increase in resistance to methotrexate in Chinese hamster ovary cells. Eur J Biochem 2001;268:3163–73.
[21] Pascal E, Tjian R. Different activation domains of Sp1 govern formation of multimers and mediate transcriptional synergism. Genes Dev 1991;5: 1646–56.
[22] de Almagro MC, Coma S, Noe V, Ciudad CJ. Polypurine hairpins directed against the template strand of DNA knock down the expression of mammalian genes. J Biol Chem 2009;284:11579–89.
[23] Abdelrahim M, Samudio I, Smith 3rd R, Burghardt R, Safe S. Small inhibitory RNA duplexes for Sp1 mRNA block basal and estrogen-induced gene expression and cell cycle progression in MCF-7 breast cancer cells. J Biol Chem 2002;277:28815–22.
[24] Rajakumar RA, Thamotharan S, Menon RK, Devaskar SU. Sp1 and Sp3 regulate transcriptional activity of the facilitative glucose transporter isoform-3 gene in mammalian neuroblasts and trophoblasts. J Biol Chem 1998;273:27474–83.
[25] Sivko GS, Sanford DC, Dearth LD, Tang D, DeWille JW. CCAAT/enhancer binding protein delta (c/EBPdelta) regulation and expression in human mammary epithelial cells: II. Analysis of activating signal transduction pathways, transcriptional, post-transcriptional, and post-translational control. J Cell Biochem 2004;93:844–56.
[26] Hajra A, Collins FS. Structure of the leukemia-associated human CBFB gene. Genomics 1995;26:571–9.
[27] Robertson G, Hirst M, Bainbridge M, Bilenky M, Zhao Y, Zeng T, et al. Genome-wide profiles of STAT1 DNA association using chromatin immunoprecipitation and massively parallel sequencing. Nat Methods 2007;4:651–7.
[28] Wong D, Teixeira A, Oikonomopoulos S, Humburg P, Lone IN, Saliba D, et al. Extensive characterization of NF-kappaB binding uncovers non-canonical motifs and advances the interpretation of genetic functional traits. Genome Biol 2011;12:R70.
[29] Valouev A, Johnson DS, Sundquist A, Medina C, Anton E, Batzoglou S, et al. Genome-wide analysis of transcription factor binding sites based on ChIP-Seq data. Nat Methods 2008;5:829–34.
[30] Guertin MJ, Lis JT. Chromatin landscape dictates HSF binding to target DNA elements. PLoS Genet 2010;6.
[31] Marco E, Garcia-Nieto R, Gago F. Assessment by molecular dynamics simulations of the structural determinants of DNA-binding specificity for transcription factor Sp1. J Mol Biol 2003;328:9–32.
[32] Amillet JM, Ferbus D, Real FX, Antony C, Muleris M, Gress TM, et al. Characterization of human Rab20 overexpressed in exocrine pancreatic carcinoma. Hum Pathol 2006;37:256–63.
[33] Habermann JK, Brucker CA, Freitag-Wolf S, Heselmeyer-Haddad K, Kruger S, Barenboim L, et al. Genomic instability and oncogene amplifications in colorectal adenomas predict recurrence and synchronous carcinoma. Mod Pathol 2011;24:542–55.
[34] Turner N, Lambros MB, Horlings HM, Pearson A, Sharpe R, Natrajan R, et al. Integrative molecular profiling of triple negative breast cancers identifies amplicon drivers and potential therapeutic targets. Oncogene 2010;29: 2013–23.
[35] Yu J, Zhao L, Wang A, Eleswarapu S, Ge X, Chen D, et al. Growth hormone stimulates transcription of the fibroblast growth factor 21 gene in the liver through the signal transducer and activator of transcription 5. Endocrinology 2012;153:750–8.
[36] Fisher FM, Estall JL, Adams AC, Antonellis PJ, Bina HA, Flier JS, et al. Integrated regulation of hepatic metabolism by fibroblast growth factor 21 (FGF21) in vivo. Endocrinology 2011;152:2996–3004.
[37] Morrison BH, Tang Z, Jacobs BS, Bauer JA, Lindner DJ. Apo2L/TRAIL induction and nuclear translocation of inositol hexakisphosphate kinase 2 during IFN-beta-induced apoptosis in ovarian carcinoma. Biochem J 2005;385:595–603.
[38] Morrison BH, Bauer JA, Lupica JA, Tang Z, Schmidt H, DiDonato JA, et al. Effect of inositol hexakisphosphate kinase 2 on transforming growth factor beta-activated kinase 1 and NF-kappaB activation. J Biol Chem 2007;282:15349–56.
[39] Maeda M, Hasegawa H, Hyodo T, Ito S, Asano E, Yuang H, et al. ARHGAP18, a GTPase-activating protein for RhoA, controls cell shape, spreading, and motility. Mol Biol Cell 2011;22:3840–52.
[40] Kim HH, van den Heuvel AP, Schmidt JW, Ross SR. Novel common integration sites targeted by mouse mammary tumor virus insertion in mammary tumors have oncogenic activity. PLoS One 2011;6:e27425.
[41] Motoi N, Suzuki K, Hirota R, Johnson P, Oofusa K, Kikuchi Y, et al. Identification and characterization of nucleoplasmin 3 as a histone-binding protein in embryonic stem cells. Dev Growth Differ 2008;50:307–20.
[42] Sakhinia E, Glennie C, Hoyland JA, Menasce LP, Brady G, Miller C, et al. Clinical quantitation of diagnostic and predictive gene expression levels in follicular and diffuse large B-cell lymphoma by RT-PCR gene expression profiling. Blood 2007;109:3922–8.
[43] Graveley BR. Sorting out the complexity of SR protein functions. RNA 2000;6:1197–211.
[44] Swartz JE, Bor YC, Misawa Y, Rekosh D, Hammarskjold ML. The shuttling SR protein 9G8 plays a role in translation of unspliced mRNA containing a constitutive transport element. J Biol Chem 2007;282:19844–53.
[45] Ding S, Shi J, Qian W, Iqbal K, Grundke-Iqbal I, Gong CX, et al. Regulation of alternative splicing of tau exon 10 by 9G8 and Dyrk1A. Neurobiol Aging 2012;33:1389–99.
[46] Gao L, Wang J, Wang Y, Andreadis A. SR protein 9G8 modulates splicing of tau exon 10 via its proximal downstream intron, a clustering region for frontotemporal dementia mutations. Mol Cell Neurosci 2007;34:48–58.
[47] Weinman J, Della Gaspera B, Dautigny A, Pham Dinh D, Wang J, Nojima H, et al. Developmental regulation of calmodulin gene expression in rat brain and skeletal muscle. Cell Regul 1991;2:819–26.
[48] Toutenhoofd SL, Foletti D, Wicki R, Rhyner JA, Garcia F, Tolon R, et al. Characterization of the human CALM2 calmodulin gene and comparison of the transcriptional activity of CALM1, CALM2 and CALM3. Cell Calcium 1998;23:323–38.
[49] Toutenhoofd SL, Strehler EE. Regulation of calmodulin mRNAs in differentiating human IMR-32 neuroblastoma cells. Biochim Biophys Acta 2002;1600: 95–104.
[50] Hsieh BS, Huang LW, Su SJ, Cheng HL, Hu YC, Hung TC, et al. Combined arginine and ascorbic acid treatment induces apoptosis in the hepatoma cell line HA22T/VGH and changes in redox status involving the pentose phosphate pathway and reactive oxygen and nitrogen species. J Nutr Biochem 2011;22: 234–41.
[51] Mazurek S, Eigenbrodt E, Failing K, Steinberg P. Alterations in the glycolytic and glutaminolytic pathways after malignant transformation of rat liver oval cells. J Cell Physiol 1999;181:136–46.
[52] Zhang H, Zhai Y, Hu Z, Wu C, Qian J, Jia W, et al. Genome-wide association study identifies 1p36.22 as a new susceptibility locus for hepatocellular carcinoma in chronic hepatitis B virus carriers. Nat Genet 2010;42:755–8.

Article IV:

THE REDOX STATE OF CYTOCHROME C MODULATES RESISTANCE TO METHOTREXATE IN HUMAN MCF7 BREAST CANCER CELLS

Susana Barros, Núria Mencia, Laura Rodríguez, Carlota Oleaga, Conceiçao Santos, Verónique Noé and Carlos J. Ciudad

PLoS ONE 8(5): e63276. doi:10.1371/journal.pone.0063276 (Impact factor: 3.534)

PLOS ONE

The Redox State of Cytochrome C Modulates Resistance to Methotrexate in Human MCF7 Breast Cancer Cells

Susana Barros[1,2☯], Núria Mencia[1☯], Laura Rodríguez[1], Carlota Oleaga[1], Conceição Santos[2], Verónique Noé[1], Carlos J. Ciudad[1]*

1 Department of Biochemistry and Molecular Biology, School of Pharmacy, University of Barcelona, Barcelona, Spain, **2** Department of Biology, CESAM, University of Aveiro, Campus Universitário de Santiago, Aveiro, Portugal

Abstract

Background: Methotrexate is a chemotherapeutic agent used to treat a variety of cancers. However, the occurrence of resistance limits its effectiveness. Cytochrome c in its reduced state is less capable of triggering the apoptotic cascade. Thus, we set up to study the relationship among redox state of cytochrome c, apoptosis and the development of resistance to methotrexate in MCF7 human breast cancer cells.

Results: Cell incubation with cytochrome c-reducing agents, such as tetramethylphenylenediamine, ascorbate or reduced glutathione, decreased the mortality and apoptosis triggered by methotrexate. Conversely, depletion of glutathione increased the apoptotic action of methotrexate, showing an involvement of cytochrome c redox state in methotrexate-induced apoptosis. Methotrexate-resistant MCF7 cells showed increased levels of endogenous reduced glutathione and a higher capability to reduce exogenous cytochrome c. Using functional genomics we detected the overexpression of GSTM1 and GSTM4 in methotrexate-resistant MCF7 breast cancer cells, and determined that methotrexate was susceptible of glutathionylation by GSTs. The inhibition of these GSTM isoforms caused an increase in methotrexate cytotoxicity in sensitive and resistant cells.

Conclusions: We conclude that overexpression of specific GSTMs, GSTM1 and GSTM4, together with increased endogenous reduced glutathione levels help to maintain a more reduced state of cytochrome c which, in turn, would decrease apoptosis, thus contributing to methotrexate resistance in human MCF7 breast cancer cells.

Citation: Barros S, Mencia N, Rodríguez L, Oleaga C, Santos C, et al. (2013) The Redox State of Cytochrome C Modulates Resistance to Methotrexate in Human MCF7 Breast Cancer Cells. PLoS ONE 8(5): e63276. doi:10.1371/journal.pone.0063276

Editor: Kalpana Ghoshal, The Ohio State University, United States of America

Received December 5, 2012; **Accepted** April 1, 2013; **Published** May 13, 2013

Funding: The work was supported by grant SAF2011- 23582 from "Plan Nacional de Investigación Científica" (Spain). The funder had no role in study design, data collection and analysis, decision to publish, or preparation of the manuscript.

Competing Interests: The authors have declared that no competing interests exist.

* E-mail: cciudad@ub.edu

☯ These authors contributed equally to this work.

Introduction

Methotrexate (MTX) is a chemotherapeutic agent widely used, alone or in combination with other chemotherapeutic agents, for the treatment of a range of cancers, such as breast cancer, osteosarcoma, head and neck cancer, lymphoma and acute lymphoblastic leukemia [1]. As a structural analogue of folic acid, MTX is a high affinity inhibitor of dihydrofolate reductase (DHFR) by competing with dihydrofolate for the active site. DHFR catalyzes the NADPH-dependent reduction of dihydrofolate to tetrahydrofolate involved in the biosynthesis of thymidylate, hypoxantine and glycine, needed for DNA synthesis [2–4]. Once DHFR is inhibited by MTX, there is suppression of DNA synthesis and cell proliferation is affected. However, the main drawback of using MTX in cancer therapy is the occurrence of resistance upon treatment, thus compromising its effectiveness. Several MTX resistance mechanisms had been described such as gene amplification of the *dhfr locus* [5,6], deficiency in MTX transport [7,8] or MTX polyglutamation [9], expression of the MDR phenotype and mutations of the target (DHFR protein) [10]. Altered gene or miRNA expression also contribute to MTX resistance such as increases in AKR1C1 [11], S100A4 [12], caveolin-1, enolase-2, PRKCA [13], DKK1, EEF1A1, and UGT1A family [14,15], and the decrease of E-Cadherin [13] or miR-224 [16].

Reduced glutathione (GSH) and Glutathione S-transferases (GSTs) have been implicated in the development of drug resistance in cancer chemotherapy [17,18]. The GSTs enzymatic family belongs to a Phase II detoxification program functioning as a cellular protection from attack by reactive electrophiles associated to environmental stresses and drugs [19]. This family is mainly responsible for the conjugation of GSH to electrophilic compounds and includes three main types, cytosolic, mitochondrial and membrane-bound microsomal. Cytosolic GSTs are divided into seven classes: alpha (A), Mu (M), Omega (O), Pi (P), Sigma (S), Theta (T) and Zeta (Z) [20–23]. GSTs are thought to be involved in the development of drug resistance via direct detoxification or by regulation of the MAP kinase pathway, specifically JNK-pathway as reviewed in [19].

Cytochrome c (cyt c) is a heme-protein bound to the mitochondrial inner membrane by an interaction with the anionic phospholipid cardiolipin, which keeps cytochrome c in its proper location and prevents its release to the cytosol [24]. Under physiological conditions, cytochrome c is responsible for the electron transfer between complexes III and IV of the mitochondrial electron transport chain whereas under oxidative stress, the peroxidase activity of cytochrome c is activated, cardiolipin becomes peroxidized, and loses its affinity for cytochrome c allowing its release to the cytosol [25,26]. Once in the cytosol, cytochrome c can only induce apoptosis in its oxidized form [27–31]. The presence of high levels of cytosolic GSH holds the released cytochrome c inactive in a reduced state, thus preventing the progression of the apoptotic cascade [32,33].

In this study, we investigated the effect of the reduction state of cytochrome c on MTX sensitivity and apoptosis and its relationship with the different GSTs overexpressed in MCF7 breast cancer cells resistant to MTX, to evaluate a possible connection between GSTs and GSH in the reduction state of cytochrome c and the development of MTX resistance.

Materials and Methods

Cell lines and cell culture

The following human cell lines were used: MCF7, MDA-MB-468 and 10^{-6} M MTX-resistant MCF7 cells from breast cancer; SaOs-2 and 10^{-6} M MTX-resistant SaOs-2 cells from osteosarcoma; and HT-29 and CaCo-2 cells from colon cancer. Resistant cells were obtained previously in the laboratory upon incubation with stepwise concentrations of MTX (Almirall, Barcelona, Spain) as described in [11]. In all experimental procedures, cells were grown in Ham's F12 medium lacking the final products of DHFR activity, glycine, hypoxanthine and thymidine (-GHT), and supplemented with 7% v/v dialyzed fetal bovine serum (GIBCO, Life Technologies, Madrid, Spain), 14 mM sodium bicarbonate (1.176 g/l), penicillin G (100 U/ml) and streptomycin (100 mg/l). Cells were maintained at 37°C in a humidified atmosphere of 5% CO_2 in air. Before reaching 70% confluence, cells were subcultured by treatment with 0.05% trypsin in PBS 1×. All these components were purchased from Sigma-Aldrich (Madrid, Spain).

Oxygen consumption assay

Cellular oxygen consumption was monitored polarographically with a Clark-type oxygen electrode using Hansatech Oxygraph Measurement System (Hansatech, Norfolk, UK). The assay was performed using 6×10^4 cells/ml in the presence or in the absence of 5 µM TMPD or 300 µM ASC in 1 ml of PBS (pH 7.4) as experimental medium at 37°C. Oxygen consumption was measured during 5 min for each condition and determined by the slope calculated directly by the Oxygraph Plus Software.

Cell viability assay

Cell viability was assessed by the MTT (3-(4,5-Dimethylthiazol-2-yl)-2,5-diphenyltetrazolium bromide) assay [34] in 6-well dishes. Cells were incubated with 500 µg of MTT and 0.270 mg of sodium succinate (Sigma-Aldrich, Madrid, Spain) and allowed to react for 2 h at 37°C. The medium was removed and 1 ml of the solubilization reagent (0,57% acetic acid and 10% SDS in DMSO (dimethyl sulfoxide)) was added (Applichem, Ecogen, Barcelona, Spain). Cell viability was measured at 570 nm in a WPA S2100 Diode Array Spectrophotometer. The results were expressed as percentage of cell survival relative to the control (untreated cells).

Microarrays

Gene expression was analyzed by hybridization to GeneChip® Human Genome U133 PLUS 2.0 microarrays from Affymetrix, containing 54,675 transcripts and variants. Total RNA for cDNA arrays was prepared from triplicate samples from both control and resistant cells using the RNAeasy Mini kit (Qiagen, Madrid, Spain) following the recommendations of the manufacturer. The integrity of the RNA species was checked using the Bioanalyzer 2100 system (Agilent, Madrid, Spain). Labeling, hybridization and detection were carried out following the manufacturer's specifications.

Microarrays data analyses

Quantification was carried out with GeneSpring GX 12.0 software (Agilent, Madrid, Spain), which allows multi-filter comparisons using data from different experiments to perform the normalization, generation of lists and the functional classification of the differentially expressed genes. The input data was subjected to preprocess baseline transformation using the RMA summarization algorithm using the median of control samples. After grouping the triplicates of each experimental condition, lists of differentially expressed genes could be generated by using volcano plot analysis. T-test unpaired was applied using asymptotic p-value computation and multiple testing correction of Benjamini-Hochberg false discovery rate, FDR. The expression of each gene was reported as the ratio of the value obtained for the resistant condition relative to the control condition after normalization and statistical analysis of the data. The corrected p-value cut-off applied was of <0.05; then the output of this statistical analysis was filtered by fold expression, selecting specifically those genes that had a differential expression of at least 2-fold.

RT-Real-Time PCR

Total RNA was extracted using the Ultraspec™ RNA reagent (Biotecx, Ecogen, Barcelona, Spain) following the manufacturer's instructions. Complementary DNA (cDNA) was synthetized in a total volume of 20 µl by mixing 1 µg of total RNA, 125 ng of random hexamers (Roche, Mannheim, Germany), in the presence of 75 mM KCl, 3 mM $MgCl_2$, 50 mM Tris-HCl buffer, pH 8.3, 10 mM dithiothreitol (Invitrogen, Life Technologies, Madrid, Spain), 20 units of RNAsin (Promega, Madrid, Spain), 0.5 mM dNTPs (Applichem, Ecogen, Barcelona, Spain) and 200 units of MLV-reverse transcriptase (Invitrogen, Life Technologies, Madrid, Spain). The reaction mix was incubated at 37°C for 1 h and the cDNA product was used for subsequent amplification.

Gene expression levels were quantified by SYBR Green RT-Real Time PCR reaction in a final volume of 20 µl with specific forward and reverse primers, using the StepOnePlus™ detection system (Applied Biosystems, Life Technologies, Madrid, Spain). The sequences of the forward and reverse primers (Sigma-Aldrich, Madrid, Spain) are given in Table 1.

Table 1. Primer sequences.

Gene	Forward (5′-3′)	Reverse (5′-3′)
GSTM1	TGAAGCCTCAGCTACCCACT	AACCAGTCAATGCTGCTCCT
GSTM4	TTTCCTCGCCTATGATGTCC	GCTGAGTATGGGCTCCTCAC
HPRT	TGCTCGAGATGTGATGAAGG	TCCCCTGTTGACTGGTCATT

The sequences for the forward and reverse primer for detection of GSTM1, GSTM4 and HPRT mRNA levels used for RT-Real Time PCR are given.
doi:10.1371/journal.pone.0063276.t001

Changes in gene expression were calculated using the quantitative ΔΔCt method and normalized against Hypoxanthine-phosphoribosyl transferase (HPRT) in each sample.

GSTM1 and GSTM4 protein levels

MCF7 cells, either sensitive or MTX-resistant, were harvested from confluent dishes and total extracts were prepared according to [14]. Total extracts (80 μg) were resolved on a 15% SDS-PAGE (AppliChem, Ecogen, Barcelona, Spain) and transferred to PVDF membranes (Immobilon P, Millipore, Madrid, Spain) using a semidry electroblotter. The membranes were probed with anti-GSTμ antibody (FL-218, sc-292368) (Santa Cruz Biotechnology Inc, Heidelberg, Germany) 1:200 dilution, OVN at 4°C. Signals were detected using ImageQuant LAS 4000 Mini Technology (Amersham, GE Healthcare Life Sciences, Barcelona, Spain) with rabbit secondary horseradish peroxidase–conjugated antibody (P0399) (Dako, Barcelona, Spain) 1:5000 dilution, for 1 h at room temperature. To normalize the results blots were reprobed with an antibody against tubulin (Cp06) (Calbiochem, Millipore, Merck, Madrid, Spain) 1:400 dilution, OVN at 4°C and detected with anti-mouse (NIF 824) (Amersham, GE Healthcare Life Sciences, Barcelona, Spain) 1:2500 dilution, for 1 h at room temperature.

Inhibition of GSTM1 and GSTM4 expression levels

GST expression was inhibited by specific PPRH-hairpins (hp), a new class of DNA-hairpin molecules able to silence gene expression [35,36]. The Triplex-Forming Oligonucleotide Target Sequence Search software (M.D. Anderson Cancer Center, Houston, TX) (spi.mdanderson.org/tfo/) was used to design the hairpins. BLAST analyses were performed to check for the specificity of each sequence. Cells were plated in 6-well dishes in 1 ml of medium the night before transfection and each hairpin was mixed with N-[1-(2,3-dioleoyloxy)propyl]-N,N,N-trimethylammonium methylsulfate (DOTAP) (Roche, Mannheim, Germany) at the appropriate oligonucleotide–DOTAP molar ratio (1:100) for 15 min at RT before lipofecting the cells. The sequences of the hairpins (Sigma-Aldrich, Madrid, Spain) are listed in Table 2.

For RNA determination, cells were transfected and total RNA was extracted 30 h later. Gene expression was quantified as described above.

For viability assays, cells were incubated with each hairpin for 24 h before MTX treatment. Survival was determined after 3 days in sensitive MCF7 cells or 6 days in resistant MCF7 and SaOs-2 cells.

Apoptosis

Apoptosis was determined by the Rhodamine 123/Propidium Iodide (PI) assay. Cells (6×10^4) were plated in 6-well dishes, and treated with the different agents (TMPD, ascorbate, veratridine) alone or in combination with MTX for the indicated times and concentrations. Then cells were incubated for 30 min with 5 μl of Rhodamine 123 (1 μg/μl). All the cells in each well were harvested and centrifuged at 800× *g* for 5 min. The cell pellet was washed twice with 1 ml of PBS 1×+1%BSA solution and resuspended in 500 μl of PBS 1×+BSA 1% solution containing 0.5 μl PI (5 μg/μl). The entire procedure was performed at 4°C. All these reagents were purchased from Sigma-Aldrich (Madrid, Spain). Samples were analyzed by flow cytometry in the Coulter Epics XL™ cytometer (Beckman, Barcelona, Spain) at an excitation wavelength of 488 nm by reading the fluorescence of rhodamine123 at 525 nm. Cells that were negative for both rhodamine123 and PI were counted as the apoptotic population. Summit v4.3 software was used to analyze the data.

GSH endogenous levels

Endogenous GSH levels were determined using the Glutathione Assay Kit, Fluorimetric (Sigma-Aldrich®) based on a fluorimetric reaction catalyzed by GSTs between monochlorobimane (MCB), a thiol probe, and GSH. Briefly, the assay was performed with 6×10^4 sensitive and resistant MCF7 cells and the formation of the fluorescent adduct GSH-monochlorobimane was monitored at 390 nm for excitation and 478 nm for emission during 1 h.

Exogenous cyt c reduction by cytoplasmic cell extracts

Cytoplasmic cell extracts were obtained from MCF7 cells. Cells were collected in ice-cold PBS by scraping and centrifuged at 1,500× *g* for 10 min. The cell pellet was resuspended in 3 ml of lysing buffer prepared according to Borutaite&Brown [29] and homogenized in Glass/Teflon Potter Elvehjem homogenizer (20 strokes). The homogenate was further centrifuged in the same conditions as above and the supernatant was further centrifuged at 22,000× *g* for 30 min and the resulting supernatant corresponds to the cytoplasmic extract. The entire procedure was performed at 4°C. The reduction of exogenous cytochrome c by cytoplasmic extracts (100 μg/ml of total protein) was followed spectrophotometrically. The analysis measured the absorbance spectra between 500 and 600 nm wavelengths after incubation for 15 min at 37°C of exogenous cytochrome c (10 μM) with cytoplasmic cell extracts from sensitive or resistant MCF7 cells. Reduction level of cytochrome c was expressed as absorbance at 550 nm minus absorbance at 535 nm and was normalized to the protein of cytosolic extract used.

In vitro Glutathionylation

The glutathionylation of MTX catalyzed by GSTs was determined *in vitro* and in cell free extracts. *In vitro*, the reaction was performed by incubating MCB (100 μM), GSH (30 μM) and GST (0.25 U) in the absence or the presence of different concentrations of MTX in 0.1 M potassium phosphate buffer pH 7.0 [37]. The reaction was performed at 37°C for 15 min and

Table 2. Hairpin sequences.

Hairpin	Sequence (5′-3′)
hpGSTM1	GAAGGGGAGGGAAGAGAGAAGTTTTTGAAGAGAGAAGGGAGGGGAAG
hpGSTM4	GGAGAAGAAGAAAAGGGGGAAGTTTTTGAAGGGGGAAAAGAAGAAGAGG
hpSC	AAGAGAAAAAGAGAAAGAAGAGAGGGTTTTTGGGAGAGAAGAAAGAGAAAAAGAGAA
hpGSTA4	AAGGGAAGGGAGGAGGAAGAAAAGTTTTTGAAAAGAAGGAGGAGGGAAGGGAA

The sequences for the polypurine reverse Hoogsteen hairpins used for specific inhibition of GSTM1, GSTM4 or GSTA4 as well as the scrambled negative control are given.

doi:10.1371/journal.pone.0063276.t002

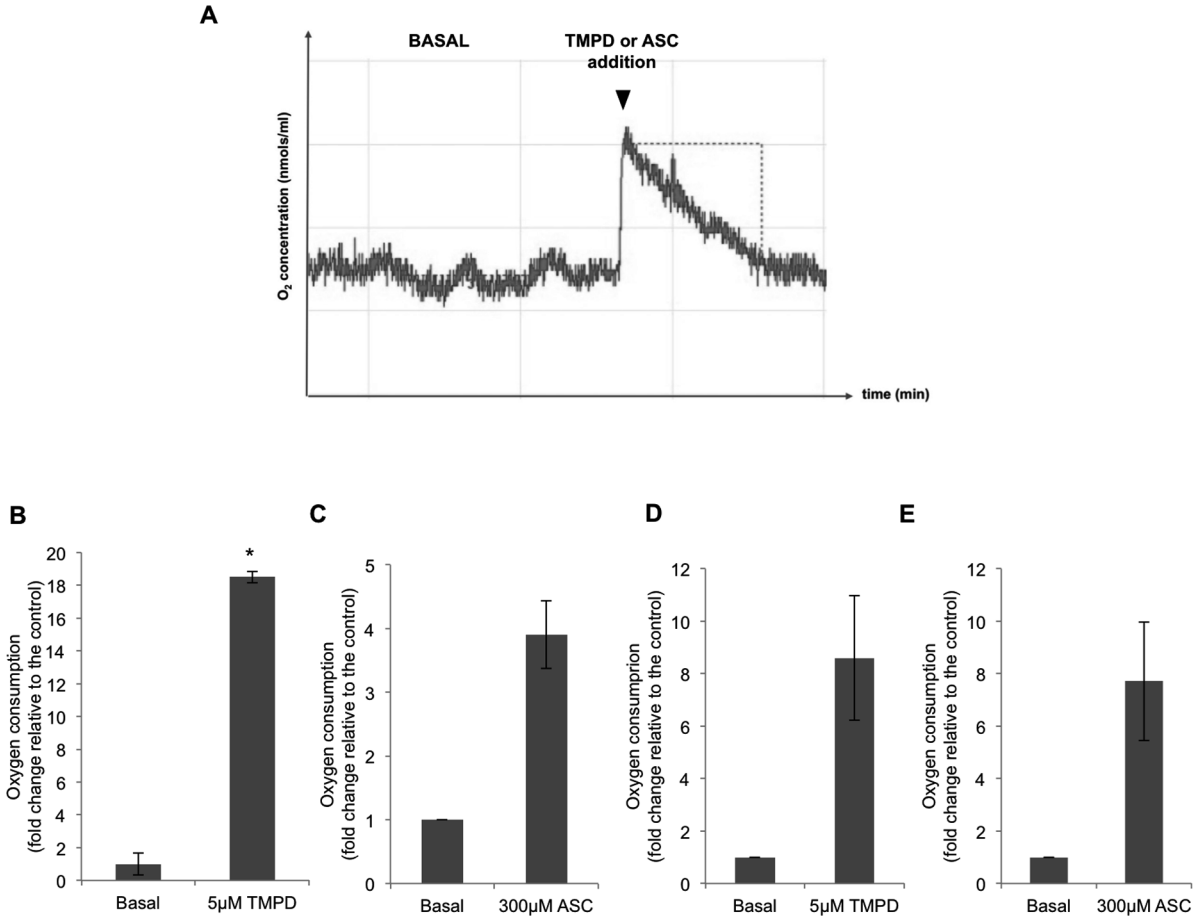

Figure 1. O_2 consumption analysis upon treatment with TMPD or ascorbate (ASC). A) Representative image of changes in O_2 concentration over time in cell extracts under basal conditions and after treatment with TMPD or ASC. The basal consumption rate in MCF7 cells (B–C) was 0.0335 nmol O_2/ml/min and 0.047 nmol O_2/ml/min in SaOs-2 cells (D–E). The results are expressed as the ratio of O_2 consumption rate in each condition relative to basal consumption levels and represent the mean value ± SE of three independent experiments. * $p<0.05$.
doi:10.1371/journal.pone.0063276.g001

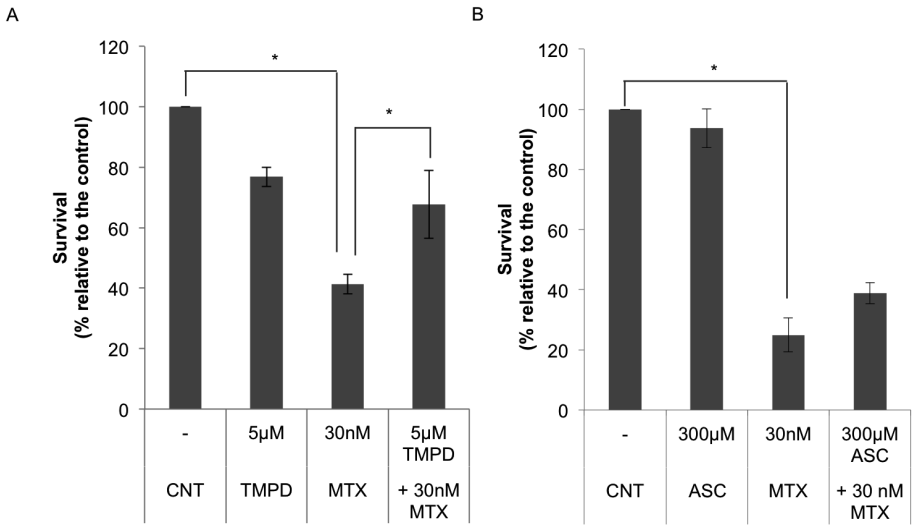

Figure 2. Effect of TMPD or ascorbate (ASC) in combination with MTX on cell viability. Cells (6×10^4) were incubated in 1 ml of medium with TMPD (A) or ASC (B) either alone or in combination with MTX at the indicated concentrations, for 3 or 6 days, respectively, and cell viability was determined using the MTT assay. TMPD or ASC were added to the cells 6 h before MTX. Results are expressed as the percentage of surviving cells compared to the control (untreated cells) and represent the mean ± SE of 3 experiments. * $p<0.05$.
doi:10.1371/journal.pone.0063276.g002

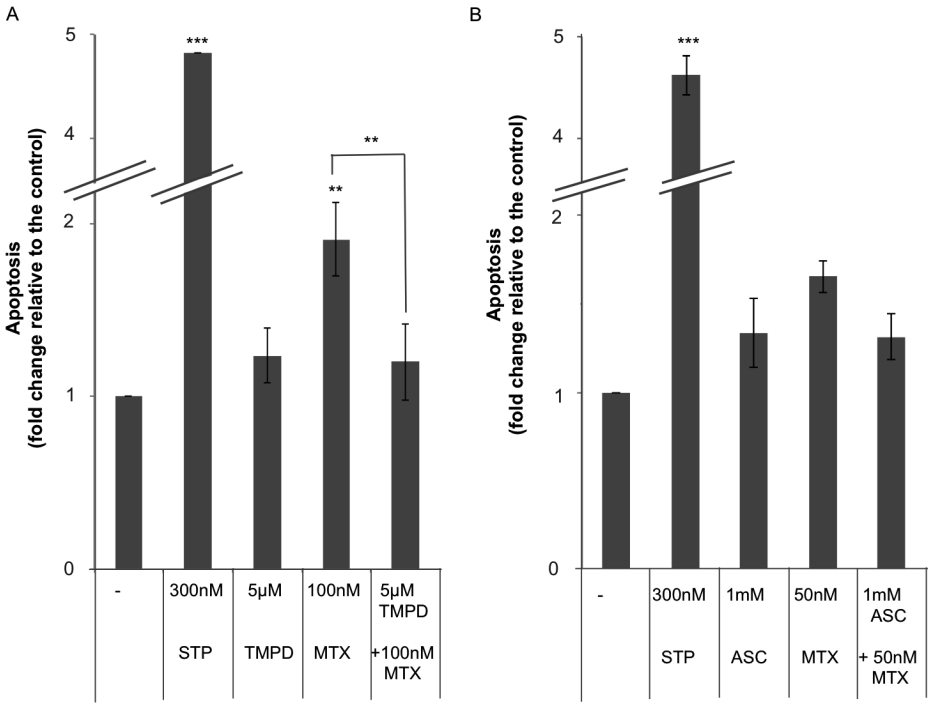

Figure 3. Effect of TMPD and ascorbate (ASC) on apoptosis induced by MTX. Cells were incubated with TMPD (A) or ASC (B) either alone or in combination with MTX at the indicated concentrations for 18 h. TMPD or ascorbate were added 12 h before MTX. Changes in mitochondrial membrane potential were determined using the Rhodamine 123/Propidium Iodide assay. Apoptosis is expressed in fold change compared to untreated cells. Results represent the mean ± SE of 3 different experiments. Staurosporine (STP) was used as a positive control. $^{**}p<0.01$, $^{***}p<0.001$.
doi:10.1371/journal.pone.0063276.g003

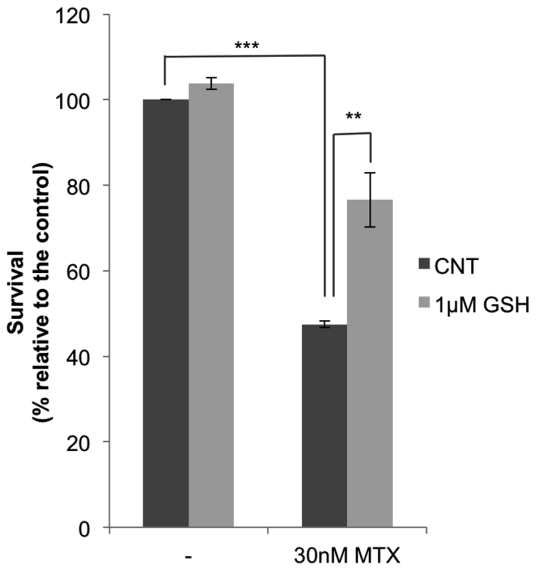

Figure 4. Effect of GSH on the cytotoxicity caused by MTX. MCF7 sensitive cells (6×10^4) were plated in 1 ml medium and treated with 1 μM GSH (light grey bars) for 2 h before incubation with MTX. Survival was assessed by the MTT assay 4 days later. Results are expressed as the percentage of survival compared to non-treated cells and represent the mean ± SE of at least 3 experiments. $^{**}p<0.01$, $^{***}p<0.001$.
doi:10.1371/journal.pone.0063276.g004

the fluorescence corresponding to the MCB-GSH adduct was measured as described above.

In cell free extracts, the reaction was performed as follows. Parental or MCF7 MTX-resistant cells (4×10^5) were harvested and washed twice with ice-cold PBS 1×. The pelleted cells were then resuspended in 100 μl of PBS 1×-1% Triton X-100, kept on ice for 15 minutes and centrifuged at 15,000× *g* for 15 minutes (4°C). The corresponding supernatant was collected (300 μg) and used for the glutathionylation reaction in the absence or in the presence of MTX for 15 min at 37°C.

MCB, reduced glutathione and GST were purchased from Sigma-Aldrich (Madrid, Spain). MCB and GSH were resuspended in DMSO and GST was resuspended at a concentration 0.25 U/μl in 0.01 M potassium phosphate pH 7.0 and 30% glycerol buffer.

Statistical analysis

Data are presented as the mean ± SE for at least three different experiments. Analyses were performed using SPSS v.18.3 software. Differences with *p*-value<0.05 were considered significant.

Results and Discussion

Effect of TMPD and ascorbate on the cytotoxicity produced by methotrexate

Tetramethylphenylenediamine (TMPD) and ascorbate (ASC) have been described as external reductants of cytochrome c both in cytosol and mitochondria [29,38,39]. In this direction, we used both agents to study the role of the reduced state of cytochrome c in the sensitivity to methotrexate.

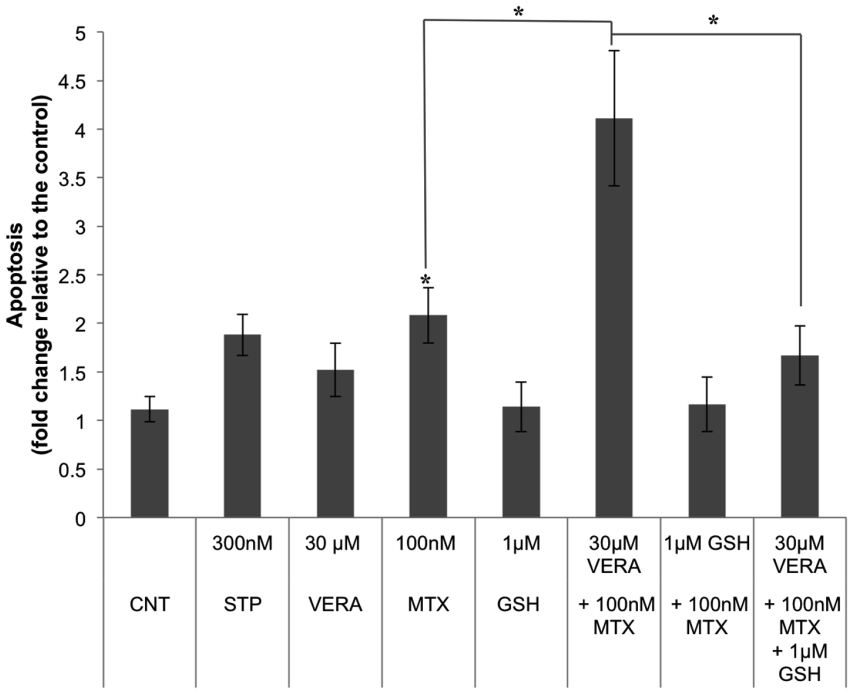

Figure 5. Effect of veratridine (VERA) and GSH on MTX induced apoptosis. Cells were incubated with veratridine alone or in combination either with MTX or MTX plus GSH, at the indicated concentrations. Veratridine was added 6 h before MTX. Incubation with exogenous GSH started 8 h before the addition of MTX. In the triple combination, cells were incubated 2 h with GSH, then veratridine was added and 6 h later, treatment with MTX was performed. Apoptosis was assessed 18 h after MTX addition by changes in mitochondrial membrane potential as determined by the Rhodamine 123/Propidium Iodide assay and it is expressed in fold change compared to untreated cells. Results represent the mean ± SE of 3 different experiments. Staurosporine (STP) was used as a positive control. * $p<0.05$.
doi:10.1371/journal.pone.0063276.g005

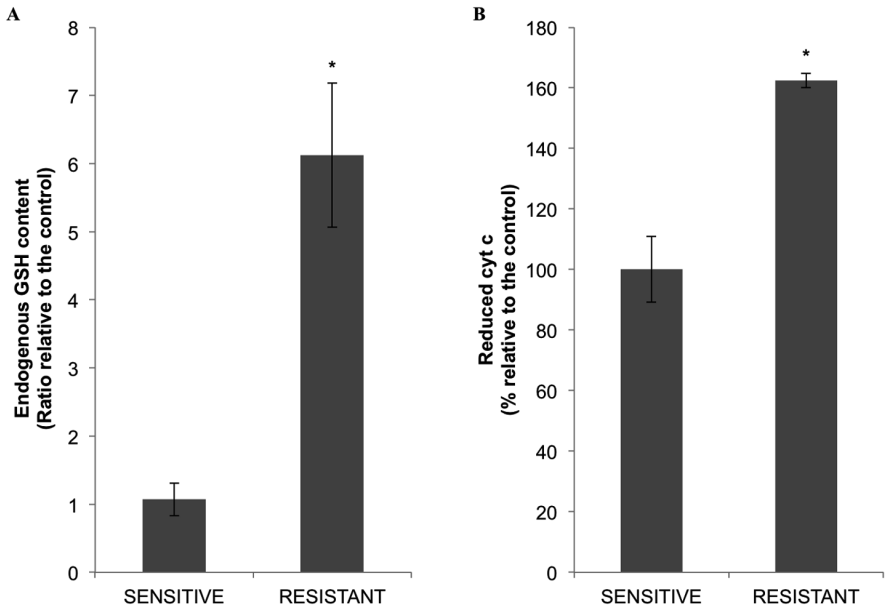

Figure 6. Endogenous GSH levels and cytochrome c redox capacity in cytosolic extracts. A) GSH endogenous levels were determined as described in Methods using cytoplasmic extracts from sensitive and MTX-resistant MCF7 cells (6×10^4). GSH content was calculated in nmols of GSH/mg of total protein (mean ± SE). Results are expressed as the ratio between resistant and sensitive cells. B) Cytoplasmic extracts from sensitive and resistant cells were incubated for 15 min with exogenous cytochrome c (10 μM). A sample with DTT and no cell extract was considered as the maximum value for cytochrome c reduction. The reduction level of cytochrome c was calculated as the difference between the absorbance at 550 nm and at 535 nm. The results are expressed as the percentage of reduction observed in the resistant extracts compared to the sensitive cells and represent the mean ± SE of at least three experiments. * $p<0.05$.
doi:10.1371/journal.pone.0063276.g006

Table 3. Differentially expressed GSTs in MCF7 MTX-resistant cells.

Gene Symbol	Raw resistant	Raw sensitive	Fold Change	Corrected *p*-value
GSTM1	129	58	2.2	0.01288
GSTM2	182	76	2.4	0.02732
GSTM4	151	67	4.8	0.02732

Microarray data analyses were performed with GeneSpring GX 12.0 software as described. For each GSTM isoform, it is expressed the mean of the raw value in sensitive and resistant cells, the fold change in expression after normalization of the data, as well as the corrected *p*-value after Benjamini-Hochberg FDR filtering.
doi:10.1371/journal.pone.0063276.t003

First, the reduction of cytochrome c by TMPD or ASC treatment in MCF7 cells was confirmed by determining the changes in O_2 consumption using an oxygraph upon treatment with these chemical reagents. One of the classic end-points to analyze mitochondrial function is to assess the changes in oxygen consumption since O_2 is the ultimate electron acceptor [40]. This method is commonly used [39,41–44], it calculates the variation of O_2 concentration over time and offers the unique advantage of being able to add other components during the experiment. The slope of the graph represents the O_2 consumption rate. As shown in figure 1, TMPD and ASC addition increased O_2 consumption in MCF7 cells by 18.5 and 3.9 fold, respectively (Figure 1, B and C). In addition, the oxygen consumption rate was also determined in SaOs-2 cells upon addition of the 2 reducing agents, TMPD and ASC, causing an increase of 8.6 and 7.7 fold, respectively (Figure 1, D and E).

MCF7 cells were incubated with 5 μM TMPD or 300 μM ascorbate, either alone or in combination with 30 nM MTX and cell viability was determined after 3 or 6 days, respectively. The incubation with TMPD and ascorbate started 6 h before the addition of MTX. The presence of TMPD or ascorbate, which alone did not cause significant cell death, decreased the cytotoxic effect of MTX (Figure 2A, B). The reduction in cytotoxicity was more evident in the presence of TMPD with a recover in cell survival of 26%. The combination of MTX with ascorbate was less effective as the presence of ascorbate only counteracted the action of MTX by 14%.

To assess whether this effect was cell type specific, different cell lines were incubated with 5 μM TMPD and then treated with MTX. The presence of TMPD also decreased the cytotoxic effect of MTX by 15.1% in MDA-MB-468 cells, by 17.5% in SaOs-2 cells, by 10.5% in HT-29 cells, and by 21% in CaCo-2 cells.

Since the cytotoxic effect of MTX decreased in the presence of TMPD or ASC, we could hypothesize that the redox state of cytochrome c might be involved in the sensitization of cells to MTX-induced apoptosis in different cell lines.

TMPD and ascorbate decrease the apoptotic effect of MTX

It has been demonstrated that MTX can induce apoptosis mediated by cytochrome c release [45,46]. For this reason, we wanted to get further insight into the role of cytochrome c redox state in MTX-induced apoptosis. Levels of apoptosis were determined by the loss of mitochondrial membrane potential (MMP) using the Rhodamine 123/Propidium Iodide assay. Incubation of MCF7 cells with 50 nM or 100 nM MTX revealed an increase in apoptosis of 1.65-fold and 1.9-fold, respectively, referred to untreated cells. Treatment with TMPD (figure 3A) or ascorbate (figure 3B) before MTX prevented this apoptotic effect by 37% and 20%, respectively. Thus, by reducing cytochrome c with either TMPD or ascorbate, we were able to decrease MTX-induced apoptosis. The preventing effect on apoptosis caused by TMPD was also demonstrated in the breast cancer cell line MDA-MB-468 as well as in HT-29 colon cancer cells.

Since TMPD was shown to be freely permeable across cytoplasmic and mitochondrial membranes [38] the reduction of cytochrome c could take place in the mitochondria or after its release, as shown by Borutaite and Brown [29]. Regardless the exact mechanism, it is clear from our results that the reduced state of cytochrome c correlates with a lower proapoptotic effect of MTX.

Effect of addition or depletion of GSH on MTX action

The redox state of cytochrome c is partially responsible for its apoptotic activity. Our results showed that exogenous reducing agents of cytochrome c were able to modulate the response towards MTX (figures 2 and 3). It has been described that GSH can reduce cytochrome c [27,31,47], and therefore we wanted to study whether GSH could exert a role in MTX resistance in MCF7 cells.

GSH is one of the most important regulators of intracellular redox balance, performing an antioxidant cell protective action, cycling between its reduced (GSH) and oxidized forms (GSSG) [48]. Reactive oxygen species (ROS) mediated apoptotic signaling is associated with a decrease of cellular GSH levels and loss of cellular redox balance [49] and high levels of GSH have been associated to drug resistance [50–52].

As shown in Figure 4, incubation with exogenous GSH decreased the cytotoxicity induced by MTX. These results suggest that a more reduced state of cytochrome c correlates with less MTX cytotoxicity, as previously observed with TMPD or ASC.

To explore the role of GSH on MTX-dependent apoptosis we used veratridine to decrease GSH levels [53]. As shown in Figure 5, the apoptotic effect provoked by the combination of veratridine plus MTX was higher than the summation of both agents by themselves. Interestingly, the addition of 1 μM GSH decreased MTX-induced apoptosis and counteracted the increase in apoptosis caused by veratridine.

These results indicate a possible role of GSH in MTX-induced apoptosis. It has been suggested that endogenous GSH contributes to maintain cytochrome c in its reduced state under physiological conditions and prevents its apoptotic effect [27,32,33,43]. A lower reduced environment caused by GSH depletion would favor cytochrome c induced apoptosis upon MTX incubation.

GSH endogenous levels were determined in cell extracts from sensitive and resistant cells. As shown in figure 6A, GSH content was 6.2 times higher in resistant cells, indicating that the detoxifying capacity of the cytoplasm in resistant cells was higher than in sensitive cells. To analyze this, exogenous cytochrome c was incubated with either sensitive or resistant cytoplasmic cell extracts. Changes in cytochrome c redox state were measured spectrophotometrically as described. The results in Figure 6B

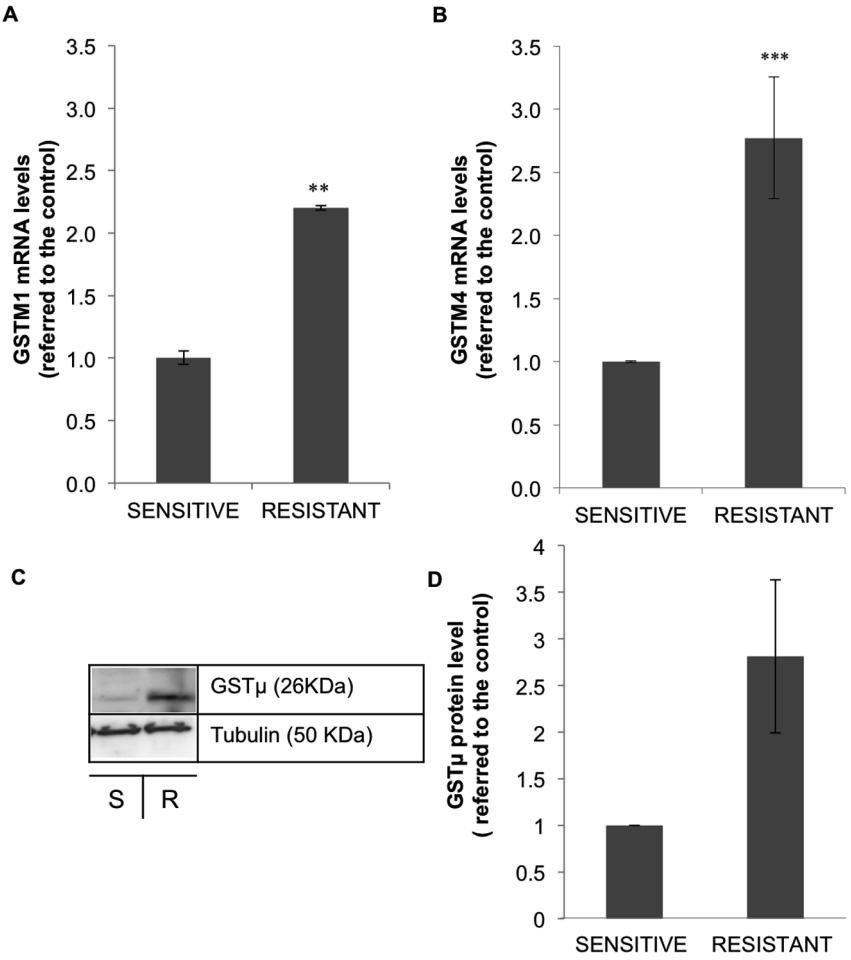

Figure 7. Validation of GSTM1 and GSTM4 overexpression in MCF7 MTX-resistant cells. GSTM1 (A) and GSTM4 (B) mRNA expression levels were determined by RT-Real Time PCR in sensitive and 10^{-6} M MTX-resistant MCF7 cells. Results are expressed as the fold changes in expression compared to sensitive cells and are the mean ± SE of at least 3 different experiments. C) GSTμ protein levels were determined by Western blot in sensitive (S) and resistant (R) cells and quantified using the ImageQuant software (GE Healthcare, Barcelona, Spain). Blots were normalized against tubulin levels. Values represent the mean ± SE of three different experiments and are expressed as fold increase in GSTμ protein levels relative to the control. $^{**}p<0.01$, $^{***}p<0.001$.
doi:10.1371/journal.pone.0063276.g007

confirmed that resistant cells had a higher capacity to reduce exogenous cytochrome c (60%). These results support the idea that the higher reduced environment present in MTX-resistant cells would contribute to overcome the apoptotic stimuli, in this case produced by MTX, and favor the resistant phenotype.

Endogenous levels of GST in sensitive and MTX-resistant MCF7 cells

Treatment with exogenous GSH prior to MTX had the same effect on cell viability that preincubation with TMPD or ascorbate, both known cytochrome c reducing agents. Therefore, an increase in GSH would keep cytochrome c reduced and could help the cells to reduce the apoptotic effect induced by MTX. To explore more in detail this possibility and its mechanism in our model of MTX resistance, we searched for genes related with GSH and the balancing redox environment of the cell.

Whole genome expression microarrays of sensitive and MTX-resistant MCF7 cells had been previously performed in the laboratory [14] and deposited in the Gene Expression Omnibus (GEO) database with series accession number GSE16648. Interestingly, analyses of the data demonstrated that different isoforms of the GST family, namely GSTM1, GSTM2 and GSTM4, were overexpressed in MCF7 resistant cells compared to their sensitive counterparts (Table 3).

Several examples in the literature have established a link between GSTM1 and GSTM4 overexpression with drug resistance [54–58], for this reason GSTM1 and GSTM4 were selected for further study. On the other hand, GSTM2 is a muscle-specific human GSTμ isoform specially enriched in in the cytoplasm of skeletal and cardiac muscle [59]. Increased or decreased expression of GSTM2 has been related to cancer predisposition or promotion, such as lung cancer [60] or ovarian teratoma [61]. However, no clear evidence between GSTM2 increased levels and drug resistance has been reported, and therefore this isoform was not further studied.

The endogenous levels of GSTM1 and GSTM4 were validated in sensitive and MTX-resistant MCF7 cells at mRNA and protein level. As it can be observed in Figure 7 both GSTM1 (A) and GSTM4 (B) mRNA levels were increased 2.2 and 2.77-fold, respectively, in MCF7 resistant cells, confirming GSTs overexpression detected in the microarray experiments. This effect was translated at the protein level. MTX-resistant MCF7 cells showed

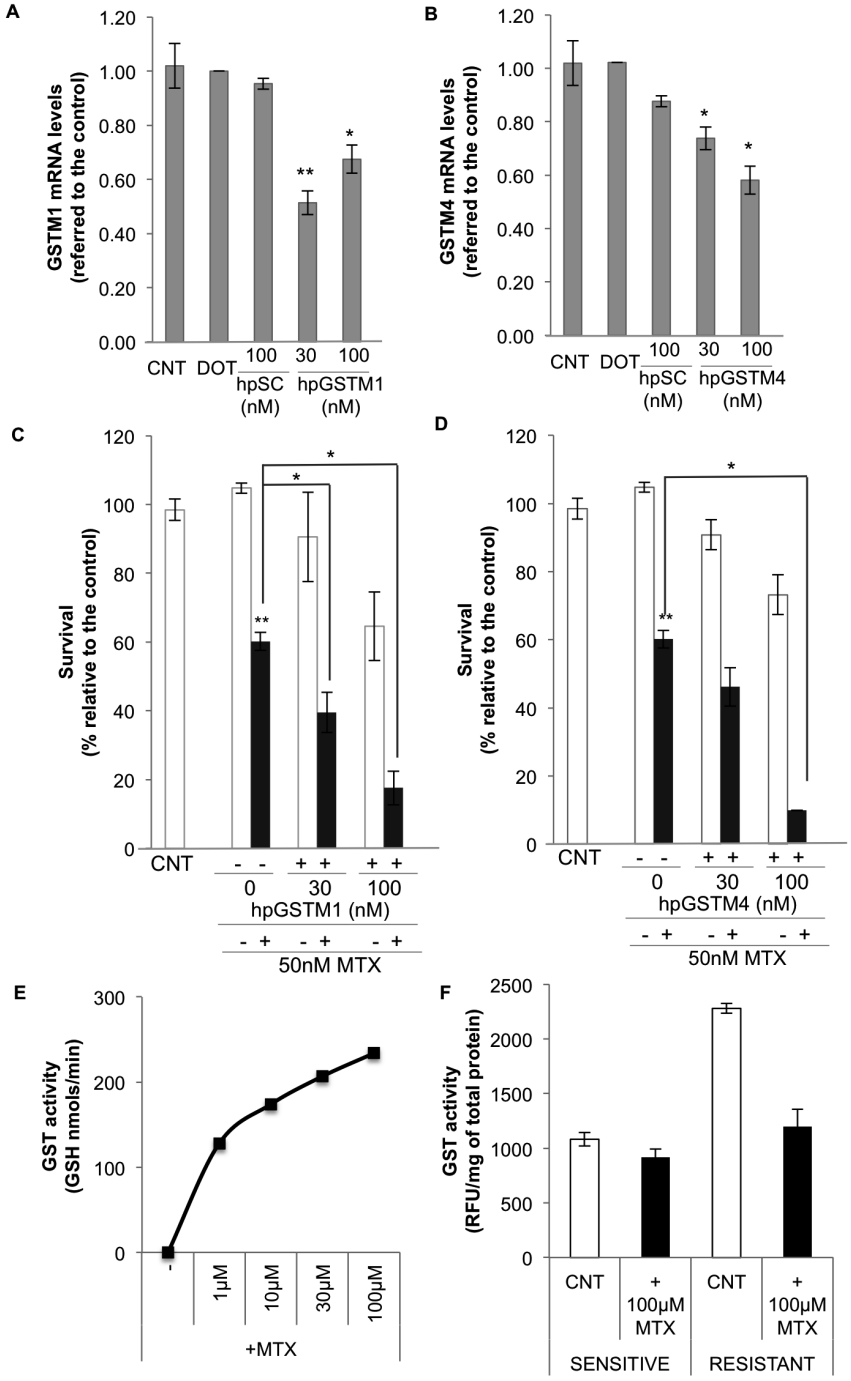

Figure 8. Effect of GSTM1 and GSTM4 inhibition on their mRNA levels and on sensitivity towards MTX. Effect on mRNA levels: MCF7 cells (6×10^4) were plated in 1 ml of medium and transfected 18 h later with specific hairpins against GSTM1 (hpGSTM1) (A) or GSTM4 (hpGSTM4) (B). mRNA levels were determined 30 h after transfection. Results are expressed as changes in expression compared to the control non-transfected cells and are the mean ± SE of at least 3 different experiments. A scrambled hairpin was used as a negative control (hpSC). Effect on MTX cytotoxicity: MCF7 cells (6×10^4) were plated in 1 ml of medium and transfected 18 h later with either hpGSTM1 (C) or hpGSTM4 (D). MTX was added 24 h after transfection and viability assayed by MTT 3 days later. Results are expressed as the percentage of cell survival compared to the control non-transfected cells and are the mean ± SE of at least 3 different experiments. *$p<0.05$, **$p<0.01$. E) *In vitro* MTX glutathionylation reaction. It was determined by calculating the differences between the fluorescence of the MCB-GSH adduct in the control reaction minus that in the presence of MTX. GST activity is expressed as nmols of GSH transferred by GST per minute. F) MTX glutathionylation reaction in cell free extracts. The formation of MCB-GSH adduct was followed by its fluorescence using cell free extracts from sensitive or resistant MCF7 cells in the absence or in the presence of MTX. Results are expressed as relative fluorescence units (RFU) per mg of total protein.
doi:10.1371/journal.pone.0063276.g008

2.8 times more GSTμ levels that sensitive cells as determined in Western blot assays (C & D).

Overexpression of different isoforms of GSTs was also detected in other MTX-resistant cell lines such as SaOs-2, HT-29 and CaCo-2 but not in MDA-MB-468 cells (GSE16648-GEO).

Inhibition of GSTM1 and GSTM4 increases the cytotoxicity produced by MTX

To establish a role of GSTs in the sensitivity to MTX, we silenced GSTM1 and GSTM4 using specific template polypurine hairpins, a new class of molecules for specific and effective gene silencing developed in the laboratory [35,36].

As it can be observed in Figure 8C & D, MTX cytotoxicity in MCF7 cells increased when either GSTM1 or GSTM4 were inhibited by specific PPRH-hairpins (Figure 8A & B), demonstrating the role of these specific GSTs in diminishing the cytotoxicity produced by MTX. Interestingly, GSTM1 and GSTM4 inhibition also increased the sensitivity to MTX in MTX-resistant cells, by 23% in the case of GSTM1 and 17% in the case of GSTM4. In a previous work performed in our laboratory, MTX-resistant MCF7 cells were found to have the *dhfr* locus amplified [14]. Therefore, it is noteworthy that inhibition of GSTM1 and GSTM4 increased the sensitivity towards MTX even in the presence of multiples copies of the *dhfr* gene. In addition, we used SaOs-2 cells as a model of MTX-resistant cell line with no amplification of the *dhfr locus* [14]. For this cell line, a hairpin against GSTA4 was used since this isoform was overexpressed in this MTX-resistant cell line. It was observed an increase in the sensitivity to MTX of 35%.

Apoptosis was also determined after incubating hairpins against GSTM1 and GSTM4 in MCF7 cells resistant to MTX. Apoptosis was increased 2.5 or 2 fold after knocking down GSTM1 and GSTM4, respectively.

As a mechanism of resistance in MTX-resistant cells, we wanted to assess whether MTX was susceptible of glutathionylation by GSTs given their role in the detoxification of exogenous compounds and drug resistance. As can be observed in Figure 8E & F, GSH can be transferred to MTX by GST activity.

Others studies relate levels of GSH with resistance to anti-tumor agents such as doxorubicin [50] and there are several examples in the literature that link increased GSH levels with breast cancer patients [62] or increased GSH levels and poor response to alkylating agents in MCF7 cells [51].

In addition, overexpression of GSTs in mammalian tumor cells has been implicated with resistance to various anticancer agents and chemical carcinogens [20,23].

In addition to their classic catalytic functions in detoxification of electrophilic compounds, GSTs are also involved in the regulation of other mechanisms that impact cell survival pathways, such as the JNK-pathway [19,63]. Interestingly, overexpression of GSTM1 [64] and GSTP [65] has been described to prevent the activation of MAPK pathway, thus avoiding the apoptosis cascade. This link with MAPK-mediated signaling could provide a possible mechanism of action of GST in drug-resistant cells. In addition, overexpression of GSTs has been associated with resistance to many therapeutic drugs [19], even if they are not GSTs substrates [17,66]. Another observation that argues in favor of GSTs playing a role in the modulation of apoptosis is the finding that Bee Venom, an inducing-apoptosis agent, increases the expression of apoptotic proteins, e.g. Bax, Bid, p53, p27, cytochrome c but decreases the expression of anti-apoptotic proteins like Bcl-2, Bcl-xL, and also GSTs [67]. Although there is no evidence of s-glutathionylation of cytochrome c *in vivo*, direct interaction between GSH and cytochrome c has been described *in vitro* [68]. Therefore, besides MTX glutathionylation, GST might help to maintain, directly or indirectly, cytochrome c in a reduced state.

According to our results, inhibition of GSTM1 and GSTM4 increases the sensitivity to MTX in sensitive cells, which is in keeping with the overexpression of these particular isoforms in breast cancer cells resistant to MTX. These observations suggest a role of GSTs in MTX drug resistance.

Conclusions

There is a relationship between cytochrome c redox state, apoptosis and development of MTX-resistance. In the presence of exogenous reducing agents of cytochrome c such as TMPD, ascorbate or GSH, MCF7 cells were less prone to apoptosis, which led to a lower MTX cytotoxicity. On the other hand, depletion of endogenous GSH using veratridine caused an increase in the apoptotic action of MTX, which was reverted by the addition of exogenous GSH. Furthermore, endogenous levels of GSH were higher in MTX-resistant MCF7 cells. These observations suggest that cytochrome c redox state modulates MTX sensitivity. This effect was not restricted to a specific cell type since treatment with TMPD also decreased MTX cytotoxicity in MDA-MB-468, SaOs-2, HT-29 and Caco-2 cells.

Inhibition of GSTM1 and GSTM4, which are overexpressed in MTX-resistant MCF7 cells, caused an increase in MTX cytotoxicity in sensitive and resistant MCF7 cells. Furthermore, inhibition of GSTA4 in MTX-resistant Saos-2 cells increased sensitivity to MTX.

In summary, we conclude that in MCF7 breast cancer cells, the overexpression of specific GSTs and increased GSH levels contribute to a more reduced environment. Thus, the presence of a more reduced cytochrome c would help the cells to avoid apoptosis and contribute to the resistant phenotype.

Acknowledgments

We thank Meryem Gonzalez and Pau Castel for their contribution to the initial phase of this work.

Author Contributions

Conceived and designed the experiments: SB NM CS VN CC. Performed the experiments: SB NM LR CO. Analyzed the data: SB NM CS VN CC. Contributed reagents/materials/analysis tools: VN. Wrote the paper: SB NM CS VN CC.

References

1. National Cancer Institute. http://www.cancer.gov.
2. Jolivet J, Cowan KH, Curt GA, Clendeninn NJ, Chabner BA (1983) The Pharmacology and Clinical Use of Methotrexate. New England Journal of Medicine 309: 1094–1104.
3. Chu E, Grem JL, Johnston PG, Allegra CJ (1996) New Concepts for the Development and Use of Antifolates. STEM CELLS 14: 41–46.
4. Blakley RL, Cocco L (1984) Dismutation of dihydrofolate by dihydrofolate reductase. Biochemistry 23: 2377–2383.
5. Noe V, Alemany C, Ciudad CJ (1995) Determination of dihydrofolate reductase gene amplification from single cell colonies by quantitative polymerase chain reaction. Anal Biochem 224: 600–603.
6. Alt FW, Kellems RE, Bertino JR, Schimke RT (1978) Selective multiplication of dihydrofolate reductase genes in methotrexate-resistant variants of cultured murine cells. J Biol Chem 253: 1357–1370.
7. Sirotnak FM, Moccio DM, Kelleher LE, Goutas LJ (1981) Relative Frequency and Kinetic Properties of Transport-defective Phenotypes among Methotrexate-

resistant L1210 Clonal Cell Lines Derived in Vivo. Cancer Research 41: 4447–4452.
8. Gorlick R, Goker E, Trippett T, Steinherz P, Elisseyeff Y, et al. (1997) Defective Transport Is a Common Mechanism of Acquired Methotrexate Resistance in Acute Lymphocytic Leukemia and Is Associated With Decreased Reduced Folate Carrier Expression. Blood 89: 1013–1018.
9. Liani E, Rothem L, Bunni MA, Smith CA, Jansen G, et al. (2003) Loss of folylpoly-gamma-glutamate synthetase activity is a dominant mechanism of resistance to polyglutamylation-dependent novel antifolates in multiple human leukemia sublines. Int J Cancer 103: 587–599.
10. Haber D, Beverley S, Kiely M, Schimke R (1981) Properties of an altered dihydrofolate reductase encoded by amplified genes in cultured mouse fibroblasts. J Biol Chem 256: 9501–9510.
11. Selga E, Noe V, Ciudad CJ (2008) Transcriptional regulation of aldo-keto reductase 1C1 in HT29 human colon cancer cells resistant to methotrexate: role in the cell cycle and apoptosis. Biochem Pharmacol 75: 414–426.
12. Mencia N, Selga E, Rico I, de Almagro MC, Villalobos X, et al. (2010) Overexpression of S100A4 in human cancer cell lines resistant to methotrexate. BMC Cancer 10: 250.
13. Selga E, Morales C, Noe V, Peinado MA, Ciudad CJ (2008) Role of caveolin 1, E-cadherin, Enolase 2 and PKCalpha on resistance to methotrexate in human HT29 colon cancer cells. BMC Med Genomics 1: 35.
14. Selga E, Oleaga C, Ramirez S, de Almagro MC, Noe V, et al. (2009) Networking of differentially expressed genes in human cancer cells resistant to methotrexate. Genome Med 1: 83.
15. de Almagro MC, Selga E, Thibaut R, Porte C, Noe V, et al. (2011) UDP-glucuronosyltransferase 1A6 overexpression in breast cancer cells resistant to methotrexate. Biochem Pharmacol 81: 60–70.
16. Mencia N, Selga E, Noe V, Ciudad CJ (2011) Underexpression of miR-224 in methotrexate resistant human colon cancer cells. Biochem Pharmacol 82: 1572–1582.
17. Tew KD (1994) Glutathione-associated enzymes in anticancer drug resistance. Cancer Res 54: 4313–4320.
18. McLellan LI, Wolf CR (1999) Glutathione and glutathione-dependent enzymes in cancer drug resistance. Drug Resist Updat 2: 153–164.
19. Townsend DM, Tew KD (2003) The role of glutathione-S-transferase in anti-cancer drug resistance. Oncogene 22: 7369–7375.
20. Hayes JD, Pulford DJ (1995) The Glut athione S-Transferase Supergene Family: Regulation of GST and the Contribution of the lsoenzymes to Cancer Chemoprotection and Drug Resistance Part I. Critical Reviews in Biochemistry and Molecular Biology 30: 445–520.
21. Armstrong RN (1997) Structure, Catalytic Mechanism, and Evolution of the Glutathione Transferases. Chemical Research in Toxicology 10: 2–18.
22. Hayes JD, McLellan LI (1999) Glutathione and glutathione-dependent enzymes represent a co-ordinately regulated defence against oxidative stress. Free Radic Res 31: 273–300.
23. Hayes JD, Flanagan JU, Jowsey IR (2004) GLUTATHIONE TRANSFERASES. Annual Review of Pharmacology and Toxicology 45: 51–88.
24. Ott M, Zhivotovsky B, Orrenius S (2007) Role of cardiolipin in cytochrome c release from mitochondria. Cell Death Differ 14: 1243–1247.
25. Kagan VE, Tyurin VA, Jiang J, Tyurina YY, Ritov VB, et al. (2005) Cytochrome c acts as a cardiolipin oxygenase required for release of proapoptotic factors. Nat Chem Biol 1: 223–232.
26. Belikova NA, Vladimirov YA, Osipov AN, Kapralov AA, Tyurin VA, et al. (2006) Peroxidase activity and structural transitions of cytochrome c bound to cardiolipin-containing membranes. Biochemistry 45: 4998–5009.
27. Hancock JT, Desikan R, Neill SJ (2001) Does the redox status of cytochrome C act as a fail-safe mechanism in the regulation of programmed cell death? Free Radic Biol Med 31: 697–703.
28. Brown GC, Borutaite V (2008) Regulation of apoptosis by the redox state of cytochrome c. Biochim Biophys Acta 1777: 877–881.
29. Borutaite V, Brown GC (2007) Mitochondrial Regulation of Caspase Activation by Cytochrome Oxidase and Tetramethylphenylenediamine via Cytosolic Cytochrome c Redox State. Journal of Biological Chemistry 282: 31124–31130.
30. Li M, Wang AJ, Xu JX (2008) Redox state of cytochrome c regulates cellular ROS and caspase cascade in permeablized cell model. Protein Pept Lett 15: 200–205.
31. Suto D, Sato K, Ohba Y, Yoshimura T, Fujii J (2005) Suppression of the pro-apoptotic function of cytochrome c by singlet oxygen via a haem redox state-independent mechanism. Biochem J 392: 399–406.
32. Vaughn AE, Deshmukh M (2008) Glucose metabolism inhibits apoptosis in neurons and cancer cells by redox inactivation of cytochrome c. Nat Cell Biol 10: 1477–1483.
33. Hancock JT, Desikan R, Neill SJ (2003) Cytochrome c, Glutathione, and the Possible Role of Redox Potentials in Apoptosis. Ann N Y Acad Sci 1010: 446–448.
34. Mosmann T (1983) Rapid colorimetric assay for cellular growth and survival: application to proliferation and cytotoxicity assays. J Immunol Methods 65: 55–63.
35. de Almagro MC, Mencia N, Noe V, Ciudad CJ (2011) Coding polypurine hairpins cause target-induced cell death in breast cancer cells. Hum Gene Ther 22: 451–463.
36. de Almagro MC, Coma S, Noe V, Ciudad CJ (2009) Polypurine hairpins directed against the template strand of DNA knock down the expression of mammalian genes. J Biol Chem 284: 11579–11589.
37. Habig WH, Pabst MJ, Jakoby WB (1974) Glutathione S-transferases. The first enzymatic step in mercapturic acid formation. J Biol Chem 249: 7130–7139.
38. Sarti P, Antonini G, Malatesta F, D'Itri E, Brunori M, et al. (1992) Spectral analysis of cytochromes in rat heart myocytes: transient and steady-state photodiode array spectrophotometry measurements. Arch Biochem Biophys 299: 8–14.
39. Nishimura G, Proske RJ, Doyama H, Higuchi M (2001) Regulation of apoptosis by respiration: cytochrome c release by respiratory substrates. FEBS Lett 505: 399–404.
40. Silva AM, Oliveira PJ (2012) Evaluation of respiration with clark type electrode in isolated mitochondria and permeabilized animal cells. Methods Mol Biol 810: 7–24.
41. Aupetit B, Emeric N, Toury R, Racadot O, Racadot J, et al. (1986) Stimulation of oxygen consumption at the cytochrome A3 level inhibits aldosterone biosynthesis from 18-hydroxycorticosterone. Biochim Biophys Acta 884: 270–275.
42. Kuznetsov AV, Schneeberger S, Seiler R, Brandacher G, Mark W, et al. (2004) Mitochondrial defects and heterogeneous cytochrome c release after cardiac cold ischemia and reperfusion. Am J Physiol Heart Circ Physiol 286: H1633–1641.
43. Ripple MO, Abajian M, Springett R (2010) Cytochrome c is rapidly reduced in the cytosol after mitochondrial outer membrane permeabilization. Apoptosis 15: 563–573.
44. Sarti P, Antonini G, Malatesta F, Brunori M (1992) Respiratory control in cytochrome oxidase vesicles is correlated with the rate of internal electron transfer. Biochem J 284 (Pt 1): 123–127.
45. Huang CC, Hsu PC, Hung YC, Liao YF, Liu CC, et al. (2005) Ornithine decarboxylase prevents methotrexate-induced apoptosis by reducing intracellular reactive oxygen species production. Apoptosis 10: 895–907.
46. Li T, Ito K, Sumi S, Fuwa T, Horie T (2009) Protective effect of aged garlic extract (AGE) on the apoptosis of intestinal epithelial cells caused by methotrexate. Cancer Chemother Pharmacol 63: 873–880.
47. Everse J, Kujundzic N (1979) Kinetics and mechanism of the reduction of horse heart ferricytochrome c by glutathione. Biochemistry 18: 2668–2673.
48. Ghibelli L, Coppola S, Fanelli C, Rotilio G, Civitareale P, et al. (1999) Glutathione depletion causes cytochrome c release even in the absence of cell commitment to apoptosis. FASEB J 13: 2031–2036.
49. Circu ML, Aw TY (2008) Glutathione and apoptosis. Free Radic Res 42: 689–706.
50. Bracht K, Boubakari, Grunert R, Bednarski PJ (2006) Correlations between the activities of 19 anti-tumor agents and the intracellular glutathione concentrations in a panel of 14 human cancer cell lines: comparisons with the National Cancer Institute data. Anticancer Drugs 17: 41–51.
51. Chen G, Waxman DJ (1994) Role of cellular glutathione and glutathione S-transferase in the expression of alkylating agent cytotoxicity in human breast cancer cells. Biochem Pharmacol 47: 1079–1087.
52. Estrela JM, Ortega A, Obrador E (2006) Glutathione in cancer biology and therapy. Crit Rev Clin Lab Sci 43: 143–181.
53. Jordan J, Galindo MF, Tornero D, Benavides A, Gonzalez C, et al. (2002) Superoxide anions mediate veratridine-induced cytochrome c release and caspase activity in bovine chromaffin cells. Br J Pharmacol 137: 993–1000.
54. Wang CH, Wu HT, Cheng HM, Yen TJ, Lu IH, et al. (2011) Inhibition of glutathione S-transferase M1 by new gabosine analogues is essential for overcoming cisplatin resistance in lung cancer cells. J Med Chem 54: 8574–8581.
55. Pasello M, Manara MC, Michelacci F, Fanelli M, Hattinger CM, et al. (2011) Targeting glutathione-S transferase enzymes in musculoskeletal sarcomas: a promising therapeutic strategy. Anal Cell Pathol (Amst) 34: 131–145.
56. Hosono N, Kishi S, Iho S, Urasaki Y, Yoshida A, et al. (2010) Glutathione S-transferase M1 inhibits dexamethasone-induced apoptosis in association with the suppression of Bim through dual mechanisms in a lymphoblastic leukemia cell line. Cancer Sci 101: 767–773.
57. Luo W, Gangwal K, Sankar S, Boucher KM, Thomas D, et al. (2009) GSTM4 is a microsatellite-containing EWS/FLI target involved in Ewing's sarcoma oncogenesis and therapeutic resistance. Oncogene 28: 4126–4132.
58. Moyer AM, Sun Z, Batzler AJ, Li L, Schaid DJ, et al. (2010) Glutathione pathway genetic polymorphisms and lung cancer survival after platinum-based chemotherapy. Cancer Epidemiol Biomarkers Prev 19: 811–821.
59. Abdellatif Y, Liu D, Gallant EM, Gage PW, Board PG, et al. (2007) The Mu class glutathione transferase is abundant in striated muscle and is an isoform-specific regulator of ryanodine receptor calcium channels. Cell Calcium 41: 429–440.
60. Tang SC, Wu MF, Wong RH, Liu YF, Tang LC, et al. (2011) Epigenetic mechanisms for silencing glutathione S-transferase m2 expression by hypermethylated specificity protein 1 binding in lung cancer. Cancer 117: 3209–3221.
61. Han I, Jeong SJ, Lee HJ, Koh W, Lee EO, et al. (2011) Proteomic analysis of mesenchymal stem-like cells derived from ovarian teratoma: potential role of glutathione S-transferase M2 in ovarian teratoma. Proteomics 11: 352–360.
62. Perry RR, Mazetta JA, Levin M, Barranco SC (1993) Glutathione levels and variability in breast tumors and normal tissue. Cancer 72: 783–787.
63. Tew KD, Townsend DM (2012) Glutathione-S-transferases as determinants of cell survival and death. Antioxid Redox Signal.

64. Cho SG, Lee YH, Park HS, Ryoo K, Kang KW, et al. (2001) Glutathione S-transferase mu modulates the stress-activated signals by suppressing apoptosis signal-regulating kinase 1. J Biol Chem 276: 12749–12755.
65. Adler V, Yin Z, Fuchs SY, Benezra M, Rosario L, et al. (1999) Regulation of JNK signaling by GSTp. EMBO J 18: 1321–1334.
66. Fan M, Chambers TC (2001) Role of mitogen-activated protein kinases in the response of tumor cells to chemotherapy. Drug Resist Updat 4: 253–267.
67. Ip S-W, Liao S-S, Lin S-Y, Lin J-P, Yang J-S, et al. (2008) The Role of Mitochondria in Bee Venom-induced Apoptosis in Human Breast Cancer MCF7 Cells. In Vivo 22: 237–245.
68. Deng H (2006) Characterization of the reaction products of cytochrome c with glutathione by mass spectrometry. Biochem Biophys Res Commun 342: 73–80.